frontiers | Research Topics

Women in heart valve disease

Edited by
Elena Aikawa, Verena Veulemans, Claudia Goettsch,
Maria Nunes and Marie Billaud

Published in
Frontiers in Cardiovascular Medicine

ISSN 1664-8714
ISBN 978-2-83252-029-1
DOI 10.3389/978-2-83252-029-1

About Frontiers

Frontiers is more than just an open access publisher of scholarly articles: it is a pioneering approach to the world of academia, radically improving the way scholarly research is managed. The grand vision of Frontiers is a world where all people have an equal opportunity to seek, share and generate knowledge. Frontiers provides immediate and permanent online open access to all its publications, but this alone is not enough to realize our grand goals.

Frontiers journal series

The Frontiers journal series is a multi-tier and interdisciplinary set of open-access, online journals, promising a paradigm shift from the current review, selection and dissemination processes in academic publishing. All Frontiers journals are driven by researchers for researchers; therefore, they constitute a service to the scholarly community. At the same time, the *Frontiers journal series* operates on a revolutionary invention, the tiered publishing system, initially addressing specific communities of scholars, and gradually climbing up to broader public understanding, thus serving the interests of the lay society, too.

Dedication to quality

Each Frontiers article is a landmark of the highest quality, thanks to genuinely collaborative interactions between authors and review editors, who include some of the world's best academicians. Research must be certified by peers before entering a stream of knowledge that may eventually reach the public - and shape society; therefore, Frontiers only applies the most rigorous and unbiased reviews. Frontiers revolutionizes research publishing by freely delivering the most outstanding research, evaluated with no bias from both the academic and social point of view. By applying the most advanced information technologies, Frontiers is catapulting scholarly publishing into a new generation.

What are Frontiers Research Topics?

Frontiers Research Topics are very popular trademarks of the *Frontiers journals series*: they are collections of at least ten articles, all centered on a particular subject. With their unique mix of varied contributions from Original Research to Review Articles, Frontiers Research Topics unify the most influential researchers, the latest key findings and historical advances in a hot research area.

Find out more on how to host your own Frontiers Research Topic or contribute to one as an author by contacting the Frontiers editorial office: frontiersin.org/about/contact

Women in heart valve disease

Topic editors

Elena Aikawa — Brigham and Women's Hospital, Harvard Medical School, United States

Verena Veulemans — University Hospital of Düsseldorf, Germany

Claudia Goettsch — RWTH Aachen University, Germany

Maria Nunes — Federal University of Minas Gerais, Brazil

Marie Billaud — Department of Surgery, Brigham and Women's Hospital, Harvard Medical School, United States

Citation

Aikawa, E., Veulemans, V., Goettsch, C., Nunes, M., Billaud, M., eds. (2023). *Women in heart valve disease*. Lausanne: Frontiers Media SA.

doi: 10.3389/978-2-83252-029-1

Author VV has received consulting fees, travel expenses, or study honoraria from Medtronic, Edwards Lifesciences, and Boston Scientific. Author EA serves on scientific board for Elastrin Therapeutics.

The remaining authors declare that the research was conducted in the absence of any commercial or financial relationships that could be construed as a potential conflict of interest

Table of contents

05 Editorial: Women in heart valve disease
Verena Veulemans, Marie Billaud, Maria Carmo P. Nunes, Claudia Goettsch and Elena Aikawa

08 Left Ventricular Remodeling in Non-syndromic Mitral Valve Prolapse: Volume Overload or Concomitant Cardiomyopathy?
Lobke L. Pype, Philippe B. Bertrand, Bernard P. Paelinck, Hein Heidbuchel, Emeline M. Van Craenenbroeck and Caroline M. Van De Heyning

22 Induced pluripotent stem cell-derived smooth muscle cells to study cardiovascular calcification
Samantha K. Atkins, Abhijeet R. Sonawane, Romi Brouwhuis, Johana Barrientos, Anna Ha, Maximillian Rogers, Takeshi Tanaka, Takehito Okui, Shiori Kuraoka, Sasha A. Singh, Masanori Aikawa and Elena Aikawa

38 Telotristat ethyl reverses myxomatous changes in mice mitral valves
Xinmei Wang, Danielle Kuban-Johnston, Pablo Lapuerta and Carla M. R. Lacerda

54 Characterization of the sex-specific pattern of angiogenesis and lymphangiogenesis in aortic stenosis
Lara Matilla, Ernesto Martín-Núñez, Mattie Garaikoetxea, Adela Navarro, Julieta Anabela Vico, Vanessa Arrieta, Amaia García-Peña, Amaya Fernández-Celis, Alicia Gainza, Virginia Álvarez, Rafael Sádaba, Natalia López-Andrés and Eva Jover

70 Glycosaminoglycans affect endothelial to mesenchymal transformation, proliferation, and calcification in a 3D model of aortic valve disease
Jonathan Alejandro Bramsen, Bridget R. Alber, Melissa Mendoza, Bruce T. Murray, Mei-Hsiu Chen, Peter Huang and Gretchen J. Mahler

81 Early and mid-term outcome of patients with low-flow–low-gradient aortic stenosis treated with newer-generation transcatheter aortic valves
Chiara Fraccaro, Giuseppe Tarantini, Stefano Rosato, Giovanni Baglio, Fausto Biancari, Marco Barbanti, Corrado Tamburino, Francesco Bedogni, Marco Ranucci, Gian Paolo Ussia, Fulvia Seccareccia and Paola D'Errigo on behalf of the OBSERVANT II Research Group

94 Safety of transesophageal echocardiography during transcatheter edge-to-edge tricuspid valve repair: A single-center experience
Katharina Hellhammer, Robert Schueler, Mareike Eißmann, Brigitte Schumacher, Alexander Wolf, Oliver Bruder, Thomas Schmitz and Moritz Lambers

99 Interactive contribution of hyperinsulinemia, hyperglycemia, and mammalian target of rapamycin signaling to valvular interstitial cell differentiation and matrix remodeling
Jessica I. Selig, H. Viviana Krug, Caroline Küppers, D. Margriet Ouwens, Felix A. Kraft, Elena Adler, Sebastian J. Bauer, Artur Lichtenberg, Payam Akhyari and Mareike Barth

116 Are acute type A aortic dissections atherosclerotic?
Nimrat Grewal, Onur Dolmaci, Evert Jansen, Robert Klautz, Antoine Driessen, Jan Lindeman and Robert E. Poelmann

frontiers | Frontiers in Cardiovascular Medicine

TYPE Editorial
PUBLISHED 13 March 2023
DOI 10.3389/fcvm.2023.1150169

OPEN ACCESS

EDITED AND REVIEWED BY
Hendrik Tevaearai Stahel,
University Hospital of Bern, Switzerland

*CORRESPONDENCE
Verena Veulemans
verena.veulemans@med.uni-duesseldorf.de

SPECIALTY SECTION
This article was submitted to Heart Valve Disease, a section of the journal Frontiers in Cardiovascular Medicine

RECEIVED 23 January 2023
ACCEPTED 22 February 2023
PUBLISHED 13 March 2023

CITATION
Veulemans V, Billaud M, Nunes MCP, Goettsch C and Aikawa E (2023) Editorial: Women in heart valve disease.
Front. Cardiovasc. Med. 10:1150169.
doi: 10.3389/fcvm.2023.1150169

Editorial: Women in heart valve disease

Verena Veulemans[1]*, Marie Billaud[2], Maria Carmo P. Nunes[3], Claudia Goettsch[4] and Elena Aikawa[5]

[1]Department of Cardiology, Pulmonology, and Vascular Diseases, University Hospital Düsseldorf, Düsseldorf, Germany, [2]Department of Surgery, Division of Thoracic and Cardiac Surgery, Brigham and Women's Hospital and Harvard Medical School, Boston, MA, United States, [3]Hospital das Clinicas, School of Medicine, Federal University of Minas Gerais, Belo Horizonte, Brazil, [4]Department of Internal Medicine I, Cardiology, Medical Faculty, RWTH Aachen University, Aachen, Germany, [5]Cardiovascular Medicine, Brigham and Women's Hospital and Harvard Medical School, Boston, MA, United States

KEYWORDS

heart valve disease (HVD), basic research, clinical research, mitral valve, CAVD (calcific aortic valve disease), LV remodeling

Editorial on the Research Topic
Women in heart valve disease

The present editorial summarizes articles published by women investigators in Frontiers Cardiovascular Medicine, Heart Valve Disease Section, and promotes the work of female scientists with a strong focus on heart valve disease. Even if women have made progress in education and science, they are largely under-represented and constitute only thirty percent of researchers worldwide, a condition known as STEM (Science, Technology, Engineering, and Math) -gap. Long-standing gender stereotypes that are frequently experienced by women may lead to a natural limitation for success, further discouraging high-potential females from entering these areas of research. Even if the presence and visibility of women are successively increasing in the medical area, their contribution to scientific fields usually lags behind men and develops slower. This exclusive collection of articles offers a view on outstanding research performed by female scientists in the field of heart valve disease.

However, ideally, gender should not have any impact on science, and we have to be careful that the empowerment of female scientific work does not end in discrimination against men. Looking back on the previous and current status quo in cardiovascular medicine and science, women still remain under-represented, including leading author positions, scientific or clinical meeting responsibilities, speaking engagements, and principal investigator roles in randomized clinical trials (1–4). Furthermore, women usually receive less research funding and more critical reviews than men (5), favoring a double-blind review process as an optimal and gender-neutral publication strategy in the future. As long as this is not routinely performed, other strategies to break the wheel of gender disparity in cardiovascular science are necessary, such as supporting educational and network platforms, which are also well-accepted for male networks and collaboration. In this context, van Spall et al. (3) provided a helpful roadmap concerning strategies to resolve long-lasting gender disparity, including monitoring key metrics by investigators, institutions, professional societies, industry and funding agencies, and scientific journals.

Regarding this collection of articles and the submission eligibility, the five handling female editors invited female researchers from their network and female scientists through research call/promotion actions on social media (Twitter, LinkedIn). Notably, male

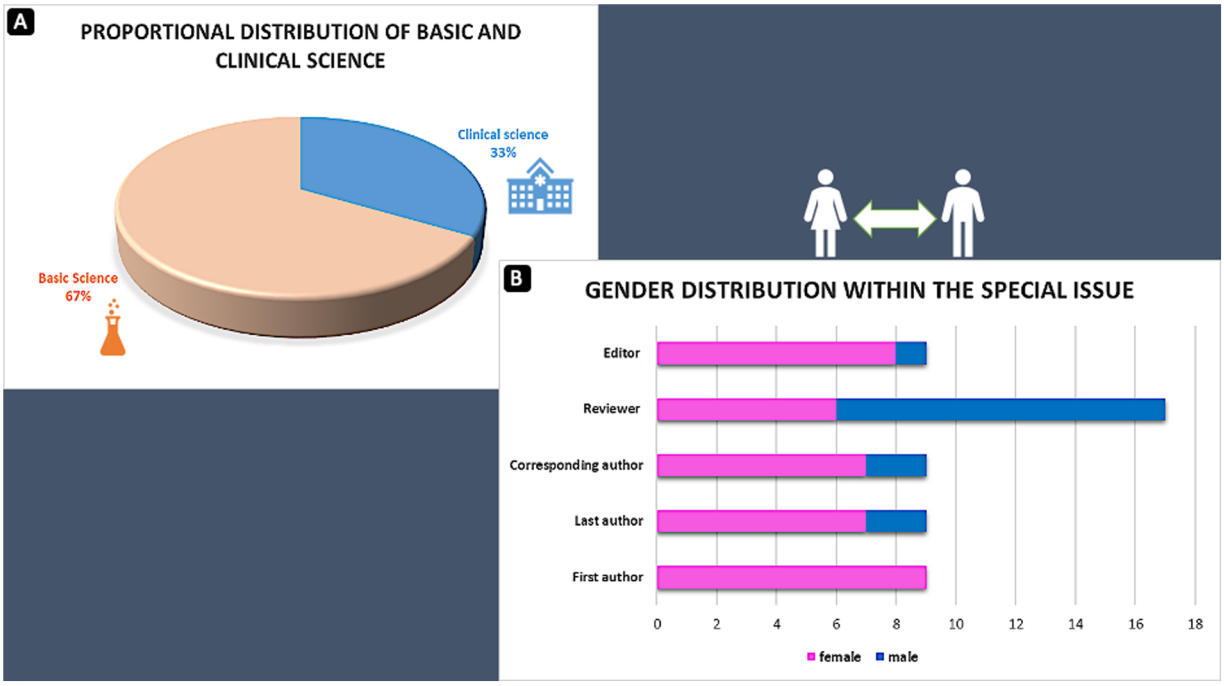

FIGURE 1
(A) Proportional distribution of basic and clinical science. (B) Gender-related responsibilities within this special issue.

researchers were also contacted to provide names for eligible women for a research contribution. All nine articles had females as first authors, while 7 out of 9 articles had a female in senior position. According to availability, the reviewer process was gender-independent and performed mainly by at least one male and one female reviewer. The handling editors made the final decision after the independent review process was finalized. Figure 1 illustrates the field research contribution and gender-related responsibilities within this special issue also involving men during the whole publication process (overall distribution of women/men: 70/30%) but with a clear focus on women in primary positions. However, as female scientists still represent a minority of first and last authors in cardiovascular research, journals should ideally blind and monitor their peer review processes to eliminate gender bias in one or another direction in the future.

Take-home message

The reported research in this section features different scientific considerations within heart valve disease, including basic and clinical research predominantly performed by women, providing an outstanding contribution to future research and facilitating greater diversity in cardiovascular research leadership.

Author contributions

VV wrote the first draft of the manuscript. All authors contributed to manuscript revision, read, and approved the submitted version.

Conflict of interest

Author VV has received consulting fees, travel expenses, or study honoraria from Medtronic, Edwards Lifesciences, and Boston Scientific. Author EA serves on scientific board for Elastrin Therapeutics.

The remaining authors declare that the research was conducted in the absence of any commercial or financial relationships that could be construed as a potential conflict of interest.

Publisher's note

All claims expressed in this article are solely those of the authors and do not necessarily represent those of their affiliated organizations, or those of the publisher, the editors and the reviewers. Any product that may be evaluated in this article, or claim that may be made by its manufacturer, is not guaranteed or endorsed by the publisher.

References

1. Mehran R, Kumar A, Bansal A, Shariff M, Gulati M, Kalra A. Gender and disparity in first authorship in cardiology randomized clinical trials. *JAMA Netw Open*. (2021) 4(3):e211043. doi: 10.1001/jamanetworkopen.2021.1043

2. Iqbal K, Kumar A, Rathore SS, Farid E, Ishaque A, Afzal H, et al. Gender and racial/ethnic disparities in award distribution by Major cardiovascular societies from 2000 to 2021. *J Am Coll Cardiol*. (2022) 80(21):2050–3. doi: 10.1016/j.jacc.2022.09.016

3. Van Spall HGC, Lala A, Deering TF, Casadei B, Zannad F, Kaul P, et al. Global CardioVascular Clinical Trialists (CVCT) forum and women as one scientific expert panel. Ending gender inequality in cardiovascular clinical trial leadership: JACC review topic of the week. *J Am Coll Cardiol*. (2021) 77(23):2960–72. doi: 10.1016/j.jacc.2021.04.038

4. Yong C, Suvarna A, Harrington R, Gummidipundi S, Krumholz HM, Mehran R, et al. Temporal trends in gender of principal investigators and patients in cardiovascular clinical trials. *J Am Coll Cardiol*. (2023) 81(4):428–30. doi: 10.1016/j.jacc.2022.10.038

5. Budden AE, Tregenza T, Aarssen LW, Koricheva J, Leimu R, Lortie CJ. Double-blind review favours increased representation of female authors. *Trends Ecol Evol*. (2008) 23(1):4–6. doi: 10.1016/j.tree.2007.07.008

frontiers | Frontiers in Cardiovascular Medicine

REVIEW
published: 12 April 2022
doi: 10.3389/fcvm.2022.862044

Left Ventricular Remodeling in Non-syndromic Mitral Valve Prolapse: Volume Overload or Concomitant Cardiomyopathy?

*Lobke L. Pype[1,2], Philippe B. Bertrand[3,4], Bernard P. Paelinck[2,5], Hein Heidbuchel[1,2], Emeline M. Van Craenenbroeck[1,2] and Caroline M. Van De Heyning[1,2]**

[1] Department of Cardiology, Antwerp University Hospital, Antwerp, Belgium, [2] Genetics, Pharmacology and Physiopathology of Heart, Vasculature and Skeleton (GENCOR) Research Group, University of Antwerp, Antwerp, Belgium, [3] Department of Cardiology, Ziekenhuis Oost-Limburg, Genk, Belgium, [4] Cardio and Organ Systems (COST) Resarch Group, Hasselt University, Hasselt, Belgium, [5] Department of Cardiac Surgery, Antwerp University Hospital, Antwerp, Belgium

Mitral valve prolapse (MVP) is a common valvular disorder that can be associated with mitral regurgitation (MR), heart failure, ventricular arrhythmias and sudden cardiac death. Given the prognostic impact of these conditions, it is important to evaluate not only mitral valve morphology and regurgitation, but also the presence of left ventricular (LV) function and remodeling. To date, several possible hypotheses have been proposed regarding the underlying mechanisms of LV remodeling in the context of non-syndromic MVP, but the exact pathophysiological explanation remains elusive. Overall, volume overload related to severe MR is considered the main cause of LV dilatation in MVP. However, significant LV remodeling has been observed in patients with MVP and no/mild MR, particularly in patients with bileaflet MVP or Barlow's disease, generating several new hypotheses. Recently, the concept of "prolapse volume" was introduced, adding a significant volume load to the LV on top of the transvalvular MR volume. Another possible hypothesis is the existence of a concomitant cardiomyopathy, supported by the link between MVP and myocardial fibrosis. The origin of this cardiomyopathy could be either genetic, a second hit (e.g., on top of genetic predisposition) and/or frequent ventricular ectopic beats. This review provides an overview of the different mechanisms and remaining questions regarding LV remodeling in non-syndromic MVP. Since technical specifications of imaging modalities impact the evaluation of MR severity and LV remodeling, and therefore might influence clinical decision making in these patients, this review will also discuss assessment of MVP using different imaging modalities.

Keywords: mitral valve prolapse, cardiomyopathy, mitral regurgitation, cardiac imaging, echocardiography, cardiac magnetic resonance (CMR) imaging, left ventricular remodeling

OPEN ACCESS

Edited by:
Verena Veulemans, University Hospital of Düsseldorf, Germany

Reviewed by:
Hoda Hatoum, Michigan Technological University, United States
Hiroyuki Kamiya, Asahikawa Medical University, Japan

****Correspondence:***
Caroline M. Van De Heyning
caroline.vandeheyning@uza.be

Specialty section:
This article was submitted to Heart Valve Disease, a section of the journal Frontiers in Cardiovascular Medicine

Received: *25 January 2022*
Accepted: *07 March 2022*
Published: *12 April 2022*

Citation:
Pype LL, Bertrand PB, Paelinck BP, Heidbuchel H, Van Craenenbroeck EM and Van De Heyning CM (2022) Left Ventricular Remodeling in Non-syndromic Mitral Valve Prolapse: Volume Overload or Concomitant Cardiomyopathy? Front. Cardiovasc. Med. 9:862044. doi: 10.3389/fcvm.2022.862044

INTRODUCTION

Mitral valve prolapse (MVP) is a common valvular disorder with a prevalence of 2–3% in the general population (1).

Abbreviations: BD, Barlow's Disease; CMR, cardiac magnetic resonance; EF, ejection fraction; EROA, effective regurgitant orifice area; FED, fibroelastic deficiency; FLNC, filamin C; LA, left atrium; LGE, late gadolinium enhancement; LV, left ventricle; MR, mitral regurgitation; MVP, mitral valve prolapse; PISA, proximal isovelocity surface area; PVC, premature ventricular contraction; TGF-β, transforming growth factor beta; TTE, transthoracic echocardiography; TTN, titin; TEE, transesophageal echocardiography.

In general, two main MVP subtypes can be distinguished that represent two ends of a disease spectrum in MVP. At one end, Barlow's disease (BD) occurs in relatively young patients (20–40 years) and is characterized by dilatation of the mitral annulus and the elongation, thickening and prolapse of both leaflets, often associated with mitral annular disjunction. At the other end, fibroelastic deficiency (FED) occurs in older patients (50–70 years) and is characterized by single leaflet or segment prolapse, chordal elongation or rupture, and thickening of the prolapsing leaflet segments (2–4). Although some patients remain asymptomatic for a long time, MVP can be associated with mitral regurgitation (MR), LV dysfunction and remodeling with heart failure, ventricular arrhythmias and sudden cardiac death (5, 6).

Left ventricular (LV) remodeling and dysfunction are important features of disease progression and worse prognosis in many cardiovascular diseases, including MVP. The underlying mechanisms of LV remodeling in MVP are only partly understood and the exact pathophysiological process remains elusive. In general, volume overload related to MR is considered the main mechanism of LV remodeling in MVP. Therefore, current guidelines recommend surgical mitral intervention in severe MR (7, 8).

However, this concept has been challenged by the observation that LV dilatation and dysfunction can be disproportionate to the degree of MR, especially in patients with BD (9–11). Disproportionate LV remodeling in MVP can be defined as LV dilatation over the age- and gender-specific upper limit of normal when corrected for MR volume. Recently, several hypotheses have been introduced to explain this disproportionate LV remodeling in MVP, including additional volume overload by the prolapse volume (12), concomitant cardiomyopathy associated with myocardial fibrosis and ventricular arrhythmias (13–15) or genetic predisposition (16). Besides syndromic forms of MVP (e.g., Marfan syndrome), there is a growing body of evidence that non-syndromic MVP is also a genetic disease, characterized by autosomal dominant (17–20) or X-linked inheritance (21).

This review will provide an overview of the proposed mechanisms regarding LV remodeling in non-syndromic MVP. Furthermore, the assessment of MVP using different imaging modalities will be discussed as their technical specifications impact the evaluation of MR severity and LV remodeling, and therefore contribute substantially to clinical decision making in these patients.

MECHANISMS OF GLOBAL LEFT VENTRICULAR REMODELING IN MITRAL VALVE PROLAPSE

Left Ventricular Remodeling Related to Volume Overload

Mitral Regurgitant Volume

It has been established that severe primary MR (including due to MVP) can present with significant hemodynamic consequences, particularly on the LV and left atrium (LA) (**Figure 1**). More specifically, LA and LV remodeling or dilatation may occur in patients with chronic MR to compensate for the increased volume load and to maintain the forward stroke volume. In this chronic compensated phase, LV ejection fraction (LVEF) is (supra) normal and LA pressure is usually not elevated. Over time, this may progress to a chronic decompensated phase characterized by a decrease in forward stroke volume, rise in LA pressure and pulmonary hypertension. Despite development of significant myocardial dysfunction, LVEF may appear preserved due to low afterload in severe MR (22). In accordance with this theory, current guideline-based clinical practice focuses on volume overload related to chronic severe MR as the main mechanism of LV dilatation in patients with MVP (7, 8). LA and LV remodeling in primary MR should be differentiated from remodeling in secondary MR, as this form of MR typically occurs as a result of significant atrial (23) or ventricular (24) dilatation, e.g., in the presence of atrial fibrillation or dilated cardiomyopathy (25).

Prolapse Volume

While volume overload related to severe MR is considered the main cause of LV dilatation in MVP, several studies have challenged this concept by reporting significant LV dilatation in patients with MVP without a significant degree of MR (9–11). Yiginer et al. (10) reported LV enlargement in a small cohort of patients with classic bileaflet MVP in the absence of significant MR. Likewise, Malev et al. (9) detected increased LV dimensions and lower global longitudinal strain in patients with classic MVP without MR. Finally, Yang et al. (11) confirmed these findings in a larger cohort of patients with less than moderate MR with ($n = 253$) and without MVP ($n = 344$) and found that more severe LV remodeling was independently associated with MVP.

A possible explanation for disproportionate LV remodeling relative to the degree of MR severity was recently proposed by El-Tallawi et al. (12). This study suggests that the total LV volume load in MVP is the sum of the transvalvular MR volume and the prolapse volume, which is defined as the end-systolic volume between the mitral annular plane and prolapsing leaflets (26) (**Figure 2A**). Especially in patients with BD and mitral annulus dilatation, the prolapse volume may contribute significantly to the total volume load. El-Tallawi et al. used cardiovascular magnetic resonance (CMR) to compare MR, prolapse volume and LV remodeling parameters in 157 patients with bileaflet prolapse (BD) or single leaflet prolapse. Despite similar transvalvular MR volumes, BD patients had significantly larger LV volumes. In addition, the prolapse volume (15.7 mL vs. 3.3 mL, $p < 0.001$) and therefore, the total volume load (59 mL vs. 42.5 mL, $p < 0.001$) were significantly larger in BD. A large prolapse volume of > 20 mL was present in 28% of BD patients. Furthermore, using the total volume load instead of transvalvular MR volume improved the correlation with LV end-diastolic volume in patients with BD, supporting the authors' concept that disproportionate LV remodeling in BD can be explained by the total volume load (12). Recently, similar findings regarding the influence of prolapse volume on LV remodeling were reported by Levy et al. who also used CMR to compare myxomatous MVP (≈BD) with FED (27). In addition, Luyten et al. have confirmed

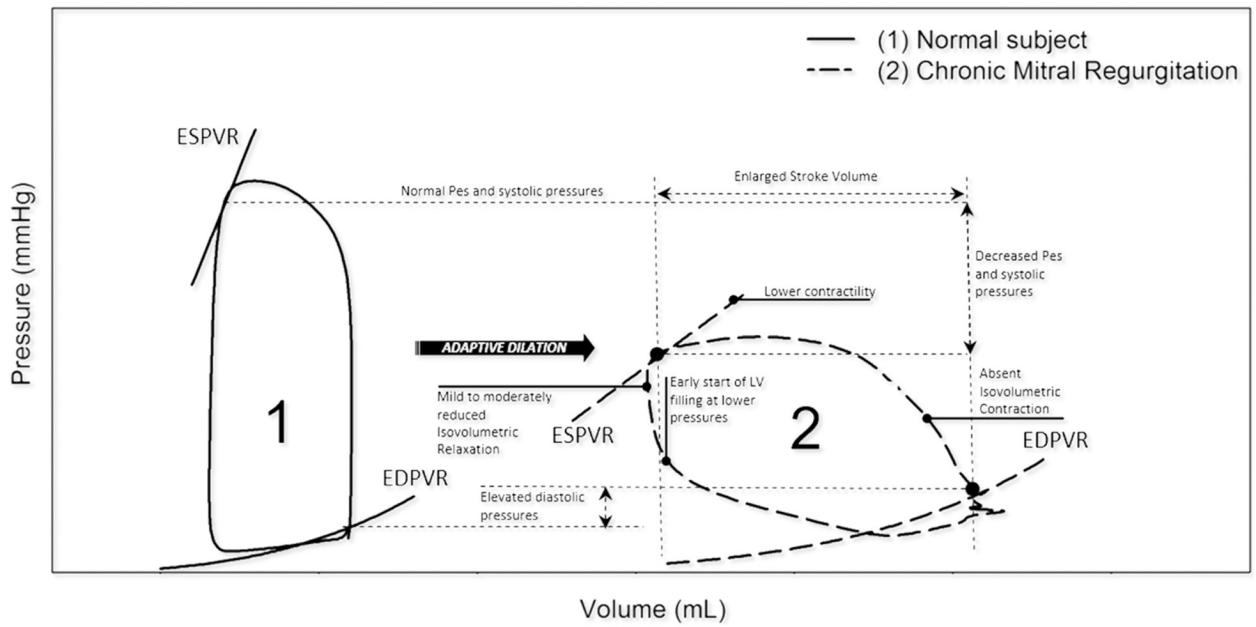

FIGURE 1 | Left ventricle pressure-volume loops in normal vs. chronic MR. In chronic MR the LV pressure-volume loop shows a rightward shift toward larger ventricular volumes with increased total stroke volume. Note that isovolumetric contraction is absent and isovolumetric relaxation is reduced. EDPVR, end-diastolic pressure-volume relation; ESPVR, end-systolic pressure-volume relation; LV, left ventricular; MR, mitral regurgitation; Pes, end-systolic pressure. Reproduced from "Invasive left ventricle pressure–volume analysis: overview and practical clinical implications" by Bastos et al. (120) Copyright by © The Author(s) 2019. Distributed under the terms of Creative Commons Attribution Non-commercial License.

the association of a large prolapse volume with significant LA and LV dilatation using echocardiography in patients with MVP and mitral annular disjunction (28).

Impact at the Cellular and Molecular Level

On a microscopic level, LV remodeling related to chronic LV volume overload is characterized by significant changes in the extracellular matrix, including alterations in collagen and matrix metalloproteinase expression (29–31). In addition, animal models have shown that extracellular matrix turnover and associated structural LV remodeling can be induced by mast cell activation and degranulation, e.g., by upregulation of the pro-inflammatory cytokine TNF-α (32–35). Furthermore, ventricular remodeling due to chronic volume overload has been associated with overexpression of transforming growth factor beta (TGF-β), which induces myocardial fibrosis through activation of fibroblasts and collagen synthesis (36). These findings need to be confirmed in human tissue to identify potential biomarkers for disease progression and it currently remains uncertain whether these molecular changes have a causative or compensatory role in the different stages of LV remodeling related to MR in MVP.

Left Ventricular Remodeling Related to an Underlying Cardiomyopathy

Another theory to explain LV remodeling in MVP, certainly when disproportionate to the degree of MR, is the existence of an underlying myocardial disease—a cardiomyopathy. While the hypothesis of MVP-related cardiomyopathy has gained a lot of interest lately, this concept was first introduced several decades ago (37, 38). Early studies found an association of MVP with LV dysfunction (37), arrhythmias (39) and histologic evidence of myocardial fibrosis (38), suggestive of a concomitant myocardial disease. However, it is important to mention that quantification of MR and LV volumes was performed using ventriculography in these early studies, meaning that precise evaluation in accordance with current guidelines was not possible. In addition, these studies usually did not specify the MVP subtype as BD or FED.

At present, there are several possible hypotheses regarding the etiology of a concomitant cardiomyopathy in MVP (**Figure 3**).

Genetic Substrate

MVP is known to be associated with several connective tissue disorders such as Marfan syndrome and Loeys-Dietz syndrome, which are beyond the scope of this review (3, 40). Accordingly, it has been suggested that non-syndromic MVP could be correlated with connective tissue diseases as well.

Similar to syndromic forms of MVP, familial inheritance by autosomal dominant (17–20) and X-linked (21) transmission has been observed in non-syndromic MVP. To date, several (candidate) genes have been identified through linkage analysis and genome wide association studies, such as *DCHS1* (dachsous cadherin-related 1) (41), *TNS1* (tensin 1) (20), *LMCD1* (LIM and cysteine rich domains 1) (20), *DZIP1* (DAZ interacting zinc finger protein 1) (42), *GLIS1* (GLIS family zinc finger 1) (43) and *FLNA* (filamin A) (21). Interestingly, a very recent meta-analysis of six genome wide association studies identified several new candidate genes associated with MVP, including genes involved in TGF-β

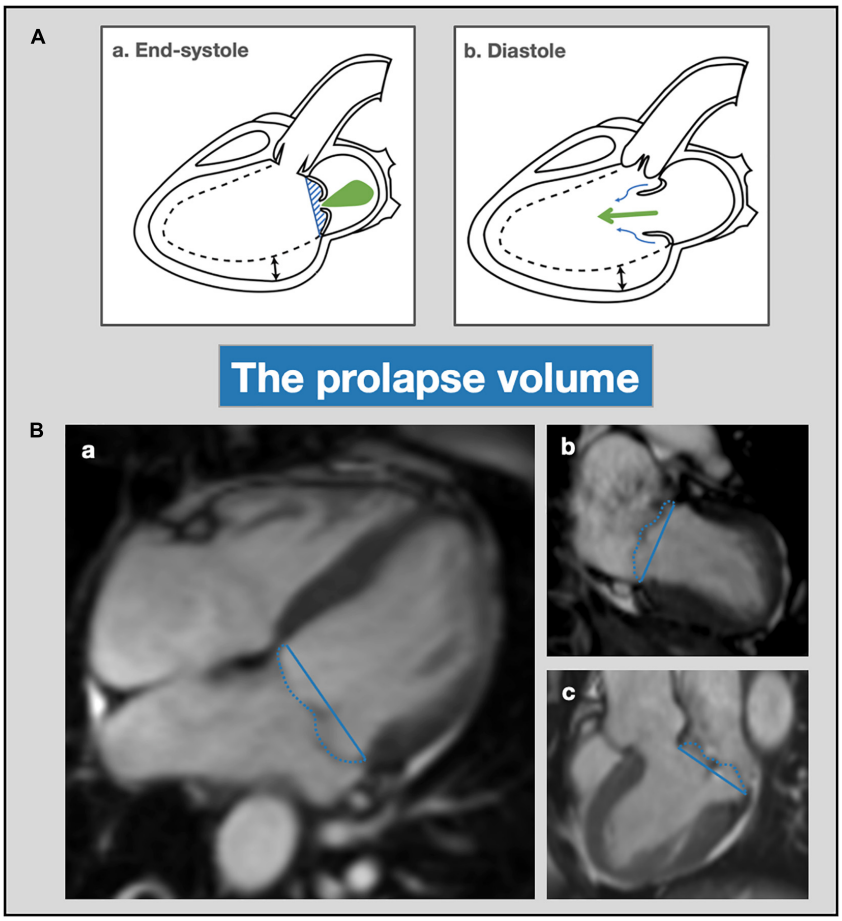

FIGURE 2 | Prolapse volume—mechanism and assessment with cardiac magnetic resonance imaging. **(A)** Schematic overview of prolapse volume as a mechanism for progressive LV remodeling (dotted line). In end-systole (a) transvalvular MR occurs (green jet) and the prolapse volume is contained beneath the mitral leaflets (blue shaded area) and delineated by the mitral annulus (blue line). In diastole (b) the prolapse volume (blue arrows) exerts an additional volume load on the left ventricle on top of the transvalvular MR volume (green arrows). **(B)** Mitral valve prolapse volume assessment with CMR. CMR cine images of patient with bileaflet mitral valve prolapse and mitral regurgitation; 4-chamber (a), 2-chamber (b) and 3-chamber (c) views. Calculation of the prolapse volume is performed as previously described (12, 26). First, the mitral valve annulus diameter is measured in each view (indicated with the blue line) in order to calculate the average mitral annulus diameter. Then, the end-systolic prolapse area is measured by tracing the area between the mitral valve leaflets and annulus in each view (dashed blue line). By dividing the prolapse area by the annulus diameters, the prolapse height can be calculated for each view. Finally, the prolapse volume can be determined by multiplying mean prolapse height with annulus area, which can be calculated using the ellipse area formula. LV, left ventricular; MR, mitral regurgitation; CMR, cardiac magnetic resonance imaging.

signaling and cardiomyopathy (44). While these genes have been related to the etiology of MVP, it is currently unclear whether they also act as a genetic substrate for disproportionate LV remodeling.

The recent association of MVP with pathogenic variants in several known cardiomyopathy genes, such as *TTN* (titin) and *FLNC* (filamin C) could explain disproportionate LV remodeling (16, 45). In 2020, Van Wijngaarden et al. (16) performed an extensive cardiac gene panel in 101 patients with MVP, predominantly BD phenotype (n = 96, 97%), in order to evaluate the genetic yield of the known causative MVP genes and detect possible new genetic variants. Interestingly, only 1 patient (1%) had a likely pathogenic variant in one of the causative MVP genes (*DCHS1*), but in 8 probands (8%) a likely pathogenic variant in four cardiomyopathy genes was observed (*DSP*, *HCN4*, *MYH6* and *TTN*), suggesting a common genetic foundation in the development of both myocardial and mitral valve disease. Most prevalent were *TTN* truncating variants (n = 5) which encode for the giant sarcomeric protein titin and are known to explain ca. 25% of patients with familial dilated cardiomyopathy (46). Furthermore, several case reports demonstrated a link between arrhythmogenic bileaflet MVP and truncating variants in the *FLNC* gene, which encodes an actin-binding protein associated with both hypertrophic and dilated cardiomyopathies (45). To date, the genetic substrate of MVP has not been linked with MR severity or LV remodeling parameters, so additional studies will be needed to elucidate the genotype-phenotype correlation and determine the role of familial screening in the future.

Furthermore, an MVP-related cardiomyopathy could be induced only in patients with a genetic substrate and an additional environmental risk factor that acts as a second hit. This mechanism has been described in dilated cardiomyopathy secondary to pregnancy, alcohol and anthracyclines (47). Most

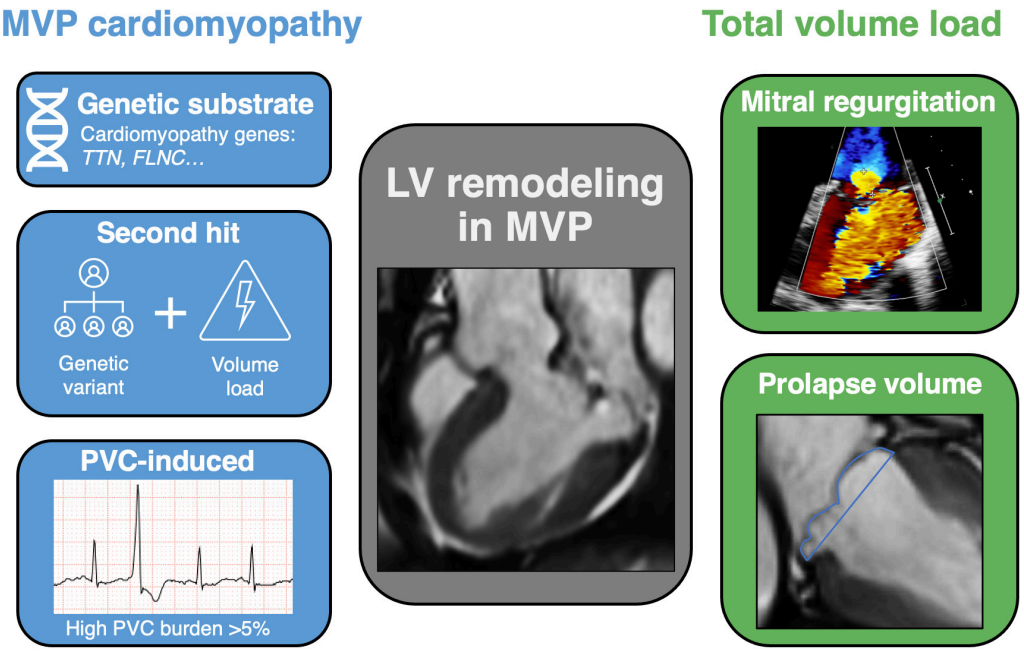

FIGURE 3 | Central image: mechanisms of left ventricular remodeling in mitral valve prolapse. Schematic view of LV remodeling mechanisms in MVP, addressing the hypothesis of a cardiomyopathy on the left and total volume load on the right. Different pathophysiological mechanisms exist regarding the development of a cardiomyopathy in MVP, including a genetic substrate, second hit phenomenon and PVC-induced remodeling. On the other hand, the excessive volume load of chronic MR itself can induce LV dilatation, especially when a significant prolapse volume is added to the total volume load. LV, left ventricular; MVP, mitral valve prolapse; MR, mitral regurgitation; CMR, cardiac magnetic resonance imaging; *TTN*, titin; *FLNC*, filamin C; PVC, premature ventricular contraction.

commonly, the culprit mutations that serve as a first hit are related to known cardiomyopathy genes, again the *TTN* gene in particular (48–50). Therefore, in the presence of a genetic substrate, the MR volume in MVP could act as a second hit to cause a dilated cardiomyopathy. In addition, prolapsing leaflets generate increased mechanical stress on the LV myocardium and papillary muscles which could induce focal fibrosis (51).

Arrhythmogenic

Supraventricular and ventricular arrhythmias have been established as a possible trigger for the development of a non-ischemic cardiomyopathy, characterized by reversible LV dysfunction and dilatation (52). In addition to tachycardia-induced cardiomyopathy, for example due to atrial fibrillation, frequent premature ventricular contractions (PVCs) are now recognized as a separate etiology of dilated cardiomyopathy (53). Whereas PVCs are frequently referred to as benign, even a low PVC-burden has been associated with increased risk of heart failure and LV dysfunction (54). The exact pathophysiology of PVC-induced cardiomyopathy is still unclear, but potential mechanisms are LV dyssynchrony and post-extrasystolic potentiation with Ca^{2+} overload (55–57).

Several studies have already demonstrated a correlation between MVP, ventricular arrhythmias and sudden cardiac death (15, 58). Complex PVCs, frequently arising from the papillary muscles or outflow tract, may induce LV dysfunction and act as a trigger for ventricular fibrillation as well (59). A significant improvement in LVEF has been observed after suppression of PVC burden with successful catheter ablation in patients with MVP, supporting the hypothesis of a PVC-induced cardiomyopathy (59, 60). Furthermore, Essayagh et al. showed that ventricular arrhythmias, defined as PVC burden >5%, ventricular tachycardia and ventricular fibrillation, are not only associated with LV dysfunction but with LA and LV dilatation as well (58). Therefore, the presence of PVCs or more complex arrhythmias appears to be an important risk factor in the process of disproportionate LV remodeling in MVP and screening with Holter monitoring should be considered.

MECHANISMS OF REGIONAL LEFT VENTRICULAR REMODELING IN MITRAL VALVE PROLAPSE

Apart from global LV remodeling, several regional LV remodeling patterns have been described in MVP.

First, focal LV hypertrophy has been observed in the basal inferolateral myocardial wall of patients with MVP, frequently coinciding with replacement fibrosis (15, 61), and the extent of basal hypertrophy has been correlated with the degree of mitral valve leaflet excursion (62). This regional hypertrophy may be triggered by dilatation of the LV base, especially in patients with mitral annular dilatation, due to increased wall tension by Laplace's law (63). Furthermore, early angiographic studies have described a reduction in LV basal wall contractility, the so-called ballerina-foot pattern (37). These regional wall

motion abnormalities have been confirmed more recently using speckle-tracking echocardiography and correlated with LV dilatation, mitral annular dilation and mitral annular disjunction (63–65). In addition to excessive regional stretch induced by posterior leaflet prolapse, abnormal contractility of the LV basal wall is thought to cause the typical systolic curling motion of the mitral annulus that is frequently referred to in patients with MVP (66, 67).

Second, it was recently hypothesized that morphological variations in mitral valve apparatus components, such as insertion of the papillary muscles, could alter (regional) LV remodeling. Moura-Ferreira et al. (68) found that apical insertion of the papillary muscles in patients with MVP induces significant changes in regional LV remodeling, such as focal thinning of the mid lateral wall and a lower global circumferential strain at this level, however, no changes in ventricular volumes or LVEF were observed. Furthermore, the prevalence of papillary muscle fibrosis was significantly higher in patients with apical papillary muscle insertion, presumably due to increased systolic traction and higher contractile force on the myocardium in these patients. Interestingly, they observed a higher burden of PVC's and non-sustained ventricular tachycardias in patients with apical insertion of the papillary muscles (68).

Finally, several other LV abnormalities have been described in patients with MVP, such as LV non-compaction (69) and asymmetric septal hypertrophy (70), however these were only reported in small series.

MITRAL VALVE PROLAPSE SUBTYPES AND THEIR IMPACT ON LEFT VENTRICULAR REMODELING

In MVP, two phenotypes can generally be distinguished—Barlow's Disease (BD) and fibroelastic deficiency (FED). While current guidelines still recommend the same assessment and treatment for both entities (7, 8), they present with important differences in histopathology, echocardiographic characteristics and arrhythmogenic risk (2).

The pathophysiology of MVP is based on myxomatous degeneration of the valve, characterized by progressive thickening and increased area of the mitral valve leaflets. The normal valve tissue consists of 3 layers: the atrialis on the atrial side, the spongiosa as a middle layer and the fibrosa on the ventricular side (5). Histopathological analysis of the mitral valve identified that BD valves are characterized by expansion of the spongiosa layer due to proteoglycan accumulation and intimal thickening of fibrosa and atrialis (71, 72). This process of myxomatous infiltration causes leaflet thickening in BD. In contrast, FED showed more leaflet thinning due to impaired production of connective tissue with deficiency of collagen, elastin and proteoglycans. However, local thickening of the prolapsing segment can be observed in FED as well (71).

Presentation of BD is frequently in asymptomatic, younger patients (< 40 years) whereas FED occurs at a more advanced age (50–70 years), e.g., after chordal rupture (4). Interestingly, Hiemstra et al. observed that patients with BD more frequently report a familial history of primary MR compared to FED (26 vs. 8%) (73). Complex ventricular arrhythmias, ranging from ventricular ectopy to sustained ventricular tachycardia or even sudden cardiac death, have been associated particularly with bileaflet prolapse (≈BD) (13, 58).

Furthermore, it seems that bileaflet myxomatous MVP or BD is the main phenotype in patients with LV remodeling disproportionate to the degree of MR. In 2012, Yiginer et al. observed LV enlargement in classic bileaflet MVP even in the absence of significant MR (10). Similar findings were reported by Malev et al. (9), who studied 78 young adults with MVP without MR, and detected lower global longitudinal strain and larger LV dimensions in patients with classic prolapse compared to non-classic prolapse. In contrast, Yang et al. found early LV remodeling in patients with MVP and less than moderate MR severity, but observed no significant difference in chamber remodeling parameters between single and bileaflet prolapse (11). Overall, the role of MVP subtype remains debatable.

THE ELUSIVE LINK BETWEEN LEFT VENTRICULAR REMODELING AND MYOCARDIAL FIBROSIS IN MITRAL VALVE PROLAPSE

An important prognostic factor in the process of LV remodeling is the presence of myocardial fibrosis, which might be focal (replacement fibrosis) or diffuse (interstitial fibrosis). In patients with MVP, focal myocardial fibrosis has been observed mainly in the basal inferolateral LV wall and papillary muscles through histopathology (15, 51, 74) or by using CMR with late gadolinium enhancement (LGE) (14, 15, 51) and an association with malignant arrhythmias and sudden cardiac death has been established (13–15, 74). Interestingly, a CMR-based analysis of patients with chronic primary MR detected a significantly higher prevalence of focal LV fibrosis in MVP compared to non-MVP MR patients (36.7 vs. 6.7%; $p < 0.001$), suggesting a unique pathophysiological mechanism beyond MR causing LV fibrosis in MVP (61). Furthermore, the presence of LGE has been associated with LV dilatation in different cohorts of primary MR patients (61, 75). These findings have been validated in a population of patients with MVP by Constant Dit Beaufils et al. (14). Moreover, they observed focal LV fibrosis even in the absence of significant MR. In addition, subgroup analysis of patients with trace-mild MR ($n = 120$) showed LV dilatation (16%) and ventricular arrhythmias (25%), even in the absence of significant volume overload, suggesting another pathophysiological mechanism (14).

Besides focal fibrosis, limited data are available regarding the presence of diffuse interstitial fibrosis in patients with MVP, which can be associated with diastolic and systolic impairment. Two studies have shown that interstitial myocardial fibrosis as quantified with T1-mapping by CMR is correlated with LV dilatation in primary MR (76), and more specifically in MVP (77). Although it is assumed that chronic MR with LV volume overload leads to diffuse myocardial fibrosis which may ultimately result in heart failure, some evidence points toward a more specific

myocardial disease in MVP. Bui et al. showed that interstitial fibrosis as assessed by T1-mapping was not related to MR severity in patients with MVP, however, this study may be underpowered due to the small sample size (77). In contrast, Kitkungvan et al. recently demonstrated that the presence of diffuse interstitial fibrosis was associated with increase in MR severity, but not with MVP in particular (78). In the future, large multicenter studies will be required to further evaluate the role of T1-mapping in the risk stratification of patients with primary MR and MVP.

LEFT VENTRICULAR REVERSE REMODELING

Several studies have demonstrated that surgical correction of severe primary MR can reverse the process of LV remodeling by eliminating chronic volume overload (79–81). The phased process of LV reverse remodeling, characterized by a decrease in LV dimensions and improvement of LV systolic function, was recently investigated by Le Tourneau et al. (81) using echocardiographic follow-up after mitral valve surgery. The initial response after surgery is a significant decrease in LV end-diastolic volume and LVEF which largely depends on the pre-operative regurgitant volume. After several months, a decrease in LV end-systolic volume and improvement of LVEF can be observed (81). Besides pre-operative MR severity, other determinants of LV reverse remodeling and normalization of LVEF are preserved LVEF and smaller LV dimensions at baseline (82, 83). Interestingly, a recent CMR study in patients with primary MR showed that mitral valve surgery can even result in reverse myocardial remodeling with a reduction in diffuse myocardial fibrosis (84).

In MVP specifically, a similar evolution with decrease in LV volumes has been demonstrated following mitral valve repair or replacement (82, 85, 86). As mentioned earlier, the total LV volume load in MVP consists of the transvalvular MR volume and the prolapse volume, which can be significant especially in bileaflet prolapse. We could therefore hypothesize that LV reverse remodeling in MVP will be optimal if the prolapse volume is corrected as well, e.g., by mitral annuloplasty and partial leaflet resection if needed in contrast to an Alfieri procedure without annuloplasty, although there are currently no data on this specific topic. Of note, a recent study by Essayagh et al. (87) showed that LV remodeling post-mitral valve repair in patients with MVP was similar between patients with and without mitral annular disjunction—which is related to the height of the prolapse volume—if the disjunction was corrected.

ASSESSMENT OF MITRAL VALVE PROLAPSE, MITRAL REGURGITATION SEVERITY AND LEFT VENTRICULAR REMODELING BY CARDIOVASCULAR IMAGING

Any study investigating MVP and LV remodeling is impacted by the limitations of the imaging method used. Therefore, clinicians should be aware of particular limitations and strengths of each modality when assessing a patient with MVP, summarized in **Table 1**.

Echocardiography

Transthoracic Echocardiography

Routine 2D TTE is generally the first-line imaging tool to diagnose MVP and usually allows for a correct identification of the prolapsing leaflet segments. However, it is important to note that the diagnosis of MVP should be made in the parasternal (or apical) long-axis view but not in the apical four-chamber view because the saddle-shaped annulus could lead to false positive diagnosis (88).

Following diagnosis of prolapse, MVP subtypes (BD vs. FED) can be differentiated by comprehensive echocardiographic assessment (**Figure 4**).

As per international society recommendations, echocardiographic assessment of MR severity should be performed using a multi-integrative approach including both qualitative and quantitative parameters (7, 8) (**Figure 5A**). In the clinical evaluation of patients with valve regurgitation, it is critical to differentiate severe from non-severe MR since the former may implicate the need for (surgical) intervention. When feasible, the proximal isovelocity surface area (PISA) method is recommended to quantify the regurgitant volume and effective regurgitant orifice area (EROA) (22).

While 2D TTE is widely used as the principal technique to investigate MR severity, several limitations have to be addressed, which can originate from specific MR characteristics, such as orifice morphology, eccentric or multiple jets. . . (**Table 1**). For example, patients with mid-late systolic MR might have a similar jet area and EROA compared to holosystolic MR, but a lower regurgitant volume (and therefore more benign outcome) due to the shorter regurgitant time interval (89). Correspondingly, the PISA radius may be variable during the cardiac cycle and increase during systole to reach a maximum in mid- to end-systole. It is important to note that not considering these limitative factors of Transthoracic Echocardiography (TTE) could lead to an overestimation of MR severity and possibly even excess surgical interventions.

Echocardiographic evaluation of LA volume and LV dimensions, LVEF and systolic pulmonary pressure is recommended in all patients with more than mild MR (22). In the context of MR, LV dilatation is defined as LV end-systolic dimension $\geq$ 40 mm (7, 8), which is less load-dependent compared to LV end-diastolic dimension. After correction for body surface area, LV end-systolic volume and end-diastolic volume can provide more insight in the degree of ventricular remodeling. In order to detect early LV dysfunction, global longitudinal strain can be considered (90, 91). Importantly, 3D echocardiography has superior accuracy compared to 2D echocardiography regarding the evaluation of LV volumes and LVEF, as it avoids foreshortening of the LV (92). The prolapse volume can be quantified using 2D TTE (28) and 3D TEE (93), although this measurement is currently not part of standard clinical practice.

TABLE 1 | Strengths and limitations of echocardiography vs. cardiac magnetic resonance imaging (CMR) in the assessment of mitral valve prolapse.

	Echocardiography		CMR	
	+	–	+	–
General	Widely available Evaluation of prolapsing leaflet/segment and MVP subtype Hemodynamic impact (filling pressures and pulmonary hypertension)	TTE: limited by poor echogenicity TEE: semi-invasive technique	Tissue characterization (T1 mapping, LGE) Accurate quantification of prolapse volume (26)	Relative contra-indications: incompatible implanted devices, claustrophobia,. . . Inaccurate measurements with arrhythmia or poor breath-holding
MR quantification	Greater sensitivity (small jets)	Mid-late systolic MR: overestimation of severity with PISA and EROA (79, 89) Eccentric jet difficult to quantify High intra- and interobserver variability (114, 115)	Lower intra- and interobserver variability (116, 117) Better correlation with outcome (110, 118)	No well-established cut-off to define severe MR Indirect method: includes prolapse volume in MR volume (100)
LV remodeling	Quick evaluation of LV volumes and function	Underestimation of LV volumes and overestimation of LV ejection fraction compared to CMR (2D > 3D echo) (119)	More accurate assessment of LV volumes (gold standard) (96, 97)	LV volumes and ejection fraction dependent on definition of LV base (100)

Transesophageal Echocardiography

Part of the limitations of TTE, such as poor echogenicity, can be overcome by using Transesophageal Echocardiography (TEE). In addition, TEE can provide a more detailed evaluation of valve geometry and dynamics, and help to characterize BD vs. FED. Benefits like higher resolution, multiplane and proximity to the mitral valve enhance MR evaluation techniques such as PISA and vena contracta compared to TTE (94). Moreover, 3D echocardiography allows for direct delineation of the vena contracta and EROA, which may improve MR severity assessment, especially if the mitral regurgitant orifice is non-circular. Furthermore, the surgical view of the mitral valve can be visualized by 3D TEE and has a high specificity and sensitivity for the diagnosis of MVP. Consequently, current international guidelines state that 3D echocardiography should be incorporated in the clinical assessment of patients with particularly complex mitral valve pathology (92).

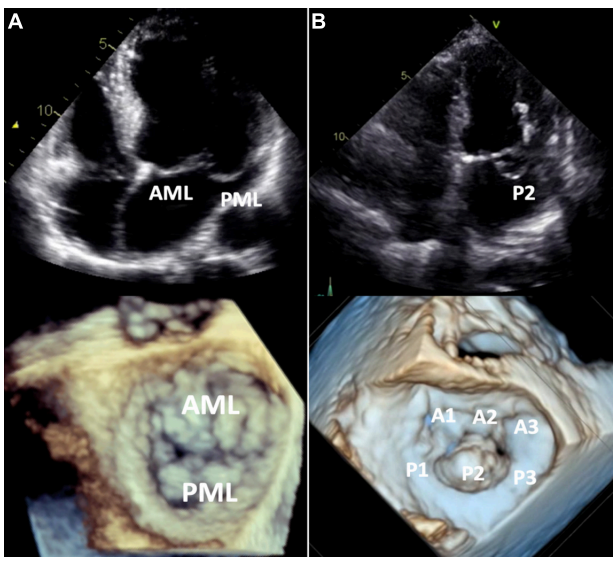

FIGURE 4 | Barlow's disease vs. fibroelastic deficiency. 2D transthoracic four-chamber view (upper panels) and 3D transesophageal focused view of the mitral valve (lower panels). **(A)** Barlow's disease with annular dilatation, thickened leaflets and bileaflet prolapse (anterior + posterior mitral leaflet). **(B)** Fibro-elastic deficiency with prolapse (flail) of the P2 segment of the posterior mitral leaflet due to chordal rupture. Mitral annulus diameter is normal in this case, but mild annular dilatation can be present. AML, anterior mitral leaflet; PML, posterior mitral leaflet.

Cardiac Magnetic Resonance Imaging

Due to the known limitations of echocardiography and therapeutic consequences of severe MR, CMR has emerged as an interesting non-invasive imaging modality for the evaluation of MVP morphology and MR severity (95). At present, CMR is generally indicated in patients with MVP when echocardiographic images are suboptimal, when there is discordance between MR severity by echocardiography and clinical findings, and to evaluate the presence of myocardial fibrosis (94). Importantly, CMR is currently considered as the gold standard for the assessment of atrial and ventricular volumes and function (96, 97).

Quantification of MR volume using CMR can be performed using direct or indirect methods. The most commonly used indirect CMR method relies on two techniques for the quantification of MR: phase-contrast imaging to measure aortic flow and short-axis cine images to quantify LV stroke volume (98, 99) (**Figure 5B**). In patients with lone MR, the LV stroke volume contains the forward stroke volume and mitral regurgitant volume. Thus, the MR volume can be calculated by subtracting the aortic forward flow from the total LV stroke volume. Importantly, in patients with MVP the LV base (at end-systole) is usually defined at the mitral valve annulus and not at the mitral valve leaflets, meaning that the calculated regurgitant volume includes the prolapse volume (100) (**Figure 5B**).

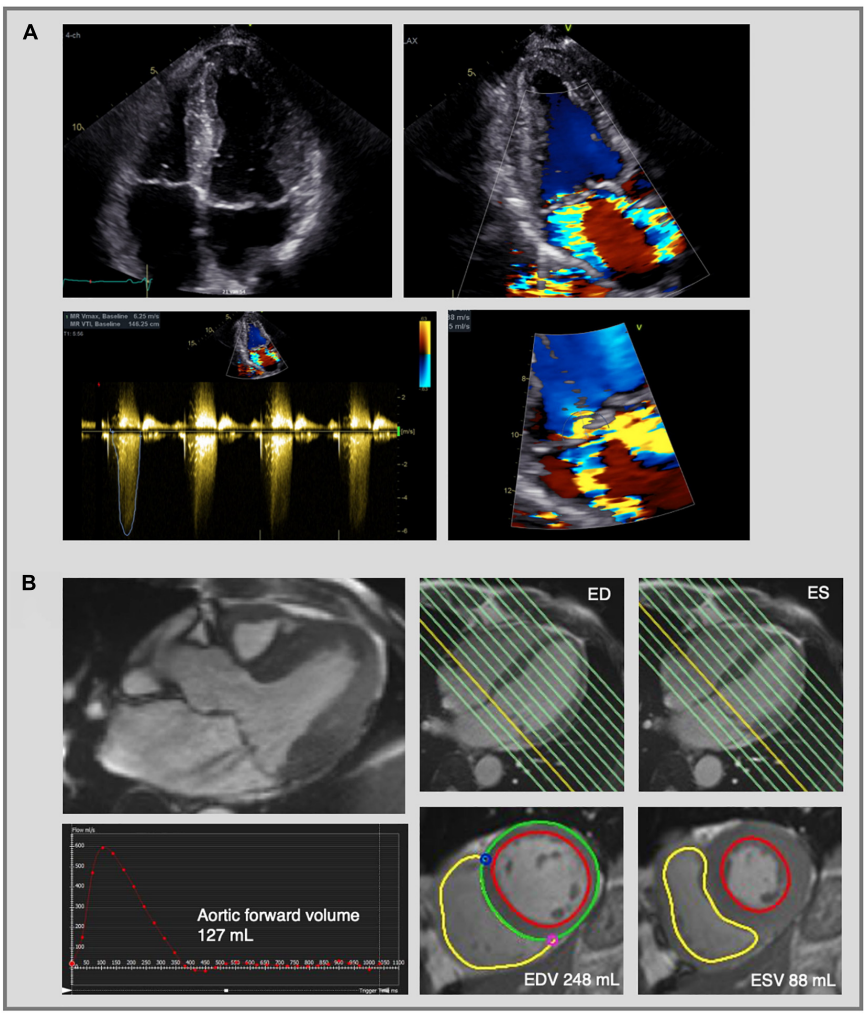

FIGURE 5 | Mitral regurgitation assessment by echocardiography and cardiac magnetic resonance imaging. Complex evaluation of moderate-severe mitral regurgitation (MR) with multiple jets in a patients with bileaflet mitral valve prolapse. **(A)** 2D transthoracic echocardiography using color flow Doppler shows two MR jets—an eccentric jet toward the intra-atrial septum and a jet toward the lateral wall. The PISA radius was measured at 8 mm, but given the multiple and eccentric jets, this parameter is not reliable to calculate the EROA and MR volume, which indicates the need for further evaluation using CMR. **(B)** CMR images of the same patient as in panel **(A)**. Three-chamber cine image shows the presence of MR with two jets (upper left image). MR volume was calculated at 33 mL using the indirect method based on the difference between LV stroke volume (EDV—ESV = 160 mL) and aortic forward volume (127 mL). The LV stroke volume was calculated from the short-axis cine images in end-diastole and end-systole (lower right images) and the aortic flow was calculated by phase-contrast imaging (lower left image). Traditionally the LV base is defined at the level of the mitral valve annulus (yellow line, upper right images) and therefore the calculated regurgitant volume includes both the transvalvular MR volume and the prolapse volume. MR, mitral regurgitation; PISA, proximal isovelocity surface area; EROA, effective regurgitant orifice area; CMR, cardiac magnetic resonance imaging; LV, left ventricle; ED, end-diastolic; ES, end-systolic; EDV, end-diastolic volume; ESV, end-systolic volume.

Moreover, CMR also allows direct quantification of MR by measuring the regurgitant flow over the mitral valve with phase-contrast imaging (101). Recently, four-dimensional (4D) flow CMR has emerged as an innovative imaging technique to quantitate MR based on a three-dimensional and time-resolved assessment of blood flow MR (102). Both in patients with primary MR and specifically in patients with MVP, quantification of mitral regurgitant volume has shown to be reproducible and feasible using 4D flow CMR (103, 104). However, this technique requires additional acquisition and post-processing time and future studies are needed to evaluate a potential clinical outcome benefit over the indirect 2D CMR technique (102).

In addition to transvalvular MR, the prolapse volume can represent a significant volume load and should be assessed in patients with MVP (12). The indirect CMR method to assess MR already incorporates the prolapse volume, therefore possibly overestimating MR severity in patients with severe bileaflet prolapse (26), while echocardiography and direct CMR methods only assess the transvalvular MR volume (**Figure 5**). Using CMR, the prolapse volume can be calculated from 4-, 3-, and 2-chamber views by measuring end-systolic mitral annulus diameter and prolapse area, as is shown in **Figure 2B** (26).

An important additional benefit of CMR in MVP, beyond accurate quantification of MR and LV volumes, is the ability

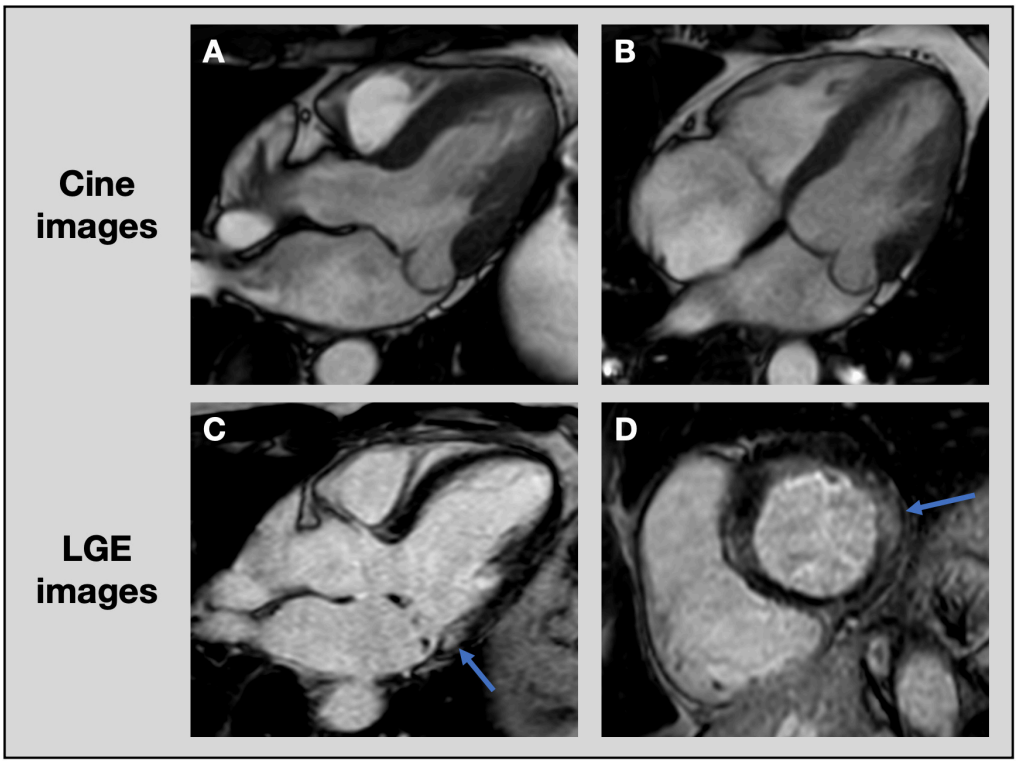

FIGURE 6 | Assessment of focal fibrosis with cardiac magnetic resonance imaging. CMR cine images of patient with posterior leaflet prolapse on 3-chamber **(A)** and 4-chamber **(B)** views. Late gadolinium enhancement images show evidence of focal fibrosis in the basal inferolateral wall (blue arrows) on 3-chamber **(C)** and short axis **(D)** views. CMR, cardiac magnetic resonance imaging; LGE, late gadolinium enhancement.

to detect focal or diffuse LV fibrosis. LGE CMR is the most accurate non-invasive technique to assess focal myocardial replacement fibrosis (**Figure 6**). Given the association of BD with ventricular arrhythmias and fibrosis, detection of LGE using CMR may improve risk stratification in these patients (13, 15, 61). In addition, T1 mapping can quantify diffuse interstitial fibrosis, demonstrated by an elevated native T1 time and extracellular volume expansion (105, 106). Although these CMR techniques are increasingly used in valvular heart disease and the extent of fibrosis is strongly associated with patient outcomes, there are currently no well-established cut-off values to refer patients for valve surgery (107).

FUTURE DIRECTIONS

Although prognosis can be benign in many patients with MVP, poor outcomes have been observed in relation to severe MR, heart failure and malignant ventricular arrhythmias (13, 58). In large cohorts of patients with primary MR, severe LV remodeling with an increase in LV dimensions and decrease in LVEF was correlated with worse prognosis, but no comparison was made between MVP and non-MVP (108–110). Moreover, outcome studies that compare patients with MVP with and without disproportionate LV remodeling are still lacking. In order to optimize treatment options and improve patient outcomes, further studies are needed to provide more insight into these different mechanisms of LV remodeling, such as severe volume overload or a genetic cardiomyopathy.

First, to assess LV remodeling related to volume overload, a careful quantification of LV volumes and MR severity is crucial, emphasizing the importance of accurate cardiac imaging techniques. An important question that still remains is the clinical and prognostic importance of the total volume load, including both MR volume and prolapse volume, especially in patients with BD. Although mitral valve repair or replacement would reduce both MR volume and prolapse volume, there are currently insufficient data to base surgical indications on total volume load instead of MR severity alone. Furthermore, optimal risk assessment and timing of mitral valve surgery is still debated in patients with MVP. Postoperative LV reverse remodeling has been observed to be less favorable in patients with LV dilatation and dysfunction prior to mitral valve surgery (81, 111). Therefore, some authors advocate for early intervention, in contrast with the current guidelines (112).

Second, if further studies confirm the hypothesis of a genetic cardiomyopathy in patients with MVP, it will be important to elucidate the genotype-phenotype relationship in order to refer patients for genetic counseling. In addition, this may provide the opportunity for familial screening, preclinical diagnosis and better follow-up.

Third, despite the established association of LGE on CMR with worse event-free survival in patients with MVP (14), the exact role of focal or diffuse LV fibrosis in the risk stratification for heart failure or malignant arrhythmias needs to be further explored. Since non-invasive detection of fibrosis is only possible using CMR, will this investigation be indicated for all patients with MVP in the future or primarily for those with the BD subtype or history of arrhythmias?

Finally, the presence of PVC's and arrythmias are a known risk factor for sudden cardiac death and LV remodeling in patients with MVP. Therefore, screening with Holter monitoring should be considered. The possible benefit from radiofrequency ablation in patients with MVP to reverse a PVC-induced cardiomyopathy and decrease the risk of malignant arrhythmias needs to be investigated further (59, 60, 113).

CONCLUSION

To conclude, severe LV dilatation and dysfunction are important markers of disease progression and may indicate worse prognosis and the need for mitral valve surgery in patients with MVP. An in-depth assessment of MR severity, LV volumes and function, and myocardial fibrosis by cardiac imaging techniques is crucial to determine patients at risk. In addition, insight in the potential mechanisms behind this process of LV remodeling is of great importance. While some interesting hypotheses have been proposed, it is currently still debated whether LV remodeling occurs only due to severe volume overload or whether an underlying cardiomyopathy may be the cause. At present, it is clear that many questions still remain unanswered and therefore large multicenter studies are needed to further elucidate mechanisms of LV remodeling, identify patients at risk and improve treatment and outcome in MVP.

AUTHOR CONTRIBUTIONS

LP, PB, and CV performed the data search and drafted the manuscript. BP, HH, and EV critically revised the draft. All authors contributed to the conceived of this work and approved the final version of the manuscript.

REFERENCES

1. Freed LA, Levy D, Levine RA, Larson MG, Evans JC, Fuller DL, et al. Prevalence and clinical outcome of mitral-valve prolapse. *N Engl J Med.* (1999) 341:1–7. doi: 10.1056/nejm199907013410101
2. van Wijngaarden AL, Kruithof BPT, Vinella T, Barge-Schaapveld D, Ajmone Marsan N. Characterization of degenerative mitral valve disease: differences between fibroelastic deficiency and Barlow's disease. *J Cardiovasc Dev Dis.* (2021) 8:23. doi: 10.3390/jcdd8020023
3. Le Tourneau T, Mérot J, Rimbert A, Le Scouarnec S, Probst V, Le Marec H, et al. Genetics of syndromic and non-syndromic mitral valve prolapse. *Heart.* (2018) 104:978–84. doi: 10.1136/heartjnl-2017-312420
4. Anyanwu AC, Adams DH. Etiologic classification of degenerative mitral valve disease: Barlow's disease and fibroelastic deficiency. *Semin Thorac Cardiovasc Surg.* (2007) 19:90–6. doi: 10.1053/j.semtcvs.2007.04.002
5. Delling FN, Vasan RS. Epidemiology and pathophysiology of mitral valve prolapse: new insights into disease progression, genetics, and molecular basis. *Circulation.* (2014) 129:2158–70. doi: 10.1161/CIRCULATIONAHA.113.006702
6. Hourdain J, Clavel MA, Deharo J-C, Asirvatham S, Avierinos JF, Habib G, et al. Common phenotype in patients with mitral valve prolapse who experienced sudden cardiac death. *Circulation.* (2018) 138:1067–9. doi: 10.1161/CIRCULATIONAHA.118.033488
7. Vahanian A, Beyersdorf F, Praz F, Milojevic M, Baldus S, Bauersachs J, et al. 2021 ESC/EACTS guidelines for the management of valvular heart disease: developed by the task force for the management of valvular heart disease of the European society of cardiology (ESC) and the European association for cardio-thoracic surgery (EACTS). *Eur Heart J.* (2021) 43:561–632. doi: 10.1093/eurheartj/ehab395
8. Otto CM, Nishimura RA, Bonow RO, Carabello BA, Erwin JP III, Gentile F, et al. 2020 ACC/AHA guideline for the management of patients with valvular heart disease: executive summary: a report of the American college of cardiology/American heart association joint committee on clinical practice guidelines. *Circulation.* (2021) 143:e35–71. doi: 10.1161/cir.0000000000000932
9. Malev E, Reeva S, Vasina L, Timofeev E, Pshepiy A, Korshunova A, et al. Cardiomyopathy in young adults with classic mitral valve prolapse. *Cardiol Young.* (2014) 24:694–701. doi: 10.1017/S1047951113001042
10. Yiginer O, Keser N, Ozmen N, Tokatli A, Kardesoglu E, Isilak Z, et al. Classic mitral valve prolapse causes enlargement in left ventricle even in the absence of significant mitral regurgitation. *Echocardiography.* (2012) 29:123–9. doi: 10.1111/j.1540-8175.2011.01544.x
11. Yang LT, Ahn SW, Li Z, Benfari G, Mankad R, Takeuchi M, et al. Mitral valve prolapse patients with less than moderate mitral regurgitation exhibit early cardiac chamber remodeling. *J Am Soc Echocardiogr.* (2020) 33:815–25e2. doi: 10.1016/j.echo.2020.01.016
12. El-Tallawi KC, Kitkungvan D, Xu J, Cristini V, Yang EY, Quinones MA, et al. Resolving the disproportionate left ventricular enlargement in mitral valve prolapse due to Barlow disease: insights from cardiovascular magnetic resonance. *JACC Cardiovasc Imaging.* (2020) 14:573–84. doi: 10.1016/j.jcmg.2020.08.029
13. Tayal B, Delling FN, Malahfji M, Shah DJ. Cardiac imaging for risk assessment of malignant ventricular arrhythmias in patients with mitral valve prolapse. *Front Cardiovasc Med.* (2021) 8:574446. doi: 10.3389/fcvm.2021.574446
14. Constant Dit Beaufils AL, Huttin O, Jobbe-Duval A, Senage T, Filippetti L, Piriou N, et al. Replacement myocardial fibrosis in patients with mitral valve prolapse: relation to mitral regurgitation, ventricular remodeling and arrhythmia. *Circulation.* (2021) 143:1763–74. doi: 10.1161/circulationaha.120.050214
15. Basso C, Perazzolo Marra M, Rizzo S, De Lazzari M, Giorgi B, Cipriani A, et al. Arrhythmic mitral valve prolapse and sudden cardiac death. *Circulation.* (2015) 132:556–66. doi: 10.1161/circulationaha.115.016291
16. van Wijngaarden AL, Hiemstra YL, Koopmann TT, Ruivenkamp CAL, Aten E, Schalij MJ, et al. Identification of known and unknown genes associated with mitral valve prolapse using an exome slice methodology. *J Med Genet.* (2020) 57:843–50. doi: 10.1136/jmedgenet-2019-106715
17. Freed LA, Acierno JS Jr., Dai D, Leyne M, Marshall JE, Nesta F, et al. A locus for autosomal dominant mitral valve prolapse on chromosome 11p15.4. *Am J Hum Genet.* (2003) 72:1551–9. doi: 10.1086/375452
18. Nesta F, Leyne M, Yosefy C, Simpson C, Dai D, Marshall JE, et al. New locus for autosomal dominant mitral valve prolapse on chromosome 13: clinical insights from genetic studies. *Circulation.* (2005) 112:2022–30. doi: 10.1161/CIRCULATIONAHA.104.516930
19. Disse S, Abergel E, Berrebi A, Houot AM, Le Heuzey JY, Diebold B, et al. Mapping of a first locus for autosomal dominant myxomatous mitral-valve prolapse to chromosome 16p11.2-p12.1. *Am J Hum Genet.* (1999) 65:1242–51. doi: 10.1086/302624
20. Dina C, Bouatia-Naji N, Tucker N, Delling FN, Toomer K, Durst R, et al. Genetic association analyses highlight biological pathways underlying mitral valve prolapse. *Nat Genet.* (2015) 47:1206–11. doi: 10.1038/ng.3383

21. Kyndt F, Gueffet J-P, Probst V, Jaafar P, Legendre A, Le Bouffant F, et al. Mutations in the gene encoding filamin A as a cause for familial cardiac valvular dystrophy. *Circulation.* (2007) 115:40–9. doi: 10.1161/CIRCULATIONAHA.106.622621
22. Lancellotti P, Tribouilloy C, Hagendorff A, Popescu BA, Edvardsen T, Pierard LA, et al. Recommendations for the echocardiographic assessment of native valvular regurgitation: an executive summary from the European association of cardiovascular imaging. *Eur Heart J Cardiovasc Imaging.* (2013) 14:611–44. doi: 10.1093/ehjci/jet105
23. Deferm S, Bertrand PB, Verbrugge FH, Verhaert D, Rega F, Thomas JD, et al. Atrial functional mitral regurgitation: JACC review topic of the week. *J Am Coll Cardiol.* (2019) 73:2465–76. doi: 10.1016/j.jacc.2019.02.061
24. Levine RA, Schwammenthal E. Ischemic mitral regurgitation on the threshold of a solution. *Circulation.* (2005) 112:745–58. doi: 10.1161/CIRCULATIONAHA.104.486720
25. O'Gara PT, Mack MJ. Secondary mitral regurgitation. *N Engl J Med.* (2020) 383:1458–67. doi: 10.1056/NEJMcp1903331
26. Vincenti G, Masci PG, Rutz T, De Blois J, Prsa M, Jeanrenaud X, et al. Impact of bileaflet mitral valve prolapse on quantification of mitral regurgitation with cardiac magnetic resonance: a single-center study. *J Cardiovasc Magn Reson.* (2017) 19:56. doi: 10.1186/s12968-017-0362-6
27. Levy F, Iacuzio L, Marechaux S, Civaia F, Dommerc C, Wautot F, et al. Influence of prolapse volume in mitral valve prolapse. *Am J Cardiol.* (2021) 157:64–70. doi: 10.1016/j.amjcard.2021.07.019
28. Luyten P, Heuts S, Cheriex E, Olsthoorn JR, Crijns HJGM, Winkens B, et al. Mitral prolapsing volume is associated with increased cardiac dimensions in patients with mitral annular disjunction. *Neth Heart J.* (2021) 30:131–9. doi: 10.1007/s12471-021-01575-6
29. Ryan TD, Rothstein EC, Aban I, Tallaj JA, Husain A, Lucchesi PA, et al. Left ventricular eccentric remodeling and matrix loss are mediated by bradykinin and precede cardiomyocyte elongation in rats with volume overload. *J Am Coll Cardiol.* (2007) 49:811–21. doi: 10.1016/j.jacc.2006.06.083
30. Zheng J, Chen Y, Pat B, Dell'italia LA, Tillson M, Dillon AR, et al. Microarray identifies extensive downregulation of noncollagen extracellular matrix and profibrotic growth factor genes in chronic isolated mitral regurgitation in the dog. *Circulation.* (2009) 119:2086–95. doi: 10.1161/circulationaha.108.826230
31. Hutchinson KR, Stewart JA Jr., Lucchesi PA. Extracellular matrix remodeling during the progression of volume overload-induced heart failure. *J Mol Cell Cardiol.* (2010) 48:564–9. doi: 10.1016/j.yjmcc.2009.06.001
32. Su X, Wei CC, Machida N, Bishop SP, Hankes GH, Dillon RA, et al. Differential expression of angiotensin-converting enzyme and chymase in dogs with chronic mitral regurgitation. *J Mol Cell Cardiol.* (1999) 31:1033–45. doi: 10.1006/jmcc.1999.0933
33. Stewart JA Jr., Wei CC, Brower GL, Rynders PE, Hankes GH, Dillon AR, et al. Cardiac mast cell- and chymase-mediated matrix metalloproteinase activity and left ventricular remodeling in mitral regurgitation in the dog. *J Mol Cell Cardiol.* (2003) 35:311–9. doi: 10.1016/s0022-2828(03)00013-0
34. Levick SP, Gardner JD, Holland M, Hauer-Jensen M, Janicki JS, Brower GL. Protection from adverse myocardial remodeling secondary to chronic volume overload in mast cell deficient rats. *J Mol Cell Cardiol.* (2008) 45:56–61. doi: 10.1016/j.yjmcc.2008.04.010
35. Chen Y, Pat B, Zheng J, Cain L, Powell P, Shi K, et al. Tumor necrosis factor-alpha produced in cardiomyocytes mediates a predominant myocardial inflammatory response to stretch in early volume overload. *J Mol Cell Cardiol.* (2010) 49:70–8. doi: 10.1016/j.yjmcc.2009.12.013
36. Zhang M, Liu X, Wu J, Yu Y, Wang Y, Gu Y. Impact of bilateral sympathetic stellate ganglionectomy on TGF-β1 signaling pathway in rats with chronic volume overload. *Front physiol.* (2020) 11:375. doi: 10.3389/fphys.2020.00375
37. Gulotta SJ, Gulco L, Padmanabhan V, Miller S. The syndrome of systolic click, murmur, and mitral valve prolapse-A cardiomyopathy? *Circulation.* (1974) 49:717–28. doi: 10.1161/01.CIR.49.4.717
38. Mason JW, Koch FH, Billingham ME, Winkle RA. Cardiac biopsy evidence for a cardiomyopathy associated with symptomatic mitral valve prolapse. *Am J Cardiol.* (1978) 42:557–62. doi: 10.1016/0002-9149(78)90623-9
39. Gooch AS, Vicencio F, Maranhao V, Goldberg H. Arrhythmias and left ventricular asynergy in the prolapsing mitral leaflet syndrome. *Am J Cardiol.* (1972) 29:611–20. doi: 10.1016/0002-9149(72)90161-0
40. Morningstar JE, Nieman A, Wang C, Beck T, Harvey A, Norris RA. Mitral valve prolapse and its motley crew-syndromic prevalence, pathophysiology, and progression of a common heart condition. *J Am Heart Assoc.* (2021) 10:e020919. doi: 10.1161/jaha.121.020919
41. Durst R, Sauls K, Peal DS, deVlaming A, Toomer K, Leyne M, et al. Mutations in DCHS1 cause mitral valve prolapse. *Nature.* (2015) 525:109–13. doi: 10.1038/nature14670
42. Toomer KA, Yu M, Fulmer D, Guo L, Moore KS, Moore R, et al. Primary cilia defects causing mitral valve prolapse. *Sci Transl Med.* (2019) 11:eaax0290. doi: 10.1126/scitranslmed.aax0290
43. Yu M, Georges A, Tucker NR, Kyryachenko S, Toomer K, Schott JJ, et al. Genome-wide association study-driven gene-set analyses, genetic, and functional follow-up suggest GLIS1 as a susceptibility gene for mitral valve prolapse. *Circ Genom Precis Med.* (2019) 12:e002497. doi: 10.1161/CIRCGEN.119.002497
44. Roselli C, Yu M, Nauffal V, Georges A, Yang Q, Love K, et al. Genome-wide association study reveals novel genetic loci: a new polygenic risk score for mitral valve prolapse. *Eur Heart J.* (2022). doi: 10.1093/eurheartj/ehac049
45. Verdonschot JAJ, Vanhoutte EK, Claes GRF, Helderman-van den Enden ATJM, Hoeijmakers JGJ, Hellebrekers DMEI, et al. A mutation update for the FLNC gene in myopathies and cardiomyopathies. *Hum Mutat.* (2020) 41:1091–111. doi: 10.1002/humu.24004
46. Herman DS, Lam L, Taylor MRG, Wang L, Teekakirikul P, Christodoulou D, et al. Truncations of titin causing dilated cardiomyopathy. *N Engl J Med.* (2012) 366:619–28. doi: 10.1056/NEJMoa1110186
47. Marstrand P, Picard K, Lakdawala NK. Second hits in dilated cardiomyopathy. *Curr Cardiol Rep.* (2020) 22:8. doi: 10.1007/s11886-020-1260-3
48. Ware JS, Li J, Mazaika E, Yasso CM, DeSouza T, Cappola TP, et al. Shared genetic predisposition in peripartum and dilated cardiomyopathies. *N Engl J Med.* (2016) 374:233–41. doi: 10.1056/NEJMoa1505517
49. Garcia-Pavia P, Kim Y, Restrepo-Cordoba MA, Lunde IG, Wakimoto H, Smith AM, et al. Genetic variants associated with cancer therapy-induced cardiomyopathy. *Circulation.* (2019) 140:31–41. doi: 10.1161/CIRCULATIONAHA.118.037934
50. Ware JS, Amor-Salamanca A, Tayal U, Govind R, Serrano I, Salazar-Mendiguchía J, et al. Genetic etiology for alcohol-induced cardiac toxicity. *J Am Coll Cardiol.* (2018) 71:2293–302. doi: 10.1016/j.jacc.2018.03.462
51. Morningstar JE, Gensemer C, Moore R, Fulmer D, Beck TC, Wang C, et al. Mitral valve prolapse induces regionalized myocardial fibrosis. *J Am Heart Assoc.* (2021) 10:e022332. doi: 10.1161/JAHA.121.022332
52. Huizar JF, Ellenbogen KA, Tan AY, Kaszala K. Arrhythmia-induced cardiomyopathy: JACC state-of-the-art review. *J Am Coll Cardiol.* (2019) 73:2328–44. doi: 10.1016/j.jacc.2019.02.045
53. Panizo JG, Barra S, Mellor G, Heck P, Agarwal S. Premature ventricular complex-induced cardiomyopathy. *Arrhythm Electrophysiol Rev.* (2018) 7:128–34. doi: 10.15420/aer.2018.23.2
54. Dukes JW, Dewland TA, Vittinghoff E, Mandyam MC, Heckbert SR, Siscovick DS, et al. Ventricular ectopy as a predictor of heart failure and death. *J Am Coll Cardiol.* (2015) 66:101–9. doi: 10.1016/j.jacc.2015.04.062
55. Cooper MW. Postextrasystolic potentiation: do we really know what it means and how to use it? *Circulation.* (1993) 88:2962–71. doi: 10.1161/01.CIR.88.6.2962
56. Ellis ER, Josephson ME. Heart failure and tachycardia-induced cardiomyopathy. *Curr Heart Fail Rep.* (2013) 10:296–306. doi: 10.1007/s11897-013-0150-z
57. Delgado V, Tops LF, Trines SA, Zeppenfeld K, Marsan NA, Bertini M, et al. Acute effects of right ventricular apical pacing on left ventricular synchrony and mechanics. *Circ Arrhythm Electrophysiol.* (2009) 2:135–45. doi: 10.1161/circep.108.814608
58. Essayagh B, Sabbag A, Antoine C, Benfari G, Yang LT, Maalouf J, et al. Presentation and outcome of arrhythmic mitral valve prolapse. *J Am Coll Cardiol.* (2020) 76:637–49. doi: 10.1016/j.jacc.2020.06.029
59. Enriquez A, Shirai Y, Huang J, Liang J, Briceno D, Hayashi T, et al. Papillary muscle ventricular arrhythmias in patients with arrhythmic mitral valve prolapse: electrophysiologic substrate and catheter ablation outcomes. *J cardiovasc Electrophysiol.* (2019) 30:827–35. doi: 10.1111/jce.13900

60. Lee A, Hamilton-Craig C, Denman R, Haqqani HM. Catheter ablation of papillary muscle arrhythmias: implications of mitral valve prolapse and systolic dysfunction. *Pacing Clin Electrophysiol.* (2018) 41:750–8. doi: 10.1111/pace.13363
61. Kitkungvan D, Nabi F, Kim RJ, Bonow RO, Khan MA, Xu J, et al. Myocardial fibrosis in patients with primary mitral regurgitation with and without prolapse. *J Am Coll Cardiol.* (2018) 72:823–34. doi: 10.1016/j.jacc.2018.06.048
62. Zia MI, Valenti V, Cherston C, Criscito M, Uretsky S, Wolff S. Relation of mitral valve prolapse to basal left ventricular hypertrophy as determined by cardiac magnetic resonance imaging. *Am J Cardiol.* (2012) 109:1321–5. doi: 10.1016/j.amjcard.2011.12.029
63. Fukuda S, Song JK, Mahara K, Kuwaki H, Jang JY, Takeuchi M, et al. Basal left ventricular dilatation and reduced contraction in patients with mitral valve prolapse can be Secondary to annular dilatation: preoperative and postoperative speckle-tracking echocardiographic study on left ventricle and mitral valve annulus interaction. *Circ Cardiovasc Imaging.* (2016) 9:e005113. doi: 10.1161/circimaging.115.005113
64. Huttin O, Pierre S, Venner C, Voilliot D, Sellal JM, Aliot E, et al. Interactions between mitral valve and left ventricle analysed by 2D speckle tracking in patients with mitral valve prolapse: one more piece to the puzzle. *Eur Heart J Cardiovasc Imaging.* (2017) 18:323–31. doi: 10.1093/ehjci/jew075
65. Castillo-Sang M, Palmer C, Truong VT, Young M, Wolking S, Alsaied T, et al. Abnormal ventricular contractile pattern associated with late systolic mitral prolapse: a two-dimensional speckle tracking study. *Int J Cardiovasc Imaging.* (2020) 36:2155–64. doi: 10.1007/s10554-020-01931-4
66. Gilbert BW, Schatz RA, VonRamm OT, Behar VS, Kisslo JA. Mitral valve prolapse. Two-dimensional echocardiographic and angiographic correlation. *Circulation.* (1976) 54:716–23. doi: 10.1161/01.cir.54.5.716
67. Perazzolo Marra M, Basso C, De Lazzari M, Rizzo S, Cipriani A, Giorgi B, et al. Morphofunctional abnormalities of mitral annulus and arrhythmic mitral valve prolapse. *Circ Cardiovasc Imaging.* (2016) 9:e005030. doi: 10.1161/CIRCIMAGING.116.005030
68. Moura-Ferreira S, Vandenberk B, Masci PG, Dresselaers T, Garweg C, Symons R, et al. Left ventricular remodelling in mitral valve prolapse patients: implications of apical papillary muscle insertion. *Eur Heart J Cardiovasc Imaging.* (2021) 22:1129. doi: 10.1093/ehjci/jeab134
69. Towbin JA. Ion channel dysfunction associated with arrhythmia, ventricular noncompaction, and mitral valve prolapse: a new overlapping phenotype. *J Am Coll Cardiol.* (2014) 64:768–71. doi: 10.1016/j.jacc.2014.06.1154
70. Chandraratna PA, Tolentino AO, Mutucumarana W, Gomez AL. Echocardiographic observations on the association between mitral valve prolapse and asymmetric septal hypertrophy. *Circulation.* (1977) 55:622–6. doi: 10.1161/01.CIR.55.4.622
71. Hjortnaes J, Keegan J, Bruneval P, Schwartz E, Schoen FJ, Carpentier A, et al. Comparative histopathological analysis of mitral valves in Barlow disease and fibroelastic deficiency. *Semin Thorac Cardiovasc Surg.* (2016) 28:757–67. doi: 10.1053/j.semtcvs.2016.08.015
72. Levine RA, Hagége AA, Judge DP, Padala M, Dal-Bianco JP, Aikawa E, et al. Mitral valve disease–morphology and mechanisms. *Nat Rev Cardiol.* (2015) 12:689–710. doi: 10.1038/nrcardio.2015.161
73. Hiemstra YL, Wijngaarden ALV, Bos MW, Schalij MJ, Klautz RJ, Bax JJ, et al. Familial occurrence of mitral regurgitation in patients with mitral valve prolapse undergoing mitral valve surgery. *Eur J Prevent cardiol.* (2019) 27:272–80. doi: 10.1177/2047487319874148
74. Han HC, Parsons SA, Teh AW, Sanders P, Neil C, Leong T, et al. Characteristic histopathological findings and cardiac arrest rhythm in isolated mitral valve prolapse and sudden cardiac death. *J Am Heart Assoc.* (2020) 9:e015587. doi: 10.1161/jaha.119.015587
75. Van De Heyning CM, Magne J, Pierard LA, Bruyere PJ, Davin L, De Maeyer C, et al. Late gadolinium enhancement CMR in primary mitral regurgitation. *Eur J Clin Invest.* (2014) 44:840–7. doi: 10.1111/eci.12306
76. Edwards NC, Moody WE, Yuan M, Weale P, Neal D, Townend JN, et al. Quantification of left ventricular interstitial fibrosis in asymptomatic chronic primary degenerative mitral regurgitation. *Circ Cardiovasc Imaging.* (2014) 7:946–53. doi: 10.1161/circimaging.114.002397
77. Bui AH, Roujol S, Foppa M, Kissinger KV, Goddu B, Hauser TH, et al. Diffuse myocardial fibrosis in patients with mitral valve prolapse and ventricular arrhythmia. *Heart.* (2017) 103:204–9. doi: 10.1136/heartjnl-2016-309303
78. Kitkungvan D, Yang EY, El Tallawi KC, Nagueh SF, Nabi F, Khan MA, et al. Extracellular volume in primary mitral regurgitation. *JACC Cardiovasc Imaging.* (2020) 14:1146–60. doi: 10.1016/j.jcmg.2020.10.010
79. Uretsky S, Gillam L, Lang R, Chaudhry FA, Argulian E, Supariwala A, et al. Discordance between echocardiography and MRI in the assessment of mitral regurgitation severity: a prospective multicenter trial. *J Am Coll Cardiol.* (2015) 65:1078–88. doi: 10.1016/j.jacc.2014.12.047
80. Uretsky S, Shah DJ, Lasam G, Horgan S, Debs D, Wolff SD. Usefulness of mitral regurgitant volume quantified using magnetic resonance imaging to predict left ventricular remodeling after mitral valve "correction". *Am J cardiol.* (2020) 125:1666–72. doi: 10.1016/j.amjcard.2020.02.045
81. Le Tourneau T, Topilsky Y, Inamo J, Mahoney DW, Suri R, Schaff HV, et al. Reverse left ventricular remodeling after surgery in primary mitral regurgitation: a volume-related phased process. *Struct Heart.* (2019) 3:383–90. doi: 10.1080/24748706.2019.1639870
82. Suri RM, Schaff HV, Dearani JA, Sundt TM, Daly RC, Mullany CJ, et al. Recovery of left ventricular function after surgical correction of mitral regurgitation caused by leaflet prolapse. *J Thorac Cardiovasc Surg.* (2009) 137:1071–6. doi: 10.1016/j.jtcvs.2008.10.026
83. Enriquez-Sarano M, Tajik AJ, Schaff HV, Orszulak TA, McGoon MD, Bailey KR, et al. Echocardiographic prediction of left ventricular function after correction of mitral regurgitation: results and clinical implications. *J Am Coll Cardiol.* (1994) 24:1536–43. doi: 10.1016/0735-1097(94)90151-1
84. Liu B, Neil DAH, Bhabra M, Patel R, Barker TA, Nikolaidis N, et al. Reverse myocardial remodeling following valve repair in patients with chronic severe primary degenerative mitral regurgitation. *JACC Cardiovasc imaging.* (2021) 15:224–36. doi: 10.1016/j.jcmg.2021.07.007
85. Sénéchal M, MacHaalany J, Bertrand OF, O'Connor K, Parenteau J, Dubois-Sénéchal IN, et al. Predictors of left ventricular remodeling after surgical repair or replacement for pure severe mitral regurgitation caused by leaflet prolapse. *Am J Cardiol.* (2013) 112:567–73. doi: 10.1016/j.amjcard.2013.04.024
86. Athanasopoulos LV, McGurk S, Khalpey Z, Rawn JD, Schmitto JD, Wollersheim LW, et al. Usefulness of preoperative cardiac dimensions to predict success of reverse cardiac remodeling in patients undergoing repair for mitral valve prolapse. *Am J Cardiol.* (2014) 113:1006–10. doi: 10.1016/j.amjcard.2013.12.009
87. Essayagh B, Mantovani F, Benfari G, Maalouf JF, Mankad S, Thapa P, et al. Mitral annular disjunction of degenerative mitral regurgitation: 3D evaluation and implications for mitral repair. *J Am Soc Echocardiogr.* (2021) 35:165–75. doi: 10.1016/j.echo.2021.09.004
88. Levine RA, Stathogiannis E, Newell JB, Harrigan P, Weyman AE. Reconsideration of echocardiographic standards for mitral valve prolapse: lack of association between leaflet displacement isolated to the apical four chamber view and independent echocardiographic evidence of abnormality. *J Am Coll Cardiol.* (1988) 11:1010–9. doi: 10.1016/s0735-1097(98)90059-6
89. Topilsky Y, Michelena H, Bichara V, Maalouf J, Mahoney DW, Enriquez-Sarano M. Mitral valve prolapse with mid-late systolic mitral regurgitation: pitfalls of evaluation and clinical outcome compared with holosystolic regurgitation. *Circulation.* (2012) 125:1643–51. doi: 10.1161/circulationaha.111.055111
90. Lancellotti P, Cosyns B, Zacharakis D, Attena E, Van Camp G, Gach O, et al. Importance of left ventricular longitudinal function and functional reserve in patients with degenerative mitral regurgitation: assessment by two-dimensional speckle tracking. *J Am Soc Echocardiogr.* (2008) 21:1331–6. doi: 10.1016/j.echo.2008.09.023
91. Mentias A, Naji P, Gillinov AM, Rodriguez LL, Reed G, Mihaljevic T, et al. Strain echocardiography and functional capacity in asymptomatic primary mitral regurgitation with preserved ejection fraction. *J Am Coll Cardiol.* (2016) 68:1974–86. doi: 10.1016/j.jacc.2016.08.030
92. Lang RM, Badano LP, Tsang W, Adams DH, Agricola E, Buck T, et al. EAE/ASE recommendations for image acquisition and display using three-dimensional echocardiography. *Eur Heart J Cardiovasc Imaging.* (2012) 13:1–46. doi: 10.1093/ehjci/jer316
93. Clavel MA, Mantovani F, Malouf J, Michelena HI, Vatury O, Jain MS, et al. Dynamic phenotypes of degenerative myxomatous mitral valve disease: quantitative 3-dimensional echocardiographic study. *Circ Cardiovasc Imaging.* (2015) 8:e002989. doi: 10.1161/CIRCIMAGING.114.002989

94. Zoghbi WA, Adams D, Bonow RO, Enriquez-Sarano M, Foster E, Grayburn PA, et al. Recommendations for noninvasive evaluation of native valvular regurgitation: a report from the american society of echocardiography developed in collaboration with the society for cardiovascular magnetic resonance. *J Am Soc Echocardiogr.* (2017) 30:303–71. doi: 10.1016/j.echo.2017.01.007
95. Van de Heyning CM, Magne J, Vrints CJ, Pierard L, Lancellotti P. The role of multi-imaging modality in primary mitral regurgitation. *Eur Heart J Cardiovasc Imaging.* (2012) 13:139–51. doi: 10.1093/ejechocard/jer257
96. Bellenger NG, Burgess MI, Ray SG, Lahiri A, Coats AJS, Cleland JGF, et al. Comparison of left ventricular ejection fraction and volumes in heart failure by echocardiography, radionuclide ventriculography and cardiovascular magnetic resonance. Are they interchangeable? *Eur Heart J.* (2000) 21:1387–96. doi: 10.1053/euhj.2000.2011
97. Grothues F, Smith GC, Moon JCC, Bellenger NG, Collins P, Klein HU, et al. Comparison of interstudy reproducibility of cardiovascular magnetic resonance with two-dimensional echocardiography in normal subjects and in patients with heart failure or left ventricular hypertrophy. *Am J Cardiol.* (2002) 90:29–34. doi: 10.1016/S0002-9149(02)02381-0
98. Myerson SG, Francis JM, Neubauer S. Direct and indirect quantification of mitral regurgitation with cardiovascular magnetic resonance, and the effect of heart rate variability. *MAGMA.* (2010) 23:243–9. doi: 10.1007/s10334-010-0222-y
99. Kramer CM, Barkhausen J, Bucciarelli-Ducci C, Flamm SD, Kim RJ, Nagel E. Standardized cardiovascular magnetic resonance imaging (CMR) protocols: 2020 update. *J Cardiovasc Magn Reson.* (2020) 22:17. doi: 10.1186/s12968-020-00607-1
100. Wolff R, Uretsky S. Defining the left ventricular base in mitral valve prolapse: impact on systolic function and regurgitation. *Int J Cardiovasc Imaging.* (2020) 36:2221–7. doi: 10.1007/s10554-020-01927-0
101. Uretsky S, Argulian E, Narula J, Wolff SD. Use of cardiac magnetic resonance imaging in assessing mitral regurgitation: current evidence. *J Am Coll Cardiol.* (2018) 71:547–63. doi: 10.1016/j.jacc.2017.12.009
102. Fidock B, Barker N, Balasubramanian N, Archer G, Fent G, Al-Mohammad A, et al. A systematic review of 4D-flow MRI derived mitral regurgitation quantification methods. *Front Cardiovasc Med.* (2019) 6:103. doi: 10.3389/fcvm.2019.00103
103. Spampinato RA, Jahnke C, Crelier G, Lindemann F, Fahr F, Czaja-Ziolkowska M, et al. Quantification of regurgitation in mitral valve prolapse with four-dimensional flow cardiovascular magnetic resonance. *J Cardiovasc Magn Reson.* (2021) 23:87. doi: 10.1186/s12968-021-00783-8
104. Fidock B, Archer G, Barker N, Elhawaz A, Al-Mohammad A, Rothman A, et al. Standard and emerging CMR methods for mitral regurgitation quantification. *Int J Cardiol.* (2021) 331:316–21. doi: 10.1016/j.ijcard.2021.01.066
105. Pradella S, Grazzini G, Brandani M, Calistri L, Nardi C, Mori F, et al. Cardiac magnetic resonance in patients with mitral valve prolapse: focus on late gadolinium enhancement and T1 mapping. *Eur Radiol.* (2019) 29:1546–54. doi: 10.1007/s00330-018-5634-5
106. Guglielmo M, Fusini L, Muscogiuri G, Baessato F, Loffreno A, Cavaliere A, et al. T1 mapping and cardiac magnetic resonance feature tracking in mitral valve prolapse. *Eur Radiol.* (2020) 31:1100–9. doi: 10.1007/s00330-020-07140-w
107. Bing R, Dweck MR. Myocardial fibrosis: why image, how to image and clinical implications. *Heart.* (2019) 105:1832–40. doi: 10.1136/heartjnl-2019-315560
108. Tribouilloy C, Grigioni F, Avierinos JF, Barbieri A, Rusinaru D, Szymanski C, et al. Survival implication of left ventricular end-systolic diameter in mitral regurgitation due to flail leaflets a long-term follow-up multicenter study. *J Am Coll Cardiol.* (2009) 54:1961–8. doi: 10.1016/j.jacc.2009.06.047
109. Grigioni F, Clavel MA, Vanoverschelde JL, Tribouilloy C, Pizarro R, Huebner M, et al. The MIDA mortality risk score: development and external validation of a prognostic model for early and late death in degenerative mitral regurgitation. *Eur Heart J.* (2018) 39:1281–91. doi: 10.1093/eurheartj/ehx465
110. Penicka M, Vecera J, Mirica DC, Kotrc M, Kockova R, Van Camp G. Prognostic implications of magnetic resonance-derived quantification in asymptomatic patients with organic mitral regurgitation: comparison with doppler echocardiography-derived integrative approach. *Circulation.* (2018) 137:1349–60. doi: 10.1161/CIRCULATIONAHA.117.029332
111. Shafii AE, Gillinov AM, Mihaljevic T, Stewart W, Batizy LH, Blackstone EH. Changes in left ventricular morphology and function after mitral valve surgery. *Am J Cardiol.* (2012) 110:403.e–8.e. doi: 10.1016/j.amjcard.2012.03.041
112. Suri RM, Aviernos JF, Dearani JA, Mahoney DW, Michelena HI, Schaff HV, et al. Management of less-than-severe mitral regurgitation: should guidelines recommend earlier surgical intervention? *Eur J Cardiothorac Surg.* (2011) 40:496–502. doi: 10.1016/j.ejcts.2010.11.068
113. Bumgarner JM, Patel D, Kumar A, Clevenger JR, Trulock KM, Popovic Z, et al. Management and outcomes in mitral valve prolapse with ventricular arrhythmias undergoing ablation and/or implantation of ICDs. *Pacing Clin Electrophysiol.* (2019) 42:447–52. doi: 10.1111/pace.13613
114. Biner S, Rafique A, Rafii F, Tolstrup K, Noorani O, Shiota T, et al. Reproducibility of proximal isovelocity surface area, vena contracta, and regurgitant jet area for assessment of mitral regurgitation severity. *JACC Cardiovasc Imaging.* (2010) 3:235–43. doi: 10.1016/j.jcmg.2009.09.029
115. Thomas N, Unsworth B, Ferenczi EA, Davies JE, Mayet J, Francis DP. Intraobserver variability in grading severity of repeated identical cases of mitral regurgitation. *Am Heart J.* (2008) 156:1089–94. doi: 10.1016/j.ahj.2008.07.017
116. Lopez-Mattei JC, Ibrahim H, Shaikh KA, Little SH, Shah DJ, Maragiannis D, et al. Comparative assessment of mitral regurgitation severity by transthoracic echocardiography and cardiac magnetic resonance using an integrative and quantitative approach. *Am J Cardiol.* (2016) 117:264–70. doi: 10.1016/j.amjcard.2015.10.045
117. Cawley PJ, Hamilton-Craig C, Owens DS, Krieger EV, Strugnell WE, Mitsumori L, et al. Prospective comparison of valve regurgitation quantitation by cardiac magnetic resonance imaging and transthoracic echocardiography. *Circ Cardiovasc Imaging.* (2013) 6:48–57. doi: 10.1161/circimaging.112.975623
118. Myerson SG, d'Arcy J, Christiansen JP, Dobson LE, Mohiaddin R, Francis JM, et al. Determination of clinical outcome in mitral regurgitation with cardiovascular magnetic resonance quantification. *Circulation.* (2016) 133:2287–96. doi: 10.1161/CIRCULATIONAHA.115.017888
119. Van De Heyning CM, Magne J, Piérard LA, Bruyère P-J, Davin L, De Maeyer C, et al. Assessment of left ventricular volumes and primary mitral regurgitation severity by 2D echocardiography and cardiovascular magnetic resonance. *Cardiovasc Ultrasound.* (2013) 11:46. doi: 10.1186/1476-7120-11-46
120. Bastos MB, Burkhoff D, Maly J, Daemen J, den Uil CA, Ameloot K, et al. Invasive left ventricle pressure–volume analysis: overview and practical clinical implications. *Eur Heart J.* (2019) 41:1286–97. doi: 10.1093/eurheartj/ehz552

Conflict of Interest: The authors declare that the research was conducted in the absence of any commercial or financial relationships that could be construed as a potential conflict of interest.

frontiers | Frontiers in Cardiovascular Medicine

TYPE Original Research
PUBLISHED 22 July 2022
DOI 10.3389/fcvm.2022.925777

OPEN ACCESS

EDITED BY
Michel Puceat,
Institut National de la Santé et de la Recherche Médicale (INSERM), France

REVIEWED BY
Ileana Manduteanu,
Institute of Cellular Biology and Pathology (ICBP), Romania
Gretchen Mahler,
Binghamton University, United States

*CORRESPONDENCE
Abhijeet R. Sonawane
asonawane@bwh.harvard.edu
Elena Aikawa
eaikawa@bwh.harvard.edu

†These authors have contributed equally to this work

SPECIALTY SECTION
This article was submitted to Heart Valve Disease, a section of the journal Frontiers in Cardiovascular Medicine

RECEIVED 21 April 2022
ACCEPTED 28 June 2022
PUBLISHED 22 July 2022

CITATION
Atkins SK, Sonawane AR, Brouwhuis R, Barrientos J, Ha A, Rogers M, Tanaka T, Okui T, Kuraoka S, Singh SA, Aikawa M and Aikawa E (2022) Induced pluripotent stem cell-derived smooth muscle cells to study cardiovascular calcification.
Front. Cardiovasc. Med. 9:925777.
doi: 10.3389/fcvm.2022.925777

Induced pluripotent stem cell-derived smooth muscle cells to study cardiovascular calcification

Samantha K. Atkins[1†], Abhijeet R. Sonawane[1,2*†], Romi Brouwhuis[1], Johana Barrientos[1], Anna Ha[1], Maximillian Rogers[1], Takeshi Tanaka[1], Takehito Okui[1], Shiori Kuraoka[1], Sasha A. Singh[1], Masanori Aikawa[1,2] and Elena Aikawa[1,2*]

[1]Center for Interdisciplinary Cardiovascular Sciences, Division of Cardiovascular Medicine, Brigham and Women's Hospital, Harvard Medical School, Boston, MA, United States, [2]Center for Excellence in Vascular Biology, Department of Medicine, Brigham and Women's Hospital, Harvard Medical School, Boston, MA, United States

Cardiovascular calcification is the lead predictor of cardiovascular events and the top cause of morbidity and mortality worldwide. To date, only invasive surgical options are available to treat cardiovascular calcification despite the growing understanding of underlying pathological mechanisms. Key players in vascular calcification are vascular smooth muscle cells (SMCs), which transform into calcifying SMCs and secrete mineralizing extracellular vesicles that form microcalcifications, subsequently increasing plaque instability and consequential plaque rupture. There is an increasing, practical need for a large scale and inexhaustible source of functional SMCs. Here we describe an induced pluripotent stem cell (iPSC)-derived model of SMCs by differentiating iPSCs toward SMCs to study the pathogenesis of vascular calcification. Specifically, we characterize the proteome during iPSC differentiation to better understand the cellular dynamics during this process. First, we differentiated human iPSCs toward an induced-SMC (iSMC) phenotype in a 10-day protocol. The success of iSMC differentiation was demonstrated through morphological analysis, immunofluorescent staining, flow cytometry, and proteomics characterization. Proteomics was performed throughout the entire differentiation time course to provide a robust, well-defined starting and ending cell population. Proteomics data verified iPSC differentiation to iSMCs, and functional enrichment of proteins on different days showed the key pathways changing during iSMC development. Proteomics comparison with primary human SMCs showed a high correlation with iSMCs. After iSMC differentiation, we initiated calcification in the iSMCs by culturing the cells in osteogenic media for 17 days. Calcification was verified using Alizarin Red S staining and proteomics data analysis. This study presents

an inexhaustible source of functional vascular SMCs and calcifying vascular SMCs to create an *in vitro* model of vascular calcification in osteogenic conditions, with high potential for future applications in cardiovascular calcification research.

KEYWORDS

calcification, cardiovascular diseases, induced pluripotent stem cells, smooth muscle cells (SMCs), proteomics and bioinformatics, stem cell differentiation and reprogramming

Introduction

Cardiovascular calcification is the lead predictor of adverse cardiovascular events, which has become the top cause of morbidity and mortality worldwide (1–3). Despite the increasing understanding of the underlying pathological mechanisms, to date there are no available pharmacological treatments to slow or stop the calcification process (4). Key players in vascular calcification are vascular smooth muscle cells (SMCs). In addition, immune cells, including macrophages, have been recently described to play a role (5–7). SMCs transform into calcifying SMCs and secrete mineralizing extracellular vesicles that form microcalcifications, subsequently increasing plaque instability and consequential plaque rupture (8, 9). Vascular disease susceptibility is hypothesized to be dependent on SMC germ layer origin, with vascular SMCs originating from all three germ layers. SMCs that contribute to calcification are thought to originate from the lateral plate mesoderm germ layer (10). On top of heterogeneity in origin, vascular SMCs also show heterogeneity in phenotype, and show phenotype plasticity as a response to environmental cues (11).

Experimental models for unraveling calcification mechanisms include human tissue samples, cell culture and animal models. The large biological differences between species, together with the limited proliferative capacity and donor to donor variability of primary SMCs in culture, make data analysis and statistical comparisons incredibly challenging (12). Primary human SMCs, like many other primary cell types, are limited by their capacity to withstand multiple passages *in vitro* and display passage-dependent expression of SMC marker proteins (13, 14). There is a significant need for large-scale, reproducible lines of SMCs to study disease mechanisms and offer potential non-invasive, therapeutic solutions. This unmet research need necessitates the development of a standardized source of human SMCs for two important reasons: (1) to create a human tissue model for studying the pathological mechanisms underlying vascular calcification; and (2) to subsequently discover novel therapeutic targets for treatment of vascular calcification. One approach to resolve the issues with passage-dependency and limited proliferative capacity in primary human cell lines is to generate such a disease model is by using human iPSCs for *in vitro* studies and screening. iPSCs can be used to create an alternative source of cell lines for disease modeling, tissue engineering, and drug screening. In this paper, we present a method to create iPSC-derived induced SMCs (iSMCs) that can calcify under osteogenic conditions to represent the disease model of atherosclerosis. In addition, we carefully defined the proteome at every stage throughout the differentiation timeline. Most previous studies of iPSC-derived SMCs have poorly defined starting cell populations with a range of phenotypically diverse iSMC end products (15). In this model, we have adapted the approach by Patsch et al., to create an inexhaustible line of iSMCs (16). We have characterized the population throughout the differentiation timeline using systems biology approaches, and we have gone a step further to recapitulate SMC calcification *in vitro*.

Materials and methods

Cell culture

Human induced pluripotent stem cells (iPSCs) derived from foreskin fibroblasts of one single donor (BJiPSCs, ATCC) were used in this study. iPSCs were cultured in mTeSR™ Plus medium (StemCell Technologies), enriched with 1% antibiotic-antimycotic (Anti-Anti, Gibco), on plates coated with Matrigel matrix (50–100 μg/ml) (Fisher Scientific). iPSCs were passaged at 70–80% confluency using ReLeSR™ (StemCell Technologies) and replated as aggregates at a dilution of 1:20. At the initial thaw, before culturing in mTeSR™ Plus medium, cells were cultured on Matrigel-coated plates in mTeSR™ Plus medium enriched with 10 μM ROCK inhibitor Y-27632 (StemCell Technologies) for 24 h. iPSCs were stored at −180°C as aggregates using mFreSR™ (StemCell Technologies), or as single cells using FreSR-S (StemCell Technologies). Each experiment was carried out in triplicate.

For flow cytometry and proteomic comparison of our iSMCs to primary SMCs, human coronary artery smooth muscle cells (hCASMCs, Promocell, three donors) were cultured in SMC

Growth Medium 2 (Promocell) supplemented with epidermal growth factor (0.5 ng/ml), insulin (5 μg/ml), basic fibroblast growth factor-B (2 ng/ml), 10% fetal bovine serum and 1% penicillin-streptomycin (P/S). For flow cytometry analysis, human umbilical vein cells (HUVECS, Lonza, one donor) were used as a negative control. HUVECs were cultured in EBM-2 Basal medium, enriched with EGM-2 supplements (Lonza) and 1% P/S. All primary cells were passaged using 0.25% Trypsin-EDTA (ATCC) and counted using Countess II (Life Technologies).

Study design and sample replicates

Induced pluripotent stem cell differentiation was carried out in three independent experiments ($n = 3$) using one single donor (BJiPSCs, ATCC) due to limited availability of commercially available donors from ATCC. For comparison to primary hCASMCs under normal and osteogenic conditions, three separate donors ($N = 3$) obtained from Promocell were used.

Induced pluripotent stem cell-induced-smooth muscle cell differentiation

For differentiation, a protocol was set up based on a previous study that reported successful differentiation of iPSCs to iSMCs (16). Three differentiations were performed on iPSCs between passages 6 and 9 from one single donor. On day 0 iPSCs were cultured as described above (see section "Cell Culture") in mTeSR™ Plus, on Matrigel-coated plates. Upon passaging, iPSCs were plated on Matrigel coated plates at a density of 40,000 cells/cm^2 in mTeSR™ Plus, enriched with 10 μM ROCK inhibitor Y27632. From here on N2B27 medium was used for culturing the cells. N2B27 consists of DMEM/F12 with 15 mM Hepes (StemCell Technologies) and Neurobasal medium (Life Technologies) at a ratio of 1:1, supplemented with 2% B27 minus vitamin A (Life Technologies), 1% N2 supplement (Life Technologies), 1% antibiotic-antimycotic solution and 0.1% β-mercaptoethanol (Life Technologies). Twenty-four hours after the iPSCs were plated, the cells were cultured in mesoderm induction media, consisting of N2B27, enriched with 8 μM CHIR99021 (StemCell Technologies) and 2.5 ng/ml BMP4 (Peprotech). The lower amount of BMP4 was the only modification to the original protocol by Patsch et al. Mesoderm induction was carried out for 3 days with no media change. At day 3 the media was replaced with SMC inducing media, containing N2B27 supplemented with 10 ng/ml PDGF-BB (Peprotech) and 2 ng/ml ActivinA (Peprotech). On day 5, the cells were removed with trypsin-EDTA (0.25%, ATCC), washed in N2B27 media and pelleted by centrifugation (150 × gravity, 5 min). To induce SMC maturation, the cells were resuspended in N2B27 media enriched with 2 μg/ml heparin (StemCell Technologies) and 2 ng/ml ActivinA (Peprotech) and plated on collagen coated wells (Corning Biocoat) at a density of 30,000 cells/cm^2. The cells were cultured with regular media changes until day 10, at which the differentiation media was replaced with SMC Growth Media 2 (SMGM2) (Promocell). Further expansion and culturing of the cells was done in SMGM2. An in-depth protocol can be found in **Supplementary Material 1**.

Osteogenic differentiation of induced-smooth muscle cells into calcifying induced-smooth muscle cells

Osteogenic differentiation of iSMCs was carried out three times ($n = 3$, 1 donor). For the osteogenic differentiation of iSMCs into calcifying (c)-iSMCs, the iSMCs were plated on 24-well plates at a density of 100,000 cells/well in SMGM2. After 24 h, calcification was induced by culturing the cells in osteogenic medium (OM), containing GlutaMAX™ DMEM, 10% FBS and 1% penicillin-streptomycin (termed normal media, NM), with addition of osteogenic factors; 10 mM dexamethasone (Fisher Scientific), 10 mM β-glycerol phosphate (Millipore Sigma) and 100 μM L-ascorbic acid 2-phosphate (Millipore Sigma). Media was refreshed every 3 days.

Immunocytochemistry

Cells were fixed in 4% paraformaldehyde (Sigma-Aldrich) for 10 min, followed by a 5-min permeabilization step with 100% methanol, washed twice with PBS for 5 min per wash. Next, the cells were blocked with 0.1% Tween (Sigma-Aldrich) and 10% normal donkey serum blocking solution (Sigma-Aldrich) in PBS at room temperature. Cells were incubated overnight at 4°C with primary antibodies; dilution of 1:100 rabbit anti-αSMA (Abcam #ab5694), 1:100 rabbit anti-Nanog (Abcam #ab21624), and 1:250 mouse anti-smMHC11 (Abcam #ab683). The cells were then incubated for 1 h at room temperature with secondary antibodies donkey anti-mouse 488 (Thermo Fisher Scientific #a21202) and donkey anti-rabbit 594 (Thermo Fisher Scientific #A21207) at 1:200 dilution. After rinsing, cells were incubated with a drop of NucBlue Fixed Cell Ready Probes Reagent (Thermo Fisher Scientific #R37606) in PBS for 5 min. Cells were stored at 4°C in the dark. Examination was done using the confocal microscope A1 (Nikon Instruments Inc), and all images were processed with Elements 3.20 software (Nikon Instruments Inc).

Flow cytometry

For flow cytometry sample preparation, the cell samples were harvested and collected in EasySep buffer (StemCell Technologies) at a concentration of 10 × 10^6 cells/ml. The samples were incubated for 20 min in the dark on ice with antibodies Alexa fluor 647 mouse anti-human TRA-1-60 (BD Biosciences), FITC mouse anti-human TRA-1-81 (BD Biosciences), PE mouse anti-human CD140b (BD Biosciences), and APC-Cy7 mouse anti-human CD31 (BD Biosciences). Next, the cell samples were diluted ten times in EasySep buffer, and centrifuged [350 × *g* × 5 min]. Supernatant was removed and the dilution step was repeated. After supernatant was removed, the cell samples were resuspended in EasySep buffer at a concentration of 3.33 × 10^6 cells/ml and filtered through a round-bottom tube with cell strainer (Falcon). The stained cell samples were analyzed using the BD FACSAria^{TM}IIu machine and the accompanied BD FACSDiva software. Acquisition of 10,000 events was made, and data analysis was performed after gating for single cell population minus cell debris.

Proteomics sample preparation

Approximately 1 × 10^6 cells from a 6-well plate were collected in 400 μl of RIPA lysis buffer with protease inhibitor cocktail (Thermo Fisher Scientific) according to the manufacturer's protocol. There are two datasets. Dataset 1 consists of the iPSCs differentiated into iSMCs (n = 3, 1 donor, time points: day 0, day 3, day 5, day 7, day 10) and a Matrigel negative control "Mgel"; **Supplementary Material 2 (Table 1)**. Dataset 2 consists of the iSMCs cultured in NM and OM collected at days 10 and 17 (n = 3, 1 donor, time points: day 10 and day 17) as well as SMCs in NM and OM from day 14 in culture (3 donors, time point: day 14); **Supplementary Material 3 (Table 2)**. The sampling time points for dataset 1 during iPSC to iSMC differentiation correspond with the specific induction protocols. Day 0 represents naïve iPSCs; day 3 represents lateral mesoderm; day 5 represents the start of SMC induction; day 7 represents a midpoint for iSMC purification; day 10 represents the endpoint for iSMC differentiation. Dataset 2 timespoints are consistent with when calcification is present as indicated by Alizarin Red staining; days 10 and 17 for iSMCs and day 14 for primary human coronary artery SMCs.

The protein content was determined by the Pierce BCA assay (Thermo Fisher Scientific). A volume equivalent to 20 μg of protein was used for further processing. Next, the samples were prepared using iST Sample Preparation Kit (PreOmics, Germany) according to the protocol provided by manufacturer, without sonication and with a 90 min incubation at 37°C. The samples processed by the iST kit were resuspended in 40 μl of LC-LOAD (PreOmics).

Mass spectrometry

Data-dependent acquisitions (DDAs, unbiased peptide sampling)–the peptides were and analyzed using the Orbitrap Fusion Lumos Tribrid mass spectrometer (Thermo Fisher Scientific) fronted with an EasySpray ion source, and coupled to an Easy-nLC1000 HPLC pump (Thermo Fisher Scientific). The peptides were separated using a dual column set-up: an Acclaim PepMap 100 C18 trap column, 75 μm × 20 mm; and a PepMap RSLC C18 EASY-Spray LC heated (45°C) column, 75 μm × 250 mm (Thermo Fisher Scientific). The gradient flow rate was 300 nl/min from 5 to 21% solvent B (acetonitrile/0.1% formic acid) for 75 min, 21 to 30 % Solvent B for 15 min, followed by 10 min of a "jigsaw wash," alternating between 5 and 95 % Solvent B. Solvent A was 0.1% formic acid. The instrument was set to 120 K resolution, and the top N precursor ions in a 3 s cycle time (within a scan range of 375–1,500 m/z; isolation window, 1.6 m/z; ion trap scan rate, normal) were subjected to collision induced dissociation (collision energy 30%) for peptide sequencing (or MS/MS). Dynamic exclusion was enabled (60 s).

Mass spectrometry/mass spectrometry data analysis

The MS/MS spectra were queried against the human (downloaded on November 21, 2018; 155,133 entries) using the HT-SEQUEST search algorithm, *via* the Proteome Discoverer (PD) Package (version 2.2, Thermo Fisher Scientific). Methionine oxidation and n-terminal acetylation were set as a variable modifications, and carbamidomethylation of cysteine was set as a fixed modification. Peptides were filtered based on a 1% false discovery rate (FDR) (17) based on the reverse database (decoy) results (18, 19). In order to quantify peptide precursors detected in the MS1 but not sequenced from sample to sample (across mass spectrometric samples in **Supplementary Material 2 (Table 1)**), we enabled the "Feature Mapper" node. Chromatographic alignment was done with a maximum retention time (RT) shift of 10 min and a mass tolerance of 10 ppm. Feature linking and mapping settings were, RT tolerance minimum of 0 min, mass tolerance of 10 ppm and signal-to-noise minimum of five. Precursor peptide abundances were based on their chromatographic intensities and total peptide amount was used for normalization. Peptides assigned to a given protein group, and not present in any other protein group, were considered as unique. Consequently, each protein group is represented by a single master protein (PD Grouping feature). We used unique and razor peptides per protein for quantification.

Proteomics dataset processing

In house scripts written in Python v3.4 (20) were used to replace missing values with zero values and to perform per-sample median normalization on master protein (more than 2 unique peptides) intensities as quantified by PD. Dataset 1 (**Supplementary Material 2 (Table 1)**) was used to analyze the differentiation time course. Dataset 2 (**Supplementary Material 2 (Table 2)**) compares the protein expression from iSMCs in NM and OM at two time points (day 10 and day 17; 1 donor, $n = 3$) to primary human coronary artery SMCs in NM and OM (day 14; 3 donors).

High dimensional clustering of protein abundances

Analysis of proteome abundance patterns over the 10 day differentiation time course was performed using a high-dimensional clustering software, XINA[1] (21). The median-normalized abundance of proteins for three independent differentiation experiments ($n = 3$, 1 donor) were combined into a single dataset for subsequent clustering analysis by time point. Clusters differentiating peak protein abundance per time point (days 0, 3, 5, 7, and 10) were prioritized. The top ten most abundant shared proteins per time point were normalized by the daily expression and plotted with labels indicating the most enriched gene ontological terms.

Day-specific proteomics analysis

The proteomics data were used to obtain the mean abundance values for each protein for days 0, 3, 5, 7 and 10 separately (**Supplementary Figure 1**). To obtain the day-specific proteins, we compared the mean abundance level $\langle p \rangle_j^d$ of a protein j and at day d to the mean $\langle p \rangle^{all}$ and standard deviation σ of all the p^{all} on all days:

$$Zscore\ Abundance\ p_j^d = \frac{(\langle p \rangle_j^d - \langle p \rangle^{all})}{\sigma}.$$

We define a protein as specific to day d if the z-score abundance is $p_j^d > 1.5$. The threshold 1.5 was chosen such that there is a balance between number of proteins specific to at least one day (**Supplementary Figures 1B,C**). This definition allowed us to utilize the full distribution of protein abundance values. The list of proteins specific to each day is given in **Supplementary Material 2 (Table 3)**.

To investigate the functional enrichment of day-specific proteins, we acquired Gene Ontology (GO) terms for each group of proteins using R (v 4.0.3) package clusterProfiler (v 3.18) (22) with adjusted p-value < 0.05 (Benjamini-Hochberg) and used AnnotationDbi R package "org.Hs.eg.db" (v 3.12) to map gene identifiers.

To perform differential abundance analysis on the proteomics data between adjacent days, we used limma (3.46) package in R (v 4.0.3) with voom transformation to remove mean variance dependence and Benjamini-Hochberg for adjusted p-value. The volcano plots were plotted using R package EnhancedVolcano (v 1.8) with adjusted p-value $<$ 10e-5 and abs(logFC) > 1 shown in color.

Alizarin red staining for smooth muscle cell calcification

Cells were stained with Alizarin Red S (Sigma Aldrich) to analyze calcium deposition. Cells were washed with PBS before being fixed with 10% formalin solution for 10 min. Afterward the cells were washed three times with distilled water. Pictures were taken using a scanner (Ricoh Aficio MP 3500) at 300 dpi.

Statistical analyses

Data was statistically analyzed using t-test or ANOVA with *post-hoc* tests using GraphPad PRISM or Qlucore Omics Explorer. ImageJ, Adobe Photoshop and Adobe Illustrator were used to process and present the images and graphs, and to create the figures. Pearson correlation was computed using cor() function in R.

Results

Induced pluripotent stem cells undergo dynamic morphological changes while transitioning to induced-smooth muscle cells

Induced pluripotent stem cells were induced into mesoderm and then SMCs. Arteries arise from the lateral plate mesoderm germ layer, and this germ layer is hypothesized to be the origin of SMCs near areas of calcification (10). To achieve a population of iSMCs capable of recapitulating the calcification process, the iPSCs were transitioned into mesoderm from day 0 to day 3, before beginning SMC differentiation. The differentiation timeline (**Figure 1A**) to induce the iPSCs into a mesoderm germ layer, and then conditioned the cells with combinations of PDGF-BB, activin A, and heparin to induce the iSMC phenotype (16). Brightfield microscopy at 20 × resolution on days: −1, 0, 3, 5, 7, and 10 demonstrate the morphological changes that take place over the differentiation time course (**Figure 1B**). The cells begin as iPSC colonies with defined

1 https://bioconductor.org/packages/release/bioc/html/XINA.html

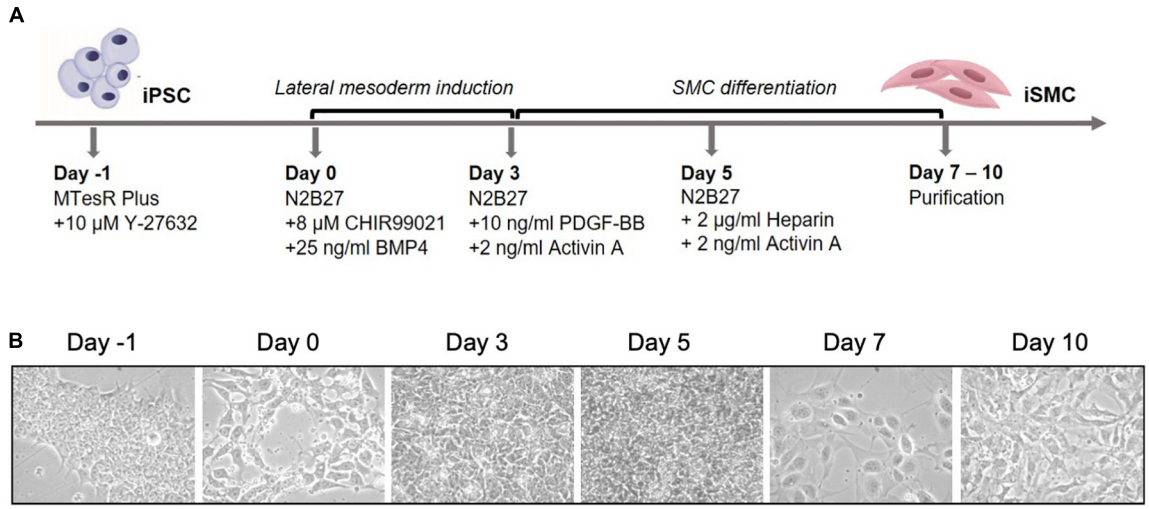

FIGURE 1
Differentiation timeline of iPSCs into iSMCs. **(A)** Schematic of the differentiation timeline and protocol. **(B)** Brightfield microscopy images of the differentiation time course from iPSCs to mesoderm and then to iSMCs (magnification = 20×). Representative images of $n = 3$ differentiation replicates.

edges (day −1) that were replated as single cells with ROCK inhibitor, and at day 0 showed the presence of small colonies with the absence of smooth and defined colony edges, typical of iPSCs treated with ROCK inhibitor (Y-27632). Over the 10-day differentiation time course, the cell morphology underwent dynamic changes that result in a stretched SMC phenotype by day 10 (**Figure 1B**).

Differentiation protocol yields high efficiency of induced-smooth muscle cells by flow cytometry

We then assessed iPSCs for the correct morphology and the expression of pluripotency markers using immunofluorescence and flow cytometry. The immunofluorescent analysis showed the iPSCs had compact colonies with well-defined edges and expressed the pluripotency marker NANOG (**Figure 2A**). Flow cytometry for pluripotency markers TRA-1-60 and TRA-1-81 indicated a 62% pluripotent cell population (**Figure 2B**). Immunofluorescent staining on day 10 for SMC markers alpha smooth muscle actin (αSMA) and myosin heavy chain 11 (MYH11) showed the clear presence of these markers (**Figure 2C**). Flow cytometry of the iSMCs at day 10 showed 96% (± 3.1%) positive for SMC membrane marker protein CD140b (PDGFRB) (**Figure 2D**). Endothelial cells (ECs) are a potential byproduct of this particular differentiation protocol (16), and the EC marker CD31 was used to verify the absence of these cells. As a negative control, flow cytometry analysis of iSMCs for EC marker CD31 and pluripotency markers TRA-1-60 plus TRA-1-81 showed low percentage (4.47 and 8% positive cells, respectively), indicative of a pure population of iSMCs (**Figure 2D**).

Induced-smooth muscle cells immunofluorescence shows OCT4 expression throughout differentiation and appearance of smooth muscle cell markers at days 7 and 10

Immunofluorescent staining performed at days 0, 3, 5, 7, and 10 on iPSC markers (**Figure 3A**) and SMC markers (**Figure 3B**) during the differentiation time course demonstrated that cells lose NANOG expression while maintaining OCT4 in the perinuclear and cytosolic regions of the iSMCs. At days 7 and 10 these cells showed strong expression of SMC markers such as αSMA and MYH11 and displayed a spindle-shape morphology, characteristic of SMCs. This may explain why the flow cytometry analysis after differentiation showed a population of cells that are positive for both pluripotency marker (TRA-1-60+TRA-1-81) and SMC marker (CD140b), as some pluripotency expression remained at day 10.

Induced pluripotent stem cell to induced-smooth muscle cell differentiation was confirmed by proteomics

A comprehensive characterization of the differentiation of iPSCs into iSMCs has not been done prior to this study.

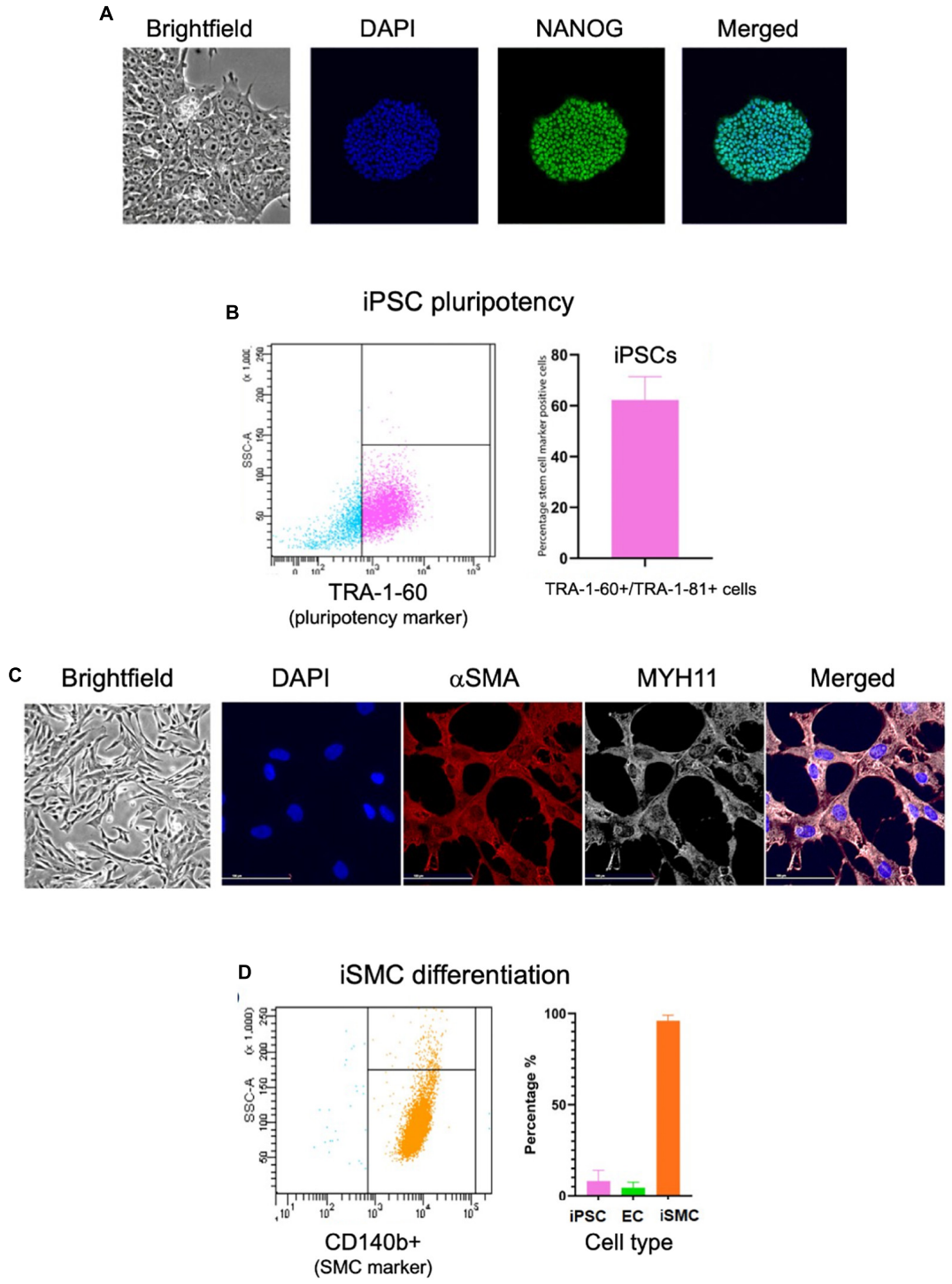

FIGURE 2
Characterization of iPSCs at day 0 and iSMCs at day 10. **(A)** Brightfield microscopy image (20× magnification) of iPSC colony morphology, and immunofluorescent staining (20× magnification) for DAPI (blue), pluripotency marker NANOG (green), and merged. **(B)** Flow cytometry analysis on iPSC pluripotency marker TRA-1-60; left side (blue dots) representative flow cytometry analysis, right side (pink dots) flow cytometry detected percentage of stem cell marker positive cells. **(C)** Brightfield microscopy of iSMCs at day 10. Immunofluorescent staining for DAPI (blue), αSMA (red), MYH11 (white) and merged. **(D)** Flow cytometry analysis on iPSC marker TRA-1-60, EC marker CD31, and iSMC marker CD140b; left side representative flow cytometry analysis, right side flow cytometry detected percentage of stem cell marker, EC marker, and SMC marker. n = 3 differentiation replicates; mean ± SEM; scale bars = 100 μm (20× magnification).

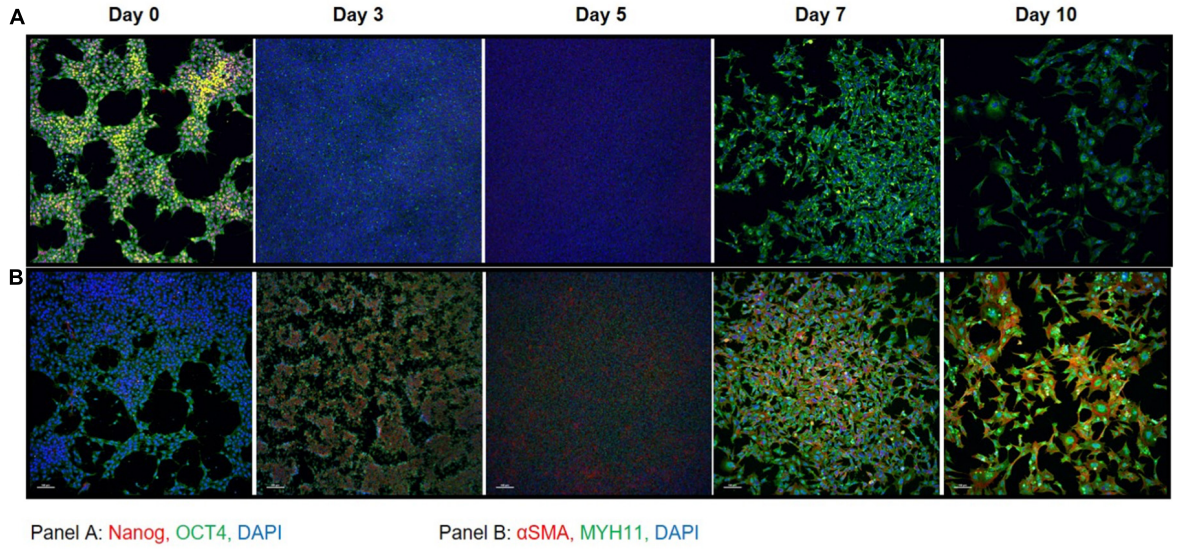

FIGURE 3
Immunocytochemistry on iPSC markers and SMC markers during differentiation. **(A)** iPSC markers NANOG (red) and OCT4 (green) with DAPI (blue) shows that OCT4 expression is maintained throughout the differentiation time course. **(B)** SMC markers αSMA (red) and MYH11 (green) with DAPI (blue) shows that by day 7 the cells express high levels of SMC marker proteins that persists through day 10. A total of 10× magnification, scale bars = 100 μm; representative images.

Previously, only prototypical markers of SMCs have been verified by Western blot at the end of the differentiation time course, but in this study, proteomics has allowed us to delve deeper into the molecular profiles throughout the differentiation process. To better understand the molecular changes along the differentiation trajectory, we collected proteomics data at five time points: Days 0, 3, 5, 7, and 10 (n = 3 differentiation replicates). First, we analyzed the data using a high-dimensional clustering tool XINA (21) to identify temporal patterns in protein expression/abundance using k-means clustering of the combined replicate data, resulting in 20 clusters (**Figure 4A**). Since this high-dimensional clustering method combined the three independent replicates, we could also confirm that each replicate exhibited similar time-resolved protein patterns since each cluster contains approximately same number of proteins from each replicate (**Figure 4B**).

A network of proteins co-expressed at the same time point is referred to as protein co-abundance and can be used to identify proteins that work together to perform a specific process or function (21). We identified clusters of co-abundant proteins at each stage of differentiation, namely, day 0 cluster number 14; day 3 cluster number 3; day 5 cluster number 20; day 7 cluster number 5, and day 10 cluster number 10 (**Figure 4C**). Day 0 notable proteins included POU5F, PODXL, and PROM1 and the top GO terms included tissue development and morphogenesis. Day 3 top GO terms indicated primitive streak formation, regulation of mesoderm development, and many other embryonic processes. Day 5 indicated fibronectin type domains. By day 7 GO terms indicated actin filament network formation, and day 10 showed collagen fibril organization, cell migration involved in sprouting angiogenesis, and muscle tissue morphogenesis, providing further evidence for successful differentiation into iSMCs.

Induced pluripotent stem cell to smooth muscle cell differentiation is marked by a metabolic to a cell morphogenesis pathway transition

Previous analysis using XINA showed general biological processes active at various days using selected protein clusters. To leverage the broad proteomics data and to look deeper into specific biological processes during the differentiation, we identified day-specific proteins using z-scored abundance (see section "Materials and Methods"). Using the differences in sample mean and global mean for all the proteins, we identified proteins with increased abundance on a particular day (**Figure 5**). For example, on day 0 we saw around 400 proteins with increased abundance such as PROM1, VSNL1, CDH1, SOX2, and POU5F1, involved in NADP metabolic and alpha-amino acid biosynthetic processes (**Figure 5A**). PROM1 modulates Rho/ROCK (23), CDH1 (E-cadherin) is required for iPSC pluripotency and self-renewal (24), and SOX2 and POU5F1 further confirmed pluripotency in our starting cell population (25). On Day 3, we found proteins MEST, VIM, and DDAH1, indicative of mesoderm formation (**Figure 5B**).

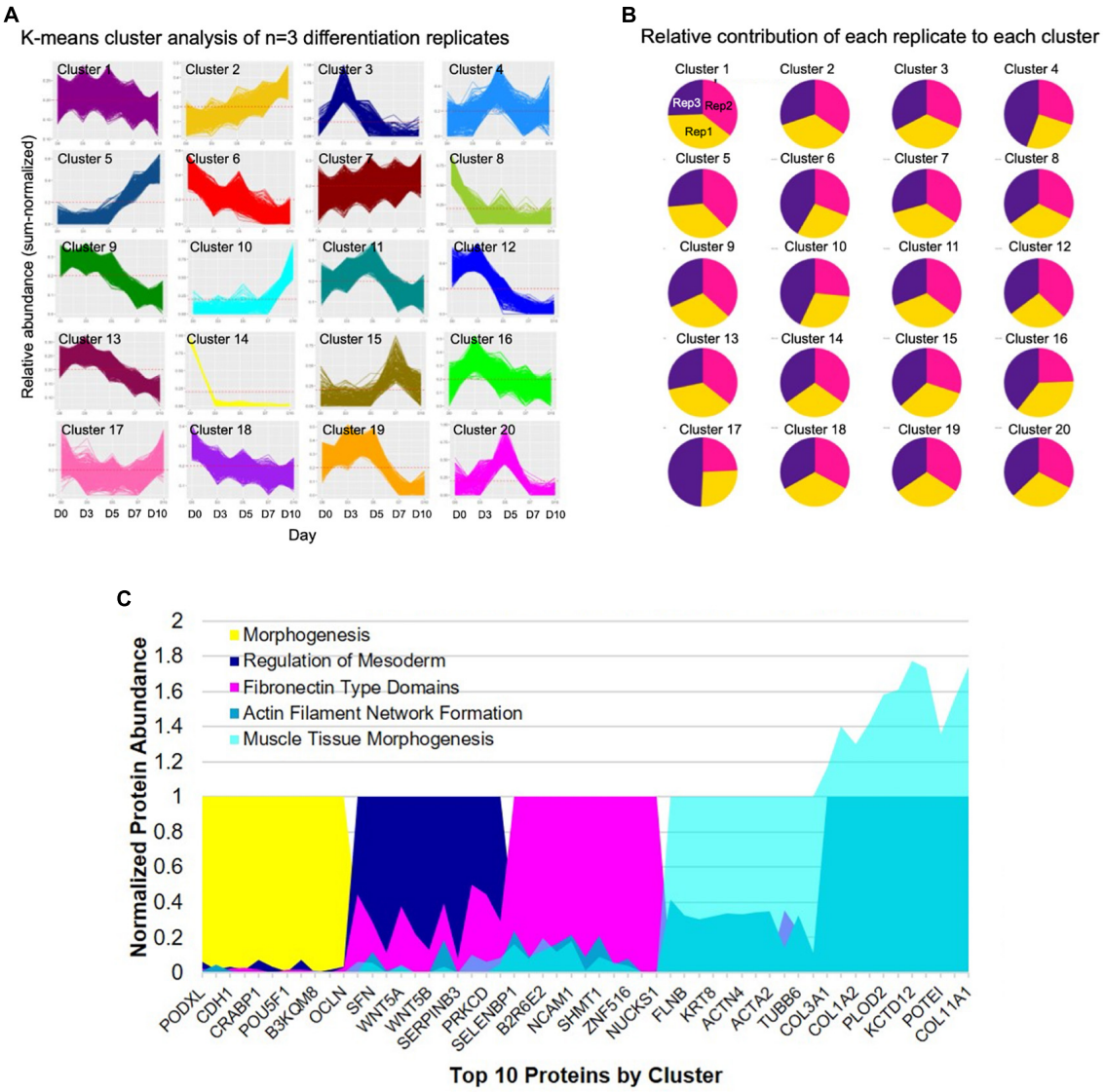

FIGURE 4
High-dimensional cluster analysis of the proteome describing the iPSC to iSMC transition. **(A)** K-means clustering analysis with 20 clusters describing the combined time-resolved protein abundances of n = 3 differentiation replicates. **(B)** Condition composition of the clusters shows equal distribution of each differentiation replicate in each cluster: yellow = replicate 1, pink = replicate 2, purple = replicate 3. **(C)** Expression of top 10 shared proteins between experimental replicates at each time point (day 0 = cluster 14; day 3 = cluster 3; day 5 = cluster 20; day 7 = cluster 5; day 10 = cluster 10) normalized by time point. String analysis on the shared proteins of each cluster was used to analyze GO terms.

MEST is known as the mesoderm-specific transcript, a negative regulator of adipogenesis (26). Vimentin upregulation is representative of mesoderm formation (27), and DDAH1 belongs to the mesoderm commitment pathway (28). The GO enrichment of 144 day 3 proteins included pathways involving RNA processing, developmental induction, ribosome biogenesis and primary lysosome.

After day 3, the cells were changed to SMC inducing media, and we saw proteins involved in chromatin remodeling, nucleosome assembly, nBAF and SWI/SNF complex (29) and establishment of spindle localization (**Figure 5C**). The first 5 days demonstrate the large switch in signaling that accompanies iPSC differentiation into iSMCs. On day 7, keratins 2 and 10 expression lead to functional enrichment of skin epidermis pathways, keratin filament pathway, mitochondrion localization, and intermediate filament cytoskeleton indicating structural formation (**Figure 5D**). Finally, proteins abundant at day 10 showed a robust SMC enrichment network, with pathways for actin filament organization, blood coagulation, cell morphogenesis, cell-substrate adhesion, and extracellular matrix organization that accompany successful iSMC differentiation (**Figure 5E**).

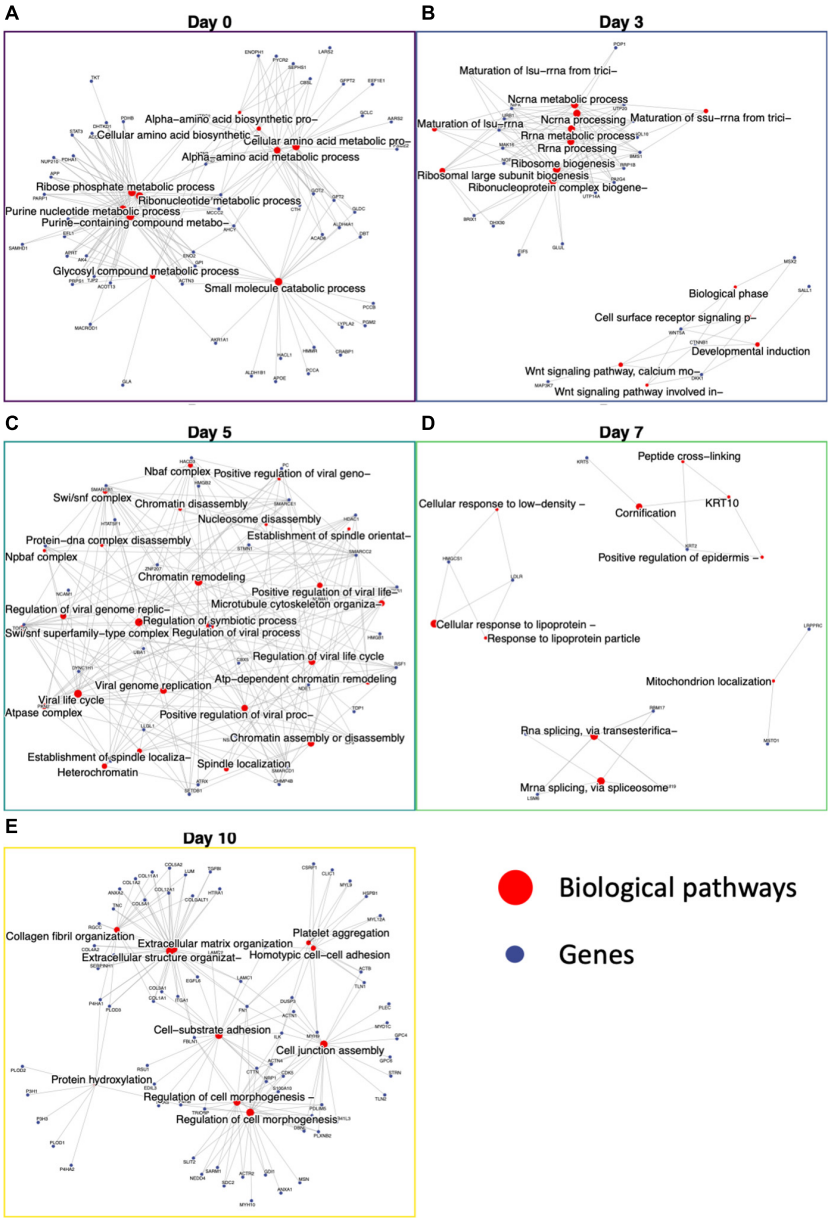

FIGURE 5
Functional enrichment of day-specific proteins accurately maps differentiation trajectory. Proteins were identified as day-specific with increase z-score abundance and function enrichment analysis was performed showing biological processes active on each day: Day 0, Day 3, Day 5, Day 7, and Day 10. **(A)** Day 0 major nodes include ribose phosphate and ribonucleotide metabolic processes. **(B)** Day 3 major nodes include RNA processing and Wnt signaling. **(C)** Day 5 nodes include chromatin assembly, disassembly, and remodeling. **(D)** Day 7 nodes include cornification and mitochondrion localization. **(E)** Day 10 nodes include extracellular matrix organization, regulation of cell morphogenesis, cell junction assembly, and cell-substrate adhesion.

Comparing proteomics from adjacent days to find activated and deactivated processes

The day specific proteins showed protein abundances on particular days with respect to overall data. To probe the activation and deactivation of processes through-out the differentiation cycle, we performed differential abundance analysis between consecutive days. The volcano plots showed significantly enriched (adjusted p-value < 0.05 and abs(logFC) > 1) proteins between samples from adjacent days as well as end points (day 0 and day 10). Day 0 vs. day 3 (Figure 6A), we saw proteins PODXL, EZR, and DNMT3B indicative of the formation of apical actin-dependent microvilli

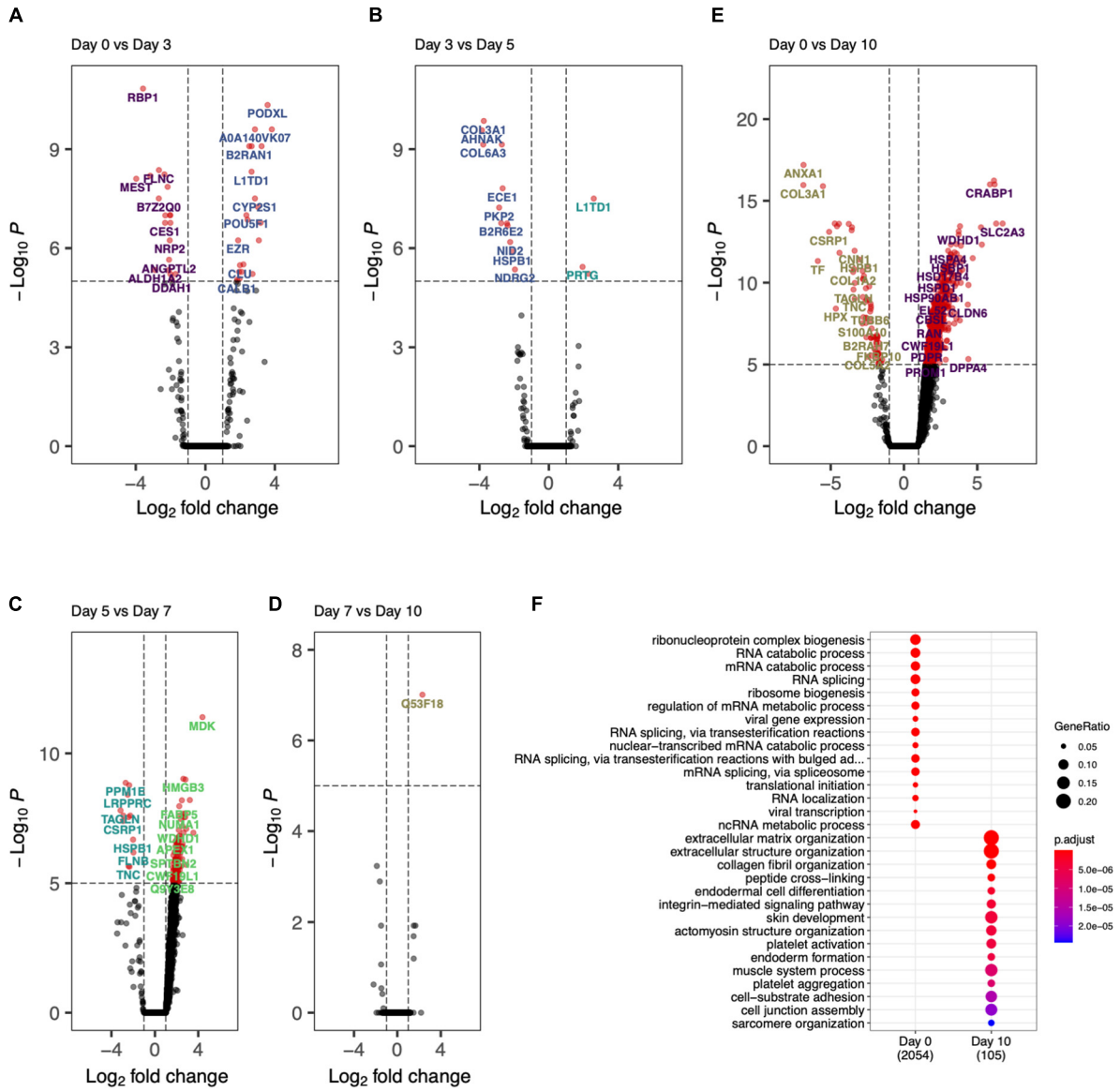

FIGURE 6
Day-to-day differential protein abundance analysis. Volcano plots of increased of previous day (shown on right with positive log fold change) vs. adjacent day (shown on left with -negative log fold change). **(A)** Day 0 vs. Day 3, **(B)** Day 3 vs. Day 5, **(C)** Day 5 vs. Day 7, **(D)** Day 7 vs. Day 10, **(E)** Day 0 vs. Day 10. **(F)** Bar chart showing the functional enriched processes on Day 0 and Day 10.

and the establishment of DNA methylation patterns during development. Comparison of day 3 with day 0 and day 5 show significant enrichment in proteins VIM, MEST, COL6A1, L1TD1, and PRTG indicating processes like intermediate filament product, mesoderm-specific transcription, and fibronectin domains (Figure 6A). Protein enrichment at day 5, (Figure 6B) showed enhancement in collagens III and VI as well as MDK, SELENBP1, APEX1, ENPP1, and HEL-S-310. GO terms associated with these proteins include phosphodiesterase I activity and protein-containing complex binding. Interestingly, protein MDK is implicated in neointima formation after arterial injuries (30), and ENPP1 is required for SMC calcification (31). Differentially expressed proteins at day 7 (Figure 6C) included SMC marker proteins TAGLN and CNN1, as well as ANXA1, which is required for SMC calcification (7). The GO terms associated with these significantly enriched proteins include cellular response to vascular endothelial growth factor stimulus and positive regulation of blood vessel endothelial cell migration. There was one significantly enriched protein at day 7 as compared to day 10, which is unannotated protein Q53F18, a WH1 domain-containing family involved in

actin polymerization[2] (**Figure 6D**). This unannotated protein could represent a potential undiscovered SMC-specific protein required for differentiation.

Finally, by comparing day 0 to day 10 (**Figures 6E,F**) there was a clear decrease in stem cell marker proteins (DPPA4) and transcriptional regulation and elongation proteins (ENO2, DUT, PHF6, TCEA1). By looking at the proteins differentially abundant at day 10, SMC marker proteins COL1A1, ANXA1, CNN1, and ACTB implicated regulation and modulation of smooth muscle contraction. This analysis showed the cell differentiation protocol not only recapitulates robust iSMCs but also sheds light on trajectory of cellular evolution, which can potentially be used in modulating the protocol to evolve different SMC subtypes.

Induced pluripotent stem cell-derived induced-smooth muscle cells show potential to calcify and have a high proteomic overlap with primary smooth muscle cells

The derived iSMCs were cultured in NM and OM to investigate the potential to calcify. Each of the three differentiations replicates were carried out to days 10 and 17, to ensure calcification under OM. iSMCs treated with OM showed high amounts of calcium deposits after 10 days, and Alizarin Red S staining for calcium deposition was used to measure calcification at day 17. This is represented by bright red color in iSMCs in OM (calcified; c-iSMCs), while iSMCs in NM remain unstained (**Figure 7A**).

The mean protein expression levels for both endpoints (days 10 and 17) in iSMCs were compared to primary SMCs cultured for 14 days in NM and OM. Representative images of Alizarin Red S staining for calcium deposition of SMCs in both media are shown as well (**Figure 7B**).

Induced-smooth muscle cells have a relatively higher expression of vimentin under both NM and OM conditions than primary SMCs. Inclusion of the protein vimentin in the correlation analysis had little effect on the Pearson's correlation of iSMCs and primary SMCs cultured in NM. Pearson's correlation values in NM were 0.788 and 0.764 with and without the inclusion of vimentin, respectively (**Figure 7C**). However, inclusion of vimentin had a much greater effect on the Pearson's correlation values under OM conditions. The Pearson's correlation between iSMCs and primary SMCs in OM was 0.561 when vimentin was included; however, the exclusion of vimentin caused a Pearson correlation of 0.88 in OM conditions (**Figure 7D**). When deciding if iSMCs should be cultured in NM or OM for prolonged time periods (17 days vs. 10 days), we show that the Pearson's correlation at Day 17 is much higher in both NM and OM as compared to Day 10, indicating higher proteomic overlap with primary cells with longer culture duration (**Figure 7E**). To conclude, iPSC-derived SMCs can be used as a high-fidelity model of primary SMCs.

Discussion

Intimal calcification is a common outcome of atherosclerosis. It is characterized by the formation of macro- and microcalcifications within the plaque, where microcalcifications contribute to plaque instability. A key cell type in the pathogenesis of atherosclerosis is SMCs, through the secretion of mineralizing EVs that accumulate and form microcalcifications (5, 8, 32–35). Primary SMCs have major limitations that complicate *in vitro* studies, by showing high passage dependency, low proliferation rate and high donor to donor variability (14). To overcome these limitations, iPSC-technology has proven to be a critical alternative, as iPSCs can be grown in large quantities due to their unlimited proliferation potential and ability to differentiate into any desired cell type. This study presented a model for studying SMC contributions in vascular calcification by differentiating iPSCs toward a calcifying SMC phenotype, as seen in vascular calcification.

The protocol for differentiation of iPSC toward iSMC through a lateral plate mesoderm intermediate was based on a previous study from Patsch et al. (16). The protocol was adapted to our cell line; for mesoderm induction BMP4 protein concentration was 10% of their protocol due cell death at higher concentrations. Immunofluorescent staining and flow cytometry analysis of pluripotency markers showed consistency in iPSC pluripotency, with high NANOG and OCT4 expression by immunocytochemistry and positive flow cytometry on markers TRA-1-60 and TRA-1-81.

A limitation of this study is the restriction to one iPS cell line. iPSC lines from different donors, and even clones from the same cell line, have been reported to vary in differentiation potential and efficiency (36, 37). This study utilized iPSC lines derived from foreskin fibroblasts, and thus the iSMCs were male-derived. Female vascular SMCs have been shown to have lower contractility, which could be due to gender-related differences in the expression of estrogen receptors (38). Therefore, the SMCs used for comparison were chosen from male donors to eliminate any confounding differences in the proteome that may be related to sex hormone signaling. For future studies, it is important to test our methods on more iPSC lines to ensure that additional donor cell lines could produce the same results.

The iPSCs were differentiated successfully toward an SMC phenotype within 10 days, showing clear SMC morphology and expression of SMC markers αSMA and MYH11. Flow cytometry analysis showed an efficiency of SMC differentiation

2 https://www.uniprot.org/uniprot/Q53F18

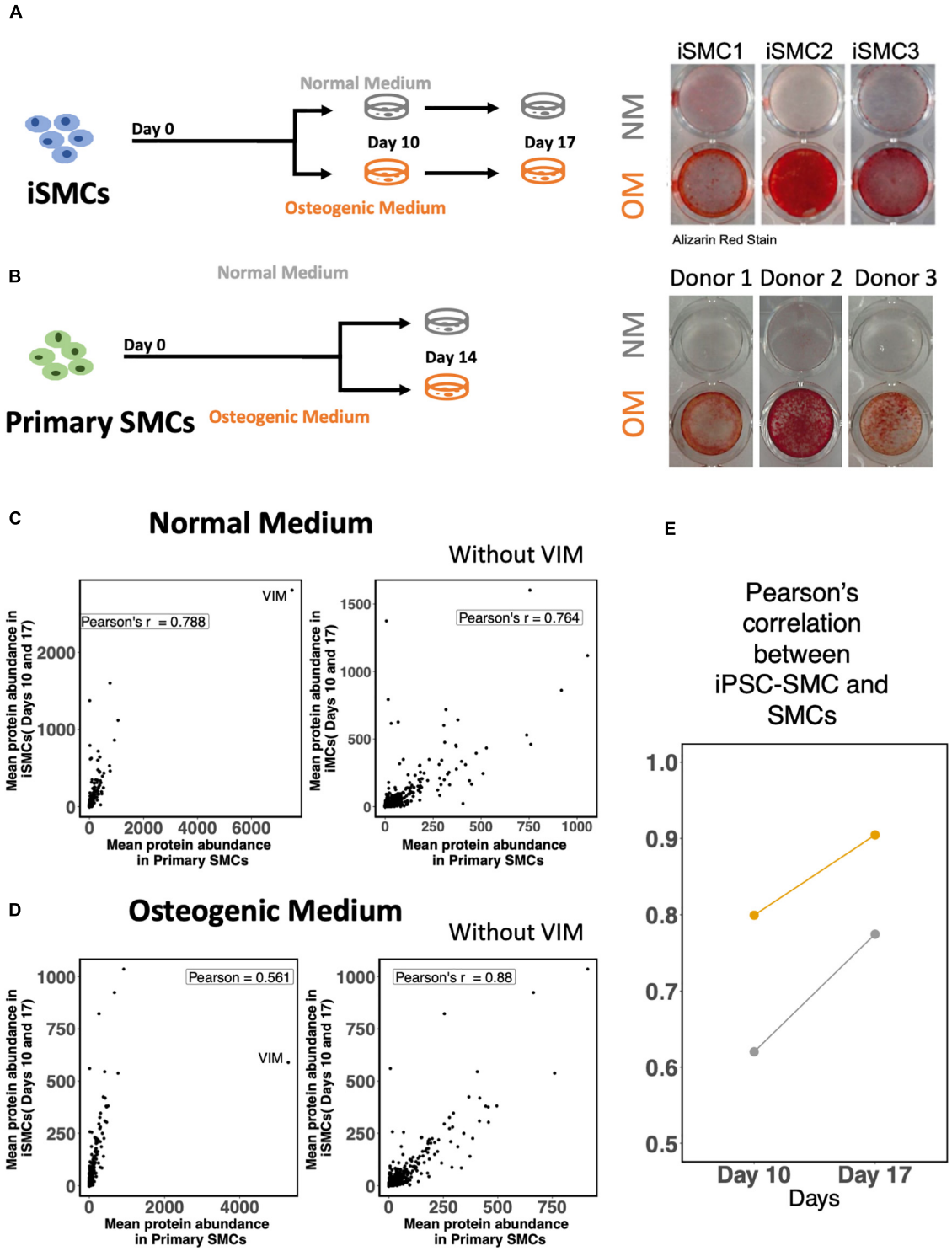

FIGURE 7
Induced-smooth muscle cells (iSMCs) calcify under osteogenic media (OM) conditions. **(A)** Study design and Alizarin Red S staining on iSMCs cultured in normal media (NM) and osteogenic media (OM) during three independent differentiations on Days 10 and 17. Bright red staining under OM conditions represents calcification in OM while no staining is observed in NM indicative of no calcification. **(B)** Study design and representative images of Alizarin Red S staining on primary SMCs cultured in normal media (NM) and osteogenic media (OM). **(C)** Pearson's correlation between mean protein abundance between iSMCs and primary SMCs cultured with and without the inclusion of the protein vimentin in the analyses under NM. **(D)** Similar plot under OM. **(E)** Pearson correlations of iSMCs with primary SMCs, without the inclusion of the protein vimentin at days 10 and 17 in NM and OM.

of 96% (n = 3) CD140b+ cells. The proteome was analyzed throughout the differentiation time course. Cells were collected at days 0 (iPSCs), 3, 5, 7, and 10 (iSMCs). The proteomics data verified a successful iPSC differentiation to iSMCs through a mesodermal intermediate. First, this was shown by an upregulation of mesodermal proteins on day 3 and followed by increasing upregulation of SMC associated proteins at day 5, 7, and 10. Analysis on biological processes showed an initial decrease of pluripotency and increase of mesodermal and other developmental processes. From day 5 to day 10 GO terms associated with muscle development and organizational processes dominated. Finally, Pearson's correlation coefficient of iSMCs with naïve hCASMCs showed a strong correlation in the expression of SMC marker proteins at days 7 and 10. Together, these results indicate a successful differentiation of iPSCs to iSMCs.

Characterizing SMCs has shown to be challenging and is not universally consistent (10). The most common marker for identification of SMCs is αSMA. However, αSMA is also expressed by other cell types such as myofibroblasts, cardiomyocytes and skeletal muscle cells, and therefore αSMA alone is not enough to define a pure population of SMCs. Other proteins have been described to be elevated in either mature SMCs or during the differentiation of SMCs, including CNN1, smooth muscle protein 22 alpha, myosin light chains, transgelin, vinculin, vimentin, desmin, tropomyosin, and CD140b. However, these markers are not specific for SMCs either. The most specific markers for mature SMCs currently known are smoothelin and MYH11, but these proteins are also dependent on SMC maturity. Due to this, characterization of SMCs is limited and fails to exclude the outcome of having cell types that show high resemblance with SMCs such as myofibroblasts (39). Because of possible mischaracterization, it is unclear whether previous studies show a pure SMC population. The extensive amount of data provided by proteomics analysis in our study enables higher certainty of proving purity of the iSMC population. This introduces a method to research the course of SMC differentiation and possibly identify novel factors required for SMC transition.

After iSMC differentiation, we initiated calcification in the iSMCs by culturing the cells in osteogenic media for up to 17 days. Alizarin Red S staining verified successful transformation of iSMCs into c-iSMCs. Proteomic analysis showed increase of Annexin 5 in c-iSMCs (data not shown). Annexin 5 has been demonstrated to play an important role in the generation of microcalcifications (40). It contributes in pathological extracellular vesicle mineralization by facilitating hydroxyapatite nucleation (41). Kegg pathway carbon metabolism, and GO terms for various metabolic processes, vesicle mediated transport and phosphate regulatory processes show up as functional enrichments in the network of proteins. These terms and pathways have previously been associated with calcification (42–44). Biological processes, which appear low in c-iSMCs included developmental processes and intracellular organizational processes such as adherens junctions, supramolecular fiber, collagen fiber and cytoskeleton organization. This indicates a less organized, less mature, more plastic and less contractile phenotype, as seen in a more synthetic (calcifying) SMC phenotype (10). More functional assays assessing contractility and proliferative capacity would help to further evaluate iSMC functional plasticity, which was not addressed herein.

Correlation analysis between the generated iSMCs cultured under NM or OM conditions showed high proteomic overlap with primary SMCs cultured under the same conditions. However, regardless of media conditioning, iSMCs showed a persistently high vimentin protein expression. When cultured in NM, the inclusion of vimentin in the correlation analysis had little effect and actually lowered the correlation coefficient when removed. In contrast, inclusion of vimentin in the correlation analysis under osteogenic media conditions had a much larger effect on the correlation coefficient, raising it from 0.561 to 0.88 upon removal. The persistence of the high vimentin protein expression may be a hallmark of iPSC-derived cell lines and should be considered in future studies. Previous differentiation experiments of iPSC-derived erythroid cells also resulted in a persistent vimentin expression that impeded enucleation (45). Other studies have shown that dedifferentiation during reprogramming may be associated with cytoskeleton remodeling to a more rudimentary state that persists even after iPSC differentiation (46). Future studies should take into consideration the possibility of 3-dimensional cell culture using hydrogels. A more physiologically relevant culture condition that recreates an *in vivo*-like microenvironment may lead to even higher overlap between iSMC ECM protein expression levels and provide a higher fidelity model.

Studying the role of SMCs during calcification using "omics" approaches is becoming more common; however, these studies are usually limited to diseased tissue and appropriate, non-diseased controls are typically lacking. Oftentimes, the initiating events of calcification are missed in tissue that has already reached an advanced disease stage by the time of diagnosis. While it is possible to identify disease-drivers at this stage, it is most likely an accumulation of several confounding metabolic events instead of initiating factors. Therefore, the premise of pharmacological intervention requires bridging the gap between disease initiation and clinical presentation. The combination of an iPSC-derived model of SMC calcification and "omics" analysis may help to identify the starting factors involved in calcification while deconvoluting the pathways involved in the end-stage disease (47). This study presents an inexhaustible source of functional iSMCs and calcifying iSMCs to create vascular calcification tissue model systems, which holds a high

potential for future applications in cardiovascular calcification research and drug discovery.

Data availability statement

The mass spectrometry proteomics data have been deposited to the ProteomeXchange Consortium via the PRIDE partner repository with the dataset identifier PXD032353.

Author contributions

SA and AS contributed equally to the manuscript. All authors listed have made a substantial, direct, and intellectual contribution to the work, and approved it for publication.

Funding

MA and EA were supported by research grants from the National Institutes of Health (R01HL126901 and R01HL149302 to MA; R01HL136431, R01HL141917, and R01HL147095 to EA) and Kowa Company, Ltd, Nagoya, Japan (A11014 to MA). The funders played no role in the design, data collection, and analysis of the studies described here, or in preparation of the present manuscript.

Conflict of interest

The authors declare that the research was conducted in the absence of any commercial or financial relationships that could be construed as a potential conflict of interest.

Publisher's note

Supplementary material

The Supplementary Material for this article can be found online at: https://www.frontiersin.org/articles/10.3389/fcvm.2022.925777/full#supplementary-material

SUPPLEMENTARY FIGURE 1
Proteomics analysis. **(A)** Snapshot of overall proteomics data divided based on highest protein abundance on each day. **(B)** Z-score Abundance (eq. 1) vs. various threshold to obtain the threshold = 1.5 showing multiplicity of 1. **(C)** Number of Day-specific proteins on each day.

References

1. Shaw LJ, Raggi P, Schisterman E, Berman DS, Callister TQ. Prognostic value of cardiac risk factors and coronary artery calcium screening for all-cause mortality. *Radiology.* (2003) 228:826–33.

2. Pagidipati NJ, Gaziano TA. Estimating deaths from cardiovascular disease: a review of global methodologies of mortality measurement. *Circulation.* (2013) 127:749–56.

3. Benjamin EJ, Muntner P, Alonso A, Bittencourt MS, Callaway CW, Carson AP, et al. Heart disease and stroke statistics-2019 update: a report from the American heart association. *Circulation.* (2019) 139:e56–528.

4. Hutcheson JD, Aikawa E, Merryman WD. Potential drug targets for calcific aortic valve disease. *Nat Rev Cardiol.* (2014) 11:218–31.

5. Goettsch C, Hutcheson JD, Aikawa M, Iwata H, Pham T, Nykjaer A, et al. Sortilin mediates vascular calcification via its recruitment into extracellular vesicles. *J Clin Invest.* (2016) 126:1323–36. doi: 10.1172/JCI80851

6. New S, Goettsch C, Aikawa M, Marchini J, Shibasaki M, Yabusaki K, et al. Macrophage-derived matrix vesicles: an alternative novel mechanism for microcalcification in atherosclerotic plaques. *Circ Res.* (2013) 113:72–7. doi: 10.1161/CIRCRESAHA.113.301036

7. Rogers MA, Buffolo F, Schlotter F, Atkins SK, Lee LH, Halu A, et al. Annexin A1-dependent tethering promotes extracellular vesicle aggregation revealed with single-extracellular vesicle analysis. *Sci Adv.* (2020) 6:eabb1244. doi: 10.1126/sciadv.abb1244

8. Hutchenson J, Goettsch C, Bertazzo S, Maldonado N, Ruiz J, Goh W, et al. Genesis and growth of extracellular vesicle-derived microcalcification in atherosclerotic plaques. *Nat Mater.* (2016) 15:335–43. doi: 10.1038/nmat4519

9. Kelly-Arnold A, Maldonado N, Laudier D, Aikawa E, Cardoso L, Weinbaum S. Revised microcalcification hypothesis for fibrous cap rupture in human coronary arteries. *Proc Natl Acad Sci USA.* (2013) 110:10741–6. doi: 10.1073/pnas.1308814110

10. Ayoubi S, Sheikh SP, Eskildsen TV. Human induced pluripotent stemcell-derived vascular smooth muscle cells: differentiation and therapeutic potential. *Cardiovasc Res.* (2017) 113:1282–93.

11. Pfaltzgraff ER, Bader DM. Heterogeneity in vascular smooth muscle cell embryonic origin in relation to adult structure, physiology, and disease. *Dev Dyn.* (2015) 244:410–6. doi: 10.1002/dvdy.24247

12. Emini Veseli B, Perrotta P, de Meyer GRA, Roth L, van der Donckt C, Martinet W, et al. Animal models of atherosclerosis. *Eur J Pharmacol.* (2017) 816:3–13.

13. Goto S, Rogers MA, Blaser MC, Higashi H, Lee LH, Schlotter F, et al. Standardization of human calcific aortic valve disease in vitro modeling reveals passage-dependent calcification. *Front Cardiovascr Med.* (2019) 6:49. doi: 10.3389/fcvm.2019.00049

14. Chang S, Song S, Lee J, Yoon J, Park J, Choi S, et al. Phenotypic modulation of primary vascular smooth muscle cells by short-term culture on micropatterned substrate. *PLoS One.* (2014) 9:e88089. doi: 10.1371/journal.pone.0088089

15. Stephenson M, Reich DH, Boheler KR. Induced pluripotent stem cell-derived vascular smooth muscle cells. *Vasc Biol.* (2020) 2:R1–15.

16. Patsch C, Challet-Meylan L, Thoma EC, Urich E, Heckel T, O'Sullivan JF, et al. Generation of vascular endothelial and smooth muscle cells from human pluripotent stem cells. *Nat Cell Biol.* (2015) 17:994–1003.

17. Benjamini Y, Hochberg Y. Controlling the false discovery rate - a practical and powerful approach to multiple testing. *J R Stat Soc Ser B.* (1995) 1:289–300.

18. Park CY, Klammer AA, Käli L, MacCoss MJ, Noble WS. Rapid and accurate peptide identification from tandem mass spectra. *J Proteome Res.* (2008) 7:3022–7.

19. Elias JE, Gygi SP. Target-decoy search strategy for increased confidence in large-scale protein identifications by mass spectrometry. *Nat Methods.* (2007) 4:207–14.

20. Schlotter F, Halu A, Goto S, Blaser MC, Body SC, Higashi H, et al. spatiotemporal multi-omics mapping generates a molecular atlas of the aortic valve and reveals networks driving disease. *Circulation.* (2018) 138:377–93. doi: 10.1161/CIRCULATIONAHA.117.032291

21. Lee LH, Halu A, Morgan S, Iwata H, Aikawa M, Singh SA. XINA: a workflow for the integration of multiplexed proteomics kinetics data with network analysis. *J Proteome Res.* (2019) 18:775–81. doi: 10.1021/acs.jproteome.8b00615

22. Yu G, Wang LG, Han Y, He QY. ClusterProfiler: an R package for comparing biological themes among gene clusters. *OMICS.* (2012) 16:284–7. doi: 10.1089/omi.2011.0118

23. Hori A, Nishide K, Yasukuni Y, Haga K, Kakuta W, Ishikawa Y, et al. Prominin-1 Modulates Rho/ROCK-Mediated Membrane Morphology and Calcium-Dependent Intracellular Chloride Flux. *Sci Rep.* (2019) 9:15911. doi: 10.1038/s41598-019-52040-9

24. Soncin F, Ward CM. The function of E-cadherin in stem cell pluripotency and self-renewal. *Genes.* (2011) 2:229–59. doi: 10.3390/genes2010229

25. Gao F, Wei Z, An W, Wang K, Lu W. The interactomes of POU5F1 and SOX2 enhancers in human embryonic stem cells. *Sci Rep.* (2013) 3:1588. doi: 10.1038/srep01588

26. Karbiener M, Glantschnig C, Pisani DF, Laurencikiene J, Dahlman I, Herzig S, et al. Mesoderm-specific transcript (MEST) is a negative regulator of human adipocyte differentiation. *Int J Obes.* (2015) 39:1733–41. doi: 10.1038/ijo.2015.121

27. Sun R, Lei L, Liu S, Xue B, Wang J, Wang J, et al. Morphological changes and germ layer formation in the porcine embryos from days 7–13 of development. *Zygote.* (2015) 23:266–76. doi: 10.1017/S0967199413000531

28. Org T, Duan D, Ferrari R, Montel-Hagen A, van Handel B, Kerényi MA. Scl binds to primed enhancers in mesoderm to regulate hematopoietic and cardiac fate divergence. *EMBO J.* (2015) 34:759–77. doi: 10.15252/embj.201490542

29. Alfert A, Moreno N, Kerl K. The BAF complex in development and disease. *Epigenetics Chromatin.* (2019) 12:19.

30. Horiba M, Kadomatsu K, Nakamura E, Muramatsu H, Ikematsu S, Sakuma S, et al. Neointima formation in a restenosis model is suppressed in midkine- deficient mice. *J Clin Invest.* (2000) 105:489–95. doi: 10.1172/JCI7208

31. Prosdocimo DA, Wyler SC, Romani AM, Charles O'neill W, Dubyak GR. Regulation of vascular smooth muscle cell calcification by extracellular pyrophosphate homeostasis: synergistic modulation by cyclic AMP and hyperphosphatemia. *Am J Physiol Cell Physiol.* (2010) 298:702–13. doi: 10.1152/ajpcell.00419.2009

32. New SEP, Aikawa E. Role of extracellular vesicles in de novo mineralization: an additional novel mechanism of cardiovascular calcification. *Arterioscler Thromb Vasc Biol.* (2013) 33:1753–8. doi: 10.1161/ATVBAHA.112.300128

33. Hutcheson JD, Maldonado N, Aikawa E. Small entities with large impact: microcalcifications and atherosclerotic plaque vulnerability. *Curr Opin Lipidol.* (2014) 25:327–32. doi: 10.1097/MOL.0000000000000105

34. Bakhshian Nik A, Hutcheson JD, Aikawa E. Extracellular Vesicles As Mediators of Cardiovascular Calcification. *Front Cardiovasc Med.* (2017) 4:78. doi: 10.3389/fcvm.2017.00078

35. Aikawa E, Nahrendorf M, Figueiredo JL, Swirski FK, Shtatland T, Kohler RH, et al. Osteogenesis Associates With Inflammation in Early-Stage Atherosclerosis Evaluated by Molecular Imaging In Vivo. *Circulation.* (2007) 116:2841–50. doi: 10.1161/CIRCULATIONAHA.107.732867

36. Hu BY, Weick JP, Yu J, Ma LX, Zhang XQ, Thomson JA, et al. Neural differentiation of human induced pluripotent stem cells follows developmental principles but with variable potency. *Proc Natl Acad Sci USA.* (2010) 107:4335–40. doi: 10.1073/pnas.0910012107

37. Ramos-Mejia V, Melen GJ, Sanchez L, Gutierrez-Aranda I, Ligero G, Cortes JL, et al. Nodal/activin signaling predicts human pluripotent stem cell lines prone to differentiate toward the hematopoietic lineage. *Mol Ther.* (2010) 18:2173–81. doi: 10.1038/mt.2010.179

38. Ma Y, Qiao X, Falone AE, Reslan OM, Sheppard SJ, Khalil RA, et al. Gender-specific reduction in contraction is associated with increased estrogen receptor expression in single vascular smooth muscle cells of female rat. *Cell Physiol Biochem.* (2010) 26:457–70. doi: 10.1159/000320569

39. Gan Q, Yoshida T, Li J, Owens GK. Smooth muscle cells and myofibroblasts use distinct transcriptional mechanisms for smooth muscle α-actin expression. *Circ Res.* (2007) 101:883–92. doi: 10.1161/CIRCRESAHA.107.154831

40. Kapustin AN, Davies JD, Reynolds JL, McNair R, Jones GT, Sidibe A, et al. Calcium regulates key components of vascular smooth muscle cell-derived matrix vesicles to enhance mineralization. *Circ Res.* (2011) 109:e1–12.

41. Blaser MC, Aikawa E. Roles and regulation of extracellular vesicles in cardiovascular mineral metabolism. *Front Cardiovasc Med.* (2018) 5:187. doi: 10.3389/fcvm.2018.00187

42. Voelkl J, Lang F, Eckardt KU, Amann K, Kuro-o M, Pasch A, et al. Signaling pathways involved in vascular smooth muscle cell calcification during hyperphosphatemia. *Cell Mol Life Sci.* (2019) 76:2077–91.

43. Leem J, Lee IK. Mechanisms of vascular calcification: the pivotal role of Pyruvate dehydrogenase kinase 4. *Endocrinol Metab.* (2016) 31:52–61. doi: 10.3803/EnM.2016.31.1.52

44. Riad A, Narasimhulu CA, Deme P, Parthasarathy SA. Novel mechanism for atherosclerotic calcification: potential resolution of the oxidation paradox. *Antioxid Redox Signal.* (2018) 29:471–83. doi: 10.1089/ars.2017.7362

45. Trakarnsanga K, Ferguson D, Daniels DE, Griffiths RE, Wilson MC, Mordue KE, et al. Vimentin expression is retained in erythroid cells differentiated from human iPSC and ESC and indicates dysregulation in these cells early in differentiation. *Stem Cell Res Ther.* (2019) 10:130. doi: 10.1186/s13287-019-1231-z

46. Boraas LC, Guidry JB, Pineda ET, Ahsan T. Cytoskeletal expression and remodeling in pluripotent stem cells. *PLoS One.* (2016) 11:e0145084. doi: 10.1371/journal.pone.0145084

47. Atkins SK, Singh SA, Aikawa E. Calcific aortic valve disease "Omics" is timely, but are we looking too late?. *JACC Basic Transl Sci.* (2020) 5:1178–80. doi: 10.1016/j.jacbts.2020.11.001

frontiers | Frontiers in Cardiovascular Medicine

TYPE Original Research
PUBLISHED 04 August 2022
DOI 10.3389/fcvm.2022.945672

OPEN ACCESS

EDITED BY
Elena Aikawa,
Brigham and Women's Hospital and Harvard Medical School, United States

REVIEWED BY
Paul Philipp Heinisch,
German Heart Centre, Germany
Meric Kocaturk,
Uludag University, Turkey

*CORRESPONDENCE
Carla M. R. Lacerda
clacerda@uttyler.edu

SPECIALTY SECTION
This article was submitted to Heart Valve Disease, a section of the journal Frontiers in Cardiovascular Medicine

RECEIVED 16 May 2022
ACCEPTED 06 July 2022
PUBLISHED 04 August 2022

CITATION
Wang X, Kuban-Johnston D, Lapuerta P and Lacerda CMR (2022) Telotristat ethyl reverses myxomatous changes in mice mitral valves. *Front. Cardiovasc. Med.* 9:945672. doi: 10.3389/fcvm.2022.945672

Telotristat ethyl reverses myxomatous changes in mice mitral valves

Xinmei Wang[1], Danielle Kuban-Johnston[2], Pablo Lapuerta[2] and Carla M. R. Lacerda[3]*

[1]Department of Bioengineering, Shenyang University, Shenyang, China, [2]Lexicon Pharmaceuticals, Basking Ridge, NJ, United States, [3]Department of Chemical Engineering, The University of Texas at Tyler, Tyler, TX, United States

Rationale: Myxomatous mitral valve degeneration is a common pathological manifestation of mitral valve regurgitation, with or without valvular prolapse. In addition to similarities between naturally occurring and serotonergic valve degeneration, an increasing body of evidence has recently suggested that serotonin signaling is a regulator of degenerative valvulopathies. Studies have found that serotonin can be synthesized locally by valvular cells and serotonin receptors in turn may be activated to promote signaling. Recently, telotristat ethyl (TE) has been introduced as a treatment for carcinoid disease, by selectively inhibiting tryptophan hydroxylase 1, the rate-limiting enzyme in peripheral serotonin synthesis. TE provides a unique tool to test inhibition of serotonin synthesis *in vivo*, without impacting brain serotonin, to further confirm the role of local serotonin synthesis on heart valves.

Objective: To confirm the link between serotonin and myxomatous valvular disease *in vivo*.

Methods and results: A hypertension-induced myxomatous mitral valve disease mouse model was employed to test the effect of TE on valvular degeneration. Circulating serotonin and local serotonin in valve tissues were tested by enzyme immunoassay and immunohistochemistry, respectively. TE was administrated in two modes: (1) parallel with angiotensin II (A2); (2) post A2 treatment. Myxomatous changes were successfully recapitulated in hypertensive mice, as determined by ECM remodeling, myofibroblast transformation, and serotonin signaling activation. These changes were at least partially reversed upon TE administration.

Conclusion: This study provides the first evidence of TE as a potential therapeutic for myxomatous mitral disease, either used to prevent or reverse myxomatous degeneration.

KEYWORDS

telotristat ethyl, serotonin, hypertension, myxomatous mitral disease, mouse model

Abbreviations: TE, telotristat ethyl; ECM, extracellular matrix; VIC, valvular interstitial cell; α-SMA, alpha-smooth muscle actin; MMP1, matrix metalloproteinase 1; TGFβ1, transforming growth factor beta 1; TPH1, tryptophan hydroxylase 1; 5HTR2b, serotonin receptor type 2B; IHC, immunohistochemistry; SBP, systolic blood pressure; Sal, saline; SalTE; combination of saline and telotristat ethyl; A2, angiotensin II; A2TE, combination of angiotensin II and telotristat ethyl.

Introduction

The most common mitral valve disorder is mitral regurgitation, often with myxomatous degeneration as the dominant pathology (1). According to the most current Heart Disease and Stroke Statistics update, the prevalence of myxomatous mitral disease is greater than 1.5% in the United States population and dramatically increases with age (1). At the macroscopic level, myxomatous mitral valve leaflets are typically elongated and distorted, leading to prolapse and improper coaptation (2). At the microscopic level, myxomatous mitral valves undergo extracellular matrix (ECM) remodeling and valvular interstitial cell (VIC) phenotype transformation (3).

Valvular homeostasis is maintained by quiescent VICs, the main cell population in normal heart valves (3, 4). In naturally occurring myxomatous mitral valve disease, accompanied or not by valve regurgitation and prolapse, quiescent VICs are transformed to activated VICs, which exhibit increased cell proliferation and enhanced expression of myofibroblastic protein markers, such as alpha-smooth muscle actin (α-SMA), matrix metalloproteinase 1 (MMP1), and transforming growth factor beta 1 (TGFβ1) (3, 5, 6). In addition, ECM remodeling occurs due to increased expression of matrix metalloproteinases (MMPs) and tissue inhibitors of MMPs, collagen degradation, proteoglycan accumulation, and elastin fiber fragmentation (3, 4). Similarly in carcinoid heart disease, patients of carcinoid syndrome develop right heart failure as right-sided heart valves develop a similar pathology (7, 8). The outflow side of the tricuspid and pulmonary valves are known to develop carcinoid plaques, largely composed of highly proliferative myofibroblastic VICs (activated VICs), deposited myxoid ECM rich in collagen and proteoglycans, which together result in valvular regurgitation (9, 10). Carcinoid plaques form more rarely on the left side due to the pulmonary circulation clearing serotonin from arterial blood, which contacts mitral and aortic valves. Despite the differences in location, the cell and molecular changes occurring in myxomatous mitral valve disease and in carcinoid heart disease are evidently similar (8). To further solidify these commonalities, serotonergic valve disease has been found to be inducible by serotonin directly in a murine model (11) or in humans undergoing the Fen-Phen diet, a combination of anorexigen drugs that increase circulating serotonin (fenfluramine and phentermine are both potent inhibitors of serotonin uptake) (12, 13). At the molecular level, serotonergic valve disease is similar to the cases described above, which culminates in potential valve failure (14).

Based on the evidence described above, it has now been demonstrated that serotonin is locally synthesized by mitral valves and regulates myxomatous pathology. Tryptophan hydroxylase 1 (TPH1), the rate-limiting enzyme for peripheral serotonin synthesis, was intensively expressed in myxomatous human and canine mitral valves (15). Additionally, serotonin receptor type 2B (5HTR2b), in company with TPH1, was increased in myxomatous mitral valves, while serotonin transporter was decreased leading its reduced metabolism (16). However, it is still unclear how serotonin circulating in plasma and serum triggers and/or mediates myxomatous mitral disease (17–19). In addition to evidence from *ex vivo* myxomatous mitral valves, other *in vitro* studies have shown that local serotonin in mitral valves can be induced by mechanical stimuli and regulates myxomatous proteins (20, 21).

However, *in vivo* studies to substantiate the role of serotonin regulation on valvulopathies are missing due to the lack of selectivity of TPH1 inhibitors. Recently, telotristat ethyl (TE) has been released for the treatment of carcinoid syndrome. TE is a specific TPH1 inhibitor (22), which does not cross the blood-brain barrier, thus not interfering with serotonin in the brain, synthesized by TPH2. Based on clinical evidence suggesting that TE works effectively to inhibit serotonin synthesis in the gut (22), we expect it to function as an effective inhibitor of serotonin synthesis by heart valves. Thus, here we hypothesized that serotonin synthesis inhibition ameliorates the severity of myxomatous mitral valve disease in hypertensive mice. To test this hypothesis, mice were rendered hypertensive by subcutaneous angiotensin II (A2) delivery with or without TE administration, and parallel groups of normotensive mice served as controls. By studying this mouse model, we aimed to: (1) confirm that mitral myxomatous changes can be induced in hypertensive mice that received a short-term A2 administration; (2) demonstrate that myxomatous changes and high blood pressure correlate with high serotonin; (3) validate the role of TE on myxomatous mitral valves in hypertensive mice; 4) elucidate the link between serotonin and myxomatous valvular disease *in vivo*.

Materials and methods

Animals

Wild-type, 6-week old C57BL6J mice of both genders were purchased from Jackson Laboratory (Bar Harbor, ME, United States). Male and female mice were housed separately and maintained under standard conditions within Animal Care Service Facility at Texas Tech University (TTU). Mice in groups of two per cage were maintained under an artificial 12-h dark-light cycle. They were allowed free access to food and water and were acclimated for five. All animal experiments followed TTU Institutional Animal Care and Use Committee (IACUC) approved protocol number T18006.

ALZET pump preparation

Mini-osmotic pumps, models 2004 or 2006 (both from ALZET, Cupertino, CA, United States) with delivery duration of 4 or 6 weeks respectively, were employed for delivery of A2

or saline. Osmotic pumps were preloaded and primed under sterile conditions following the protocol from the manufacturer. Loading solutions were sterile A2 (Millipore Sigma, Burlington, MA, United States) in 0.9% (w/v) saline (Fisher Scientific, Hampton, NH, United States) or sterile 0.9% saline (Sal). Preloaded pumps were primed in sterile 0.9% saline in an incubator at 37°C for at least 40 or 60 h depending on pump model, prior to subcutaneous implantation. In study 1 – prevention mode, mini-osmotic pumps model 2004 filled with A2 delivered 1 μg/kg/min at a flow rate of 0.25 μL/h to achieve 0.8 mg of A2 total per 20 g animal for period of 4 weeks. In study 2 – reversal mode, mini-osmotic pumps model 2006 filled with A2 delivered 1 μg/kg/min at a flow rate of 0.15 μL/h to achieve 1.2 mg of A2 total per 20 g animal for a period of 6 weeks.

Subcutaneous pump implantation surgery

Right after acclimation, mice underwent implantation of subcutaneous mini-osmotic pumps. Anesthesia chamber was pre-filled with 4% isoflurane (Patterson Veterinary, Greeley, CO, United States) with 2 L/min oxygen flow. After mouse was transferred into chamber, isoflurane was reduced to 2%, and mouse was transferred to a nose cone in ventral recumbence. Eyes were covered by ophthalmic lubricant ointment. Slow release SR Buprenorphine (Wildlife Pharmaceuticals, Windsor, CO, United States) at dose 0.05 mg/kg was administered pre-emptively *via* injection to control pain for 72 h. The skin between the shoulder to the mid-back was shaved and aseptically wiped with 70% alcohol and 4% chlorhexidine gauze sponges for 4 times. Subsequently, animal was immediately transferred to a clean procedural table with a heat pad underneath and covered by a sterile disposable towel. A mid-scapular incision (∼ 10 mm) was made by a sterile blade to open the dorsal skin, and a subcutaneous pocket was created by inserting sterile scissors to fit mini-osmotic pumps. A mini-osmotic pump pre-filled with A2 or saline vehicle was implanted into the pocket. To finalize the surgery procedure, each incision was closed with two 7-mm Reflex wound closure clips (Harvard Apparatus, Holliston, MA, United States). After the surgery, each mouse was transferred to a cage with a clean towel in and a heat pad under to prevent hypothermia and allowed to wake up. All mice were weighed and tattooed on the tail for identification purposes. After surgery, mice were transferred to a new cage and housed in pairs. Mice were maintained under standard conditions at TTU Animal Care Service Facility for 4 or 6 weeks.

Inducing myxomatous changes and their reversal

Two studies were performed separately and animals were divided into 4 groups (Sal, A2, SalTE, A2TE) in each study. In the first study – prevention mode, ALZET model 2004 pumps preloaded with A2 or saline vehicle (A2 negative control) were surgically implanted into 100 mice (50 males and 50 females) with or without TE administration in parallel for 4 weeks. Briefly, TE was administered daily as described below as the pumps delivered 1 μg/kg/min saline or A2 for 28 days to each animal in pertinent groups. In the second study – reversal mode, ALZET pumps model 2004 or 2006 preloaded with A2 or saline vehicle (A2 negative control) were surgically implanted into 100 mice (50 males and 50 females). Mice implanted with model 2006 pumps received 1 μg/kg/min saline or A2 for 42 days. Mice implanted with model 2004 pumps received 1 μg/kg/min saline or A2 for 28 days followed by a late administration of TE in the last 2 weeks, to reverse previously developed myxomatous changes. Complete experimental details of these two studies are summarized in Table 1.

Telotristat ethyl was provided by Lexicon Pharmaceuticals (Basking Ridge, NJ, United States). TE was prepared as a suspension in 0.25 % (w/v) methylcellulose (Spectrum, New Brunswick, NJ, United States) to a final concentration of 0.24 g/mL TE. Each mouse was fed 25 μL TE solution once each day by oral gavage to achieve 300 mg/kg/day, a dose at which

TABLE 1 Experimental design.

Study	Group	Experimental period	Mini-osmotic pump model	Loading solution	Number of Mice			TE administration
					Male	Female	Total	
Prevention	Sal	4 weeks	2004	Sal	14	10	24	Not Applied
	SalTE		2004	Sal	10	16	26	Applied for 4 weeks
	A2		2004	A2	14	10	24	Not Applied
	A2TE		2004	A2	12	14	26	Applied for 4 weeks
Reversal	Sal	6 weeks	2006	Sal	12	12	24	Not Applied
	SalTE		2004	Sal	10	14	24	Applied in the last 2 weeks
	A2		2006	A2	14	12	26	Not Applied
	A2TE		2004	A2	14	12	26	Applied in the last 2 weeks

dose peripheral serotonin was significantly reduced in mice guts, without inducing side effects.[2] TE was administered either in parallel or post-A2 treatment until the day before euthanasia.

Blood pressure *in vivo* measurement

Blood pressure measurements were conducted using the CODA non-invasive blood pressure system (Kent Scientific, Torrington, CT, United States) every 4 days over the complete experimental period. The procedure followed the owner's manual from Kent Scientific. A CODA controller was connected to a laptop installed with CODA software (CODA 4.1), and a warming platform was preset to 38 ^{o}C. After mice were properly placed in pre-warmed holders, their tails entered the CODA cuff assembly with the occlusion cuff close to tail base and the volume pressure recording (VPR) sensor distal to the O-cuff. Both O-cuff and VPR sensor were connected to the CODA controller. Data tables were created by the system containing systolic, diastolic, and mean blood pressures. Statistical differences on blood pressure among treatments were assessed by multiple comparison tests following one-way ANOVA and $p < 0.05$ were considered significant.

Exsanguination and heart collection

At the end of *in vivo* treatments (4 or 6 weeks), mice underwent carbon dioxide asphyxiation. After mice ceased breathing, they were weighed and transferred to an operation bench. The death was confirmed by cervical dislocation. Subsequently, blood was collected through the abdominal aorta and hearts were collected through a thoracic incision. Blood samples were immediately supplemented with 0.1% ethylenediaminetetraacetic acid (Fisher Scientific) and stored at −20°C for future serotonin enzyme-linked immunosorbent assay. Hearts were washed at least 3 times in phosphate-buffered saline [PBS, 137 mM sodium chloride, 2.7 mM potassium chloride, 4.3 mM sodium phosphate dibasic and 1.46 mM potassium phosphate monobasic (all from Fisher Scientific)] supplemented with 0.1% ethylenediaminetetraacetic acid, followed by fixation in 4% formaldehyde (Fisher Scientific). Paired Student's *t*-test was performed to assess the significant differences on animal weight changes with age. $P < 0.05$ were considered significant.

Circulating serotonin quantification

The total concentration of serotonin circulating in blood was determined by serotonin isolation from blood proteins followed by a serotonin enzyme-linked immunosorbent assay (Enzo Life Science, Farmingdale, NY, United States). Briefly, blood samples were centrifuged, then precipitated in 9 volumes of ethanol at −80°C overnight to remove hemoglobin and other proteins after complete cell lysis (23). Serotonin was enriched in the supernatant ethanol layer and vacuum concentrated. Enzyme-linked immunosorbent assay was performed following the manufacturer's protocol. The average and standard deviation in each group were calculated from eight biological replicates. Statistical differences on circulating serotonin among treatments were assessed by multiple comparison tests following one-way ANOVA, and $p < 0.05$ were considered significant.

Histology and histological staining

Histological slide preparation

Mouse hearts were symmetrically bisected across the center of the ventricles. After fixation in formaldehyde, dehydration, clearing and paraffin infiltration, heart sections were paraffin-embedded in tissue cassettes with left ventricles next to each other. Tissue-embedded paraffin blocks were sliced into 4 μm slices by a rotary microtome and slices placed onto poly-L-lysine coated glass slides (Fisher Scientific). Sections were air dried overnight prior to deparaffinization in xylenes and subsequent rehydration prior to staining.

Modified russell-movat pentachrome stain

Mitral valve sections were stained by a Movat-Russell modified pentachrome stain kit (American MasterTech, Lodi, CA, United States). The staining procedure followed the protocol recommended by the manufacturer. Elastic fibers and nuclei were stained black and dark purple, respectively. Polysaccharides, muscle and collagen were stained in sequence by alcian blue, the combination of crocein scarlet and acidic fuchsine, and alcoholic saffron in greenish blue, red, and yellow, respectively. Sections were allowed to air dry and mounted with Permount mounting medium (Fisher Scientific) and cover glasses. Bright-field images were acquired using a color camera (DFC295) of Leica DMI6000 B microsystem (Leica Microsystems, Buffalo Grove, IL, United States). Valve thicknesses were measured at the base of the leaflets on histological sections using a scale bar in LAS X microscope software (Leica Microsystems). Average values and standard deviations of thickness measurement were calculated from 26 images from at least 6 biological replicates. Statistical differences on valve thickness among treatments were assessed by multiple comparison tests following one-way ANOVA, and $p < 0.05$ were considered significant.

Immunohistochemistry

To investigate differences in expression of protein markers on mitral valves receiving different treatments, Immunohistochemistry (IHC) was performed using a commercial ready-to-use kit (BioVision, Milpitas, CA,

United States). The protocol provided by the manufacturer was followed. First, peroxidase block was applied to tissue sections for 10 min. After 10 s wash in water, sections were immersed in pre-boiled sodium citrate buffer (10 mM sodium citrate, 0.05% Tween 20 (both from Fisher Scientific), pH 6.0) and immediately transferred to a pre-heated steamer. The requirement of heat-induced antigen retrieval step depended on the primary antibody applied later. In this study, antigen retrieval was employed in the staining of 5HTR2b, TGFβ1, and MMP1. Sections were then cooled in cold water and incubated with protein blocking solution for 10 min. Primary antibodies were applied to tissue sections and incubated for 30–60 min without drying. Primary antibodies employed were mouse monoclonal anti-TPH (Millipore Sigma) at a final concentration of 2 μg/mL, mouse monoclonal anti-smooth muscle actin (Fisher Scientific) at a final concentration of 1.25 μg/mL, rabbit polyclonal anti-5HTR2b (Novus Biologicals, Centennial, CO, United States) at a final concentration of 2.4 μg/mL, rabbit polyclonal anti-TGFβ1 (Abcam, Cambridge, United Kingdom) at a final concentration of 5 μg/mL, rabbit polyclonal anti-MMP1 (Invitrogen, Carlsbad, CA, United States) at a final concentration of 0.92 μg/mL. After primary antibody binding, another 30-min incubation with HRP polymer was performed, followed by washes in PBS and water in sequence. Positive expression of proteins was visualized in a dark brown color after a 10 min reaction with diaminobenzidine chromogen. Lastly, nuclei were labeled by hematoxylin (Electron Microscopy Sciences, Hatfield, PA, United States) in dark purple, and sections were washed in water for 20 min for better coloration. Sections were mounted with Fluoromount-G hydrophilic mounting medium (Southern Biotech, Birmingham, AL, United States) and cover glasses after air drying. Bright-field images were acquired as above. For the quantitative evaluation of each protein marker, at least 4 biological replicates in each treatment group were tested. Protein expression was quantified in MATLAB R2018b (MathWorks, Natick, MA, United States), where the total stained area in pixels was measured from at least 4 biological replicates after background and noise were removed by thresholding. Significant differences in protein expression were assessed by Kruskal-Wallis and multiple comparison tests. $P < 0.05$ were considered significant.

Results

All mice were initially normotensive

In the prevention study, average weights of animals increased from 21.5 3.5 g to 22.6 3.7 g in 4 weeks, while in the reversal study, average weights increased from 22.0 2.8 g to 25.0 3.2 g in 6 weeks. In both cases, weights of males were always higher than those of females, with no significant differences observed across treatments (**Supplementary Figures 1A,B**).

In both prevention and reversal studies, blood pressure baseline was measured from 100 animals the day before surgeries, and animals were all normotensive initially (**Figures 1A,B**). Blood pressure baselines in reversal study were higher than those from prevention study, due to a different size of occlusion cuff used in reversal study. In both cases, there was no significant difference on blood pressure baseline between males and females, as shown on **Figures 1A,B**.

Hypertension was successfully induced by subcutaneous angiotensin II delivery in mice

Systolic, diastolic and mean blood pressures of each animal were measured every 4 days over the entire experimental periods of both studies. Since paired systolic, diastolic and mean blood pressures showed the same trends, only systolic blood pressures (SBP) are reported here and were used to assess differences across treatments.

In the prevention study, SBPs from Sal and SalTE groups overlaid throughout the entire experimental period, and were much lower than SBPs from A2-treated groups on each measurement date (**Figure 2A**). However, the parallel administration of A2TE ceased the increase in blood pressure after day 21. This demonstrates that A2 dramatically elevated blood pressure from 149.6 35.6 mmHg to 203.8 34.6 mmHg in mice, and sustained TE administration seemed to reverse A2-induced hypertension, as indicated by a less increase in blood pressure from 142.7 32.2 mmHg to 185.8 36.7 mmHg in 4 weeks. To further evaluate the effects of A2 and/or TE on blood pressure, blood pressures from final measurements were compared across treatments, as shown in **Figure 2B**. Final day blood pressures from angiotensin groups (A2 and A2TE) were significantly higher than those from saline groups (Sal and SalTE). Moreover, TE decreased blood pressure in A2TE but not SalTE. The main findings are 1) A2 significantly induced hypertension in mice within 4 weeks; 2) TE reversed A2-induced hypertension in mice, without effects in normotensive mice.

In the reversal study, TE was administered in the last 2 weeks of the total 6 weeks of A2 treatment. Consistently with the observations from the prevention study, A2 largely induced high blood pressure from 153.9 37.0 mmHg to 178.4 42.6 mmHg, which was reversed by TE supplementation, where blood pressure was elevated from 150.2 32.0 mmHg to 164.9 28.8 mmHg (**Figure 3A**). On the other hand, TE administration did not result in differences in blood pressure among saline groups (**Figure 3A**). Again, endpoint blood pressures before and after TE administration (Day 29 and Day 41) were compared across treatments. Before TE administration (Day 29), blood pressures in angiotensin groups (A2 and A2TE)

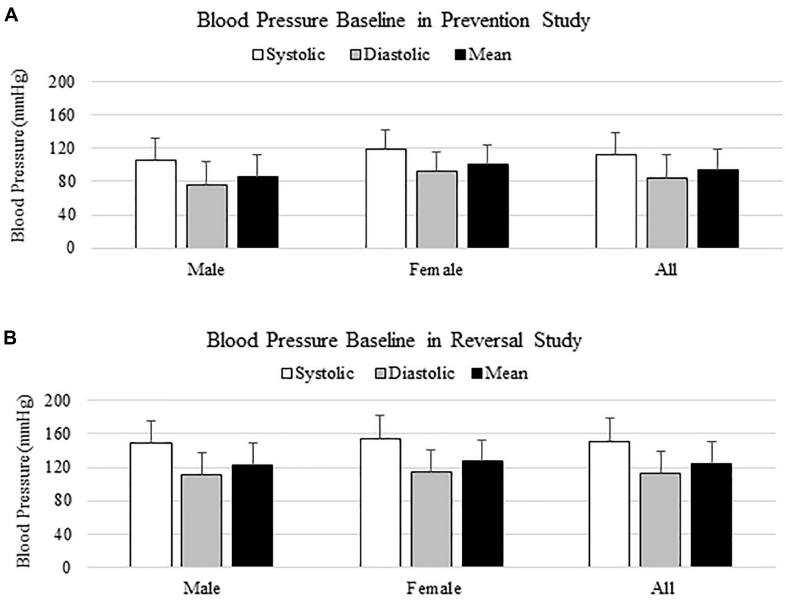

FIGURE 1
Blood pressure baseline in prevention **(A)** and reversal **(B)** studies.

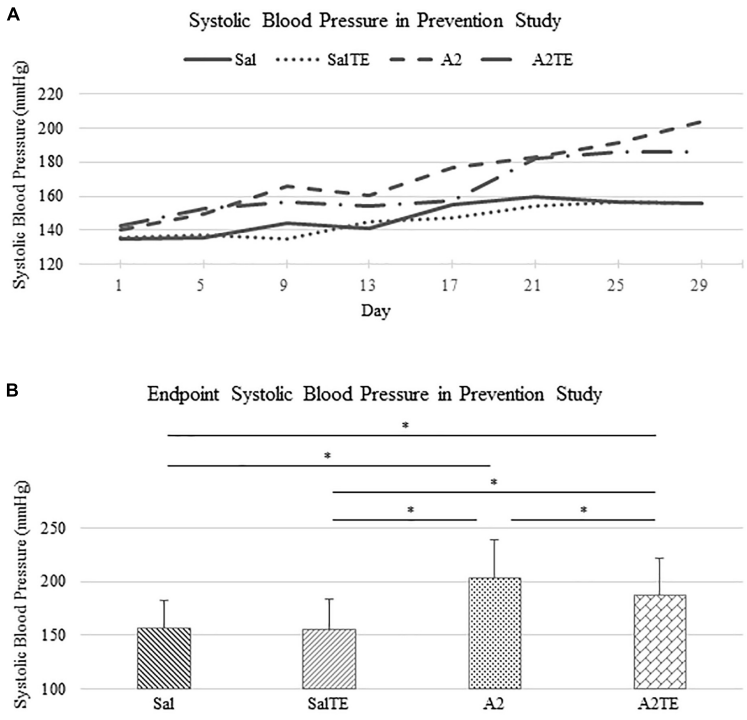

FIGURE 2
(A) Systolic blood pressure changes with time in hypertensive and normotensive mice in prevention study. **(B)** Endpoint (Day 29) systolic blood pressure comparison across treatments. Asterisk indicates significant difference ($p < 0.05$).

were significantly higher than those from saline groups (Sal and SalTE) (Figure 3B). After 2 weeks along with TE administration (Day 41), blood pressure was continuously increased by A2, but this change was prevented by TE (Figure 3B). However, TE administration did not cause a change in saline group (SalTE). By the end of the experiment, blood pressures from A2 group

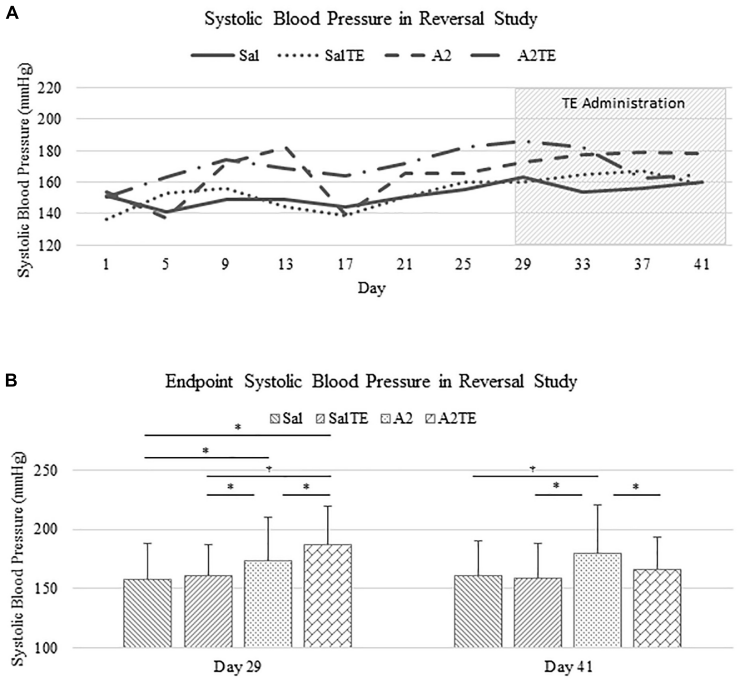

FIGURE 3
(A) Systolic blood pressure changes with time in hypertensive and normotensive mice in reversal study. **(B)** Endpoint (Day 29 and 41) systolic blood pressure comparison across treatments. Asterisk indicates significant difference ($p < 0.05$).

were significantly higher than those from the other 3 groups, indicating an impact of TE on A2-induced high blood pressure.

These findings demonstrate that A2 continuously increased blood pressure in mice for 6 weeks, but the resulting high blood pressure was significantly reversed by TE administration. Data from both studies suggested that A2 successfully induced hypertension in mice and TE counteracted this effect in either parallel or late administration.

Angiotensin II and telotristat ethyl synergistically reduce circulating serotonin in mice

Circulating serotonin levels were compared across treatments. In the prevention study, A2 significantly reduced circulating serotonin in mice, compared to Sal group that served as normotensive control (**Figure 4A**). Concentrations of circulating serotonin in TE-treated mice were significantly lower than those in the corresponding Sal or A2 groups (**Figure 4A**), as expected. However, the inhibitory effect of TE on serotonin was higher in the presence of A2 (**Figure 4A**). TE reduced circulating serotonin from 2952.51 to 1862.00 ng/mL on average in normotensive mice, and the inhibition efficiency is 36.94%. On the other hand, TE decreased 62.46% circulating serotonin in hypertensive mice, with average levels of 1838.82 and 690.33 ng/mL, respectively.

Similar results of circulating serotonin concentrations were observed in reversal study, where TE was administered following the treatment with A2 or Sal. A2 reduced circulating serotonin after 6 weeks (**Figure 4B**), although not significantly. The 2-week administration of TE significantly reduced serotonin levels in blood compared to those in corresponding Sal and A2 (**Figure 4B**). Moreover, the lowest concentration of serotonin appeared in A2TE as before (**Figure 4B**). These data suggested that longer A2 treatment slightly reduced serotonin level, while TE always effectively inhibited circulating serotonin. Moreover, this inhibitory effect was maximized in combination with A2. Circulating serotonin was reduced by TE from 2497.15 to 1634.61 ng/mL in normotensive mice and from 1978.64 to 1016.05 ng/mL in hypertensive mice, resulting 34.54 and 48.65% reductions, respectively.

Myxomatous changes on mitral valves were observed in hypertensive mice, and reversed by a parallel telotristat ethyl administration

Myxomatous remodeling was evaluated on Movat stains and IHC of myxomatous markers. ECM disorganization was

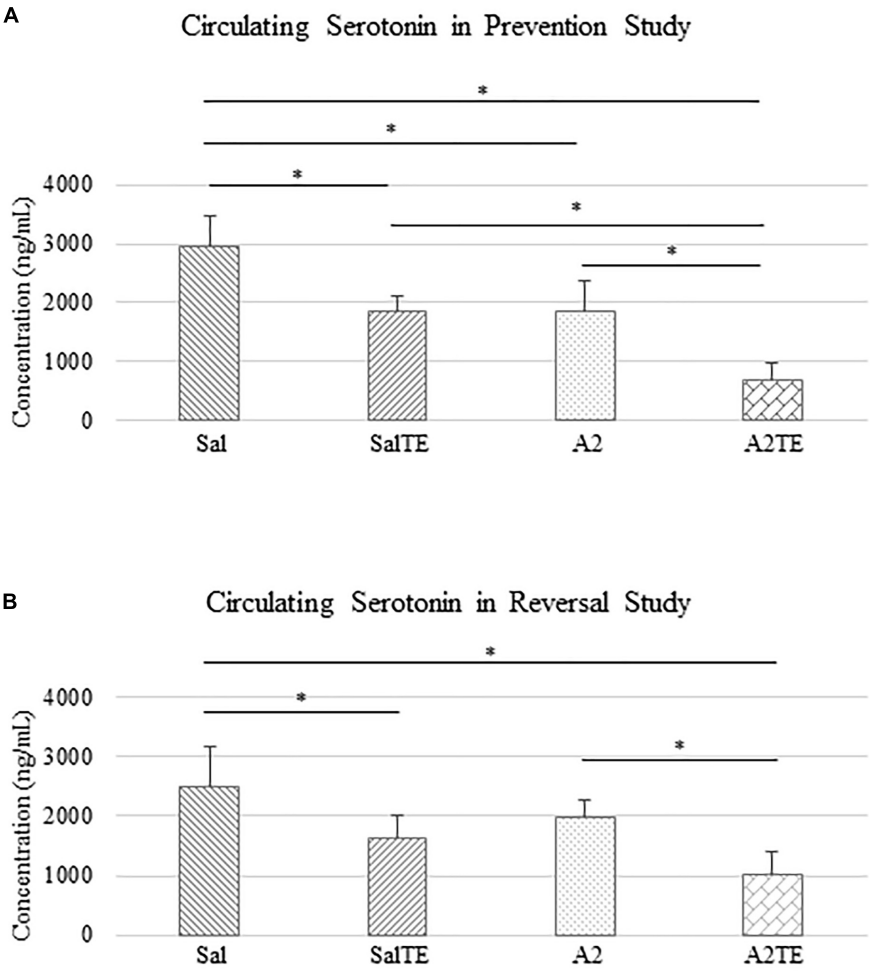

FIGURE 4
Circulating serotonin level comparison across treatments in prevention **(A)** and reversal **(B)** studies. Asterisk indicates significant difference ($p < 0.05$).

assessed by Movat stains, where collagen, proteoglycans, and elastic fibers were colored in yellow, greenish blue, and black, respectively. The most easily observed ECM component is proteoglycan, as indicated by greenish blue tint throughout the sections (**Figure 5A**). In addition, black elastic fibers dominated the atrialis layer facing the left atrium. A much more condensed blue tint appeared in mitral valves of A2-treated mice, indicating that proteoglycan accumulation was induced by A2 (**Figure 6A**), with less yellow (collagen fibers). Whereas, this proteoglycan overproduction combined with collagen fragmentation was not observed in the presence of TE (**Figure 6A**). Mitral valve thickening did not occur in short-term (4 week prevention study) A2 supplementation (**Supplementary Figure 2A**).

Expression of five myxomatous markers were assessed by IHC in mitral valves from the same animals employed for Movat stains. Positive expression of protein markers was stained in dark brown, indicating affected regions. In general, excess MMP1 was produced by mitral valves that received A2 (**Figures 5A,B**). Parallel treatment with TE lowered MMP1 level compared to corresponding Sal or A2 specimens (**Figures 5A,B**). Activated phenotype transformation was significantly enhanced in mitral valves in hypertensive mice, as suggested by plaques of strong positive α-SMA stain (**Figures 6A,B**). As expected, parallel administration of TE reduced A2-induced cell activation. TGFβ1 showed the same trend as α-SMA, with its expression significantly increased in hypertensive mice but reversed by TE (**Figures 6A,B**). TPH1 and 5HTR2b expression levels were highly increased in hypertensive mice, and diminished by TE administration (**Figures 7A,B**). Moreover, their expression was also lowered by TE in normotensive mice. Based on these observations, the prevention study uncovered that ECM proteoglycans and myxomatous markers (MMP1, α-SMA, TGFβ1, TPH1, and 5HTR2b) were overproduced in mitral valves of hypertensive mice, and these changes were reversed by TE.

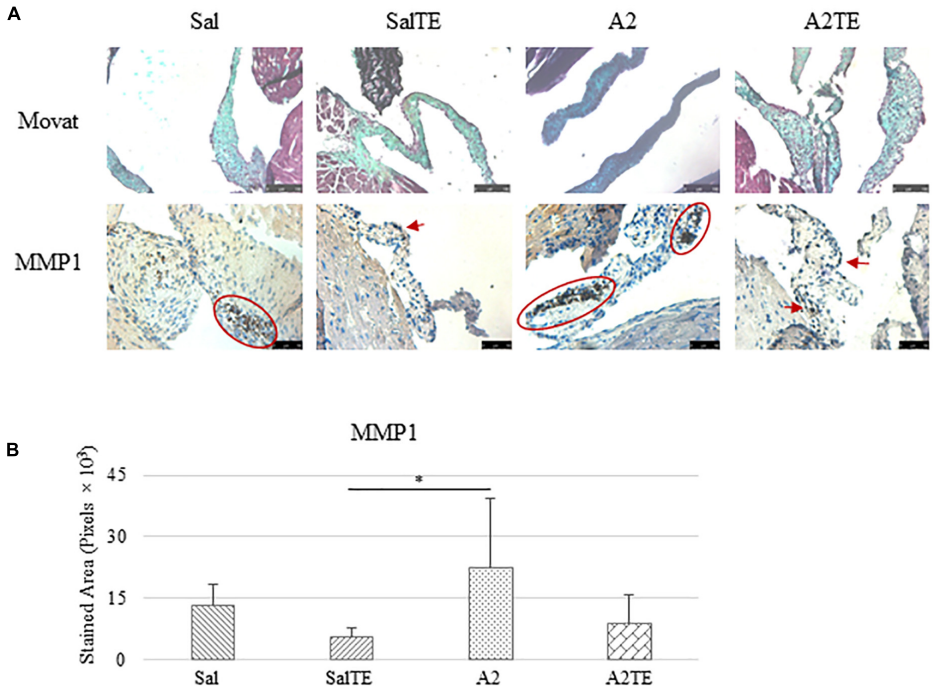

FIGURE 5
(A) Investigation of mitral valve ECM remodeling by Movat stain and MMP1 IHC in prevention study. Major positive IHC stains were highlighted by circles and arrows. Scale bar on Movat images: 100 μm. Scale bar on IHC images: 50 μm. **(B)** Quantification of MMP1 expression determined by total stained area in pixels that measured from 4 biological replicates in MATLAB. Asterisk indicates significant difference ($p < 0.05$).

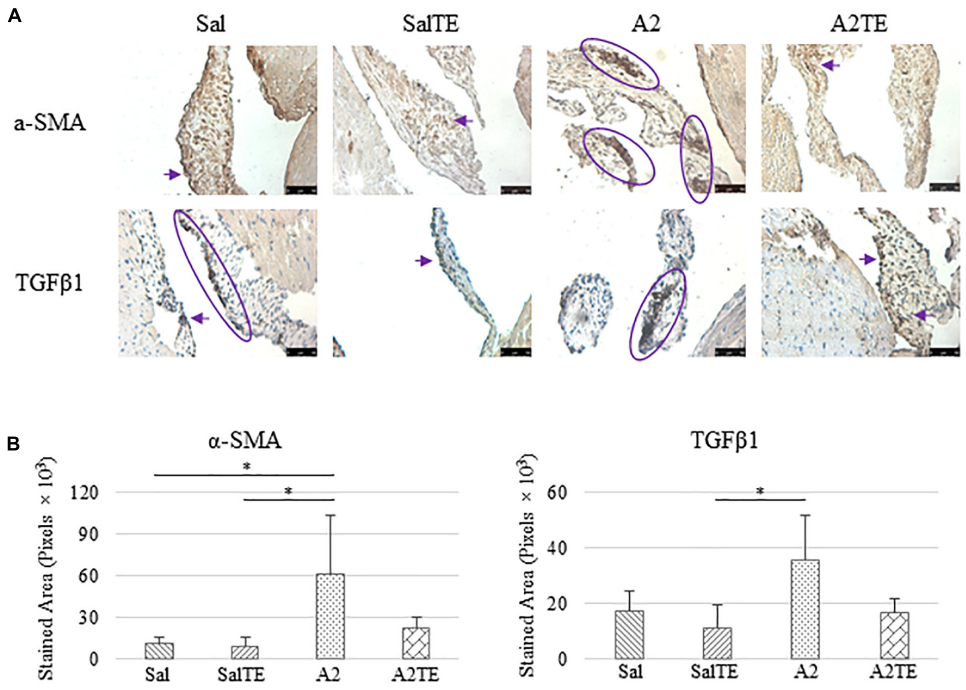

FIGURE 6
(A) Investigation of mitral valve VIC activation by IHC examinations on α-SMA and TGFβ1 in prevention study. Major positive IHC stains were highlighted by circles and arrows. Scale bar: 50 μm. **(B)** Quantification of their expression determined by total stained area in pixels that measured from 4 biological replicates in MATLAB. Asterisk indicates significant difference ($p < 0.05$).

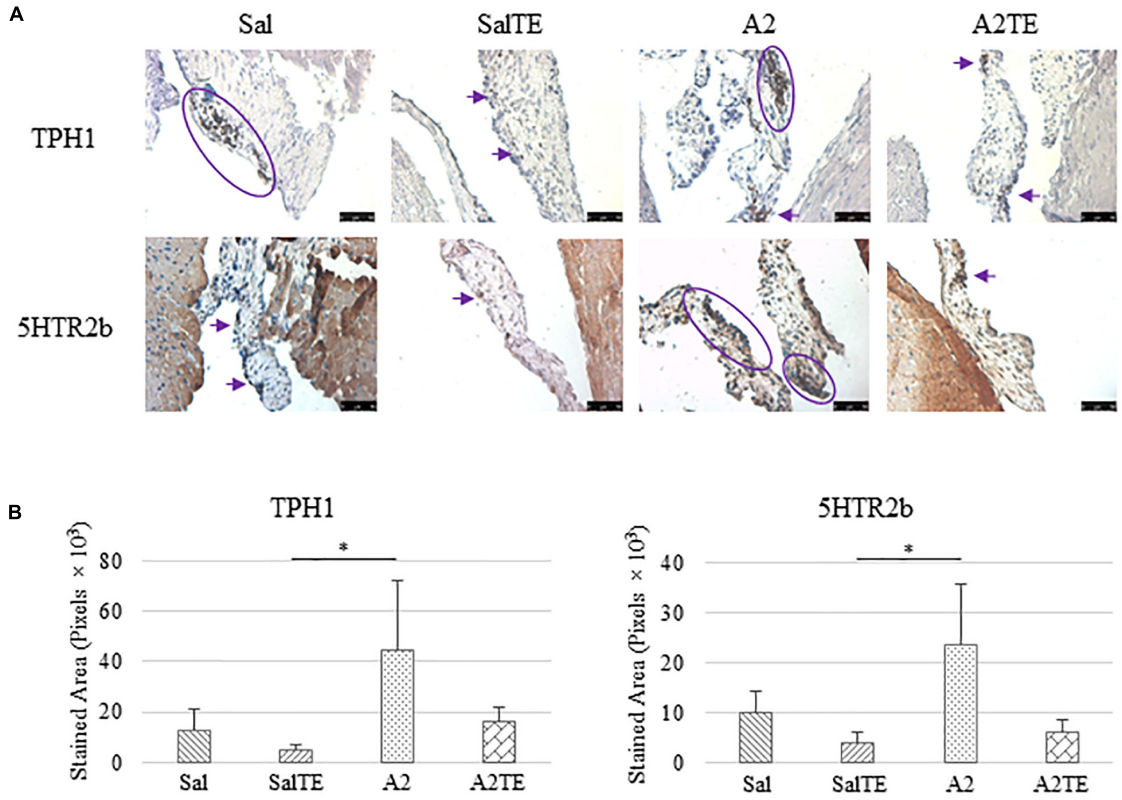

FIGURE 7
(A) Investigation of local serotonin signaling in mitral valve by IHC examinations on TPH1 and 5HTR2b in prevention study. Major positive IHC stains were highlighted by circles and arrows. Scale bar: 50 μm. **(B)** Quantification of their expression determined by total stained area in pixels that measured from 4 biological replicates in MATLAB. Asterisk indicates significant difference ($p < 0.05$).

Myxomatous changes on mitral valves were observed in hypertensive mice, and reversed by a late telotristat ethyl administration

Consistently with the observations from the prevention study, the reversal study showed that proteoglycans accumulated in A2-treated mitral valves, as suggested by a higher density of greenish blue stain (**Figure 8A**), and this was effectively reversed by a 2-week late administration of TE. As before, MMP1, α-SMA, TGFβ1, TPH1, and 5HTR2b were assessed in mitral valves obtained from the reversal study. In general, they all presented similar trends as those observed from the prevention study. MMP1 (**Figures 8A,B**) expression was higher in hypertensive than normotensive mice, and in both cases, TE decreased MMP1 expression. α-SMA and TGFβ1 (**Figures 9A,B**) levels were significantly increased by A2, and these trends were reversed by TE. Also in agreement with the prevention study, TPH1 and 5HTR2b (**Figures 10A,B**) expression levels in mitral valves were always higher in hypertensive mice, but decreased upon TE administration. In addition to the significant changes on myxomatous proteins, mitral valves were significantly thickened by A2, compared to those from normotensive animals (**Supplementary Figure 2B**). The major finding from the reversal study is that ECM proteoglycans and all protein markers were overproduced in mitral valves of hypertensive mice, and these changes were at least partially reversed by a 2-week late TE administration.

Discussion

Angiotensin II has been known to induce hypertension in mice and its effect has been validated in several studies (24, 25). Our goal was to employ this model as an inducer of myxomatous disease and use it as a tool to uncover the role of serotonin in myxomatous mitral disease. Previously, hypertension was been successfully induced *via* chronic systemic A2 infusion in mice with mitral valves presenting myxomatous changes (26). Additional indirect evidence suggested that A2 is a contributor to the progress of myxomatous mitral disease (27, 28). The SBP reported for C57BL/6J at age 8–14 weeks, is 120 mmHg, (29) which is comparable to our experimental results.

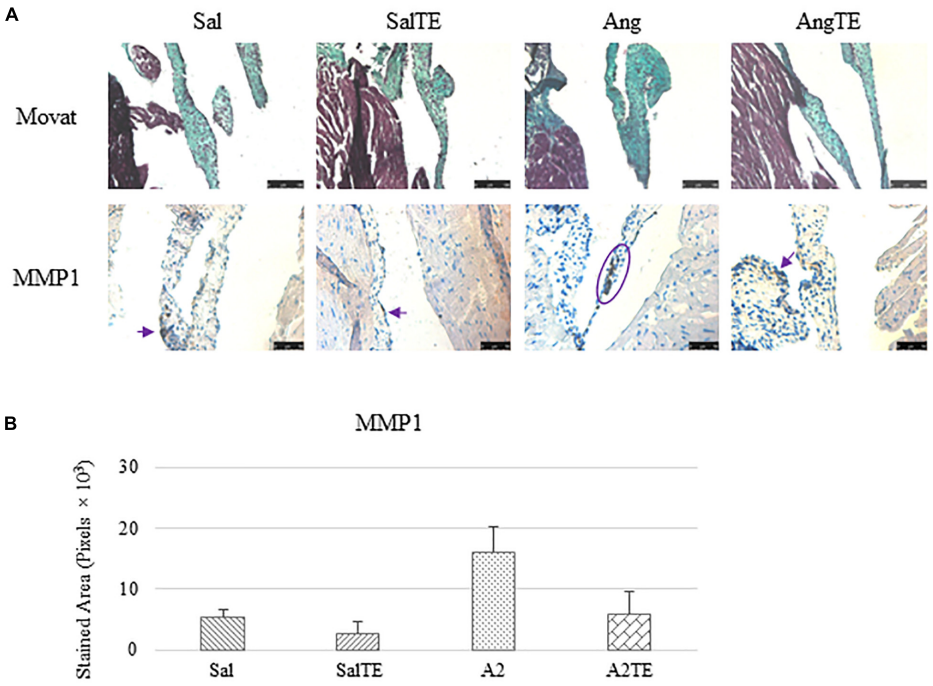

FIGURE 8
(A) Investigation of mitral valve ECM remodeling by Movat stain and MMP1 IHC in reversal study. Major positive IHC stains were highlighted by circles and arrows. Scale bar on Movat images: 100 μm. Scale bar on IHC images: 50 μm. **(B)** Quantification of MMP1 expression was determined by total stained area in pixels that measured from 4 biological replicates in MATLAB. Asterisk indicates significant difference ($p < 0.05$).

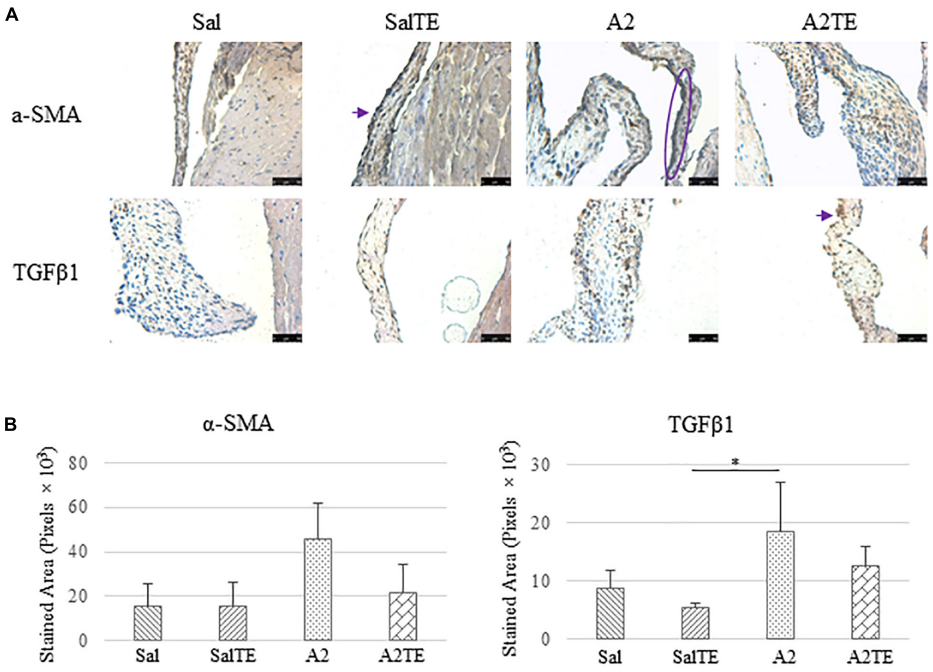

FIGURE 9
(A) Investigation of mitral valve VIC activation by IHC examinations on α-SMA and TGFβ1 in reversal study. Major positive IHC stains were highlighted by circles and arrows. Scale bar: 50 μm. **(B)** Quantification of their expression determined by total stained area in pixels that measured from 4 biological replicates in MATLAB. Asterisk indicates significant difference ($p < 0.05$).

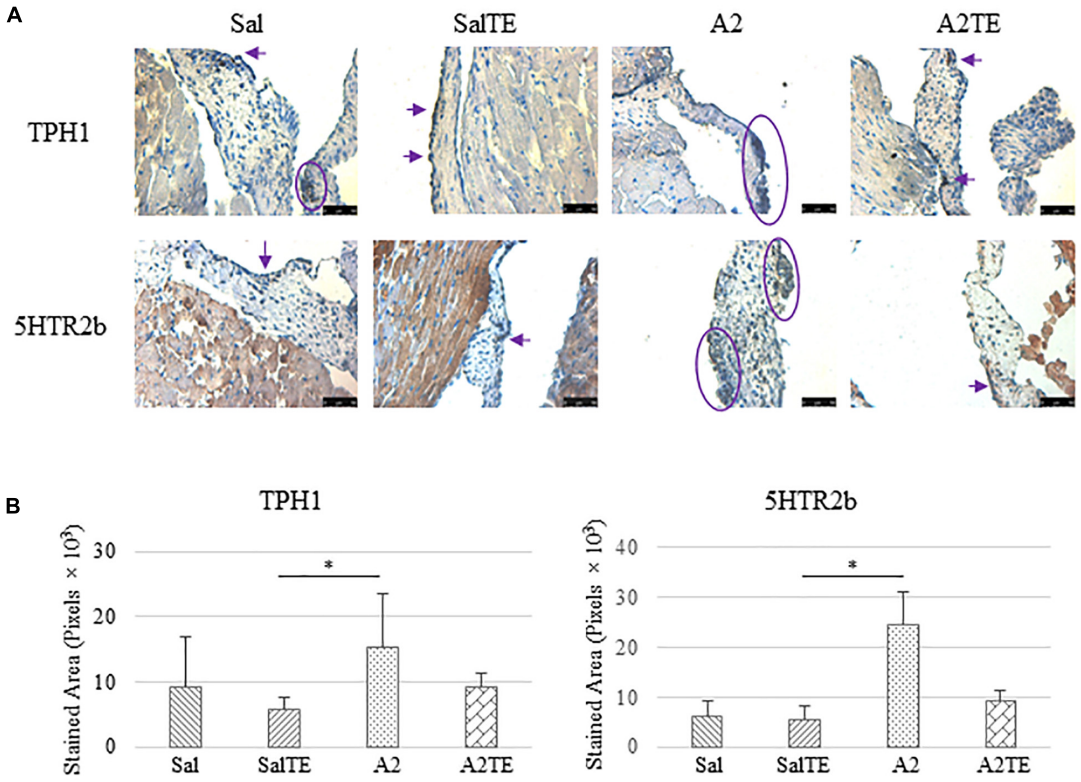

FIGURE 10
(A) Investigation of local serotonin signaling in mitral valve by IHC examinations on TPH1 and 5HTR2b in reversal study. Major positive IHC stains were highlighted by circles and arrows. Scale bar: 50 μm. **(B)** Quantification of their expression determined by total stained area in pixels that measured from 4 biological replicates in MATLAB. Asterisk indicates significant difference ($p < 0.05$).

It has been demonstrated that blood pressure increases with age in mice, as it does in humans (30–32). In both studies presented here, TE administration seemed to curb the effect of A2 on blood pressure, while maintaining the blood pressure of normotensive animals. Moreover, females were more responsive to TE effect on blood pressure reduction, which might be a consequence of higher dose of TE due to lower body weight. Several lines of evidence demonstrated that high levels of circulating serotonin upregulates blood pressure, due to its contractile effect on vascular smooth muscle cells (33, 34). This could explain why lower serotonin (due to TE administration) counteracted A2-induced hypertension in mice. However, this TE-induced blood pressure drop was not observed in humans, when TE was studied as a treatment for carcinoid syndrome (22).

Currently, there is limited evidence showing the alteration of circulating serotonin level in hypertensive subjects. Blood samples collected from hypertensive and normotensive human showed no significant difference on serotonin levels (35). Additional studies implied that the correlation between blood serotonin and hypertension still remains controversial (36, 37). In our work, serotonin was downregulated by TE administration in both hypertensive and normotensive mice. The decrease in serotonin in hypertensive mice may be due to the interplay between serotonin and A2, which might not happen to the same extent in clinical systemic hypertension. It has been suggested that serotonin level was reduced in platelets while elevated in plasma in hypertensive mice, although the total content in the blood remained constant (38). In agreement with this, human studies proposed that platelet serotonin level decreased with hypertension due to a reduced uptake rate by serotonin transporter (39, 40). A2 administration in rodents was previously reported to significantly promote the level of 5-hydroxyindoleacetic acid, a serotonin metabolite (41), indicating that A2 accelerates serotonin metabolism, which could potentially explain the differences in serotonin levels measured throughout our treatments groups.

In addition to A2, the alteration of circulating serotonin in hypertensive mice could be due to myxomatous mitral remodeling, although serotonin synthesized by heart valve leaflets may be too low compared to the amount carried by platelets. However, it is still debated how circulating serotonin is affected by myxomatous changes due to variable experimental and clinical evidence. Higher plasma serotonin level was identified in dogs with degenerative mitral valve disease (17). However, this is in disagreement with another study, where

plasma serotonin remained unchanged between healthy dogs and those with myxomatous mitral degeneration while platelet serotonin was elevated in dogs with myxomatous mitral disease and part of healthy dogs (18). On another study, both plasma and platelet serotonin levels were unchanged in dogs with myxomatous mitral degeneration compared to healthy ones (19), although local serotonin in mitral valves was a well-established regulator of myxomatous changes (5, 18). Based on these current observations from dogs, it seems that the correlation of circulating serotonin and myxomatous mitral disease is highly case- and breed-dependent, which might be also the case in mice. More importantly, the presence of A2 amplified the inhibitory effect of TE on serotonin. To the best of our knowledge, this is the first study identifying the synergistic effect of A2 and TE on circulating serotonin in a hypertensive animal model, although the changes of circulating serotonin with hypertension and myxomatous disease were independently studied previously.

The extent of proteoglycan stain appeared increased in hypertensive mice, despite rodent leaflets not showing the classic valvular architecture (42). The overproduction of proteoglycans in myxomatous mitral valves has been frequently observed in other animal and human studies (43–45), and this change is marked as a characteristic of myxomatous degeneration. Along with proteoglycan accumulation, it has been demonstrated that elastin content is upregulated in myxomatous mitral valve (45), whereas this was not clearly observed in this study, potentially due to its form of diffuse fragmentation. Therefore, we believe that myxomatous remodeling on mitral valves was successfully initiated in hypertensive mice, and restricted by TE administration.

The effects of serotonin, A2 and their combination on heart valves were studied previously in mice, where both *in vivo* and *in vitro* models were recruited (46). In their study, either serotonin or A2 administration elevated blood pressure and contributed to valve thickening, ECM remodeling and myofibroblastic transformation. In addition, their combination synergistically enhanced these changes. These evidence supports our observations from mitral valves that received A2. Beyond the agreement with previous findings, our study discovered a novel strategy for prevention or reversal of myxomatous mitral disease by selectively inhibiting peripheral serotonin. According to the results from the current study and previous ones, myxomatous markers are tightly regulated by peripheral serotonin.

It has been previously reported that phenotype transformation preferably affects the atrialis layer in the early phase of naturally occurring myxomatous mitral degeneration and ventricularis layer in serotonergic valves (45, 47). In line with previous suggestions, plaques with positive α-SMA expression were only identified in mitral valves of hypertensive mice, with a higher incidence on the atrialis edge. However, the area of α-SMA-positive stains was vastly reduced in mitral valves of hypertensive mice that received TE administration. In this case, VIC activation in mitral valves is regulated by serotonin, as proposed in another study (20). Along with the overexpression of serotonin signaling proteins, TGFβ1 as well as its receptors are elevated in myxomatous mitral valves, as supported by several studies (5, 48). On the other hand, TGFβ1 cooperated with mechanical stimuli and contributed to the progress of myxomatous changes (49), consistently with the observation of TGFβ1 increase in hypertensive mice. Most importantly, these myxomatous changes were reversed upon TE administration, indicating A2-induced myxomatous degeneration is mediated by serotonin signals.

It has been proposed that serotonin signals regulate myxomatous mitral valve degeneration and cross-talks with multiple other signaling pathways such as TGFβ (5). There may be two sources of serotonin acting upon heart valves, and these are circulating serotonin from blood and locally synthesized by heart valve cells (44). As discussed above, the exact link between serotonin and myxomatous mitral degeneration is still missing, although serotonin level in blood decreased with hypertension-induced myxomatous changes in this mouse model. Local serotonin signaling was evaluated by expression of its synthetic enzyme (TPH1) and receptor (5HTR2b) on mitral valves. Both proteins were increased in hypertensive mice, and at least partially diminished due to TE administration. These findings are supported by *in vitro* studies, where TPH1 and 5HTR2b were shown upregulated in spontaneous and mechanically induced myxomatous mitral degeneration (15, 20, 21, 50). The overexpression of serotonin proteins by A2 indicates that the activation of serotonin signaling along with VIC activation. Conversely, low serotonin due to TE administration relieves the need for receptor expression, and subsequently reduces the requirement for an expanded serotonin signaling machinery. This is the potential principle by which TE reverses myxomatous changes and prevents phenotype transformation from quiescent VICs to activated VICs.

Limitations of this experimental design include no dose response studies, inability to deliver TE locally, among other technical challenges. First, TE was only studied at a dose of 300 mg/kg previously validated in mice. In addition, the dose received by each animal is slightly variable due to the changes in body weight. Second, fluctuations in blood pressures indicate that A2 delivery by ALZET pumps may not always have been at a constant rate. Third, valve thicknesses were measured at the base of the leaflets on histological sections, which relies on perpendicular embedding of the valve leaflet. This is not only an experimental challenge, but it also means that the free edges of the leaflets, potentially containing most of the remodeled areas, were not measured due to potential embedding inaccuracies. Next, the mouse model was chosen as a basis of comparison for future studies with genetic models, but more conclusive experimentation is needed with larger animals. Finally, it is unclear how TE is distributed in the bloodstream to inhibit

serotonin synthesis locally on valve leaflets. Drug delivery strategies will be needed to complement our current results. Despite these limitations, the studies presented here were able to show that VIC phenotypic transformation, serotonin signaling activation, ECM remodeling and TGFβ1 overexpression were triggered by A2-induced hypertension in mice, and in turn, these pathological changes could be reversed by inhibiting serotonin synthesis.

Conclusion

This is the first *in vivo* model comprehensively studying the link between serotonin and myxomatous mitral valve disease, as well as uncovering the regulatory role of serotonin on myxomatous valvular disease. Myxomatous changes were successfully recapitulated in a hypertensive mouse model, as determined by ECM remodeling, myofibroblast transformation, serotonin synthesis, and TGFβ1 overexpression. Most importantly, the progress of myxomatous changes on mitral valves could be arrested upon serotonin inhibition by TE, which was effective in both modes of parallel and late administration. This study identifies a potential treatment for myxomatous mitral valve disease.

Data availability statement

The original contributions presented in this study are publicly available. This data can be found here: https://www.dropbox.com/sh/waqlanzzfkbnq0y/AADGRf704R6WefrVKjWfGLMOa?dl=0.

Ethics statement

The animal study was reviewed and approved by the Texas Tech University IACUC.

Author contributions

XW: conceptualization and design, investigation, data collection, data analysis and interpretation, and manuscript writing. DK-J and PL: conceptualization and design and financial support. CL: conceptualization and design, investigation, data collection, financial support, data analysis and interpretation, manuscript review and editing, final approval of the manuscript, and project administration. All authors contributed to the article and approved the submitted version.

Funding

This work was fully funded by a Lexicon Pharmaceuticals Investigator-Initiated Study contracted to Texas Tech University.

Acknowledgments

We acknowledged Animal Care Services at Texas Tech University for their support and assistance on animal maintenance during acclimation and subcutaneous implantation surgery preparation.

Conflict of interest

DK-J and PL were employed by Lexicon Pharmaceuticals. Lexicon Pharmaceuticals is the company that released telotristat ethyl for treatment of other serotonin diseases and is interested in evaluating its potential to treat valvular diseases.

The remaining authors declare that the research was conducted in the absence of any commercial or financial relationships that could be construed as a potential conflict of interest.

Publisher's note

Supplementary material

The Supplementary Material for this article can be found online at: https://www.frontiersin.org/articles/10.3389/fcvm.2022.945672/full#supplementary-material

SUPPLEMENTARY FIGURE 1
Monitor of animal weight in prevention **(A)** and reversal **(B)** studies. Asterisk indicates significant difference ($p < 0.05$).

SUPPLEMENTARY FIGURE 2
Comparison of mitral valve thicknesses, as at the base of the leaflets, across treatments in prevention **(A)** and reversal **(B)** studies. Asterisk indicates significant difference ($p < 0.05$).

References

1. Benjamin EJ, Muntner P, Alonso A, Bittencourt MS, Callaway CW, Carson AP, et al. Heart disease and stroke statistics—2019 update: A report from the American heart association. *Circulation.* (2019) 139:e56–528. doi: 10.1161/CIR.0000000000000659

2. Salhiyyah K, Yacoub MH, Chester AH. Cellular mechanisms in mitral valve disease. *J Cardiovasc Transl Res.* (2011) 4:702–9. doi: 10.1007/s12265-011-9318-7

3. Liu AC, Joag VR, Gotlieb AI. The emerging role of valve interstitial cell phenotypes in regulating heart valve pathobiology. *Am J Pathol.* (2007) 171:1407–18. doi: 10.2353/ajpath.2007.070251

4. Hinton RB, Yutzey KE. Heart valve structure and function in development and disease. *Annu Rev Physiol.* (2011) 73:29–46. doi: 10.1146/annurev-physiol-012110-142145

5. Orton EC, Lacerda CMR, MacLea HB. Signaling pathways in mitral valve degeneration. *J Vet Cardiol.* (2012) 14:7–17. doi: 10.1016/j.jvc.2011.12.001

6. Wang X, Lee J, Ali M, Kim J, Lacerda CMR. Phenotype transformation of aortic valve interstitial cells due to applied shear stresses within a microfluidic chip. *Ann Biomed Eng.* (2017) 45:2269–80. doi: 10.1007/s10439-017-1871-z

7. Fox DJ, Khattar RS. Carcinoid heart disease: Presentation, diagnosis, and management. *Heart.* (2004) 90:1224–8. doi: 10.1136/hrt.2004.040329

8. Grozinsky-Glasberg S, Grossman AB, Gross DJ. Carcinoid heart disease: From pathophysiology to treatment - "something in the way it moves". *Neuroendocrinology.* (2015) 101:263–73. doi: 10.1159/000381930

9. Pellikka PA, Tajik AJ, Khandheria BK, Seward JB, Callahan JA. Carcinoid heart disease. Clinical and echocardiographic spectrum in 74 patients. *Circulation.* (1993) 87:1188–96. doi: 10.1161/01.cir.87.4.1188

10. Jian B, Xu J, Connolly J, Savani RC, Narula N, Liang B, et al. Serotonin mechanisms in heart valve disease I: Serotonin-induced up-regulation of transforming growth factor-beta1 via G-protein signal transduction in aortic valve interstitial cells. *Am J Pathol.* (2002) 161:2111–21. doi: 10.1016/s0002-9440(10)64489-6

11. Gustafsson BI, Tømmerås K, Nordrum I, Loennechen JP, Brunsvik A, Solligård E, et al. Long-term serotonin administration induces heart valve disease in rats. *Circulation.* (2005) 111:1517–22. doi: 10.1161/01.CIR.0000159356.42064.48

12. Connolly JM, Bakay MA, Fulmer JT, Gorman RC, Gorman JH III, Oyama MA, et al. Fenfluramine disrupts the mitral valve interstitial cell response to serotonin. *Am J Pathol.* (2009) 175:988–97. doi: 10.2353/ajpath.2009.081101

13. Rothman RB, Baumann MH. Serotonergic drugs and valvular heart disease. *Expert Opin Drug Saf.* (2009) 8:317–29. doi: 10.1517/14740330902931524

14. Hutcheson JD, Setola V, Roth BL, Merryman WD. Serotonin receptors and heart valve disease-It was meant 2B. *Pharmacol Ther.* (2011) 132:146–57. doi: 10.1016/j.pharmthera.2011.03.008

15. Disatian S, Lacerda CMR, Orton EC. Tryptophan hydroxylase 1 expression is increased in phenotype-altered canine and human degenerative myxomatous mitral valves. *J Heart Valve Dis.* (2010) 19:71–8.

16. Disatian S, Orton EC. Autocrine serotonin and transforming growth factor beta 1 signaling mediates spontaneous myxomatous mitral valve disease. *J Heart Valve Dis.* (2009) 18:44–51.

17. Arndt JW, Reynolds CA, Singletary GE, Connolly JM, Levy RJ, Oyama MA. Serum serotonin concentrations in dogs with degenerative mitral valve disease. *J Vet Intern Med.* (2009) 23:1208–13. doi: 10.1111/j.1939-1676.2009.0378.x

18. Cremer SE, Singletary GE, Olsen LH, Wallace K, Häggström J, Ljungvall I, et al. Serotonin concentrations in platelets, plasma, mitral valve leaflet, and left ventricular myocardial tissue in dogs with myxomatous mitral valve disease. *J Vet Intern Med.* (2014) 28:1534–40. doi: 10.1111/jvim.12420

19. Mangklabruks T, Surachetpong SD. Plasma and platelet serotonin concentrations in healthy dogs and dogs with myxomatous mitral valve disease. *J Vet Cardiol.* (2014) 16:155–62. doi: 10.1016/j.jvc.2014.05.003

20. Lacerda CMR, Kisiday J, Johnson B, Orton EC. Local serotonin mediates cyclic strain-induced phenotype transformation, matrix degradation, and glycosaminoglycan synthesis in cultured sheep mitral valves. *Am J Physiol Heart Circ Physiol.* (2012) 302:H1983–90. doi: 10.1152/ajpheart.00987.2011

21. Lacerda CMR, Maclea HB, Duncana CG, Kisidaya JD, Christopher Ortona E. Human myxomatous mitral valves exhibit focal expression of cartilage-related proteins. *J Hypertens Cardiol.* (2012) 1:21–30.

22. Kulke MH, Hörsch D, Caplin ME, Anthony LB, Bergsland E, Öberg K, et al. Telotristat ethyl, a tryptophan hydroxylase inhibitor for the treatment of carcinoid syndrome. *J Clin Oncol.* (2017) 35:14–23. doi: 10.1200/JCO.2016.69.2780

23. Wawrzyniak R, Kosnowska A, Macioszek S, Bartoszewski R, Jan Markuszewski M. New plasma preparation approach to enrich metabolome coverage in untargeted metabolomics: Plasma protein bound hydrophobic metabolite release with proteinase K. *Sci Rep.* (2018) 8:9541. doi: 10.1038/s41598-018-27983-0

24. Xue B, Pamidimukkala J, Hay M. Sex differences in the development of angiotensin II-induced hypertension in conscious mice. *Am J Physiol Heart Circu Physiol.* (2004) 288:H2177–84. doi: 10.1152/ajpheart.00969.2004

25. Gletsu N, Doan TN, Cole J, Sutliff RL, Bernstein KE. Angiotensin II-induced hypertension in mice caused an increase in insulin secretion. *Vasc Pharmacol.* (2005) 42:83–92. doi: 10.1016/j.vph.2005.01.006

26. Thalji N, Hagler MA, Verzosa GC, Suri RM, Miller JD. Evidence for time-dependent and adaptive mechanisms in the mitral valve following prolonged angiotensin II infusion. *FASEB J.* (2015) 29:764.2.

27. Geirsson A, Singh M, Ali R, Abbas H, Li W, Sanchez JA, et al. Modulation of transforming growth factor- signaling and extracellular matrix production in myxomatous mitral valves by angiotensin II receptor blockers. *Circulation.* (2012) 126:S189–97. doi: 10.1161/circulationaha.111.082610

28. Boudoulas KD, Boudoulas H. Floppy mitral valve (FMV)/mitral valve prolapse (MVP) and the FMV/MVP syndrome: Pathophysiologic mechanisms and pathogenesis of symptoms. *Cardiology.* (2013) 126:69–80. doi: 10.1159/000351094

29. Mattson DL. Comparison of arterial blood pressure in different strains of mice. *Am J Hypertens.* (2001) 14:405–8. doi: 10.1016/S0895-7061(00)01285-1

30. Barsha G, Denton KM, Mirabito Colafella KM. Sex- and age-related differences in arterial pressure and albuminuria in mice. *Biol Sex Differ.* (2016) 7:57. doi: 10.1186/s13293-016-0110-x

31. Wirth A, Wang S, Takefuji M, Tang C, Althoff TF, Schweda F, et al. Age-dependent blood pressure elevation is due to increased vascular smooth muscle tone mediated by G-protein signalling. *Cardiovasc Res.* (2016) 109:131–40. doi: 10.1093/cvr/cvv249

32. Gros R, Van Wert R, You X, Thorin E, Husain M. Effects of age, gender, and blood pressure on myogenic responses of mesenteric arteries from C57BL/6 mice. *Am J Physiol Heart Circ Physiol.* (2017) 282:H380–8. doi: 10.1152/ajpheart.2002.282.1.h380

33. Van Nueten JM, Janssens WJ, Vanhoutte PM. Serotonin and vascular reactivity. *Pharmacol Res Commun.* (1985) 17:585–608.

34. Watts SW, Morrison SF, Davis RP, Barman SM. Serotonin and blood pressure regulation. *Pharmacol Rev.* (2012) 64:359–88. doi: 10.1124/pr.111.004697

35. Missouris CG, Cappuccio FP, Varsamis E, Barron JL, Carr E, Markandu ND, et al. Serotonin and heart rate in hypertensive and normotensive subjects. *Am Heart J.* (1998) 135:838–43. doi: 10.1016/S0002-8703(98)70043-2

36. Kerr PG, Argiles A, Charles M. Whole blood serotonin levels are markedly elevated in patients on dialytic therapy. *Am J Nephrol.* (1992) 12:14–8. doi: 10.1159/000168411

37. Watts SW, Davis RP. 5-Hydroxtryptamine receptors in systemic hypertension: An arterial focus. *Cardiovasc Ther.* (2011) 29:54–67. doi: 10.1111/j.1755-5922.2010.00173.x

38. Singh P, Fletcher TW, Li Y, Rusch NJ, Kilic F. Serotonin uptake rates in platelets from angiotensin II-induced hypertensive mice. *Health.* (2013) 05:31–9. doi: 10.4236/health.2013.54a005

39. Guicheney P, Baudouin-Legros M, Valtier D, Meyer P. Reduced serotonin content and uptake in platelets from patients with essential hypertension : Is a ouabain-like factor involved?. *Thromb Res.* (1987) 45:289–97. doi: 10.1016/0049-3848(87)90218-0

40. Ding YA, Chou TC, Huan R. Are platelet cytosolic free calcium, serotonin concentration and blood viscosity different between hypertensive and normotensive subjects?. *Cardiology.* (1994) 85:76–81. doi: 10.1159/000176650

41. Medelsohn FAO, Jenkins TA, Berkovic SF. Effects of angiotensin II on dopamine and serotonin turnover in the striatum of conscious rats. *Brain Res.* (1993) 613:221–9. doi: 10.1016/0006-8993(93)90902-Y

42. Rabkin E, Aikawa M, Stone JR, Fukumoto Y, Libby P, Schoen FJ, et al. Activated interstitial myofibroblasts express catabolic enzymes and mediate matrix remodeling in myxomatous heart valves. *Circulation.* (2001) 104:2525–32. doi: 10.1161/hc4601.099489

43. Elangbam CS, Wehe JG, Barton JC, Krull DL, Nyska A, Crabbs T, et al. Evaluation of glycosaminoglycans content and 5-hydroxytryptamine 2B receptor in the heart valves of Sprague-Dawley rats with spontaneous mitral valvulopathy - A possible exacerbation by dl-amphetamine sulfate in Fischer 344 rats?. *Exp Toxicol Pathol.* (2006) 58:89–99. doi: 10.1016/j.etp.2006.08.001

44. Lacerda CMR, MacLea HB, Kisiday JD, Orton EC. Static and cyclic tensile strain induce myxomatous effector proteins and serotonin in canine mitral valves. *J Vet Cardiol.* (2012) 14:223–30. doi: 10.1016/j.jvc.2011.12.002

45. Connell PS, Han RI, Grande-Allen KJ. Differentiating the aging of the mitral valve from human and canine myxomatous degeneration. *J Vet Cardiol.* (2012) 14:31–45. doi: 10.1016/j.jvc.2011.11.003

46. Perez J, Diaz N, Tandon I, Plate R, Martindale C, Balachandran K. Elevated serotonin interacts with angiotensin-ii to result in altered valve interstitial cell contractility and remodeling. *Cardiovasc Eng Technol.* (2018) 9:168–80.

47. Disatian S, Ehrhart EJ III, Zimmerman S, Orton EC. Interstitial cells from dogs with naturally occurring myxomatous mitral valve disease undergo phenotype transformation. *J Heart Valve Dis.* (2008) 17:402–11.

48. Hagler MA, Hadley TM, Zhang H, Mehra K, Roos CM, Schaff HV, et al. TGF-β signalling and reactive oxygen species drive fibrosis and matrix remodelling in myxomatous mitral valves. *Cardiovasc Res.* (2013) 99:175–84. doi: 10.1093/cvr/cvt083

49. Merryman WD, Lukoff HD, Long RA, Engelmayr GC Jr., Hopkins RA, Sacks MS. Synergistic effects of cyclic tension and transforming growth factor-β1 on the aortic valve myofibroblast. *Cardiovasc Pathol.* (2007) 16:268–76. doi: 10.1016/j.carpath.2007.03.006

50. Driesbaugh KH, Branchetti E, Grau JB, Keeney SJ, Glass K, Oyama MA, et al. Serotonin receptor 2B signaling with interstitial cell activation and leaflet remodeling in degenerative mitral regurgitation. *J Mol Cell Cardiol.* (2018) 115:94–103. doi: 10.1016/j.yjmcc.2017.12.014

frontiers | Frontiers in Cardiovascular Medicine

TYPE Original Research
PUBLISHED 12 September 2022
DOI 10.3389/fcvm.2022.971802

OPEN ACCESS

EDITED BY
Elena Aikawa,
Brigham and Women's Hospital and Harvard Medical School, United States

REVIEWED BY
Ishita Tandon,
University of Arkansas, United States
Adrien Lupieri,
Brigham and Women's Hospital and Harvard Medical School, United States

*CORRESPONDENCE
Natalia López-Andrés
natalia.lopez.andres@navarra.es
Eva Jover
eva.jover.garcia@navarra.es

†These authors have contributed equally to this work and share first authorship

‡These authors have contributed equally to this work and share last authorship

SPECIALTY SECTION
This article was submitted to Heart Valve Disease, a section of the journal Frontiers in Cardiovascular Medicine

RECEIVED 17 June 2022
ACCEPTED 11 August 2022
PUBLISHED 12 September 2022

CITATION
Matilla L, Martín-Núñez E, Garaikoetxea M, Navarro A, Vico JA, Arrieta V, García-Peña A, Fernández-Celis A, Gainza A, Álvarez V, Sádaba R, López-Andrés N and Jover E (2022) Characterization of the sex-specific pattern of angiogenesis and lymphangiogenesis in aortic stenosis.
Front. Cardiovasc. Med. 9:971802.
doi: 10.3389/fcvm.2022.971802

Characterization of the sex-specific pattern of angiogenesis and lymphangiogenesis in aortic stenosis

Lara Matilla†, Ernesto Martín-Núñez†, Mattie Garaikoetxea, Adela Navarro, Julieta Anabela Vico, Vanessa Arrieta, Amaia García-Peña, Amaya Fernández-Celis, Alicia Gainza, Virginia Álvarez, Rafael Sádaba, Natalia López-Andrés*‡ and Eva Jover*‡

Cardiovascular Translational Research, Navarrabiomed, Hospital Universitario de Navarra (HUN), Universidad Pública de Navarra (UPNA), IdiSNA, Pamplona, Spain

Objective: We aim to analyze sex-related differences in angiogenesis and lymphangiogenesis in aortic valves (AVs) and valve interstitial cells (VICs) from aortic stenosis (AS) patients.

Approach and Results: Totally 230 patients (59% men) with severe AS undergoing surgical valve replacement were recruited. The density of total neovessels was higher in AVs from men as compared to women. Both small and medium neovessels were more abundant in men's AVs. Accordingly, male AVs exhibited higher CD31 and VE-cadherin expressions. The levels of the pro-angiogenic markers, such as vascular endothelial growth factor (VEGF)-A, VEGF receptor (VEGFR)1, VEGFR2, insulin-like growth factor-binding protein-2 (IGFBP-2), interleukin (IL)-8, chemerin, and fibroblast growth factor (FGF)-7, were increased in AVs from men. Transforming growth factor-β expression was higher in male AVs. The expression of antiangiogenic molecules thrombospondin (Tsp)-1, endostatin, and CD36 was upregulated in male AVs, although the levels of Tsp-2, IL-4, IL-12p70, and chondromodulin-1 were similar between both sexes. The number of lymphatic vessels and the expression of the lymphangiogenic markers Lyve-1 and D2-40 was higher in men's AV as well as VEGF-C, VEGF-D, and VEGFR3. Multivariate analyses adjusted for confounders further validated the sex-dependent expression of these targets. VICs isolated from men's AVs secreted higher amounts of the pro-angiogenic factors, VEGF-A, VEGFR1, IGFBP-2, and FGF-7, as well as the pro-lymphangiogenic factors, VEGF-C, VEGF-D, and VEGFR3, than women without changes in antiangiogenic markers.

Conclusion: Our data show that aberrant angiogenic and lymphangiogenic cues are over-represented in male AVs. Importantly, the VIC is a relevant source

10.3389/fcvm.2022.971802

of multiple morphogens involved in angiogenesis and lymphangiogenesis likely endowing the AV of men with the predominant calcific AS phenotypes.

KEYWORDS

aortic stenosis, sex, valve interstitial cells, angiogenesis, lymphangiogenesis

Highlights

- Angiogenesis and lymphangiogenesis processes are different in men and women with AS, being over-represented in men.
- AVs from men presented a higher density of blood and lymphatic vessels accompanied by higher expression of pro-angiogenic and lymphatic factors, while in women angiogenesis might result from the downregulation of physiologic angiogenic inhibitors.
- VICs are a relevant source of pro-angiogenic and lymphangiogenic molecules, especially in men.

Introduction

Aortic stenosis (AS) is a major health problem that affects 2 to 7% of individuals older than 65 years (1). There are currently no pharmacological strategies to prevent, delay, or reverse AS (2). Inflammation, fibrosis, apoptosis, calcification, and angiogenesis are fundamental to the progression of AS and endow the aortic valve (AV) with fibro-calcific phenotypes (3). AS is more prevalent in men, and recent evidence shows clear sex-specific differences in clinical presentation and patient management (4, 5). We have recently described that for the same AS severity, AVs and valve interstitial cells (VICs) from men presented more inflammation, apoptosis, calcification, and diminished extracellular matrix remodeling than AVs and VICs from women (6).

The pathophysiological role of angiogenesis and lymphangiogenesis in AS remains unknown. Valve avascularity is seemly abrogated in AS (7) and the extent of neovascularization is well-correlated with the burden of the disease (8, 9). Angiogenic factors have been found to co-localize with osteopontin and osteocalcin in the late stage of heavily thickened and calcified atherosclerotic plaques (8, 10). It seems now to become evident that angiogenesis may promote calcific AS (11). Neovascularization is speculated to be a maladaptive response to the extensive valve cusp thickening during fibrosclerotic stages and the enhanced requirements of oxygen supply (12). It might also contribute to perpetuating osteogenesis in advanced calcified AVs similarly to that occurring during endochondral bone formation (13, 14). Contradictory data reveal an association between neovessel formation and inflammation (12, 15). Pro-angiogenic vascular endothelial growth factor (VEGF)-A and its receptors VEGFR1 and VEGFR2 have been associated with inflammation in AS patients (12). However, some recent data suggest that aberrant angiogenesis may instead precede inflammation (15). Furthermore, lymphatic vessels have been detected in AVs from AS patients (16–18). Lymphangiogenic growth factors, such as VEGF-C, VEGF-D, and VEGFR3, are over-expressed in AVs from AS patients (18).

Owing to pericyte-like differentiation, the VIC may support neovascularization in AS (19, 20) but also be a major contributor to the myofibroblast (21) and osteoblast pools (22–24). Interestingly, VICs secrete VEGF-A (3, 20, 25) and are one of the proposed sources of pro-lymphangiogenic factors VEGF-C and VEGF-D and its receptor VEGFR3 (18). Noteworthy, early transcriptomic analyses revealed over-represented angiogenic pathways in male porcine VICs (26). A recent publication has also shown that the angiogenic secretome varies with sex in porcine VICs (27). However, the information about sex-specific differences in angiogenesis and lymphangiogenesis in human AS is scarce and remains understudied. Our work aimed to provide a thorough descriptive characterization of sex-related angiogenic and lymphangiogenic signatures in patients with AS. To that, histological, molecular, and cellular approaches have been employed.

Abbreviations: AS, aortic stenosis; AU, arbitrary units; AV, aortic valve; BMP, bone morphogenetic protein; CCL2, C-C motif chemokine ligand 2; Chm-1, chondromodulin-1; ERG, erythroblast transformation-specific related gene; FBS, fetal bovine serum; FGF, fibroblast growth factor; IL, interleukin; IGFBP-2, insulin-like growth factor-binding protein-2; TGF-β, tissue growth factor-beta; Tsp, thrombospondin; VEGF, vascular endothelial growth factor; VEC, valve endothelial cell; VIC, valve interstitial cell; WB, western blot.

Materials and methods

Clinical cohort

This study, prospective and observational, involved a total of 230 patients with severe AS (28) referred to Hospital Universitario de Navarra for surgical AV replacement from June 2013 to October 2020. AS was defined as AV area ≤ 1 cm^2 and/or transaortic mean pressure gradient > 40 mm Hg. The presence of moderate or severe concomitant valvular disease, malignant tumor, infective endocarditis, diabetes mellitus, and chronic inflammatory diseases were exclusion criteria for the study.

All patients were evaluated by transthoracic echocardiography. Venous blood was drawn on admission for surgery for Measurement of brain natriuretic peptide (BNP) and other routine laboratory parameters.

Informed consent was obtained from each patient. The study protocol conforms to the ethical guidelines of the 1975 Declaration of Helsinki as reflected in a previous approval by the institution's human research committee (Comité Ético de Experimentación Clínica. Gobierno de Navarra, Departamento de Salud; Ethics numbers 17/2013 and PI2019/59).

AV leaflets harvested from AS patients were dissected into three pieces. One "healthier" part was dedicated to VICs isolation ($n = 26$) to guarantee the *in vitro* viability and expansion of the VICs with physiologic-like phenotypes; another one was paraffin-embedded and the last one was used for protein and RNA extractions. The dissection of the samples dedicated to molecular and histological analyses ($n = 230$) was aimed to get equal parts of the leaflet/s with comparable amounts of calcific, fibrotic, and "healthy" tissue to avoid biasing ulterior analyses. Different remodeling or pathological processes have been described depending on the location of the leaflet (e.g., different mechanobiological stimulation) during the progression of the AS. Accordingly, no independent leaflets were used for different purposes. Moreover, all AVs were processed and analyzed without knowing the sex of the donor to avoid biased results.

Cell isolation and culture

Human VICs were isolated from 26 AVs (14 men and 12 women from the whole cohort of 230 AVs processed in this manuscript) obtained during surgical AV replacement. VICs from each patient were isolated and individually assayed, as previously described (29). In brief, AVs were minced and enzymatically digested with buffered-collagenase type 2 (240 U/mg) for 1 h and were pelleted by centrifugation. VICs were cultured in DMEM F-12 medium (Gibco) supplemented with 20% fetal bovine serum (FBS) (Gibco), 1% Penicillin/Streptomycin (Lonza), 5 µg/ml insulin (Sigma Aldrich), and 10 ng/ml of fibroblast growth factor (FGF-2) (Novus Biological) at 37°C and 5% CO_2 in a saturation humidified incubator (Panasonic). This growing media has been adapted from previous publications (30) and allows for the expansion of VICs upon isolation and until reaching the required cell number for further *in vitro* experiments. The VIC phenotype of isolated cells was confirmed by vimentin and alpha-smooth muscle actin (α-SMA) immunocytochemistry. Experiments were performed in serum-starvation conditions (1% FBS) in multiwell plates (Sarstedt) for 2 days. The aim of serum starvation in our experimental settings is three-fold: first, to induce quiescent-like phenotypes of isolated VICs (30); second, to deplete the content of growth factors (such as VEGFs) (31) in FBS that may mask these released by VICs; and third, to deplete the content of potential physiologic inhibitors of ectopic calcification that has been strongly linked to angiogenesis *in vivo* (32).

Histology and immunohistochemistry evaluation

Histological determinations in AVs were performed in 5 µm-thick paraffin-embedded serial sections following the protocol of Leica BOND-Polymer Re-fine Detection automatic immunostainer (Leica). All solutions were filled into the bottle-Bond Open Container (Leica) and registered on a computer using the Leica Biosystem program. The immunostaining program protocol includes fixative solution, bond wash solution, blocking with a common immunohistochemistry blocker, and incubation with the following primary antibodies: CD31 (Santa Cruz Biotechnology), VE-cadherin (Abcam), glycophorin-A (Santa Cruz Biotechnology), CD34 (Santa Cruz Biotechnology), D2-40 (Leica), erythroblast transformation-specific related gene (ERG, Roche), VEGF-A (Santa Cruz Biotechnology), VEGFR3 (Santa Cruz Biotechnology), IGFBP-2, Tsp-1, TGF-β, and Lyve-1 (Santa Cruz Biotechnology). After primary antibody incubation, slides were incubated with secondary poly-HRP-IgG. The signal was revealed by using a DAB substrate. Incubation with no primary antibodies was carried out as negative controls.

AV structure, vessels, and inflammatory infiltrates were visualized by hematoxylin/eosin staining (Panreac/Bio-optica). Total vessels, blood vessels, and lymphatic vessels were counted in 168 AS valves and normalized to the surface (mm^2). For total neovessels, CD31 and VE-cadherin and complementary hematoxylin/eosin staining were used. The presence of blood vessels was assessed in ERG immunostaining and further confirmed by glycophorin-A (detecting erythrocytes) and CD34. Cross-sectional blood vessels were classified according to their size: small (S, with 2 to 3 endothelial cells), medium (M, more than 3 endothelial cells), or hypertrophied (H, with more than 2 to 3 layers of vascular smooth muscle cells), and were normalized to the total number of vessels. Double

Lyve-1 with CD31 and CD34 staining and D2–40 staining was performed to identify and count lymphatic vessels. Lyve-1 positive macrophages were excluded from the lymphatic vessel count as reported by Syvaranta et al. (18). All the counting was performed by two different blinded observers using the different immunohistochemistry profiles to reinforce the results.

Histological and immunohistochemistry preparations were imaged using a bright field in an automated image analysis system (Nikon). In brief, arbitrary fields per section were imaged at 50, 100, 200, or 400X magnification, as appropriate. The whole slide was imaged without knowing the sex of the donor and kept for ulterior batch analyses of the amount and type of vessels. Accordingly, no arbitrary fields were imaged and any digital image quantification has been normalized either to the total number of vessels or to the total area of the histological preparation (mm^2). The most representative images were displayed in the figures along the manuscript.

ELISA

CD31, VE-cadherin, VEGF-A, VEGFR1, VEGFR2, IGFBP2, IL-8, Chemerin, FGF-7, TGF-β, Tsp-1, Tsp-2, IL-4, IL-12p70, endostatin, VEGF-C, VEGF-D, and VEGFR3 were measured in AVs extracts and cells supernatants according to the manufacturer's instructions (R&D Systems). Known yields of total protein were assayed by ELISA. For the study of secretomes, equal volumes of cell supernatants were loaded upon confirming no differences in cell densities (by protein quantification of the corresponding cell monolayers) among biological replicates.

Real-time reverse transcription PCR

Total RNA from cells and AVs was extracted with Trizol Reagent (Canvas). The first-strand of cDNA was synthesized according to the manufacturer's instructions (Bio-Rad). Quantitative PCR analysis was performed with SYBR green PCR technology (Bio-Rad) (Chm-1: Forward-GGAGGAGATG CTCTGTTTGG and Reverse-GGAAATAGACGCTGGG AACA; Lyve-1: Forward-GGTTCCAGTGAGCCGACAGT and Reverse-TGCACGAGTTAGTCCAAGTATCAGA; D2-40: Forward-ACCAGTCACTCCACGGAGAAA and Reverse-GGT CACTGTTGACAAACCATCT). Relative quantification was achieved with MyiQ (Bio-Rad) software according to the manufacturer's instructions. Data were normalized to 18S (Forward: CGCCGCTAGAGGTGAAATTC and Reverse: TCTTGGCAAATGCTTTCGC), HPRT (Forward: TTGCTT TCCTTGGTCAGGCA and Reverse: ATCCAACACTTCG TGGGGTC), β-actin (Forward: GCCGCCAGCTCACCAT and Reverse: TCGATGGGGTACTTCAGGGT), and GADPH (Forward: ACCAGCCCCAGCAAGAGCACAAG and Reverse: TTCAAGGGGTCTACATGGCAACTG) levels, and expressed as fold-change relative to men. All PCRs were performed at least in triplicate for each experimental condition.

Western blot analysis

Aliquots of 10 to 20 μg of total proteins were prepared and electrophoresed from AV extracts on SDS polyacrylamide gels (4–15% polyacrylamide, Mini-PROTEANTGX Stain-Free, BioRad) and transferred to Hybond-C Extra nitrocellulose membranes (BioRad). Membranes were incubated with primary antibodies for CD36 (Santa Cruz Biotechnology) and β-actin (Sigma-Aldrich); and with secondary antibodies for mice and rabbits (GE Healthcare). Blot densitometry analyses were performed using Image Lab software. β-actin and stain free were used as loading controls for normalization and the net band densitometry was expressed as fold changes of arbitrary units (AU). Positive blots were detected with a chemiluminescence method (ECL, Amersham Biosciences) and images acquired with the Chemidoc MP Imaging system (Bio-Rad). All western blots were performed at least in triplicate for each experimental condition. Semiquantitative analyses were performed by band densitometry using the Image Lab software (Bio-Rad).

Statistical analyses

Patients' data were summarized using frequencies and percentages, means, and standard deviations (SD). Data normality were assessed through Shapiro–Wilk's test and the Kolmogorov–Smirnov test (with Lilliefors p-value). Quantitative variables were analyzed by student's t–test or the Mann–Whitney U test if the normality was not met. Univariate linear regressions models were fitted for all continuous variables. Categorical variables were expressed as percentages and compared using the $\chi 2$ test or the Fisher exact test, as appropriate. The effect of sex on demographic, clinical, and analytic-related variables was assessed in two steps. First, univariate linear regressions models were fitted for all continuous variables. Similarly, univariate logistic regression models were used to estimate the odds ratios of categorical variables. These steps allowed us to identify the variables that differed significantly between sexes and that therefore could be potential confounders. To adjust for the potential confounders found by the univariate analyses, a second analysis step was added where the adjusted effect of sex over the analyzed variables was modeled using linear and logistic multivariate regression models, as appropriate. In brief, based on the magnitude of the effect and the p-values calculated in the univariate models, age, statin use, and total cholesterol levels were used as covariates of the multivariate models. For each variable, an adjusted model was fitted to calculate the odds ratio (OR). The absence of multicollinearity was guaranteed by making use of the Variance

TABLE 1 Clinical and demographical data of AS patients.

Variable	Male	Female	Total	*p*–value
N (%)	136 (59)	94 (41)	230	
Age, Mean ± SD	69.7 ± 9.3	73.1 ± 8.4	71.1 ± 9.1	0.003
BMI, Mean ± SD	29.0 ± 4.1	29.2 ± 5.4	29.1 ± 4.7	0.777
DM, *n (%)*	47 (28.8)	28 (25.2)	75 (27.4)	0.581
Renal insufficiency, *n (%)*	9 (5.5)	9 (8.1)	18 (6.6)	0.460
HTA, *n (%)*	115 (70.6)	71 (64.0)	186 (67.9)	0.292
Drug medicines				
ACEI, *n (%)*	39 (24.1)	28 (25.5)	67 (24.6)	0.886
ARB, *n (%)*	45 (27.8)	22 (20.0)	67 (24.6)	0.154
Diuretics, *n (%)*	82 (50.3)	63 (56.8)	145 (52.9)	0.325
β-blockers, *n (%)*	53 (32.5)	29 (26.1)	82 (29.9)	0.284
Statins, *n (%)*	120 (73.6)	54 (48.6)	174 (63.5)	<0.001
Biochemical analyses				
TGAs (mg/dL), Mean ± SD	109.4 ± 63.3	106.0 ± 39.9	108.1 ± 55.1	0.627
Total cholesterol (mg/dL), Mean ± SD	166.8 ± 37.4	190.7 ± 39.7	176.4 ± 40.0	<0.001
Echocardiographic parameters				
Max gradient, Mean ± SD	77.1 ± 19.0	80.9 ± 21.0	78.6 ± 19.9	0.132
Mean gradient, Mean ± SD	49.0 ± 13.2	52.0 ± 14.0	50.2 ± 13.5	0.080
EF %, Mean ± SD	64.3 ± 12.9	66.5 ± 11.4	65.2 ± 12.3	0.161

SD, standard deviation; BMI, body mass index; DM, diabetes mellitus; HTA, artery hypertension; ACEi, Angiotensin-converting enzyme inhibitor; ARB, Angiotensin II receptor blocker; TGA, triglyceride acids; EF, ejection fraction.

Inflation Factor for each independent variable. The adjusted *p*-value was therefore calculated as the *p*-value of the sex covariate in the multivariate model that was adjusted for the variables chosen in step one. A *p*-value of < 0.05 was considered statistically significant. All analyses in the clinical cohort were performed using the R statistical package, v. 3.6 (R Foundation for Statistical Computing. Vienna, Austria). GraphPad Software Inc. was used for *in vitro* analyses.

Results

Clinical parameters in AS patients

A total amount of 230 patients (59% men) were recruited. Men were significantly younger than women and exhibited higher height and weight, with no differences in body mass index, and lower total cholesterol, as expected according to previous publications (6, 33). Clinical and demographical data of the AS patients included in this manuscript have been summarized in Table 1.

Men-derived AVs present more neovessels than women's

Neovascularization was found in 73% of the AVs. In men, the frequency was 72%, whereas in women, it was 74%. Neovessel counting in hematoxylin-eosin preparations revealed that AVs from men exhibited more density of neovessels than women's [0.50 ± 0.66 for men vs. 0.29 ± 0.28 for women (vessels/mm^2)] (Figures 1A,B). Neovascularization was further validated using complementary immunohistochemical and molecular analyses. AVs from men were more positive for CD31 and VE-cadherin than women's (Figure 1A). Accordingly, men AVs exhibited higher CD31 [2,117 ± 1,598 for men vs. 1,579 ± 1,083 for women (pg/ml)] (Figure 1C) and VE-cadherin levels [1,676 ± 1,284 for men vs. 1,177 ± 884 for women (pg/ml)] (Figure 1D) than AVs from women measured by ELISA. Importantly, multivariate analyses adjusting for confounding factors (age, statins treatment, and total cholesterol) further confirmed a lower density of neovessels/mm^2 (OR = −0.2, $p = 0.037$), CD31 (OR = −532.87, $p = 0.02$), and VE-cadherin expression (OR = −415.31, $p = 0.0025$) in women AVs compared to men's (Table 2).

The presence of blood vessels was further assessed with ERG immunohistochemistry (Figure 1E) and confirmed in hematoxylin-eosin staining. The analysis revealed that men presented a greater amount of blood vessels than women [0.37 ± 0.36 for men vs. 0.24 ± 0.24 for women (blood vessels/mm^2)] (Figures 1E,F). Small or medium-sized blood vessels were the most prevalent among the AVs. Men's AVs had higher densities for small and medium-sized blood vessels than women's [0.43 ± 0.24 for men vs. 0.33 ± 0.28 for women (small vessels/total vessels); 0.53 ± 0.31 for men vs.

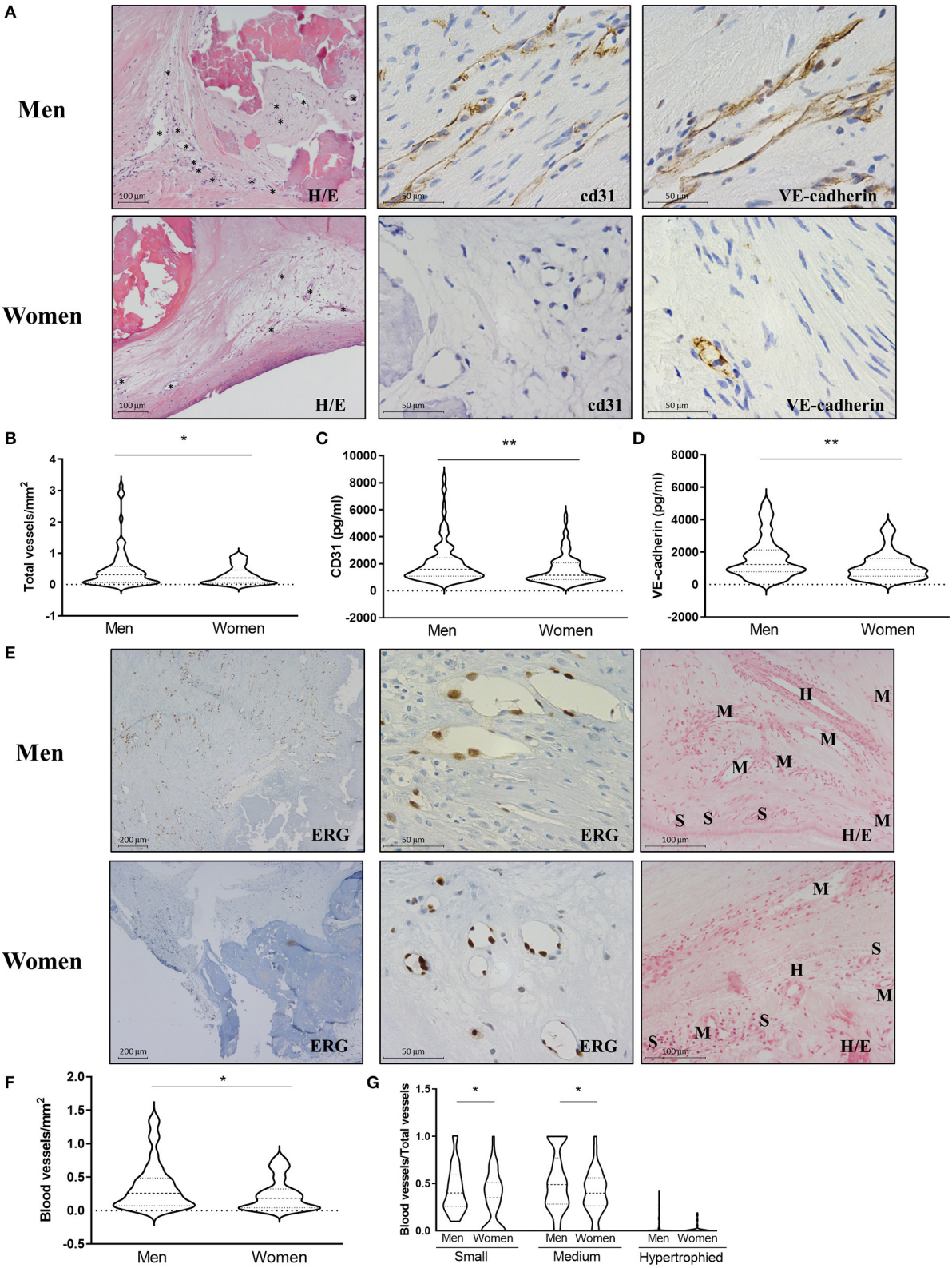

FIGURE 1
Sex differences in neovessels density in AVs from AS patients. Representative microphotographs of AV sections from men and women AS patients stained for hematoxylin/eosin and immunostained for CD31 and VE-cadherin AV tissue **(A)**. Asterisk indicates neovessels. Total vessel density in

(Continued)

FIGURE 1 (Continued)
AVs from men and women **(B)**. Protein expressions of CD31 and VE-cadherin in tissue homogenates from AVs of AS patients were measured by ELISA **(C,D)**. Representative microphotographs immunostained for the blood vessel marker ERG at low and high magnification and stained for hematoxylin/eosin for blood vessel size **(E)**. Blood vessel density **(F)** according to their size **(G)**. CD31, cluster differentiation 31; VE-cadherin, vascular endothelial cadherin; ERG: ETS-related gene. Different sample sizes were assayed depending on the analytical methods used. $N = 99$ for men and $N = 69$ for women by histology. $N = 131$ for men and $N = 87$ for women by ELISA. $^{*}p < 0.05$ vs men, $^{**}p < 0.01$ vs. men.

0.41 ± 0.22 for women (medium vessels/total vessels)]. There were no differences in hypertrophied vessels (arterioles) density between the sexes [0.03 ± 0.07 for men vs. 0.02 ± 0.05 for women (hypertrophied vessels/total vessels)] (Figures 1E–G). Multivariate analyses adjusting for confounders confirmed a significant lower density of blood vessels/mm^2 (OR = −0.17, $p = 0.01$) and medium-sized vessels/total vessels in women AVs than in men (OR = −0.14, $p = 0.05$) (Table 2). No significant differences were reported for small and hypertrophic-sized vessels.

The expression of both pro-angiogenic and anti-angiogenic factors was increased in AVs from men

The expression of VEGF-A was increased in AVs from men as compared to women as evidenced by the representative immunostaining displayed in Figure 2A and its further quantification [413 ± 300 for men vs. 335 ± 164 for women (pg/ml)] (Figure 2B). In addition, VEGFR1 [744 ± 562 for men vs. 566 ± 157 for women (pg/ml)] (Figure 2C) and VEGFR2 [89 ± 50 for men vs. 72 ± 29 for women (pg/ml)] (Figure 2D) levels were higher in men-derived AVs than in women. Additional pro-angiogenic factors were assessed in AV from patients with AS. The expression of IL-8 was increased in men's AVs as compared to women's [194 ± 407 for men vs. 39 ± 39 for women (pg/ml)] (Figure 2E). Both immunostaining and protein quantification of IGFBP2 revealed a consistent increment in AVs from men [450 ± 331 for men vs. 359 ± 254 for women (pg/ml)] (Figures 2F,G). Chemerin expression was also significantly augmented in men's AVs [494 ± 422 for men vs. 382 ± 253 for women (pg/ml)] (Figure 2H). Levels of FGF-7, other known angiogenic growth factor, were similarly higher in AVs from men as compared to women [427 ± 132 for men vs. 373 ± 91 for women (pg/ml)] (Figure 2I). All the protein expression levels were measured by ELISA. Additional multivariate analyses corroborated that IL-8 and FGF7 expression was lower in women AVs than in men counterparts (OR = −179.48, $p = 0.001$; OR = −64.95, $p = 0.001$, respectively) after adjusting for confounders (age, statins treatment, and total cholesterol). Statistical trends were reported for VEGF-A, VEGFR1, VEGFR2, and IGFBP2 but they did not reach statistical significance (Table 2).

TABLE 2 Multivariate analyses after adjusting for confounder factors in the study cohort.

Variable	OR[a] (95% CI)	Adjusted *p*–value
Neovessels/mm^2	−0.2 (−0.39; −0.01)	0.037
CD31 (pg/mL)	−532.87 (−980.24; −85.49)	0.02
VE–cadherin (pg/mL)	−415.31 (−778.03; −52.59)	0.025
Angiogenic targets		
Blood vessels/mm^2	−0.17 (−0.3; −0.04)	0.01
Small vessels/total vessels	−0.1 (−0.22; 0.03)	0.122
Medium vessels/total vessels	−0.14 (−0.27; 0)	0.05
Hypertrophied vessels/total vessel	−0.02 (−0.05; 0)	0.103
VEGF–A (pg/mL)	−71.5 (−152.83; 9.84)	0.085
VEGFR1 (pg/mL)	−131.76 (−288.47; 24.95)	0.099
VEGFR2 (pg/mL)	−11.54 (−24.91; 1.84)	0.091
IL−8 (pg/mL)	−179.48 (−281.49; −77.46)	0.001
IGFBP−2 (pg/mL)	−77.45 (−177.93; 23.03)	0.131
FGF−7 (pg/mL)	−64.95 (−102.43; −27.47)	0.001
TGF–β (pg/mL)	−57.14 (−85.89; −28.39)	<0.001
Tsp−1 (pg/mL)	−3.85 (−5.93; −1.77)	<0.001
Tsp−2 (pg/mL)	−368.12 (−789.43; 53.19)	0.087
IL−4 (pg/mL)	−1.37 (−7.5; 4.76)	0.661
IL−12p70 (pg/mL)	−19.24 (−34.58; −3.9)	0.014
Endostatin (pg/mL)	−197.81 (−356.02; −39.6)	0.014
CD36 (A.U.)	−0.41 (−0.73; −0.08)	0.014
Chm−1 (mRNA)	−0.01 (−0.04; 0.03)	0.746
Lymphangiogenic targets		
Lymphatic vessels/mm^2	−0.02 (−0.04; 0)	0.045
Lyve−1 (mRNA)	−0.92 (−3.32; 1.48)	0.453
D2–40 (mRNA)	−0.01 (−0.02; 0)	0.041
VEGF–C (pg/mL)	−79.05 (−138.38; −19.73)	0.009
VEGF–D (pg/mL)	−21.54 (−43.3; 0.22)	0.052
VEGFR3 (pg/mL)	−24.6 (−66.14; 16.94)	0.246

[a]Sex.

Of special interest, TGF-β, a pleiotropic protein that can be either pro- or anti-angiogenic, (34) was also elevated in AVs from men [361 ± 72 for men vs. 335 ± 67 for women (pg/ml)] (Figures 3A,B) by immunostaining and ELISA. Such lower expression of TGF-β in women compared to men AVs was further confirmed by multivariate analyses after adjusting for the confounding factors stated above (OR = −57.14, $p < 0.001$).

10.3389/fcvm.2022.971802

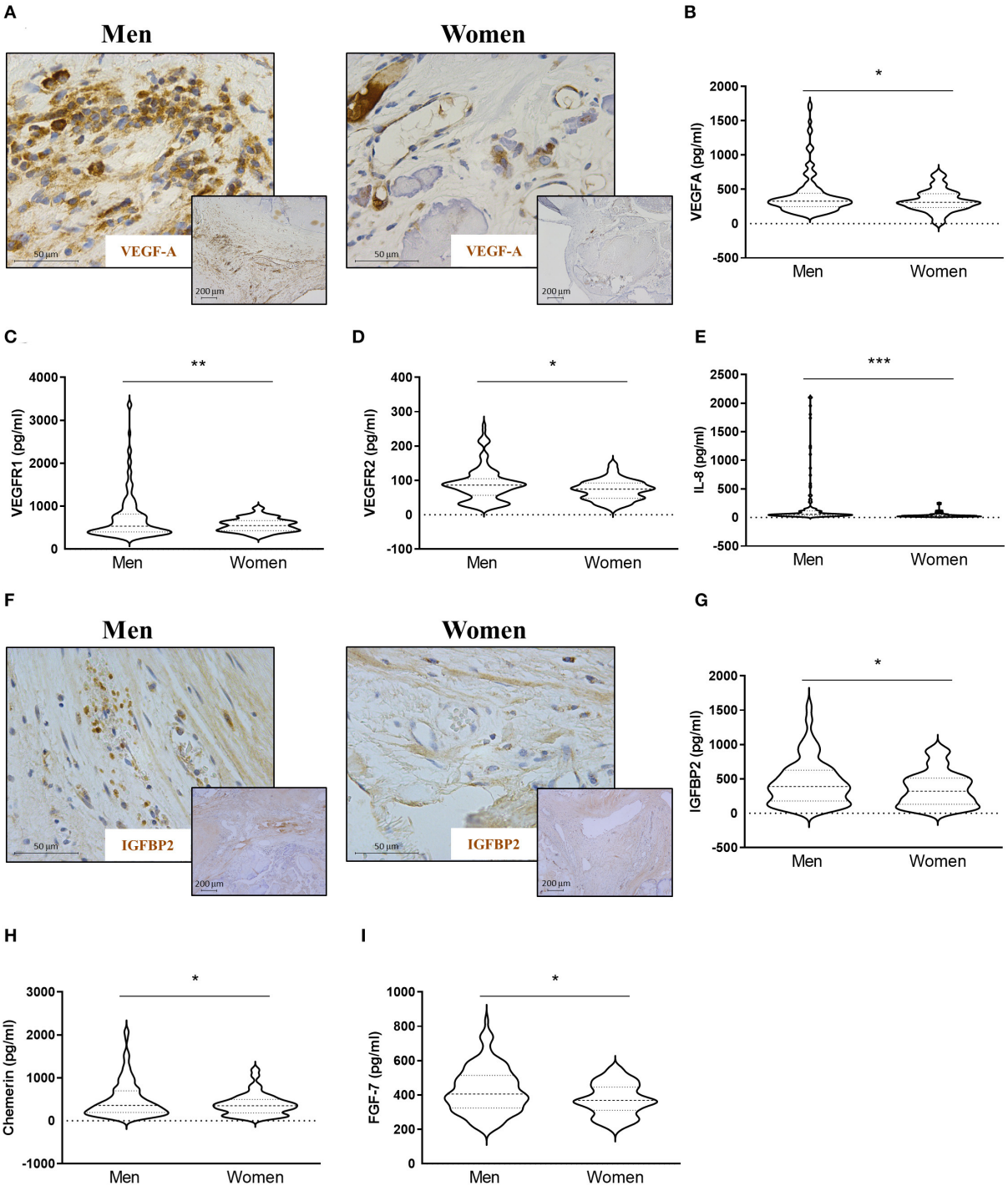

FIGURE 2
Sex differences in pro-angiogenic markers in AVs from AS patients. Representative microphotographs of AV sections from AS patients immunostained for VEGFA **(A)**. Protein expressions of VEGFA **(B)**, VEGFR1 **(C)**, VEGFR2 **(D)**, and IL-8 **(E)** in tissue homogenates from AVs of AS patients were measured by ELISA. Representative microphotographs are immunostained for IGFBP2 **(F)**. Protein expressions of IGFBP2 **(G)**, chemerin **(H)**, and FGF-7 **(I)** were measured by ELISA. VEGF: vascular endothelial growth factor; IL, interleukin; IGFBP, insulin-like growth factor binding protein. $N = 132$ for men and $N = 86$ for women by ELISA. *$p < 0.05$ vs. men, **$p < 0.01$ vs. men, ***$p < 0.001$ vs. men.

10.3389/fcvm.2022.971802

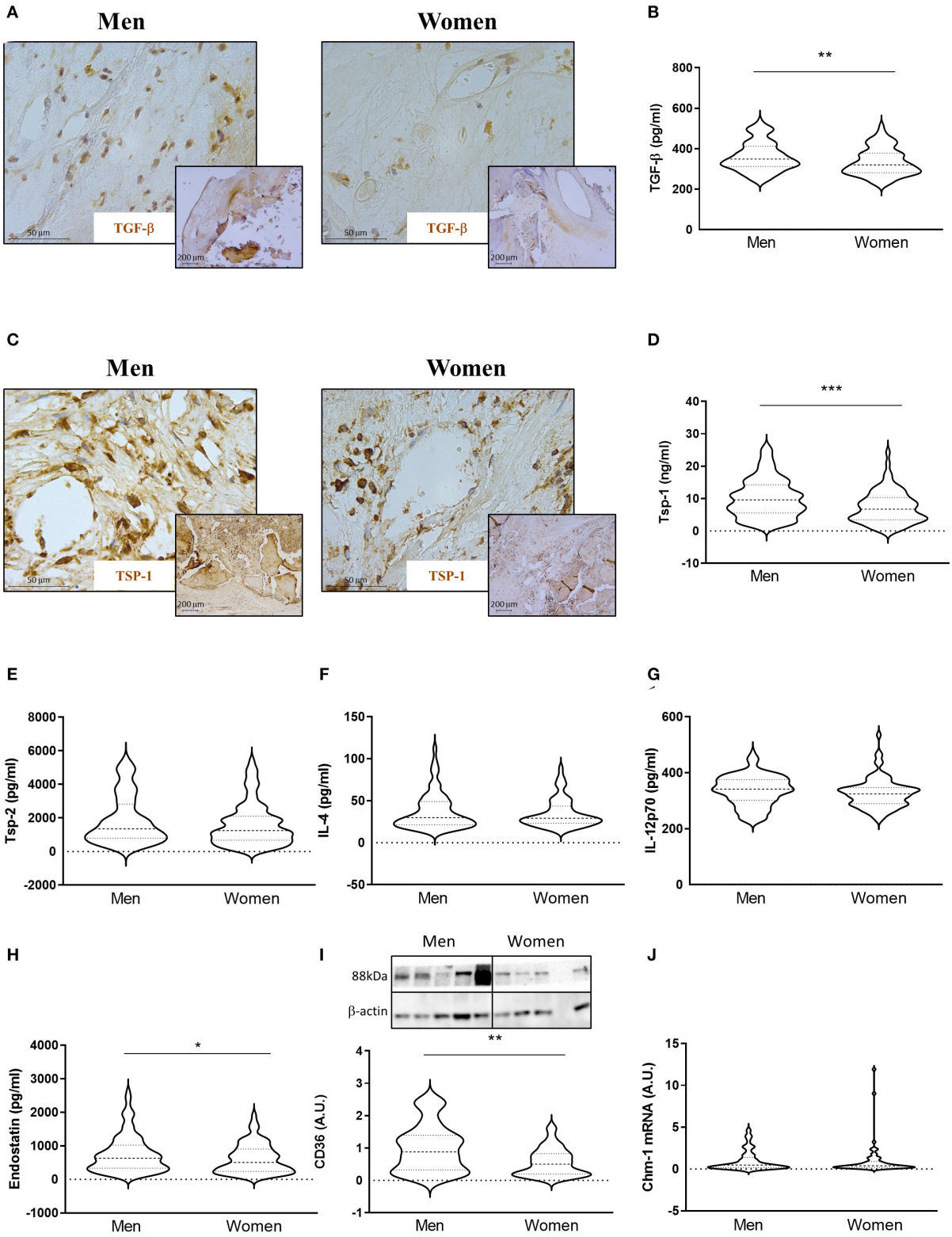

FIGURE 3
Sex differences in anti-angiogenic markers in AVs from AS patients. Representative microphotographs of AV sections from AS patients immunostained for TGF-β **(A)** and Tsp-1 **(C)**. Protein expressions of TGF-β **(B)**, Tsp-1, Tsp-2, IL-4, IL-12p70, and endostatin **(D–H)** in tissue homogenates from AVs of AS patients were measured by ELISA. Protein expression levels of CD36 by WB **(I)** and mRNA levels of Chm-1 **(J)** in AVs of AS patients. TGF-β, transforming growth factor-beta; Tsp, thrombospondin; IL, interleukin; Chm-1, chondromodulin-1. Different sample sizes were assayed depending on the analytical methods used. $N = 132$ for men and $N = 86$ for women by ELISA. $N = 42$ men and $N = 43$ women by WB. $N = 11$ men and $N = 62$ women by RT-qPCR. *$p < 0.05$ vs. men, **$p < 0.01$ vs. men, ***$p < 0.001$ vs. men.

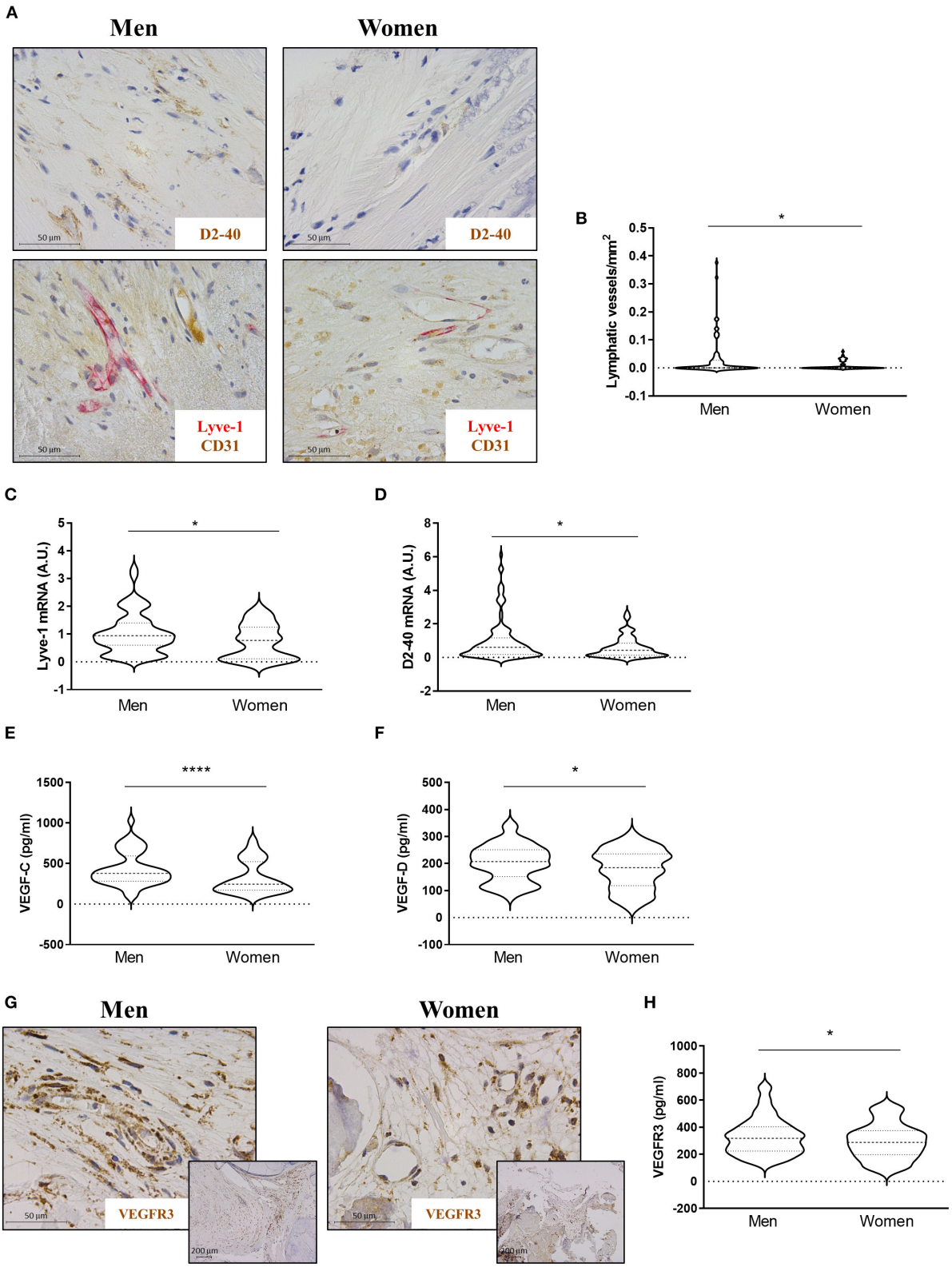

FIGURE 4
Sex differences in lymphangiogenesis in AVs from AS patients. Representative microphotographs of AV sections from AS patients immunostained for D2-40 and Lyve-1/CD31 **(A)**. Total lymphatic vessel density in AVs from men and women was measured by D2-40

(Continued)

FIGURE 4 (Continued)
and Lyve-1/CD31 immunostaining **(B)**. mRNA expression levels of Lyve-1 **(C)** and D2-40 **(D)** in AVs of AS patients. Protein expressions of VEGF-C and VEGF-D in tissue homogenates from AVs of AS patients were measured by ELISA **(E,F)**. Representative microphotographs are immunostained for VEGFR3 **(G)**. Protein expression of VEGFR3 **(H)** in whole AV tissue was measured by ELISA. VEGF: vascular endothelial growth factor. Different sample sizes were assayed depending on the analytical methods used. $N = 99$ for men and $N = 69$ for women by histology. $N = 116$ for men and $N = 70$ for women by RT-qPCR. $N = 133$ for men and $N = 87$ for women by ELISA. *$p < 0.05$ vs. men, ****$p < 0.0001$ vs. men.

We next investigated the expression of anti-angiogenic molecules. Immunohistochemical analyses showed higher expression of Tsp-1 in AVs from men (Figure 3C). This finding was further confirmed using quantitative analysis. Accordingly, AVs from men presented increased levels of Tsp-1 [10 ± 6 for men vs. 7 ± 5 for women (ng/ml)] (Figure 3D), whereas no changes were found in Tsp-2 expression [1897 ± 1446 for men vs. 1621 ± 1266 for women (pg/ml)] (Figure 3E). While IL-4 [38 ± 22 for men vs. 35 ± 17 for women (pg/ml)] (Figure 3F) and IL-12p70 [337 ± 54 for men vs. 327 ± 53 for women (pg/ml)] (Figure 3G) levels were similar in AVs from men and women, endostatin expression was elevated in men AVs as compared to women's [761 ± 557 for men vs. 616 ± 434 for women (pg/ml)] (Figure 3H). All of the previously mentioned markers were measured by ELISA. The expression of the scavenger receptor CD36 was also higher in men's AVs [1 ± 0.72 for men vs. 0.56 ± 0.42 for women (A.U.)] (Figure 3I) in WB. Similar mRNA levels of Chondromodulin-1 (Chm-1) were found in AVs in men and women [0.07 ± 0.08 for men vs. 0.07 ± 0.13 for women (A.U.)] (Figure 3J). Multivariate analyses adjusting for confounders also corroborated a significant downregulated expression of Tsp-1 (OR = −3.85, $p < 0.001$), IL-12p70 (OR = −19.24, $p = 0.014$), endostatin (OR = −197.81, $p = 0.014$), and CD36 (OR = −0.41, $p = 0.014$), with a statistical but not significant trend for Tsp-2 (OR = −368.12, $p = 0.087$), in women AVs as compared to men's (Table 2).

AVs from men exhibited increased lymphangiogenesis

The presence of lymphatic vessels in AVs was assessed with D2-40 and Lyve-1/CD31 (Figure 4A). Lymphatic vessels were found in 46.15% of the stenotic AVs, with no significant differences between men (48.33%) and women (43.18%). The number of lymphatic vessels per sample preparation was higher in AVs from men than in women [0.033 ± 0.07 for men vs. 0.008 ± 0.02 for women (lymphatic vessels/mm^2)] (Figure 4B). In line with these results, the quantification of the mRNA of Lyve-1 [1.02 ± 0.73 for men vs. 0.73 ± 0.62 for women (A.U.)] and D2-40 [0.035 ± 0.043 for men vs. 0.021 ± 0.022 for women (A.U.)] showed an increase in men's AVs (Figures 4C,D). The expression levels of the lymphangiogenic molecules VEGF-C [434 ± 207 for men vs. 326 ± 198 for women (pg/ml)] and VEGF-D [203 ± 66 for men vs. 180 ± 72 for women (pg/ml)] were higher in AVs from men as compared to women by ELISA (Figures 4E,F). VEGFR3 immunostaining showed greater expression in neovessels in AVs from men as compared to women's AVs (Figure 4G). Accordingly, VEGFR3 ELISA expression was augmented in whole AV tissue from men with AS [333 ± 136 for men vs. 296 ± 130 for women (pg/ml)] (Figure 4H). Importantly, multivariate analyses adjusting for confounding factors further confirmed a significant lower density of lymphatic vessels (OR = −0.02, $p = 0.045$) in women AVs than in men (OR = −0.14, $p = 0.05$) (Table 2). Moreover, the lower expression in women AVs of the lymphangiogenic markers D2-40 and VEGF-C was validated by multivariate analyses after adjusting for confounding factors (OR = −0.01, $p = 0.041$; and OR = –79.05, $p = 0.009$, respectively), with a statistical trend for VEGF-D (OR = −21.54, $p = 0.052$) (Table 2).

Production of pro-angiogenic, anti-angiogenic, and lymphangiogenic factors in human aortic VICs isolated from men and women with AS

VICs were isolated from male- or female-derived AVs from AS patients. Our results showed that VICs from men presented higher expression of VEGF-A [891 ± 706 for men vs. 541 ± 423 for women (pg/ml)] (Figure 5A) and VEGFR1 (375 ± 94 for men vs. 218 ± 72 for women [pg/ml)] (Figure 5B) as compared to VICs isolated from women. However, VEGFR2 levels did not differ between male and female VICs [221 ± 37 for men vs. 241 ± 61 for women (pg/ml)] (Figure 5C). An increase in IGFBP-2 secretion was found in men's VICs as compared to women's [71776 ± 33455 for men vs. 51004 ± 22946 for women (pg/ml)] (Figure 5D). Pro-angiogenic FGF-7 was higher in men's VICs supernatant as compared to women's [27926 ± 13059 for men vs. 20776 ± 9119 for women (pg/ml)] (Figure 5E). The expression of TGF-β [132 ± 51 for men vs. 151 ± 62 for women (pg/ml)], Tsp-1 [227 ± 145 for men vs. 248 ± 188 for women (pg/ml)], endostatin [101930 ± 29452 for men vs. 99215 ± 24532 for women (pg/ml)], and Chm-1 [1.08 ± 0.52 for men vs. 0.99 ± 0.63 for women (A.U.)] did not differ between men- and women-derived VICs (Figures 5F-I). Interestingly, VICs isolated from men exhibited

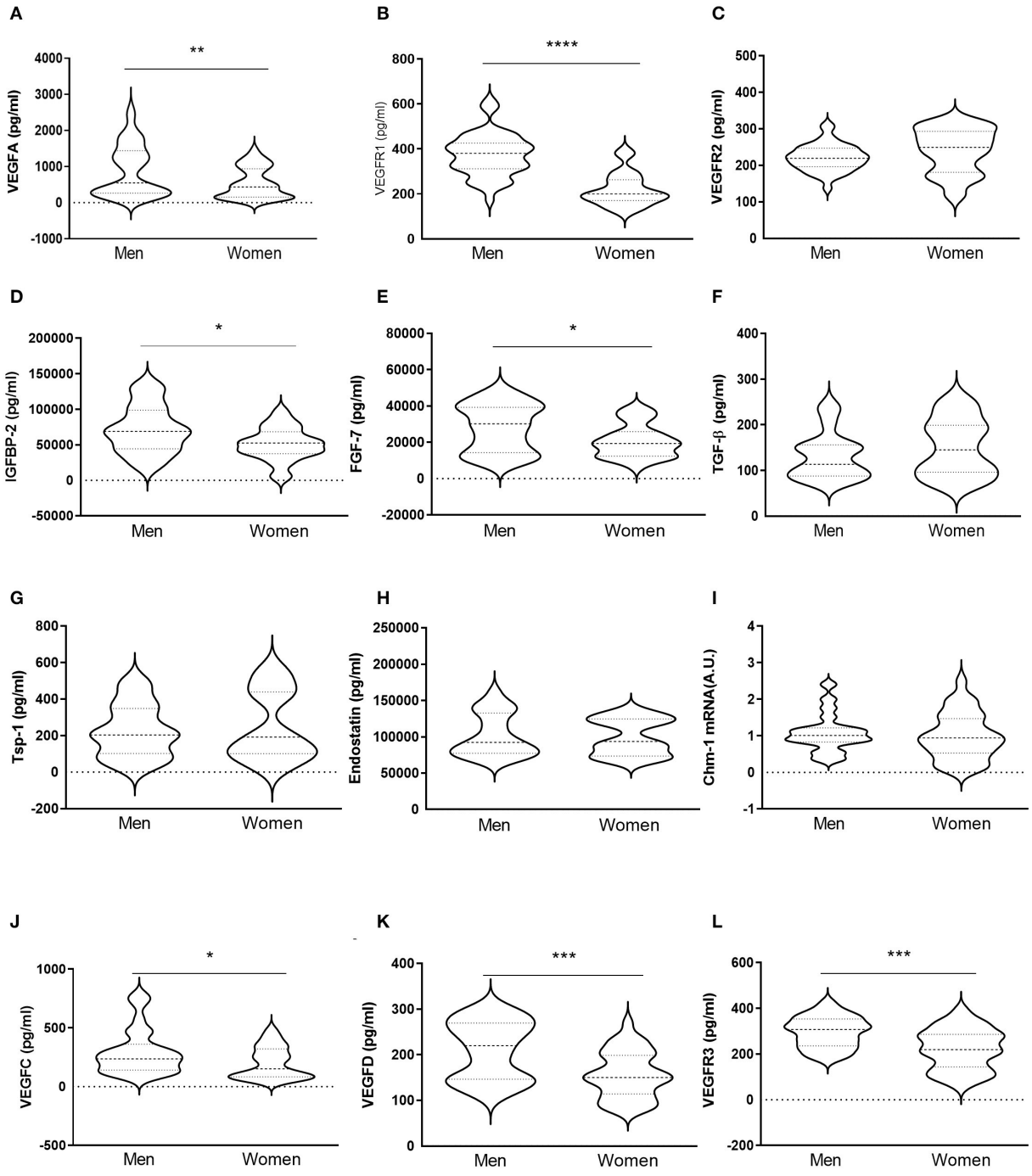

FIGURE 5
In vitro sex-comparative analysis of pro-angiogenic, anti-angiogenic, and lymphangiogenic markers in human aortic VICs. Protein expression of pro-angiogenic factors VEGF-A, VEGFR1, VEGFR2, IGFBP-2, and FGF-7 in VICs isolated from male and female-derived AVs from AS patients **(A–E)** measured from the supernatant by ELISA. Protein levels of TGF-β, Tsp-1, and endostatin in VICs from AVs of AS patients **(F–H)** were determined from the supernatant by ELISA. mRNA expression levels of Chm-1 **(I)**. Protein expression of lymphangiogenic factors VEGF-C, VEGF-D, and VEGFR3 **(J–L)** in the supernatant by ELISA. VEGF: vascular endothelial growth factor; IGFBP: insulin-like growth factor binding protein; FGF: fibroblast growth factor; TGF-β: transforming growth factor-beta; Tsp: thrombospondin; Chm-1: chondromodulin-1. $N = 24$ for men and $N = 12$ for women. *$p < 0.05$ vs. men, **$p < 0.01$ vs. men, ***$p < 0.001$ vs. men, ****$p < 0.0001$ vs. men.

higher levels of the lymphangiogenic factors VEGF-C [298 ± 193 for men vs. 202 ± 134 for women (pg/ml)], VEGF-D [210 ± 64 for men vs. 156 ± 51 for women (pg/ml)], and VEGFR3 [296 ± 68 for men vs. 222 ± 89 for women (pg/ml)] (Figures 5J-L). All these markers were measured by ELISA on cell supernatants.

10.3389/fcvm.2022.971802

Discussion

Our data demonstrate for the first time the sex-related differences in angiogenesis and lymphangiogenesis in AVs and in isolated VICs from men and women with AS. Results presented here show that AVs from men exhibit higher densities of blood and lymphatic neovessels than those from women, even after adjusting for confounding factors, such as age, total cholesterol, and statin intake. In men's AVs and VICs, there is an angiogenic switch characterized by an imbalance between pro- and anti-angiogenic factors, with subsequent activation of angiogenesis. Moreover, our *in vitro* results using primary VICs isolated from AS patients reinforce the idea that VICs are a major player regulating neovascularization of the AV in AS with a marked sex-specific pattern. Thus, male-derived VICs exhibited higher pro-angiogenic and lymphangiogenic capacity than female-derived VICs.

The information about the relevance of angiogenesis in AVs is scarce, even more for lymphangiogenesis. Previous studies have shown that both phenomena are induced in AVs from AS patients (15, 17, 18), likely contributing to the harmful accumulation of inflammatory cells and calcification. The loss of avascularity in the AV seems to respond to the enhanced requirement of oxygen supply within the extensive thickening and calcification occurring during the progression of AS. The extent of neovascularization correlates with the burden of AS (8, 9) and is associated with osteogenesis and calcification in the cardiovascular territory (8, 10). Small and medium-sized vessels and arterioles have been previously described in AVs from AS patients (18). Our results also reveal that small and medium-sized neovessels are the predominant forms of neovascularization in the AV of patients with AS, especially in men compared to women. The presence of both blood and lymphatic vessels was associated with lymphocytic infiltrates in 86% of cases in a small cohort of AS patients (17). In rheumatic valves, the presence of inflammatory infiltrates as well as the expression VEGF have been described in areas of neoangiogenesis (9). The relationship between angiogenesis and inflammation remains, however, controversial. On one hand, it has been proposed that inflammation could precede and promote angiogenesis (35). On the other hand, it has been described that elastic fiber fragmentation leads to aberrant angiogenesis and which precedes inflammation in aortic valve diseases (15). In our study, neovessels were also located near the inflammatory foci, the calcification nodules, and the endothelial layer. Both processes have been demonstrated to be over-represented in AVs among men than women in a similar cohort (6). The network of neovessels may facilitate rapid transit of inflammatory cells and pro-calcifying molecules. However, all the patients present similar severity of AS, being difficult to conclude whether angiogenesis could precede or follow inflammatory infiltration.

The source of neovessels has been a matter of debate in the last years. Initially, it was postulated that one source of this neovascularization could come from valve endothelial cells (VECs) (17). Both VICs and VECs in coculture could undergo pericyte differentiation and angiogenic sprouting, respectively (19). Recently, it has been confirmed that VICs isolated from AS patients are angiogenic cells and could differentiate into perivascular cells and secrete VEGF-A (20). Herein, we extend those findings by demonstrating that VEGF-A and other factors that contribute to angiogenesis are found in conditioned media from VICs isolated from diseased patients, with marked sex differences. Up to now, only two studies described sex differences in angiogenesis potentially relevant to the progression of AS but based on isolated VICs from porcine AVs (26, 27). McCoy and co-workers were the first to describe that VEGFR2 levels were five-fold higher in isolated VICs from male as compared to female cells (26). These results are consistent with our observations describing that male AVs expressed higher levels of VEGFR2 relative to female counterparts, although these findings have not been seen *in vitro*. Nevertheless, male VICs exhibited higher VEGF-A, VEGFR1, IGFBP-2, and FGF-7 than female VICs, without major changes in the expression of anti-angiogenic molecules. Recently, Nelson and coworkers evidenced that male quiescent VICs secrete lower levels of VEGF-A than female VICs, while VEGF-A is upregulated upon VIC activation and reaches expression levels comparable to female VICs (27). Interestingly, in our study, we evidenced that VEGF-A levels were higher in male VICs than in female's isolated from AS patients. The overall secretome and proteome of VICs isolated from end-stage stenotic AVs might show differences compared to those found in control non-diseased swine AV such as these used in previous publications (27).

Interestingly, TGF-β was overexpressed in male AVs, as it has been previously described by McCoy et al. (26). It is well known that TGF-β induces calcification and differentiation of VICs into myofibroblastic cells (36), so increased levels of this cytokine may be related to a greater degree of calcification in male patients (37) rather than to its antiangiogenic role. Concerning antiangiogenic factors, AVs from women exhibited reduced levels of Tsp-1 and endostatin as compared to men, with no differences in Tsp-2 expression. Tsps are highly conserved calcium-binding matricellular proteins regulating angiogenesis but also inflammation and extracellular matrix remodeling, and their contribution to such mechanisms might be different according to the sex. For instance, Tsp-1 is significant for initial fibro-inflammatory response and Tsp-2 for proliferative and remodeling phases within neoangiogenesis (38). Although the evidence suggesting an association between Tsp-1 and AS is limited, it seems that the expression of Tsp-1 is similar in fibrosclerotic and stenotic AVs compared to controls (39). Of note, Tsp-1 can activate TGF-β and bind CD36 to actively

participate in fibrotic processes (40). Accordingly, women AVs exhibited lower TGF-β and CD36 and presented exacerbated extracellular matrix remodeling and low inflammatory profiles (6). In contrast, Tsp-2 levels were higher in fibrotic and stenotic AVs than in control ones (39). Tsp-2 has been associated with myofibroblast proliferation and neovascularization in the AV (39), both of which are also higher in men-derived AVs. However, our results did not show differences between the sexes. In contrast with previous publications, our study compares the expression profiles of Tsps in AVs from end-stage severe forms of AS rather than fibrosclerotic vs. stenotic AVs. That might explain, at least in part, the discrepancies among our results and previous publications. Other anti-angiogenic factor, endostatin, has been found to be increased in AS patients and associated to calcification (11). In consequence, its expression is decreased in women AVs, which presented lower degree of calcification for the same AS severity (6). It has been postulated that the presence of endostatin could indicate that anti-angiogenic processes are also activated during the development of AS (11) and in line with our results in men-derived AVs might fail to resolve the aberrant loss of avascularity during the progression of AS.

Lymphangiogenesis mainly consists of the growth of lymphatic vessels from pre-existing neovessels in which the endothelial cell component exposed to VEGF-C and -D may differentiate into lymphatic endothelial cells (41). Lymphatic vessel density was higher in men's AVs than in women's. Moreover, male AVs presented higher levels of Lyve-1, VEGF-C, VEGF-D, and VEGFR3 suggesting that this process could be decreased in women. Although VEGF-C levels were not found to be overexpressed in AS valves, there is evidence that it is secreted by VICs and that increased levels of it correlate with a greater transvalvular pressure gradient (18). Consistently, VICs from men exhibited higher secretion of VEGF-C, VEGF-D, and VEGFR3. Interestingly, increased amounts of VEGFR3 in men's AVs could explain the observed differences in the presence and localization of lymphatic vessels as it has been reported for control and stenotic AVs (18). A high expression of VIC-derived VEGF-C may recruit blood endothelial cells from the valvular angiogenic sprouts to differentiate into lymphatic endothelial cells (42).

The overall higher angiogenic and lymphangiogenic profiles in men compared to women may also contribute to the development of fibro-calcific phenotypes in AS in men. Endochondral bone formation is regulated by systemically and locally acting growth factors, such as VEGFs and their receptors. VEGF-A has been proven to regulate bone formation toward the activation of angiogenesis (43). We and others have found increased inflammation, osteogenesis, and calcification in men compared to women (6, 26, 44). VIC-derived pro-angiogenic and pro-lymphangiogenic morphogens may sustain early AV thickening and sclerosis. In men-derived VICs, with higher osteoblastic profiles, these molecules may further promote osteoblast differentiation and AV-to-bone replacement.

In conclusion, angiogenesis and lymphangiogenesis are different in men and women with AS. AVs from men presented more neovessels as well as an imbalance between pro- and anti-angiogenic factors. Our study provides new molecular and cellular insights on the pathogenesis of AS with relevant sex-specific signatures that might be clinically relevant to the development of sex-tailored therapeutic strategies.

Limitations

This study had several limitations. First, we have not been able to perform the histological staining and characterization of vessels in the total sample, which could have provided us with greater robustness in our Histopathological results with respect to the molecular analyses. Second, we only have paraffin-embedded tissue, which facilitates the sectioning of the calcified tissue and better morphology, but we lose information due to the inability to label certain molecules. Third, we have not explored the role of VECs in angiogenesis and lymphangiogenesis. Future *in vitro* studies comparing the activation of angiogenic and lymphangiogenic pathways in VICs undergoing osteogenic differentiation would be appropriate to parallel findings in end-stage clinical samples. Moreover, it would be useful to search for therapeutic targets capable to revert or prevent these pathological events.

Data availability statement

The original contributions presented in the study are included in the article/Supplementary material, further inquiries can be directed to the corresponding authors.

Ethics statement

The study protocol involving human participants was approved by the Comité Ético de Experimentación Clínica, Gobierno de Navarra - Departamento de Salud (Ethics numbers 17/2013 and PI2019/59) and complied with ethical standards of the Declaration of Helsinki. Written informed consent to participate in this study was obtained from all participants.

Author contributions

NL-A and EJ conceived and designed the study. LM, EM-N, MG, JV, AN, VA, AG-P, AF-C, AG, VA, and RS performed the data. LM, EM-N, MG, JV, AN, VA, AG-P, AF-C, AG, VA, RS, EJ, and NL-A analyzed and interpreted the data. LM, EJ, and NL-A led the design and drafted the

article. All authors contributed to the article and approved the submitted version.

Funding

This work was supported by a Miguel Servet contract (CP13/00221) and by Fondo de Investigaciones Sanitarias (PI18/01875; PI21/00280) from the Instituto de Salud Carlos III - FEDER. LM was supported by a PFIS Ph.D. studentship (FI19/00302). EJ was supported by a Sara Borrell postdoctoral fellowship (CD19/00251). EM-N was supported by a Margarita Salas postdoctoral fellowship (ULL-MS-P14). MG was supported by a Miguel Servet Foundation Ph.D. studentship.

Conflict of interest

The authors declare that the research was conducted in the absence of any commercial or financial relationships that could be construed as a potential conflict of interest.

Publisher's note

References

1. Maffeis C, Rossi A, Faggiano P. Aortic valve stenosis burden: where we are now? *Int J Cardiol.* (2021) 339:128–9. doi: 10.1016/j.ijcard.2021.07.032

2. Baumgartner H, Falk V, Bax JJ, De Bonis M, Hamm C, Holm PJ, et al. 2017 Esc/Eacts guidelines for the management of valvular heart disease. *Eur Heart J.* (2017) 38:2739–91. doi: 10.1016/j.rec.2017.12.013

3. Syvaranta S, Helske S, Laine M, Lappalainen J, Kupari M, Mayranpaa MI, et al. Vascular endothelial growth factor-secreting mast cells and myofibroblasts: a novel self-perpetuating angiogenic pathway in aortic valve stenosis. *Arterioscler Thromb Vasc Biol.* (2010) 30:1220–7. doi: 10.1161/ATVBAHA.109.198267

4. Bienjonetti-Boudreau D, Fleury MA, Voisine M, Paquin A, Chouinard I, Tailleur M, et al. Impact of sex on the management and outcome of aortic stenosis patients. *Eur Heart J.* (2021) 42:2683–91. doi: 10.1093/eurheartj/ehab242

5. DesJardin JT, Chikwe J, Hahn RT, Hung JW, Delling FN. Sex differences and similarities in valvular heart disease. *Circ Res.* (2022) 130:455–73. doi: 10.1161/CIRCRESAHA.121.319914

6. Matilla L, Garaikoetxea M, Arrieta V, Garcia-Pena A, Fernandez-Celis A, Navarro A, et al. Sex-Differences in Aortic Stenosis: Mechanistic Insights and Clinical Implications. *Front Cardiovasc Med.* (2022) 9:818371. doi: 10.3389/fcvm.2022.818371

7. Aikawa E, Whittaker P, Farber M, Mendelson K, Padera RF, Aikawa M, et al. Human semilunar cardiac valve remodeling by activated cells from fetus to adult: implications for postnatal adaptation, pathology, and tissue engineering. *Circulation.* (2006) 113:1344–52. doi: 10.1161/CIRCULATIONAHA.105.591768

8. Collett GD, Canfield AE. Angiogenesis and pericytes in the initiation of ectopic calcification. *Circ Res.* (2005) 96:930–8. doi: 10.1161/01.RES.0000163634.51301.0d

9. Rajamannan NM, Nealis TB, Subramaniam M, Pandya S, Stock SR, Ignatiev CI, et al. Calcified rheumatic valve neoangiogenesis is associated with vascular endothelial growth factor expression and osteoblast-like bone formation. *Circulation.* (2005) 111:3296–301. doi: 10.1161/CIRCULATIONAHA.104.473165

10. Acharya A, Hans CP, Koenig SN, Nichols HA, Galindo CL, Garner HR, et al. Inhibitory role of notch1 in calcific aortic valve disease. *PLoS ONE.* (2011) 6:e27743. doi: 10.1371/journal.pone.0027743

11. Chalajour F, Treede H, Ebrahimnejad A, Lauke H, Reichenspurner H, Ergun S. Angiogenic activation of valvular endothelial cells in aortic valve stenosis. *Exp Cell Res.* (2004) 298:455–64. doi: 10.1016/j.yexcr.2004.04.034

12. Soini Y, Salo T, Satta J. Angiogenesis is involved in the pathogenesis of nonrheumatic aortic valve stenosis. *Hum Pathol.* (2003) 34:756–63. doi: 10.1016/S0046-8177(03)00245-4

13. Deckers MM, Karperien M, van der Bent C, Yamashita T, Papapoulos SE, Lowik CW. Expression of vascular endothelial growth factors and their receptors during osteoblast differentiation. *Endocrinology.* (2000) 141:1667–74. doi: 10.1210/endo.141.5.7458

14. Hu K, Olsen BR. Osteoblast-Derived Vegf regulates osteoblast differentiation and bone formation during bone repair. *J Clin Invest.* (2016) 126:509–26. doi: 10.1172/JCI82585

15. Hinton RB, Juraszek AL, Opoka AM, Landis BJ, Smith JM, Mecham RP, et al. Early aberrant angiogenesis due to elastic fiber fragmentation in aortic valve disease. *J Cardiovasc Dev Dis.* (2021) 8:75. doi: 10.3390/jcdd8070075

16. Kholova I, Dragneva G, Cermakova P, Laidinen S, Kaskenpaa N, Hazes T, et al. Lymphatic vasculature is increased in heart valves, ischaemic and inflamed hearts and in cholesterol-rich and calcified atherosclerotic lesions. *Eur J Clin Invest.* (2011) 41:487–97. doi: 10.1111/j.1365-2362.2010.02431.x

17. Steiner I, Krbal L, Dominik J. Blood vessels and lymphatics in calcific aortic stenosis–in support of its inflammatory pathogenesis. *Cesk Patol.* (2010) 46:33–6.

18. Syvaranta S, Helske S, Lappalainen J, Kupari M, Kovanen PT. Lymphangiogenesis in aortic valve stenosis–novel regulatory roles for valvular myofibroblasts and mast cells. *Atherosclerosis.* (2012) 221:366–74. doi: 10.1016/j.atherosclerosis.2011.12.034

19. Arevalos CA, Berg JM, Nguyen JM, Godfrey EL, Iriondo C, Grande-Allen KJ. Valve interstitial cells act in a pericyte manner promoting angiogensis and invasion by valve endothelial cells. *Ann Biomed Eng.* (2016) 44:2707–23. doi: 10.1007/s10439-016-1567-9

20. Gendron N, Rosa M, Blandinieres A, Sottejeau Y, Rossi E, Van Belle E, et al. Human aortic valve interstitial cells display proangiogenic properties during calcific aortic valve disease. *Arterioscler Thromb Vasc Biol.* (2021) 41:415–29. doi: 10.1161/ATVBAHA.120.314287

21. Kramann R, Schneider RK, DiRocco DP, Machado F, Fleig S, Bondzie PA, et al. Perivascular gli1+ progenitors are key contributors to injury-induced organ fibrosis. *Cell Stem Cell.* (2015) 16:51–66. doi: 10.1016/j.stem.2014.11.004

22. Bostrom K, Watson KE, Horn S, Wortham C, Herman IM, Demer LL. Bone morphogenetic protein expression in human atherosclerotic lesions. *J Clin Invest.* (1993) 91:1800–9. doi: 10.1172/JCI116391

23. Brighton CT, Lorich DG, Kupcha R, Reilly TM, Jones AR, Woodbury RA. 2nd. The pericyte as a possible osteoblast progenitor cell. *Clin Orthop Relat Res.* (1992) (275):287–99. doi: 10.1097/00003086-199202000-00043

24. Kramann R, Goettsch C, Wongboonsin J, Iwata H, Schneider RK, Kuppe C, et al. Adventitial Msc-like cells are progenitors of vascular smooth muscle cells and drive vascular calcification in chronic kidney disease. *Cell Stem Cell.* (2016) 19:628–42. doi: 10.1016/j.stem.2016.08.001

25. Porras AM, Westlund JA, Evans AD, Masters KS. Creation of Disease-Inspired Biomaterial environments to mimic pathological events in early calcific aortic valve disease. *Proc Natl Acad Sci U S A.* (2018) 115:E363–E71. doi: 10.1073/pnas.1704637115

26. McCoy CM, Nicholas DQ, Masters KS. Sex-Related differences in gene expression by porcine aortic valvular interstitial cells. *PLoS ONE.* (2012) 7:e39980. doi: 10.1371/journal.pone.0039980

27. Nelson V, Patil V, Simon LR, Schmidt K, McCoy CM, Masters KS. Angiogenic secretion profile of valvular interstitial cells varies with cellular sex and phenotype. *Front Cardiovasc Med.* (2021) 8:736303. doi: 10.3389/fcvm.2021.736303

28. Neumann FJ, Sousa-Uva M. 'Ten Commandments' for the 2018 Esc/Eacts guidelines on myocardial revascularization. *Eur Heart J.* (2019) 40:79–80. doi: 10.1093/eurheartj/ehy855

29. Sadaba JR, Martinez-Martinez E, Arrieta V, Alvarez V, Fernandez-Celis A, Ibarrola J, et al. Role for Galectin-3 in Calcific Aortic Valve Stenosis. *J Am Heart Assoc.* (2016) 5:4360. doi: 10.1161/JAHA.116.004360

30. Latif N, Quillon A, Sarathchandra P, McCormack A, Lozanoski A, Yacoub MH, et al. Modulation of human valve interstitial cell phenotype and function using a fibroblast growth factor 2 formulation. *PLoS ONE.* (2015) 10:e0127844. doi: 10.1371/journal.pone.0127844

31. Riu F, Slater SC, Garcia EJ, Rodriguez-Arabaolaza I, Alvino V, Avolio E, et al. The adipokine leptin modulates adventitial pericyte functions by autocrine and paracrine signalling. *Sci Rep.* (2017) 7:5443. doi: 10.1038/s41598-017-05868-y

32. Hsu HHT, Artigues A, Villar MT. Induction of calcification by serum depletion in cell culture: a model for focal calcification in aortas related to atherosclerosis. *Lipids Health Dis.* (2008) 7:2. doi: 10.1186/1476-511X-7-2

33. Matilla L, Jover E, Garaikoetxea M, Martin-Nunez E, Arrieta V, Garcia-Pena A, et al. Sex-Related signaling of aldosterone/mineralocorticoid receptor pathway in calcific aortic stenosis. *Hypertension.* (2022) 79(8):1724–37. doi: 10.1161/HYPERTENSIONAHA.122.19526

34. Pardali E, Goumans MJ. ten Dijke P. Signaling by members of the Tgf-beta family in vascular morphogenesis and disease trends. *Cell Biol.* (2010) 20:556–67. doi: 10.1016/j.tcb.2010.06.006

35. Walsh DA, Pearson CI. Angiogenesis in the pathogenesis of inflammatory joint and lung diseases. *Arthritis Res.* (2001) 3:147–53. doi: 10.1186/ar292

36. Jian B, Narula N, Li QY, Mohler ER, 3rd, Levy RJ. Progression of Aortic Valve Stenosis: Tgf-Beta1 is present in calcified aortic valve cusps and promotes aortic valve interstitial cell calcification via apoptosis. *Ann Thorac Surg.* (2003) 75:457–65. doi: 10.1016/S0003-4975(02)04312-6

37. Aggarwal SR, Clavel MA, Messika-Zeitoun D, Cueff C, Malouf J, Araoz PA, et al. Sex differences in aortic valve calcification measured by multidetector computed tomography in aortic stenosis. *Circ Cardiovasc Imaging.* (2013) 6:40–7. doi: 10.1161/CIRCIMAGING.112.980052

38. Bornstein P, Agah A, Kyriakides TR. The role of thrombospondins 1 and 2 in the regulation of cell-matrix interactions, collagen fibril formation, and the response to injury. *Int J Biochem Cell Biol.* (2004) 36:1115–25. doi: 10.1016/j.biocel.2004.01.012

39. Pohjolainen V, Mustonen E, Taskinen P, Napankangas J, Leskinen H, Ohukainen P, et al. increased thrombospondin-2 in human fibrosclerotic and stenotic aortic valves. *Atherosclerosis.* (2012) 220:66–71. doi: 10.1016/j.atherosclerosis.2011.10.003

40. Adams JC, Lawler J. The thrombospondins. *Cold Spring Harb Perspect Biol.* (2011) 3:a009712. doi: 10.1101/cshperspect.a009712

41. Jeltsch M, Kaipainen A, Joukov V, Meng X, Lakso M, Rauvala H, et al. Hyperplasia of lymphatic vessels in Vegf-C transgenic mice. *Science.* (1997) 276:1423–5. doi: 10.1126/science.276.5317.1423

42. Karkkainen MJ, Haiko P, Sainio K, Partanen J, Taipale J, Petrova TV, et al. Vascular endothelial growth factor C is required for sprouting of the first lymphatic vessels from embryonic veins. *Nat Immunol.* (2004) 5:74–80. doi: 10.1038/ni1013

43. Gerber HP, Vu TH, Ryan AM, Kowalski J, Werb Z, Ferrara N. Vegf couples hypertrophic cartilage remodeling, ossification and angiogenesis during endochondral bone formation. *Nat Med.* (1999) 5:623–8. doi: 10.1038/9467

44. Simard L, Cote N, Dagenais F, Mathieu P, Couture C, Trahan S, et al. sex-related discordance between aortic valve calcification and hemodynamic severity of aortic stenosis: is valvular fibrosis the explanation? *Circ Res.* (2017) 120:681–91. doi: 10.1161/CIRCRESAHA.116.309306

frontiers | Frontiers in Cardiovascular Medicine

TYPE Original Research
PUBLISHED 29 September 2022
DOI 10.3389/fcvm.2022.975732

OPEN ACCESS

EDITED BY
Maria Nunes,
Federal University of Minas Gerais, Brazil

REVIEWED BY
Sasha A. Singh,
Department of Medicine, Brigham and Women's Hospital and Harvard Medical School, United States
Ishita Tandon,
University of Arkansas, United States

*CORRESPONDENCE
Gretchen J. Mahler
gmahler@binghamton.edu

SPECIALTY SECTION
This article was submitted to Heart Valve Disease, a section of the journal Frontiers in Cardiovascular Medicine

RECEIVED 22 June 2022
ACCEPTED 14 September 2022
PUBLISHED 29 September 2022

CITATION
Bramsen JA, Alber BR, Mendoza M, Murray BT, Chen M-H, Huang P and Mahler GJ (2022) Glycosaminoglycans affect endothelial to mesenchymal transformation, proliferation, and calcification in a 3D model of aortic valve disease.
Front. Cardiovasc. Med. 9:975732.
doi: 10.3389/fcvm.2022.975732

Glycosaminoglycans affect endothelial to mesenchymal transformation, proliferation, and calcification in a 3D model of aortic valve disease

Jonathan Alejandro Bramsen[1], Bridget R. Alber[2], Melissa Mendoza[1], Bruce T. Murray[3], Mei-Hsiu Chen[4], Peter Huang[3] and Gretchen J. Mahler[1]*

[1]Department of Biomedical Engineering, Binghamton University, Binghamton, NY, United States, [2]Department of Biomedical Engineering, George Washington University, Washington, DC, United States, [3]Department of Mechanical Engineering, Binghamton University, Binghamton, NY, United States, [4]Department of Mathematics and Statistics, Binghamton University, Binghamton, NY, United States

Calcific nodules form in the fibrosa layer of the aortic valve in calcific aortic valve disease (CAVD). Glycosaminoglycans (GAGs), which are normally found in the valve spongiosa, are located local to calcific nodules. Previous work suggests that GAGs induce endothelial to mesenchymal transformation (EndMT), a phenomenon described by endothelial cells' loss of the endothelial markers, gaining of migratory properties, and expression of mesenchymal markers such as alpha smooth muscle actin (α-SMA). EndMT is known to play roles in valvulogenesis and may provide a source of activated fibroblast with a potential role in CAVD progression. In this study, a 3D collagen hydrogel co-culture model of the aortic valve fibrosa was created to study the role of EndMT-derived activated valvular interstitial cell behavior in CAVD progression. Porcine aortic valve interstitial cells (PAVIC) and porcine aortic valve endothelial cells (PAVEC) were cultured within collagen I hydrogels containing the GAGs chondroitin sulfate (CS) or hyaluronic acid (HA). The model was used to study alkaline phosphatase (ALP) enzyme activity, cellular proliferation and matrix invasion, protein expression, and calcific nodule formation of the resident cell populations. CS and HA were found to alter ALP activity and increase cell proliferation. CS increased the formation of calcified nodules without the addition of osteogenic culture medium. This model has applications in the improvement of bioprosthetic valves by making replacements more micro-compositionally dynamic, as well as providing a platform for testing new pharmaceutical treatments of CAVD.

KEYWORDS

calcific aortic valve disease, chondroitin sulfate, hyaluronic acid, mechanobiology, fibrosa layer

Introduction

Calcific aortic valve disease (CAVD) is characterized as a complex and multi-factorial progression involving altered matrix organization and dysregulated crosstalk between resident cell populations of the aortic microenvironment, ultimately leading to a disrupted tri-layer organization of the aortic valve, the presence of calcium deposits, and inhibited valve function (1). This multi-step cascade of events results in an estimated 130,000 deaths annually in the USA (2). Valve replacement surgery is currently the only reliable treatment option, and these inert replacements lack the ability to biologically integrate and function long-term. Tissue engineering is a promising approach to help decrease the societal burden of CAVD by creating biologically inspired and mimetic valve replacements. Developing precise models of healthy and diseased valves could accelerate the transition of tissue engineered valves from bench to bedside. This study developed a platform for studying the aortic valve microenvironment to better understand matrix remodeling and how it plays a role in matrix mineralization. The platform can have applications in the improvement of bioprosthetic valves by making replacements more micro-compositionally dynamic, thereby addressing a major limitation in current tissue engineered constructs, as well as providing a platform for testing new pharmaceutical treatments of CAVD.

Valve interstitial cells (VICs) are critical to the function and overall homeostasis of the aortic valve (3). VICs and their extracellular matrix (ECM) proteins are known to play a role in both the early stages of valvulogenesis (4–6) and in aortic valve disease progression (7, 8). The adult aortic valve has three semilunar leaflets, each characterized by distinct ECM. The fibrosa layer is composed of circumferentially aligned collagen I fibers, the spongiosa is composed of collagen and randomly oriented proteoglycans rich in glycosaminoglycans (GAGs), and the ventricularis is composed of primarily radially orientated elastin (9). Early aortic valve disease includes ECM remodeling, cell proliferation, and increased alkaline phosphatase (ALP) activity (10–13). ALP promotes calcification by reducing pyrophosphate and osteopontin *via* hydrolysis (14). Late-stage aortic valve disease is characterized by the presence of calcific nodules on the aortic valve fibrosa and a disruption of the valvular ECM organization (15). Specifically, GAGs have been shown to relocate to the fibrosa layer in diseased valves and have been implicated in facilitating disease progression due to their localization near calcific nodules (16–18).

Endothelial to mesenchymal transformation (EndMT) is a phenomenon described by endothelial cells' loss of endothelial markers such as platelet endothelial cell adhesion molecule-1 (PECAM-1), gaining of mesenchymal cell markers such as alpha smooth muscle actin (α-SMA), and gaining of migratory properties (19). EndMT plays a major role in the early stages of valve development (20), has been implicated in valvular pathology, and may serve as a mechanism to replenish adult interstitial cell populations (21). Previous work has shown that GAGs induce EndMT in an *in vitro* porcine cell model, and mesenchymally transformed cells and GAGs are found near calcified nodules in diseased human valves (17). Later studies showed that GAGs also promote calcification in an *in vitro* model with porcine cells (22). In the current study, the 3D model with porcine aortic valve cells simulated the aortic valve fibrosa layer and was used to study the role of EndMT-derived activated valve interstitial cells (aVICs) on the progression of CAVD. Although 3D models have been applied elsewhere (23–26), some incorporating GAGs (27–30), questions remain on the role of the ECM on aVIC behavior and how these EndMT-derived cells may contribute to the onset and progression of matrix mineralization (31). Here, a 3D collagen I hydrogel scaffold containing chondroitin sulfate (CS) or hyaluronic acid (HA) and seeded with porcine aortic valve endothelial and interstitial cells was used to study EndMT-derived aVICs by quantifying: (1) ALP activity, (2) calcified nodule formation *via* Alizarin Red S (ARS) staining, and (3) cell phenotype and protein expression with immunocytochemistry, flow cytometry, cellular invasion, and proliferation assays.

Materials and methods

Cell isolation and culture

Porcine aortic valve cell isolation and culture have previously been described (17, 32). Briefly, porcine aortic valve interstitial cells (PAVIC) and porcine aortic valve endothelial cells (PAVEC) were obtained from freshly slaughtered pigs at a local abattoir. Cells were pooled from young (6–8 months) females or castrated males. Following isolation *via* collagenase digestion (600 U/mL collagenase type II, Worthington Biochemical Corporation, Lakewood, NJ, USA) PAVIC were grown in Dulbecco's Modified Eagle Medium (DMEM, Invitrogen, Waltham, MA, USA) supplemented with 1% penicillin-streptomycin (Pen-Strep, Invitrogen) and 10% fetal bovine serum (FBS, VWR, Radnor, PA, USA). PAVEC were grown on 50 μg/mL rat tail collagen I (Corning Life Sciences, Tewksbury, MA, USA)-coated flasks and in medium supplemented with 50 U/mL heparin sulfate (Sigma-Aldrich, St. Louis MO, USA). PAVIC and PAVEC were used between passages 3 and 5. During experiments, medium was changed every 48 h with the PAVIC formulation.

3D hydrogel preparation

A 3D collagen hydrogel co-culture model of the aortic valve microarchitecture was created to recapitulate late-stage disease conditions (i.e., GAG infiltration of the fibrosa layer) *in vivo*.

The hydrogels were formed by seeding PAVIC into and PAVEC on top of the hydrogels. Briefly, PAVIC (1×10^6 cells/mL) were suspended within a solution containing ice-cold 3× DMEM, 18 MΩ water, FBS, 0.1 M sodium hydroxide (NaOH), and rat tail collagen I. Then, 300 μL was pipetted into a 24-well plate (Corning) and allowed to crosslink at 37°C for 1 h. Following incubation, PAVEC (95,000 cells/cm^2) were added on top of hydrogel constructs in PAVIC medium. Four conditions were used: 1.5 mg/mL collagen (control), 2.2 mg/mL collagen (stiffness control), 1.5 mg/mL collagen + 20 mg/mL CS (chondroitin sulfate A sodium salt from bovine trachea, Sigma-Aldrich), and 1.5 mg/mL collagen + 20 mg/mL HA (hyaluronic acid sodium salt from *Streptococcus equi*, Sigma-Aldrich). Previous work showed that 2.2 mg/mL collagen gels can serve as stiffness controls for 1.5 mg/mL collagen gels with 20 mg/mL GAG-supplementation (17). All cultures were incubated at 37°C and 5% CO_2 for 2 weeks before analysis. Cells were cultured for 14 days to mimic previous relevant studies, which demonstrated significant calcific nodule formation while also maintaining cell viability in 14 day valve cell co-cultures (22, 31, 33).

Alizarin Red S assay

Alizarin Red S (ARS) (Sigma-Aldrich) was used to quantify calcific nodule formation (33, 34). Briefly, hydrogels were washed with 1× phosphate buffered saline (PBS, Omnipur®, Baltimore, MD, USA) and fixed with 4% paraformaldehyde (PFA, Sigma-Aldrich) overnight at 4°C. A 40 mM ARS stain solution was added, and then rinsed with 1× PBS. Bright field images were taken using a Nikon Eclipse Ts2 at 20× magnification to visualize ARS-stained area. After imaging, a 10% acetic acid solution was used to release ARS and a 10% ammonium hydroxide solution was used to neutralize. Absorbance was measured with a plate reader at 405 nm and concentration was calculated using a standard curve (35).

Alkaline phosphatase assay

Alkaline phosphatase was used to investigate early stage valve disease progression. After 2 weeks of growth, gels were enzymatically digested with a 600 U/mL collagenase type II solution (Worthington Biochemical Corporation). Once cells were in solution, they were rinsed with 1× PBS *via* centrifugation, resuspended in sterile 18 MΩ water, and sonicated for 20 min. An ALP substrate (pNPP, Sigma-Aldrich) was then added to each cell lysate, and read at 405 nm using a plate reader, and concentration was calculated using a standard curve of p-nitrophenol (Sigma-Aldrich). P-nitrophenol values were normalized to total protein content in hydrogels obtained with Bradford assays (Sigma-Aldrich).

Immunocytochemistry

Immunocytochemistry techniques were used to co-label α-SMA and PECAM-1. A detailed protocol was described by Dahal et al. (17). Following 2 weeks of growth, hydrogels were rinsed with 1× PBS and fixed overnight at 4°C with 4% PFA. Samples were then permeabilized with 0.2% Triton X-100 (Sigma-Aldrich) and blocked with 1% bovine serum albumin (BSA, Rockland™, Limerick, PA, USA) diluted in 1× PBS overnight at 4°C. Primary antibodies for α-SMA (Abcam ab125044) at a 1:100 dilution and for PECAM-1 (P2B1, DHSB) at 2 μg/mL were both added in 1× PBS and incubated overnight at 4°C. Dilutions of 1:1000 of secondary antibodies for α-SMA [Goat Anti-Rabbit IgG H&L Alexa Fluor® 488 (ab150077)] and PECAM-1 [Goat Anti-Mouse IgG H&L Alexa Fluor® 568 (A11008)] were added. Samples were incubated for 2 h at room temperature (RT) and protected from light. Secondary antibodies were rinsed and DRAQ-5 (ThermoFisher Scientific, 62251) was added at a dilution of 1:1000 and incubated for 30 min at RT and protected from light. Hydrogels were then imaged using a Zeiss LSM 880 Two-Photon confocal microscope. An image analysis code was implemented in MATLAB to compute the amount of α-SMA expression relative to DNA content.

Fluorescence activated cell sorting

Flow cytometry-based FACS (fluorescence-activated cell sorting) was used to quantitatively evaluate resident cell populations. Hydrogels were rinsed with 1× PBS and digested using 400 μL of a 600 U/mL collagenase solution for 1–2 h, with agitation every 30 min. Once the cells were free from the matrix, the solution was centrifuged at 106°× *g* for 5 min and the cells were rinsed once with 1× PBS and then resuspended in FACS buffer (25 mM HEPES + 2 mM EDTA + 2% FBS in 1× PBS). The cell suspension for each condition was then transferred into a well of a U-bottom 96-well plate, centrifuged at 106°× *g*, resuspended in 100 μL of primary antibody for extracellular marker PECAM-1 (P2B1, DHSB) at 2 μg/mL, and incubated on ice for 30 min. Samples were then centrifuged at 106°× *g*, resuspended in 1:100 of secondary antibody Goat-Anti-Mouse IgG H&L Alexa Fluor® 647 (ab150115), and incubated on ice for 30 min before centrifugation. The cell solution was then fixed and permeabilized by incubating the suspension in BD Biosciences Fix/Perm buffer (554714) for 20 min at RT and protected from light. The buffer was then removed, samples were resuspended in 100 μL of primary antibody for intracellular marker α-SMA (ab125044) at a 1:50 dilution, and incubated for 30 min on ice. The samples were then centrifuged at 106°× *g*, resuspended in 1:100 of secondary antibody Goat Anti-Rabbit IgG H&L Alexa Fluor® 488 (ab150077), and incubated

on ice for 30 min before centrifugation and resuspension in FACS buffer for analysis. Negative controls with only secondary antibody stains were also evaluated to quantify both cell autofluorescence and non-specific binding of the secondary antibodies. Solutions were processed with the BD FACS Aria II flow cytometer and analyzed using FlowJo v10 software.

CellTrace^{TM} analysis

To track generational activity of resident cell populations, CellTrace^{TM} (ThermoFisher Scientific, Waltham, MA, USA) proliferation kits were used to stain PAVICs and PAVECs individually. Following the manufacturer's protocol, after trypsinizing, PAVICs were resuspended in 1× PBS and then incubated with the CellTrace^{TM} CFSE Proliferation Kit (ThermoFisher C34554) stock solution diluted in DMSO (Invitrogen) for 20 min at 37°C, protected from light. Culture media was then added and incubated for 5 min before removing free dye from the solution. The PAVIC suspension was then centrifuged and resuspended in ice-cold 3× DMEM, 18 MΩ water, and FBS before adding NaOH and collagen I to form hydrogels. Gels were incubated for 1 h at 37°C to crosslink. The staining process was repeated for PAVECs using the CellTrace^{TM} Far Red Proliferation Kit (Thermofisher C34564). PAVECs were then resuspended in warm PAVIC medium before being plated on top of hydrogels. Gels were grown for 2 weeks and either imaged intact (Zeiss LSM 880) or digested with a 600 U/mL collagenase type II solution to extract cells and rinsed with 1× PBS, before analyzing with the BD FACS Aria II flow cytometer. Proliferation activity, also referred to as generational activity, was assessed by quantifying cell divisions of PAVICs and PAVECs using the FlowJo proliferation modeling tool. Z-stack confocal images of CellTrace^{TM}-stained intact hydrogels were taken and cellular invasion activity was quantified in MATLAB, thereby probing resident cell and matrix activity.

Data processing and statistical analysis

All data were processed, analyzed, and graphed in GraphPad Prism 9. Non-parametric Kruskal–Wallis tests with Dunn's *post hoc* multiple comparisons tests were used to test differences among all experimental groups due to small sample sizes. Sharpiro–Wilks tests were used to verify the normality assumptions. The Spearman's correlation coefficient was used to measure the association between the number of cells invaded and the average distances traveled when the normality assumptions were violated. A p-value < 0.05 was considered statistically significant. Experimental sample sizes (n) were specified in figure legends.

Results

Disease progression analysis

Following 14 days in culture, samples were analyzed for both early stage ALP activity and late-stage calcification with ARS assays. All conditions demonstrated ALP activity less than 0.11 mg p-nitrophenol/mg protein, and GAGs conditions showed no significant difference in ALP activity when compared to the 1.5 mg/mL collagen-only controls. The 2.2 mg/mL collagen stiffness control was significantly higher than both experimental GAG conditions, suggesting that stiffness contributed more significantly to early stage disease than GAG presence (**Figure 1A**).

Alizarin Red S staining was used to locate calcific nodule formation in hydrogels. Intact hydrogels stained with ARS were imaged (**Figures 1D–G**) and analyzed using ImageJ. ARS stain quantification with a plate reader showed that an increase in stiffness (2.2 mg/mL collagen) induced calcification, and 20 mg/mL CS further significantly induced matrix mineralization. However, HA did not exhibit the same effect (**Figure 1B**). Stain quantification results were consistent with those from the quantification of the stained area in ARS images (**Figure 1C**).

Protein expression

Hydrogels were co-stained for PECAM-1 (endothelial marker) and α-SMA (activated fibroblast marker) to determine protein expression and cell transformation after 14 days. Confocal images (**Figures 2A–D**) showed an increase in α-SMA expression in conditions containing the GAGs CS and HA. A semi-quantitative analysis of α-SMA expression in MATLAB verified a significant increase of α-SMA expression in GAGs conditions compared to 1.5 mg/mL collagen controls (**Figure 2E**).

To quantify α-SMA and PECAM-1 expression, hydrogels were digested, immunocytochemistry staining was used, and cells were analyzed with flow cytometry using a standardized gating procedure in the FlowJo software. Across the four conditions, the percentage of PAVECs (+PECAM-1, −α-SMA) remained consistent (**Figure 3A**). The number of transformed cells (+PECAM-1, +α-SMA) increased in the presence of CS (**Figure 3B**). The number of PAVICs (−PECAM-1, −α-SMA) decreased in the presence of CS when compared to controls. The 2.2 mg/mL collagen stiffness control condition also had a lower number of PAVICs when compared to 1.5 mg/mL collagen condition (**Figure 3C**). CS conditions resulted in a higher percentage of aVICs (−PECAM-1, +α-SMA) when compared to HA and 1.5 mg/mL collagen conditions. Similarly, the 2.2 mg/mL collagen stiffness controls also had a significant increase in aVICs when compared to 1.5 mg/mL collagen

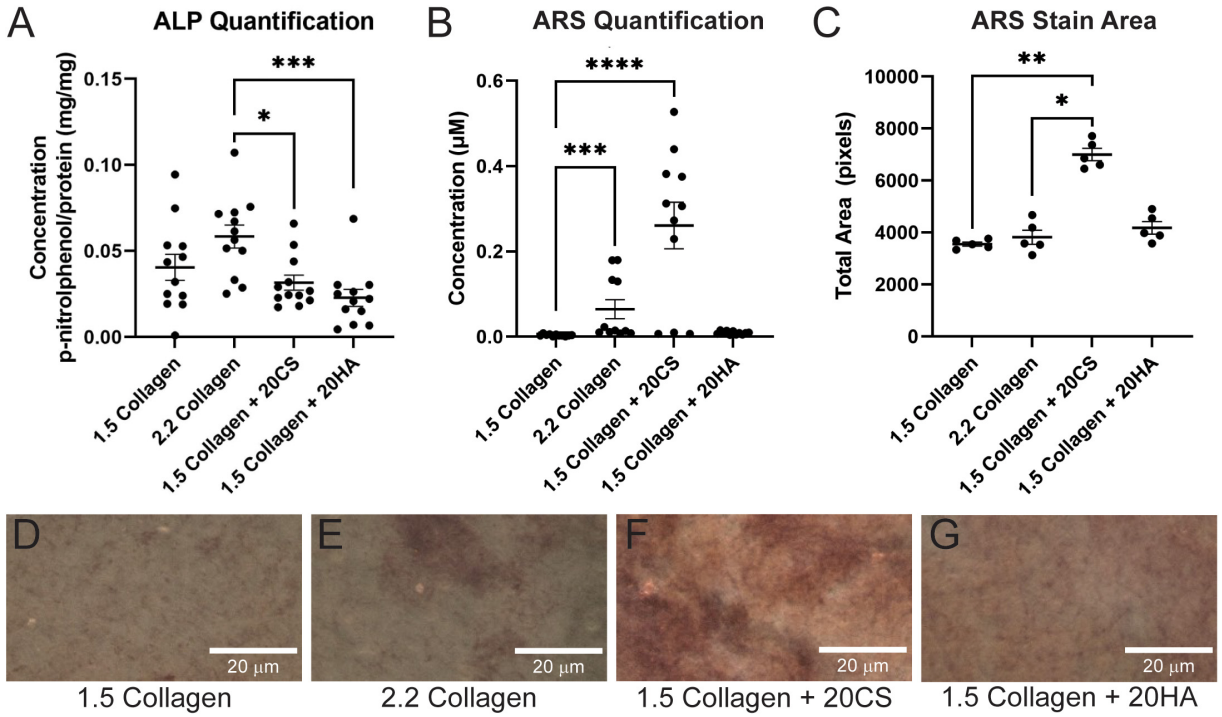

FIGURE 1
Chondroitin sulfate promotes calcific nodule formation and glycosaminoglycans (GAGs) do not produce increased alkaline phosphatase (ALP) activity. **(A)** ALP quantification in mg p-nitrophenol per mg protein (mg/mg) of digested hydrogels. $n = 12$. **(B)** Quantification of ARS-stained digested hydrogel samples. $n = 11$. **(C)** ARS stain area processed with ImageJ. $n = 5$. Data represented as mean ± SEM. **(D–G)** Brightfield images of intact ARS-stained hydrogels using a Nikon Eclipse Ts2 at 20×. Statistical significance was determined with a non-parametric Kruskal–Wallis test with Dunn's *post-hoc* test. $*p < 0.05$, $**p < 0.01$, $***p < 0.001$, and $****p < 0.0001$. Scale bars = 20 μm.

controls (Figure 3D). Results from the confocal images and semi-quantitative analysis of relative α-SMA expression were similar, both indicating increases in α-SMA expression in the presence of CS (Figures 2E, 3B,D).

Cellular invasion

To investigate cellular invasion rates, confocal z-stack images of intact hydrogels were taken at four fields of view in four biological replicates and analyzed. PAVECs and PAVICs were stained individually with CellTrace^{TM} Far Red and CellTrace^{TM} CSFE, respectively, before seeding onto and into hydrogels. After 2 weeks, hydrogels were imaged, and PAVECs that had deviated from the seeded monolayer were visualized (Figures 4A–D) and quantified using a MATLAB script. Examples of MATLAB centroid tracking for each condition were shown (Figures 4E–H) with an example of the invasion analysis (Figure 4L). The average number of invaded cells was significantly higher for the 2.2 mg/mL collagen (stiffness control) and HA conditions when compared to cells within control hydrogels (1.5 mg/mL collagen) (Figure 4I). Similarly, the average distance invaded was significantly greater for 2.2 mg/mL collagen and HA conditions, and there was an insignificant increase in average distance invaded for the CS conditions when compared to the 1.5 mg/mL collagen control (Figure 4J). Overall, conditions with GAGs promoted greater invasion rates. There was a positive correlation (Spearman's $r = 0.63$, P-value $= 0.009$) between the number of cells that invaded and the average distance they traveled (Figure 4K).

Proliferation

Flow cytometry analysis of CellTrace^{TM}-stained cells was used to assess *in vitro* proliferation activity in the model. CellTrace^{TM} tracking dyes halve in fluorescence intensity with each cellular division, and the relative fluorescence of each cell measured *via* flow cytometry can provide insight into which generation each cell belongs to. Flow cytometry analysis demonstrated an increase in the number of cellular divisions, represented as a generation number (G0 = initial generation, increasing to as much as G4), in samples with CS (Figures 5C,H) and HA (Figures 5D,I) when compared to 1.5 mg/mL (Figures 5A,F) and 2.2 mg/mL (Figures 5B,G) collagen controls for both PAVECs and PAVICs. Specifically, CS

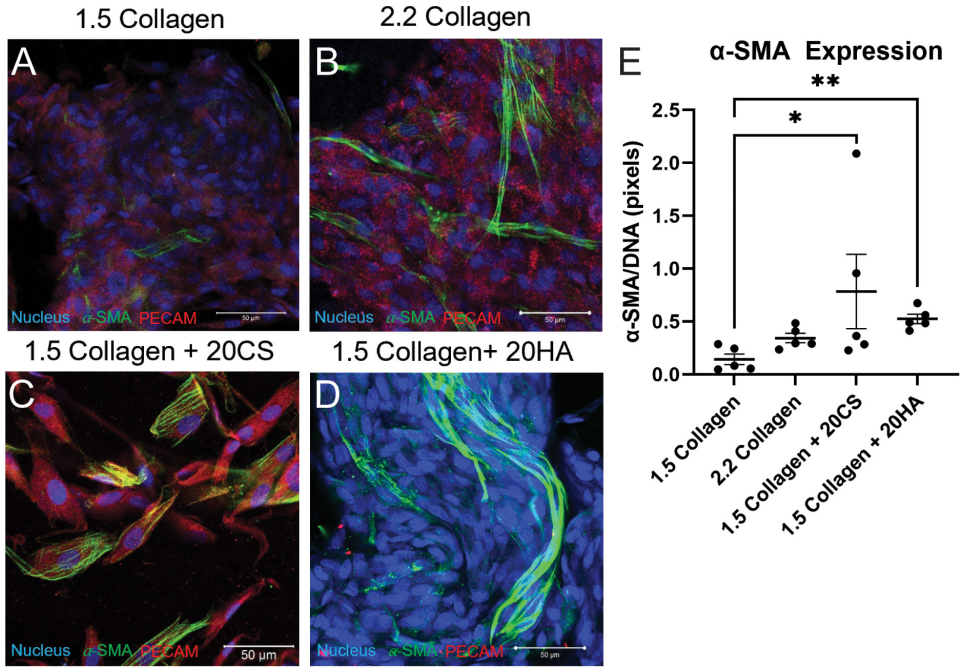

FIGURE 2
Glycosaminoglycans (GAGs) conditions express higher α-SMA per unit DNA than controls. **(A–D)** Confocal images of intact hydrogels co-stained for α-SMA (green), PECAM-1 (red), and DNA (blue) after 14 days of growth. Scale bars = 50 μm. **(E)** α-SMA expression quantified using a MATLAB script, represented as pixels of α-SMA (green signal) per pixels DNA (blue signal). Data represented as mean ± SEM. Statistical significance was determined with a non-parametric Kruskal–Wallis test with Dunn's *post-hoc* test. *$p < 0.05$ and **$p < 0.01$. $n = 5$.

induced the greatest proliferation activity (G4) in both PAVECs and PAVICs (**Figures 5E,J**).

Discussion

This study developed an *in vitro* 3D collagen hydrogel model of the aortic valve fibrosa, simulating late-stage CAVD progression in the fibrosa layer by incorporating GAGs into 3D collagen I hydrogels. The model was used to study enzyme activity, cellular proliferation, protein expression, and calcific nodule formation of the resident cell populations. Two GAGs, CS and HA, were incorporated to investigate the role of EndMT-derived aVIC activity in matrix mineralization, and these GAG conditions were found to alter cellular behavior in addition to hydrogel stiffness without the addition of osteogenic medium.

One limitation of the current study is that sex was not addressed. Cells were isolated from female or castrated male pigs. Previous work has shown that there are sex-related differences in gene expression, matrix remodeling, angiogenesis, and early osteogenic markers in porcine and rat aortic valve interstitial cells (36–40). Additionally, previous work has shown that cardiac fibroblasts can be isolated from rats or mice and maintained for a longer period in a quiescent state by decreasing the stiffness of the culture matrix and limiting the nutrient content of the cell culture medium to 2% serum (41), or porcine VIC myofibroblast differentiation can be blocked by culturing with fibroblast growth factor (FGF-2) (42). The control medium used in the current study contained 10% serum without FGF-2, and this alone may have contributed to valve cell differentiation toward myofibroblasts. CS and HA both increased α-SMA expression (**Figures 2**, **3**), invasion rates (**Figure 4**), and proliferation activity (**Figure 5**). Additionally, CS conditions yielded a higher level of calcific nodule formation (**Figure 1**), suggesting that alterations in ECM composition are leading to pathological matrix remodeling. Similar ECM alterations were seen in developmental conditions, but these environments lack disruptive matrix mineralization (20, 43). This model also supplements the understanding of the relationship between changing ECM composition and cellular behavior, including eventual pathological consequences. A better understanding of how ECM composition affects cellular behavior could improve tissue engineered heart valves. Understanding the fate of EndMT-derived aVICs could help to direct interstitial cells toward matrix regeneration/reconstruction, for example, or EndMT could provide a viable drug target for CAVD treatment.

This work indicated that HA does not stimulate either early or late-stage disease (**Figure 1**). However, Stephens et al. discovered the presence of HA local to calcific

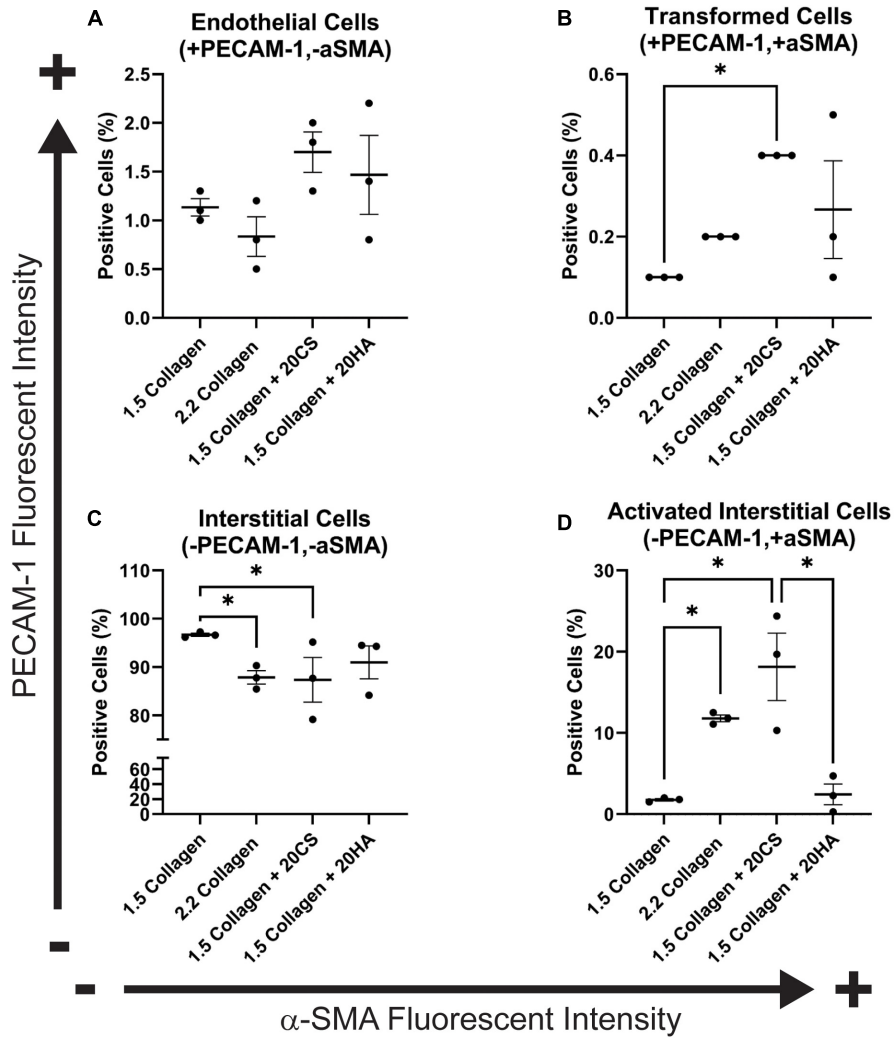

FIGURE 3
Flow cytometry analysis of protein expression shows an increase in transformed cells in glycosaminoglycans (GAGs) conditions, and an increase in activated interstitial cells in the presence of chondroitin sulfate (CS). Following 14 days of growth, hydrogels were degraded, and isolated cells were processed using a BD FACS Aria II flow cytometer. Cells were stained with α-SMA (Alexa Fluor® 488) and PECAM-1 (Alexa Fluor® 647). **(A)** Endothelial cells (positive for PECAM-1 and negative for α-SMA). **(B)** Cells that have undergone transformation (positive for both PECAM-1 and α-SMA). **(C)** Interstitial cells (negative for PECAM-1 and α-SMA) and **(D)** Activated interstitial cells (negative for PECAM-1 and positive for a-SMA). Data represented as mean ± SEM. Statistical significance was determined with a non-parametric Kruskal–Wallis test with Dunn's *post-hoc* test. $^*p < 0.05$. $n = 3$.

nodules in diseased human valves, indicating a potentially upregulating effect of HA on calcific nodule formation (16). Baugh et al. (44) found that HA increased calcification in rat interstitial cells whereas Ohri et al. (45) demonstrated HA to have a hampering effect on matrix mineralization in glutaraldehyde-fixed bovine pericardium. Masters et al. revealed that HA increased porcine valvular interstitial cell activity and ECM production, indicating that HA plays an important role in cardiac morphogenesis and remodeling (27, 46). Alternatively, Porras et al. demonstrated that pathological concentrations of HA and CS were not sufficient to cause *in vitro* disease progression in porcine VICs (29). Although there are discrepancies in the effect that HA has on calcification and disease progression, HA appears to have an overall regulatory effect on valve function. These results confirmed that HA did not exacerbate late-stage mineralization, but did induce significant alterations in cellular behavior (increased proliferation, α-SMA expression, and invasion rates), when compared to collagen-only controls. Lei et al. found that the incorporation of HA into tissue engineered scaffolds seeded with porcine cells promoted cell-mediated tissue remodeling, increased matrix density and stiffness, and regulated tissue contraction (47). Similarly, the current study provides evidence that HA may play a role in matrix

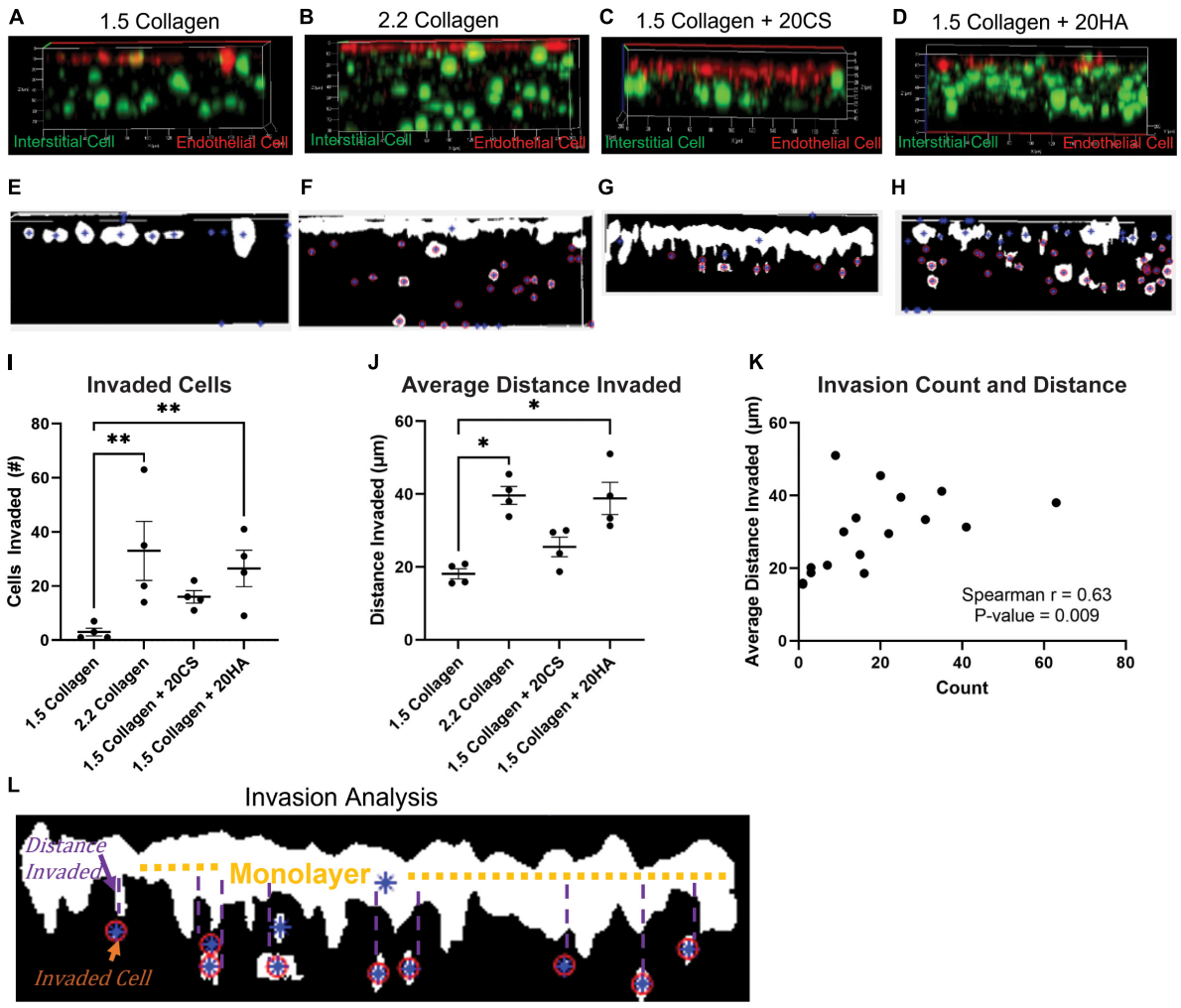

FIGURE 4
Glycosaminoglycans (GAGs) conditions promote cellular invasion. **(A–D)** Z-stack confocal images taken with a Zeiss LSM 880 Two-Photon confocal microscope. Interstitial cells were stained with CellTrace CSFE-Green (green) and endothelial cells with CellTrace Far-Red (red) prior to hydrogel seeding. Red cells that have migrated from the cell monolayer are classified as invaded. **(E–H)** Examples of MATLAB processed z-stack images used to quantify **(I)** the number of invaded cells and **(J)** the average distance each cell travelled. Data represented as mean ± SEM. $n = 4$. Statistical significance was determined with a non-parametric Kruskal–Wallis test with Dunn's *post hoc* test. $^{*}p < 0.05$, $^{**}p < 0.01$, $^{***}p < 0.001$, $^{****}p < 0.0001$. **(K)** Average distance invaded plotted against the number of cells invaded. Non-parametric Spearman's correlation was estimated to evaluate if there was linear association (Spearman's $r = 0.63$, with P-value $= 0.009$). **(L)** Example of the invasion analysis and centroid tracking. Blue stars are identified cells, and red circles are cells that are counted as invaded cells. Average distance is calculated as distance the cell has deviated from the monolayer.

regeneration and could be a potential tool for directing tissue activity toward non-pathological matrix remodeling. Recapitulating the role of HA in valvulogenesis could yield greater insight into improved methods for scaffolding and selection of biomaterials for novel tissue engineered valves (47, 48).

In contrast to HA, CS conditions were shown to induce late-stage mineralization (**Figure 1**), significant α-SMA expression (**Figure 2**), and increased proliferation rates. This suggests a possible cascade of events that resulted from an increase in EndMT-derived aVIC, which have higher expression of α-SMA (22). Dahal et al. also showed that CS increased pro-calcific markers (myofibroblastic and osteoblastic gene expression) and collagen I production by porcine aVICs (22). Additionally, Mendoza et al. demonstrated that 20 mg/mL CS contributed to CAVD progression in a microfluidic 3D model using PAVIC and PAVEC (35). Interestingly, HA was also shown to increase EndMT-related activity and proliferation levels, but to a lesser extent than CS, and did not result in the same late-stage disease as CS did within the *in vitro* model. Porras et al. also found that CS was effective in retaining lipoproteins classical to

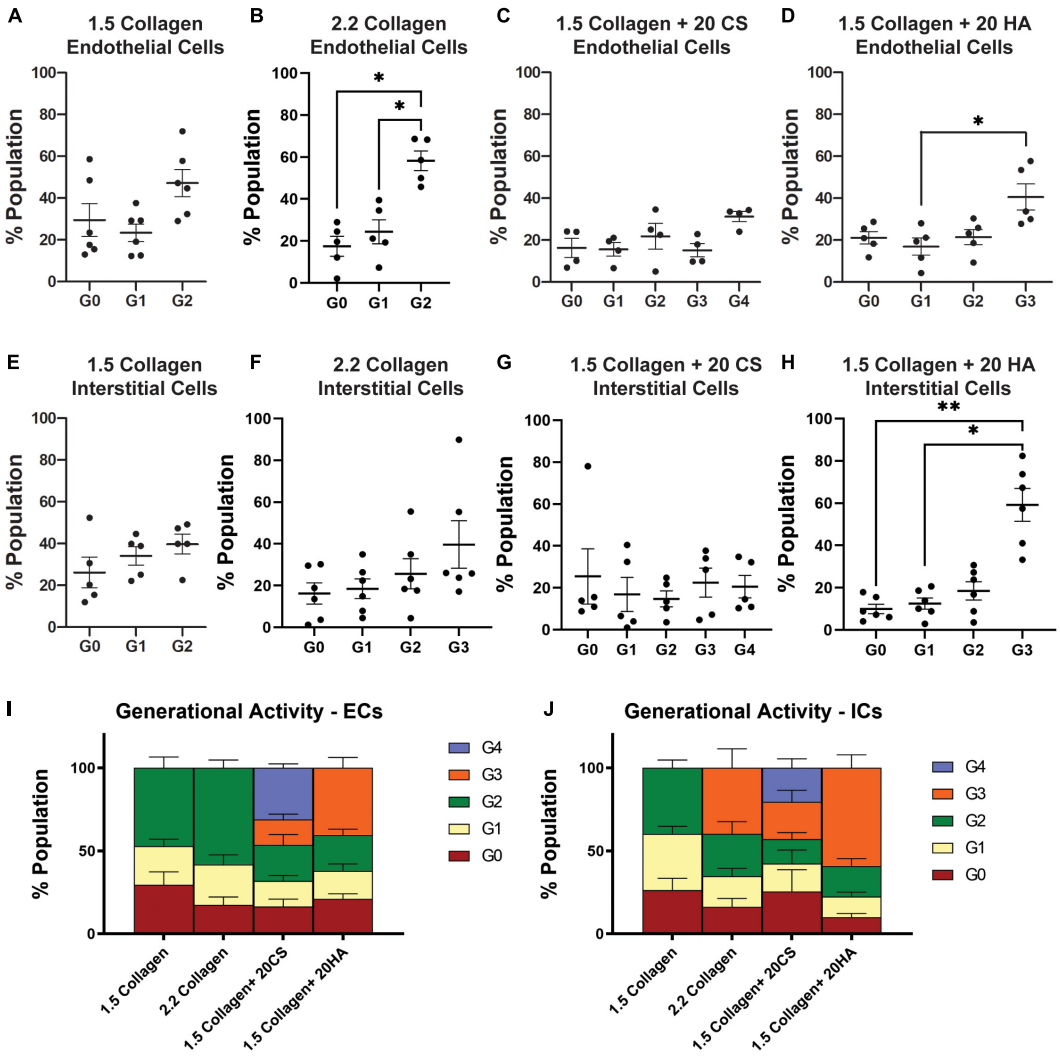

FIGURE 5
Glycosaminoglycans (GAGs) conditions promote higher levels of cellular proliferation in endothelial and interstitial cells. Interstitial cells were stained with CellTrace CSFE-Green and endothelial cells with CellTrace Far-Red prior to hydrogel seeding. Flow cytometry processing (BC FACS Aria II) was used to measure fluorescence of cells extracted from digested hydrogels after 14 days of growth. FlowJo's proliferation toolbox was used for analysis. **(A–D)** Generational activity for endothelial cells stained with CellTrace Far-Red across four conditions. **(E–H)** Generational activity for interstitial cells stained with CellTrace CSFE across four conditions. **(I)** Population percentages of each generation and each condition for endothelial cells. **(J)** Population percentages of each generation and each condition for interstitial cells. Data represented as mean ± SEM. *$p < 0.05$ and **$p < 0.01$.

early disease markers in a model containing porcine cells, indicating that CS alone may promote a fibrocalcific response (29). Understanding the differences and relationship between these two GAG types could provide guidance in designing engineered scaffolds or disease models. For example, Lei et al. used HA and CS to supplement bioprosthetic heart valve constructs, and concluded that when used together, these GAGs decreased calcification when compared to scaffolds without GAGs (49). This information can contribute to enhanced fabrication of bioprosthetic valves, and can aid in choosing appropriate cell sources for enhanced valvular matrix regeneration properties and the prevention of disease conditions. Further work can focus on the integration of both HA and CS into the 3D model, thereby exploring their relationship.

Conclusion

We have developed a 3D cell culture model of CAVD by incorporating GAGs into a collagen I hydrogel seeded with porcine aortic valve cells. Findings suggest that the altered ECM containing CS may yield matrix mineralization *via* EndMT-mediated aVICs. In conditions containing HA,

matrix mineralization was not present, despite increased levels of EndMT when compared to controls (increased α-SMA expression and cellular invasion). The role of EndMT in valvulogenesis is well-studied, and EndMT is also associated with adult diseases, including cancer (50). The role of EndMT in CAVD disease progression still remains unknown, and this model contributes to the knowledge gap. Leveraging non-calcific EndMT as a tool for directing matrix reconstruction and using natural biomaterials, such as HA and CS, could significantly benefit the production of bioengineered valves. Specifically, this work demonstrates that HA supplementation could be a viable option for long-term scaffolding. Further, this model could also provide a platform for testing new pharmaceutical treatments of late-stage CAVD.

Data availability statement

The raw data supporting the conclusions of this article will be made available by the authors, without undue reservation.

Author contributions

BM, PH, M-HC, and GM secured the funding. JB, BA, and MM performed the experiments and collected the data. JB, BA, and M-HC conducted the formal data analysis. JB and BA wrote the manuscript. MM, BM, PH, M-HC, and GM reviewed and edited the manuscript. All authors contributed to the article and approved the submitted version.

Funding

This work was supported by National Science Foundation (NSF) CMMI 1919438 (GM, BM, PH, and M-HC) and Clifford D. Clark Diversity Fellowship (JB).

Acknowledgments

We thank Log City Meats LLC in Dundee, NY for providing porcine aortic valves.

Conflict of interest

Log City Meats LLC in Dundee, NY for provided porcine aortic valves.

Publisher's note

References

1. Myasoedova VA, Ravani AL, Frigerio B, Valerio V, Moschetta D, Songia P, et al. Novel pharmacological targets for calcific aortic valve disease: prevention and treatments. *Pharmacol Res.* (2018) 136:74–82.

2. Virani SS, Alonso A, Aparicio HJ, Benjamin EJ, Bittencourt MS, Callaway CW, et al. Heart Disease and stroke statistics-2021 update: a report from the American heart association. *Circulation.* (2021) 143:e254–743. doi: 10.1161/CIR.0000000000000950

3. Rutkovskiy A, Malashicheva A, Sullivan G, Bogdanova M, Kostareva A, Stensløkken KO, et al. Valve interstitial cells: the key to understanding the pathophysiology of heart valve calcification. *J Am Heart Assoc.* (2017) 6:e006339.

4. Butcher JT, Markwald RR. Valvulogenesis: the moving target. *Philos Trans R Soc Lond B Biol Sci.* (2007) 362:1489–503. doi: 10.1098/rstb.2007.2130

5. Yang J-H, Wylie-Sears J, Bischoff J. Opposing actions of Notch1 and VEGF in post-natal cardiac valve endothelial cells. *Biochem Bioph Res Co.* (2008) 374:512–6. doi: 10.1016/j.bbrc.2008.07.057

6. Combs MD, Yutzey KE. Heart valve development: regulatory networks in development and disease. *Circ Res.* (2009) 105:408–21.

7. Farrar EJ, Pramil V, Richards JM, Mosher CZ, Butcher JT. Valve interstitial cell tensional homeostasis directs calcification and extracellular matrix remodeling processes via RhoA signaling. *Biomaterials.* (2016) 105:25–37. doi: 10.1016/j.biomaterials.2016.07.034

8. Liu M, Li F, Huang Y, Zhou T, Chen S, Li G, et al. Caffeic acid phenethyl ester ameliorates calcification by inhibiting activation of the AKT/NF-κB/NLRP3 Inflammasome pathway in human aortic valve interstitial cells. *Front Pharmacol.* (2020) 11:826. doi: 10.3389/fphar.2020.00826

9. Butcher JT, Mahler GJ, Hockaday LA. Aortic valve disease and treatment: the need for naturally engineered solutions. *Adv Drug Deliver Rev.* (2011) 63:242–68. doi: 10.1016/j.addr.2011.01.008

10. Rajamannan NM, Subramaniam M, Rickard D, Stock SR, Donovan J, Springett M, et al. Human aortic valve calcification is associated with an osteoblast phenotype. *Circulation.* (2003) 107:2181–4.

11. Porras AM, Shanmuganayagam D, Meudt JJ, Krueger CG, Hacker TA, Rahko PS, et al. Development of aortic valve disease in familial hypercholesterolemic swine: implications for elucidating disease etiology. *J Am Heart Assoc.* (2015) 4:e002254.

12. Yu B, Hafiane A, Thanassoulis G, Ott L, Filwood N, Cerruti M, et al. Lipoprotein(a) induces human aortic valve interstitial cell calcification. *JACC Basic Transl Sci.* (2017) 2:358–71.

13. Bonetti A, Marchini M, Ortolani F. Ectopic mineralization in heart valves: new insights from in vivo and in vitro procalcific models and promising perspectives on noncalcifiable bioengineered valves. *J Thorac Dis.* (2019) 11:2126–43. doi: 10.21037/jtd.2019.04.78

14. Towler DA. Molecular and cellular aspects of calcific aortic valve disease. *Circ Res.* (2013) 113:198–208.

15. Otto CM. Calcific aortic stenosis–time to look more closely at the valve. *N Engl J Med.* (2008) 359:1395–8. doi: 10.1056/NEJMe0807001

16. Stephens EH, Saltarrelli JG, Baggett LS, Nandi I, Kuo JJ, Davis AR, et al. Differential proteoglycan and hyaluronan distribution in calcified aortic valves. *Cardiovasc Pathol.* (2011) 20:334–42. doi: 10.1016/j.carpath.2010.10.002

17. Dahal S, Huang P, Murray BT, Mahler GJ. Endothelial to mesenchymal transformation is induced by altered extracellular matrix in aortic valve endothelial cells. *J Biomed Mater Res A.* (2017) 105:2729–41. doi: 10.1002/jbm.a.36133

18. Artiach G, Carracedo M, Seime T, Plunde O, Laguna-Fernandez A, Matic L, et al. Proteoglycan 4 is increased in human calcified aortic valves and enhances valvular interstitial cell calcification. *Cells.* (2020) 9:684. doi: 10.3390/cells9030684

19. Piera-Velazquez S, Jimenez SA. Endothelial to mesenchymal transition: role in physiology and in the pathogenesis of human diseases. *Physiol Rev.* (2019) 99:1281–324.

20. Bischoff J. Endothelial-to-mesenchymal transition. *Circ Res.* (2019) 124:1163–5.

21. Kovacic JC, Dimmeler S, Harvey RP, Finkel T, Aikawa E, Krenning G, et al. Endothelial to mesenchymal transition in cardiovascular disease: JACC state-of-the-art review. *J Am Coll Cardiol.* (2019) 73:190–209.

22. Dahal S, Bramsen JA, Alber BR, Murray BT, Huang P, Chen MH, et al. Chondroitin sulfate promotes interstitial cell activation and calcification in an in vitro model of the aortic valve. *Cardiovasc Eng Technol.* (2021) 13:481–94. doi: 10.1007/s13239-021-00586-z

23. Hjortnaes J, Goettsch C, Hutcheson JD, Camci-Unal G, Lax L, Scherer K, et al. Simulation of early calcific aortic valve disease in a 3D platform: a role for myofibroblast differentiation. *J Mol Cell Cardiol.* (2016) 94:13–20. doi: 10.1016/j.yjmcc.2016.03.004

24. Jenke A, Kistner J, Saradar S, Chekhoeva A, Yazdanyar M, Bergmann AK, et al. Transforming growth factor-β1 promotes fibrosis but attenuates calcification of valvular tissue applied as a three-dimensional calcific aortic valve disease model. *Am J Physiol Heart Circ Physiol.* (2020) 319:H1123–41. doi: 10.1152/ajpheart.00651.2019

25. Vadana M, Cecoltan S, Ciortan L, Macarie RD, Tucureanu MM, Mihaila AC, et al. Molecular mechanisms involved in high glucose-induced valve calcification in a 3D valve model with human valvular cells. *J Cell Mol Med.* (2020) 24:6350–61. doi: 10.1111/jcmm.15277

26. Cecoltan S, Ciortan L, Macarie RD, Vadana M, Mihaila AC, Tucureanu M, et al. High glucose induced changes in human vec phenotype in a 3d hydrogel derived from cell-free native aortic root. *Front Cardiovasc Med.* (2021) 8:714573. doi: 10.3389/fcvm.2021.714573

27. Rodriguez KJ, Piechura LM, Masters KS. Regulation of valvular interstitial cell phenotype and function by hyaluronic acid in 2-D and 3-D culture environments. *Matrix Biol.* (2011) 30:70–82. doi: 10.1016/j.matbio.2010.09.001

28. Hjortnaes J, Camci-Unal G, Hutcheson JD, Jung SM, Schoen FJ, Kluin J, et al. Directing valvular interstitial cell myofibroblast-like differentiation in a hybrid hydrogel platform. *Adv Healthc Mater.* (2015) 4:121–30. doi: 10.1002/adhm.201400029

29. Porras AM, Westlund JA, Evans AD, Masters KS. Creation of disease-inspired biomaterial environments to mimic pathological events in early calcific aortic valve disease. *Proc Natl Acad Sci USA.* (2018) 115:E363–71. doi: 10.1073/pnas.1704637115

30. Meerman M, Driessen R, Van Engeland NCA, Bergsma I, Steenhuijsen JLG, Kozono D, et al. Radiation induces valvular interstitial cell calcific response in an in vitro model of calcific aortic valve disease. *Front Cardiovasc Med.* (2021) 8:687885. doi: 10.3389/fcvm.2021.687885

31. Hjortnaes J, Shapero K, Goettsch C, Hutcheson JD, Keegan J, Kluin J, et al. Valvular interstitial cells suppress calcification of valvular endothelial cells. *Atherosclerosis.* (2015) 242:251–60.

32. Butcher JT, Penrod AM, Garcia AJ, Nerem RM. Unique morphology and focal adhesion development of valvular endothelial cells in static and fluid flow environments. *Arterioscler Thromb Vasc Biol.* (2004) 24:1429–34. doi: 10.1161/01.ATV.0000130462.50769.5a

33. Richards J, El-Hamamsy I, Chen S, Sarang Z, Sarathchandra P, Yacoub MH, et al. Side-specific endothelial-dependent regulation of aortic valve calcification: interplay of hemodynamics and nitric oxide signaling. *Am J Pathol.* (2013) 182:1922–31. doi: 10.1016/j.ajpath.2013.01.037

34. Gregory CA, Gunn WG, Peister A, Prockop DJ. An Alizarin red-based assay of mineralization by adherent cells in culture: comparison with cetylpyridinium chloride extraction. *Anal Biochem.* (2004) 329:77–84. doi: 10.1016/j.ab.2004.02.002

35. Mendoza M, Chen MH, Huang P, Mahler GJ. Shear and endothelial induced late-stage calcific aortic valve disease-on-a-chip develops calcium phosphate mineralizations. *Lab Chip.* (2022) 22:1374–85. doi: 10.1039/d1lc00931a

36. McCoy CM, Nicholas DQ, Masters KS. Sex-related differences in gene expression by porcine aortic valvular interstitial cells. *PLoS One.* (2012) 7:e39980. doi: 10.1371/journal.pone.0039980

37. Masjedi S, Lei Y, Patel J, Ferdous Z. Sex-related differences in matrix remodeling and early osteogenic markers in aortic valvular interstitial cells. *Heart Vessels.* (2017) 32:217–28. doi: 10.1007/s00380-016-0909-8

38. Porras AM, Mccoy CM, Masters KS. Calcific aortic valve disease: a battle of the sexes. *Circ Res.* (2017) 120:604–6. doi: 10.1161/CIRCRESAHA.117.310440

39. Zhang B, Miller VM, Miller JD. Influences of sex and estrogen in arterial and valvular calcification. *Front Endocrinol.* (2019) 10:622. doi: 10.3389/fendo.2019.00622

40. Nelson V, Patil V, Simon LR, Schmidt K, Mccoy CM, Masters KS. Angiogenic secretion profile of valvular interstitial cells varies with cellular sex and phenotype. *Front Cardiovasc Med.* (2021) 8:736303. doi: 10.3389/fcvm.2021.736303

41. Landry NM, Rattan SG, Dixon IMC. An improved method of maintaining primary murine cardiac fibroblasts in two-dimensional cell culture. *Sci Rep.* (2019) 9:12889. doi: 10.1038/s41598-019-49285-9

42. Cushing MC, Mariner PD, Liao JT, Sims EA, Anseth KS. Fibroblast growth factor represses Smad-mediated myofibroblast activation in aortic valvular interstitial cells. *FASEB J.* (2008) 22:1769–77. doi: 10.1096/fj.07-087627

43. Aikawa E, Whittaker P, Farber M, Mendelson K, Padera RF, Aikawa M, et al. Human semilunar cardiac valve remodeling by activated cells from fetus to adult: implications for postnatal adaptation, pathology, and tissue engineering. *Circulation.* (2006) 113:1344–52. doi: 10.1161/CIRCULATIONAHA.105.591768

44. Baugh L, Watson MC, Kemmerling EC, Hinds PW, Huggins GS, Black LD III. Knockdown of CD44 expression decreases valve interstitial cell calcification in vitro. *Am J Physiol Heart Circ Physiol.* (2019) 317:H26–36. doi: 10.1152/ajpheart.00123.2018

45. Ohri R, Hahn SK, Hoffman AS, Stayton PS, Giachelli CM. Hyaluronic acid grafting mitigates calcification of glutaraldehyde-fixed bovine pericardium. *J Biomed Mater Res A.* (2004) 70:328–34. doi: 10.1002/jbm.a.30088

46. Masters KS, Shah DN, Leinwand LA, Anseth KS. Crosslinked hyaluronan scaffolds as a biologically active carrier for valvular interstitial cells. *Biomaterials.* (2005) 26:2517–25. doi: 10.1016/j.biomaterials.2004.07.018

47. Lei Y, Bortolin L, Benesch-Lee F, Oguntolu T, Dong Z, Bondah N, et al. Hyaluronic acid regulates heart valve interstitial cell contraction in fibrin-based scaffolds. *Acta Biomater.* (2021) 136:124–36. doi: 10.1016/j.actbio.2021.09.046

48. Velasco-Rodriguez B, Diaz-Vidal T, Rosales-Rivera LC, García-González CA, Alvarez-Lorenzo C, Al-Modlej A, et al. Hybrid methacrylated gelatin and hyaluronic acid hydrogel scaffolds. Preparation and systematic characterization for prospective tissue engineering applications. *Int J Mol Sci.* (2021) 22:6758. doi: 10.3390/ijms22136758

49. Lei Y, Ning Q, Tang Y, Wang Y. Exogenous hyaluronic acid and chondroitin sulfate crosslinking treatment for increasing the amount and stability of glycosaminoglycans in bioprosthetic heart valves. *J Mater Sci Mater Med.* (2019) 30:38. doi: 10.1007/s10856-019-6237-7

50. Mina S, Huang P, Murray B, Mahler G. The role of shear stress and altered tissue properties on endothelial to mesenchymal transformation and tumor-endothelial cell interaction. *Biomicrofluidics.* (2017) 11:044104. doi: 10.1063/1.4991738

frontiers | Frontiers in Cardiovascular Medicine

TYPE Original Research
PUBLISHED 06 October 2022
DOI 10.3389/fcvm.2022.991729

OPEN ACCESS

EDITED BY
Verena Veulemans,
University Hospital of
Düsseldorf, Germany

REVIEWED BY
Pierfrancesco Agostoni,
Hospital Network Antwerp
(ZNA), Belgium
Orlando Parise,
Maastricht University, Netherlands

*CORRESPONDENCE
Giuseppe Tarantini
giuseppe.tarantini.1@unipd.it

†The OBSERVANT II Research Group is provided in the Supplementary material

SPECIALTY SECTION
This article was submitted to
Heart Valve Disease,
a section of the journal
Frontiers in Cardiovascular Medicine

RECEIVED 11 July 2022
ACCEPTED 09 September 2022
PUBLISHED 06 October 2022

CITATION
Fraccaro C, Tarantini G, Rosato S, Baglio G, Biancari F, Barbanti M, Tamburino C, Bedogni F, Ranucci M, Ussia GP, Seccareccia F and D'Errigo P (2022) Early and mid-term outcome of patients with low-flow–low-gradient aortic stenosis treated with newer-generation transcatheter aortic valves.
Front. Cardiovasc. Med. 9:991729.
doi: 10.3389/fcvm.2022.991729

Early and mid-term outcome of patients with low-flow–low-gradient aortic stenosis treated with newer-generation transcatheter aortic valves

Chiara Fraccaro[1], Giuseppe Tarantini[1]*, Stefano Rosato[2], Giovanni Baglio[3], Fausto Biancari[4,5], Marco Barbanti[6], Corrado Tamburino[6], Francesco Bedogni[7], Marco Ranucci[8], Gian Paolo Ussia[9], Fulvia Seccareccia[2] and Paola D'Errigo[2] on behalf of the OBSERVANT II Research Group[†]

[1]Interventional Cardiology Unit, Department of Cardiac, Thoracic, Vascular Sciences and Public Health, University of Padua, Padua, Italy, [2]Centro Nazionale per la Salute Globale, National Center for Global Health, Istituto Superiore di Sanità Italiana, Roma, Italy, [3]Italian National Agency for Regional Healthcare Services, Rome, Italy, [4]Clinica Montevergine, GVM Care & Research, Mercogliano, Italy, [5]Heart and Lung Center, Helsinki University Hospital, University of Helsinki, Helsinki, Finland, [6]Division of Cardiology, A.O.U. Policlinico "G. Rodolico—San Marco", University of Catania, Catania, Italy, [7]Interventional Cardiology Unit, IRCCS Policlinico San Donato, Milan, Italy, [8]Department of Cardiothoracic and Vascular Anesthesia and ICU, IRCCS Policlinico San Donato, Milan, Italy, [9]Department of Cardiovascular Sciences, Campus Bio-Medico University of Rome, Rome, Italy

Patients with non-paradoxical low-flow–low-gradient (LFLG) aortic stenosis (AS) are at increased surgical risk, and thus, they may particularly benefit from transcatheter aortic valve replacement (TAVR). However, data on this issue are still limited and based on the results with older-generation transcatheter heart valves (THVs). The aim of this study was to investigate early and mid-term outcome of TAVR with newer-generation THVs in the setting of LFLG AS. Data for the present analysis were gathered from the OBSERVANT II dataset, a national Italian observational, prospective, multicenter cohort study that enrolled 2,989 consecutive AS patients who underwent TAVR at 30 Italian centers between December 2016 and September 2018, using newer-generation THVs. Overall, 420 patients with LVEF $\leq$50% and mean aortic gradient $<$40 mmHg were included in this analysis. The primary outcomes were 1-year all-cause mortality and a combined endpoint including all-cause mortality and hospital readmission due to congestive heart failure (CHF) at 1 year. A risk-adjusted analysis was performed to compare the outcome of LFLG AS patients treated with TAVR (n = 389) with those who underwent surgical aortic valve replacement (SAVR, n = 401) from the OBSERVANT I study. Patients with LFLG AS undergoing TAVR were old (mean age, 80.8 $\pm$ 6.7 years) and with increased operative risk (mean EuroSCORE II, 11.5 $\pm$ 10.2%). VARC-3 device success was 83.3% with 7.6% of moderate/severe paravalvular leak. Thirty-day mortality was 3.1%. One-year all-cause mortality was 17.4%, and

the composite endpoint was 34.8%. Chronic obstructive pulmonary disease (HR 1.78) and EuroSCORE II (HR 1.02) were independent predictors of 1-year mortality, while diabetes (HR 1.53) and class NYHA IV (HR 2.38) were independent predictors of 1-year mortality or CHF. Compared with LFLG AS treated with SAVR, TAVR patients had a higher rate of major vascular complications and permanent pacemaker, while SAVR patients underwent more frequently to blood transfusion, cardiogenic shock, AKI, and MI. However, 30-day and 1-year outcomes were similar between groups. Patients with non-paradoxical LFLG AS treated by TAVR were older and with higher surgical risk compared with SAVR patients. Notwithstanding, TAVR was safe and effective with a similar outcome to SAVR at both early and mid-term.

KEYWORDS

low-flow–low-gradient, aortic stenosis, transcatheter aortic valve replacement, valvular heart disease, left ventricular dysfunction

Introduction

Transcatheter aortic valve replacement (TAVR) is as effective and safe as surgical aortic valve replacement (SAVR), and it has become the first-choice therapy in increased risk patients with severe aortic stenosis (AS) as well as otherwise lower-risk elderly (1). LFLG AS is present in about 5% to 10% of patients with or without ischemic cardiomyopathy (2). Left ventricular impairment is reversible after valve replacement when due to afterload mismatch or partially reversible when cardiomyopathy or myocardial fibrosis subsided. The treatment of these patients is challenging, and SAVR entails an increased operative mortality ranging from 6 to 30% (3–9). TAVR seems to be promising in this setting because of its increasing procedural safety (short operative time and no need for extracorporeal circulation with consequent better myocardial protection), as well as hemodynamic performance of transcatheter devices (10). However, TAVR downsides remain, such as post-procedural paravalvular leak (PVL) and need for permanent pacemaker (PPM), that might be detrimental in the setting of an already impaired LVEF (11, 12). To date, evidence supporting the value of TAVR in this setting is lacking (13–16).

In the last decade, the Italian Ministry of Health promoted the monitoring throughout the country of data regarding the treatments and outcomes of all patients affected by severe AS, which were collected into two national datasets: OBSERVANT I and OBSERVANT II. The primary aim of this study was to assess, in the large national study OBSERVANT II, the early and mid-term outcome of TAVR performed with newer-generation THVs in the setting of LFLG AS. Moreover, the secondary aim was to compare the outcome of these patients with that of patients who underwent SAVR included in the OBSERVANT I study (17).

Materials and methods

Data source

Data for this analysis were gathered from the OBSERVANT II datasets. OBSERVANT II was a national observational, prospective, multicenter cohort study that enrolled 2,989 consecutive AS patients who underwent TAVR at 30 Italian centers of cardiology between December 2016 and September 2018 (18–20). Twenty-eight centers met the data quality criteria required by the study protocol, and their data were included in the present analysis. The study protocol was approved by local ethics committees, and the recruited patients gave their consent to participate in this study. Data on baseline characteristics, operative details, and adverse events occurred during the index hospitalization were prospectively collected in an electronic case report form. Data on adverse events occurred after hospital discharge were gathered by a linkage with the National Hospital Discharged Records database provided by the Italian Ministry of Health and other administrative databases available through a collaboration with the Italian National Program for Outcome Evaluation (PNE-AGENAS). Linking to these national registries guaranteed complete follow-up data on outcomes at 1-year follow-up. For the secondary analysis, aimed at comparing outcomes between TAVR and SAVR patients, the SAVR historical cohort was obtained from the OBSERVANT I dataset that enrolled 7,618 consecutive AS patients who underwent TAVR (1,911 patients) or SAVR (5,707 patients) at 93 Italian centers between December 2010 and June 2012 (21).

Study population

Out of the 2,989 patients who underwent TAVR for severe AS and included in the OBSERVANT II dataset, 420 patients

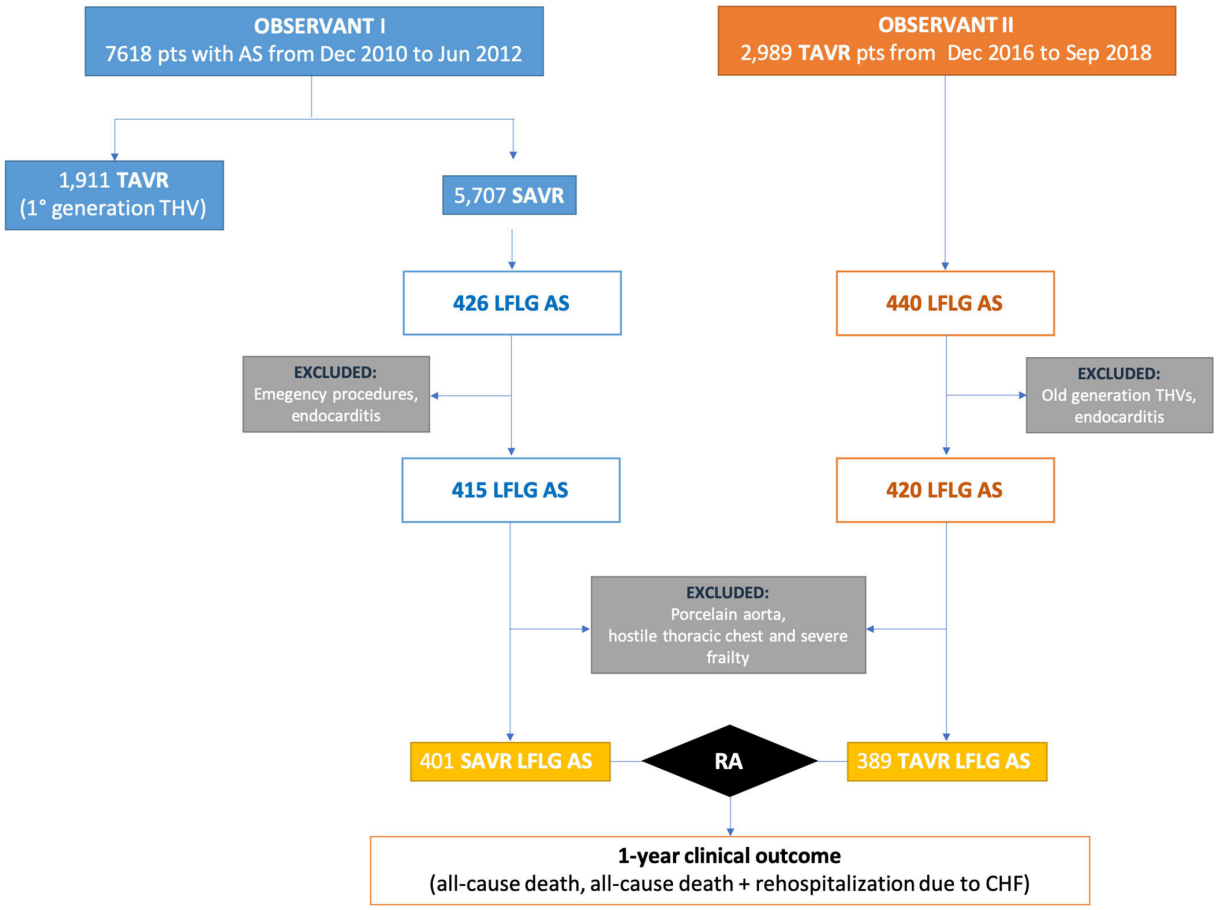

FIGURE 1
Study flowchart. AS, aortic stenosis; LFLG, low-flow–low-gradient; RA, risk adjustment; SAVR, surgical aortic valve replacement; TAVR, transcatheter aortic valve replacement.

met the following inclusion criteria of this analysis: (1) left ventricular ejection fraction (LVEF) ≤50% and (2) mean aortic transvalvular gradient <40 mmHg. Only those patients receiving new-generation THVs (Acurate, Boston Scientific, MA, USA; Evolut R and PRO, Medtronic, Minneapolis, MN, USA; Lotus, Boston Scientific, Marlborough, MA, USA; Portico, Abbott Vascular, Santa Clara, CA, USA; Sapien 3, Edwards Lifesciences Corp., Irvine, CA, USA; Engager, Medtronic 3F Therapeutics, Santa Ana, CA, USA) were included in this study. Active endocarditis was an exclusion criterion. Furthermore, LFLG TAVR patients ($n = 389$) from the OBSERVANT II dataset were compared with patients who underwent SAVR from the OBSERVANT I dataset ($n = 401$) (21). Active endocarditis, porcelain aorta, hostile chest, emergency procedure, and grade 3 of frailty based on the geriatric status scale (GSS) index (22) were exclusion criteria for this sub-analysis (Figure 1).

Outcomes

The primary outcomes were 1-year all-cause mortality and the composite of mortality and hospital readmission due to congestive heart failure (CHF) at 1 year (this endpoint has been adopted as a surrogate of futility). The secondary outcomes were 30-day mortality and the following adverse events occurring during the index hospitalization: stroke, conversion to cardiac surgery, complication at the left ventricular apex, major vascular injury, acute kidney injury, post-operative change in estimated glomerular filtration rate (e-GFR), myocardial infarction (MI), permanent pacemaker (PPM) implantation, cardiogenic shock, infections, red blood cell transfusion, procedure for cardiac tamponade, as well as valve prosthesis performance defined as the mean and peak post-procedural transvalvular gradient and paravalvular regurgitation. Major vascular injury was

TABLE 1 Baseline characteristics of patients with LFLG AS included in OBSERVANT II dataset.

Variables	Missing	Total cohort ($n = 420$)
Age, years	0	80.8 ± 6.7
Female sex	0	147 (35.0)
BMI, kg/m^2	3	25.8 ± 4.4
Diabetes	1	135 (32.2)
Coronary artery disease	3	150 (36.0)
1 Vessel		74 (17.7)
2 Vessels		27 (6.5)
3 Vessels/LM		49 (11.8)
Previous myocardial infarction	2	
<90 days		13 (3.1)
>90 days		100 (23.8)
Previous PCI	1	95 (22.7)
Previous cardiac surgery	0	106 (25.2)
Previous CABG	0	81 (19.3)
Previous aortic surgery	1	19 (4.5)
Other prior cardiac surgery procedures	0	37 (8.8)
COPD	0	81 (19.3)
Oxygen therapy	3	16 (3.8)
e-GFR (ml/min/1.73 m^2)	1	
≥45–60		108 (25.8)
≥30–45		109 (26.0)
≥15–30		30 (7.2)
<15		18 (4.3)
Dialysis	1	18 (4.3)
Neurological dysfunction	0	8 (1.9)
Porcelain aorta	5	22 (5.3)
Hostile chest	10	6 (1.5)
Peripheral artery disease	3	103 (24.7)
Liver disease	2	4 (1.0)
Pulmonary hypertension	0	34 (8.1)
Active cancer	2	16 (3.8)
EuroSCORE II, %	9	11.5 ± 10.2
EuroSCORE II >4 %	9	347 (84.4)
Frailty classes	0	
0		228 (54.3)
1		98 (23.3)
2		87 (20.7)
3		7 (1.7)
Critical preoperative status	0	16 (3.8)
NYHA classes	3	
I		2 (0.5)
II		82 (19.7)
III		293 (70.3)
IV		40 (9.6)
Unstable angina	0	29 (6.9)
Hemoglobin level, gr/dl	6	11.9 ± 1.7
Albumin level, gr/l	126	3.9 ± 0.7
AVA, cm^2	21	0.7 ± 0.2
AV pick gradient, mmHg	18	50.2 ± 13.5
AV mean gradient, mmHg	0	29.6 ± 7.7
AV annulus diameter, mm	227	23.3 ± 2.5
Mitral regurgitation	1	
No/trivial		33 (8.5)
Mild		180 (46.6)
Moderate		162 (42.0)
Severe		44 (11.4)
LVEF, %	0	37.6 ± 8.6
30–50%		352 (83.8)
≤30%		68 (16.2)

Continuous variables are reported as mean and standard deviation. Categorical variables are reported as counts and percentages (in parentheses).
AV, aortic valve; AVA, aortic valve area; BMI, body mass index; CABG, coronary artery bypass grafting; COPD, chronic obstructive pulmonary disease; e-GFR, estimated glomerular filtration rate; LVEF, left ventricular ejection fraction; NYHA, New York Heart Association; PCI, percutaneous coronary intervention.

defined as any vascular complication at peripheral access site requiring surgical or endovascular intervention. Infectious complications were defined as clinically proven surgical site infections, infections involving organs, and sepsis. Technical success, device success, and early safety were reported according to VARC-3 definitions (23). Moreover, the major adverse cardiac and cerebrovascular event (MACCE) was considered as a primary outcome of interest for the comparison between TAVR and SAVR groups. MACCE was defined as a composite of all-cause mortality, stroke, myocardial infarction, and/or coronary revascularization.

Statistical analysis

Continuous variables were reported as means and standard deviations. Categorical variables were reported as counts and percentages. Missing data were not replaced. Differences between TAVR and SAVR groups were evaluated by the χ^2 or Fisher exact test for categorical variables and by the *t*-test for continuous variables. Multivariate Cox proportional hazards regression models were used to identify independent predictors of 1-year mortality and 1-year composite endpoint of mortality and hospital readmission due to CHF in the TAVR population. Moreover, for the secondary aim multivariate Cox regression models were used to compare

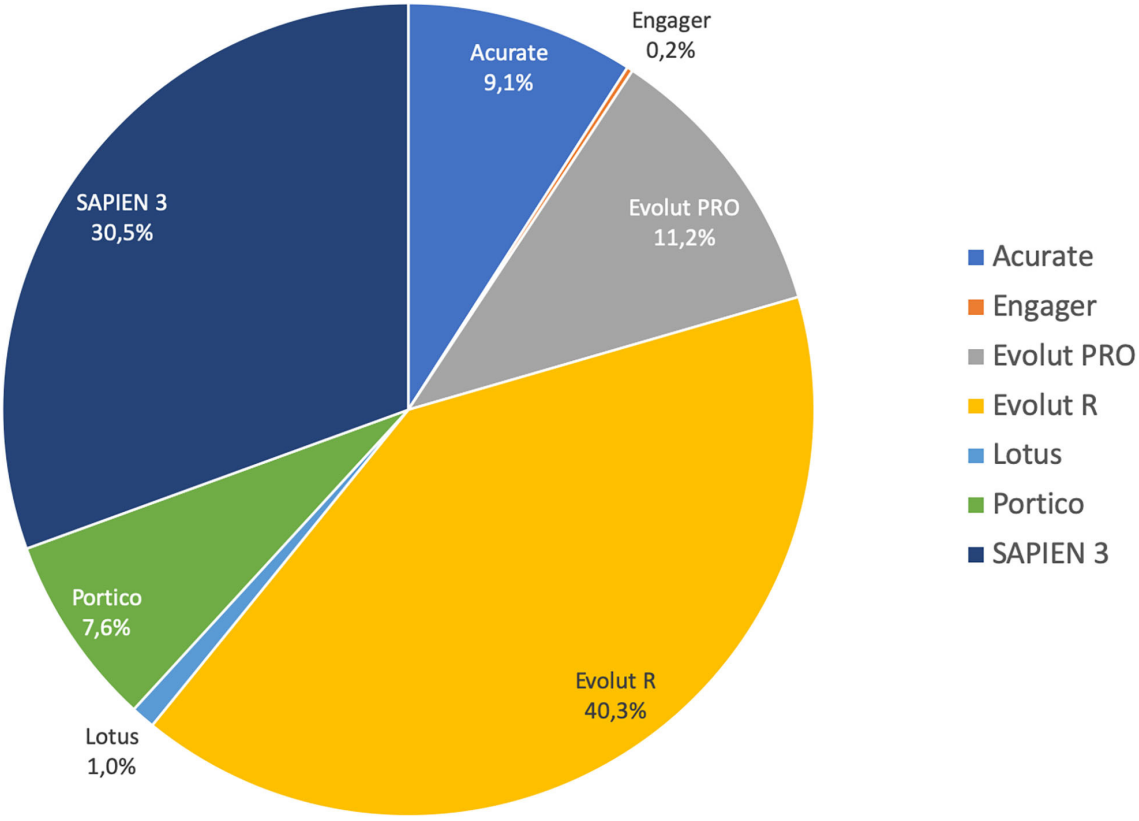

FIGURE 2
Pie chart showing the proportion of different devices implanted.

1-year death, 1-year mortality + CHF, and 1-year MACCE between TAVR and SAVR patients. To validate the results obtained from this analysis, a propensity score approach with the inverse probability of treatment weighting (IPTW) method was used (Supplementary material). $P < 0.05$ was set for statistical significance. Statistical analyses were performed using SAS statistical software version 9.4 (SAS Institute, Cary, NC, USA).

Results

Baseline characteristics of LFLG TAVR

The mean age of TAVR patients was 81 years, and 65% were men. About one-third of them had diabetes and coronary artery disease. EuroSCORE II >4% was present in 84% of cases, and NYHA class ≥ III in 79.9% of them. The mean LVEF was 38%, and the mean transvalvular aortic gradient was 29 mmHg. A concomitant moderate-to-severe mitral regurgitation was observed in more than half of patients. Baseline clinical and echocardiographic characteristics are summarized in Table 1.

Early outcome after TAVR for LFLG AS

Most of the procedures were performed through a transfemoral approach (87%) using a self-expandable THV. The proportions of employed THVs are summarized in Figure 2. The rates of aortic valve pre- and post-dilatation were 31 and 18%, respectively. Mechanical circulatory support was needed in 1.4% of cases. Technical success was observed in 92% of cases. The device success rate at 30 days was 83% and early safety 68%. The mean transvalvular gradient significantly decreased from 29 mmHg to 8 mmHg ($p < 0.001$). Thirty-day mortality was 3.1%. Other early outcomes are summarized in Table 2.

One-year outcome after TAVR for LFLG AS

One-year follow-up was complete in all patients. One-year all-cause mortality was 17.4%. The rate of hospital readmission due to CHF was 24.3%, and the rate of composite outcome was 34.8%. Kaplan–Meyer estimates of 1-year all-cause mortality and of combined all-cause mortality or CHF are shown in

Figure 3. Predictors of 1-year mortality were chronic obstructive pulmonary disease and EuroSCORE II (Table 3). Predictors of combined 1-year composite outcome were diabetes and NYHA class IV before intervention (Table 4). The type of THV was not selected in the stepwise model for any of the considered outcomes, and even forcing that variable into the models, it did not reach any statistical significance.

Outcome after SAVR or TAVR for LFLG AS

Four-hundred and one patients underwent SAVR, and 389 patients underwent TAVR. SAVR patients were younger, less frail, and symptomatic, with a less impaired LV function which resulted in a lower EuroSCORE II (Supplementary Table 1). Still SAVR patients had a higher prevalence of CAD requiring concomitant CABG. Despite such differences, the unadjusted rates of 30-day mortality (SAVR, 4.5% TAVR, 3.3%, $p = 0.407$) and stroke (SAVR, 1.3%; TAVR 1.8%, $p = 0.540$) were similar between groups. However, SAVR patients required more frequently blood transfusion and suffered AKI, MI, and cardiogenic shock requiring longer intensive care unit stay. TAVR had a higher rate of major vascular complications, need for permanent pacemaker and residual PVL (Table 5). The reduction in post-procedural mean transvalvular gradient was lower in SAVR patients compared with TAVR patients (Figure 4). At 1 year, all-cause death was 14.0% after SAVR and 16.7% after TAVR ($p = 0.284$). About one-third of patients have died or required hospitalization for CHF, without significant difference between groups (33.2% after SAVR and 34.4% after TAVR; $p = 0.704$). An adjusted Cox proportional hazards analysis showed that survival, freedom from death or rehospitalization due to CHF, and freedom from MACCE were similar after SAVR and TAVR (Figure 5). The IPTW analysis (Supplementary Figures 1–5) confirmed the results observed with the adjusted Cox proportional hazards analysis.

TABLE 2 Early outcome of LFLG TAVR group.

Variables	Total cohort ($n = 420$) Missing	
Technical success	0	386 (91.9)
Device success	0	350 (83.3)
Early safety	0	286 (68.1)
30-day mortality	0	13 (3.1)
Valve migration	2	7 (1.7)
Bailout TAVR-in-TAVR	0	8 (1.9)
Myocardial infarction	0	1 (0.2)
Major vascular complications	0	8 (1.9)
Complications at the apex	1	1 (0.2)
Permanent pacemaker	0	46 (11.0)
Moderate–severe PVL	0	32 (7.6)
Conversion to surgery	2	1 (0.2)
Stroke	0	8 (1.9)
Cardiogenic shock	2	8 (1.9)
Blood transfusion	2	46 (11.0)
AKI	1	11 (2.6)
Sepsis	0	2 (0.5)
Cardiac tamponade	0	4 (1.0)
Intensive care unit hospital stay (days)	32	1.4 ± 2.2

Continuous variables are reported as mean and standard deviation. Categorical variables are reported as counts and percentages (in parentheses).
AKI, acute kidney injury; PVL, paravalvular leak.

Discussion

The main findings of this study including a large series of patients with non-paradoxical LFLG AS treated with the last-generation THVs can be summarized as follows: (1) TAVR appears to be a safe treatment strategy in this high-risk population, with a 30-day mortality rate lower than that expected by an estimated operative risk; (2) one-third of the patients experienced death and/or rehospitalization due to CHF during the first year; and (3) TAVR-treated patients were older, more frail, and with a higher surgical risk compared with SAVR-treated patients. Notwithstanding, TAVR was as safe and effective as SAVR at early and mid-term (Figure 6, Central Illustration).

To the best of our knowledge, this is the largest series evaluating the outcome of TAVR performed with modern THVs devices in patients with LFLG AS. The risk profile of our study population was similar to that of the 287 patients with LFLG AS undergoing TAVR with similar devices included in the TOPAS trial (16). In that registry, Ribeiro et al. observed a favorable early outcome of TAVR in their high-risk cohort, with mortality rates of 3.8 and 20.1% at 30 days and 1 year, respectively, which are similar to the results of this study (3.1 and 17.4%, respectively). The minimally invasive nature of TAVR that avoids the use of extracorporeal circulation and the risk of myocardial injury, the prevalent transfemoral approach, and better hemodynamic performance and low delivery profile of most recent THVs, as well as increasing experience, might have contributed to these results. Indeed, prior series including older-generation devices reported less favorable results. In fact, in the GARY registry (14), hospital mortality was 7.8% and 1-year mortality was 32.2% among LFLG AS patients treated with TAVR.

However, about one-third of our population still may die or have a recurrence of CHF within the first year after TAVR. These findings are similar to the figures observed in the TOPAS trial (16). Similarly, a poor outcome was observed in 33% of patients in the PARTNER trial (24), whereas the rate of death, stroke, or rehospitalization was 27% in the PARTNER 2A trial

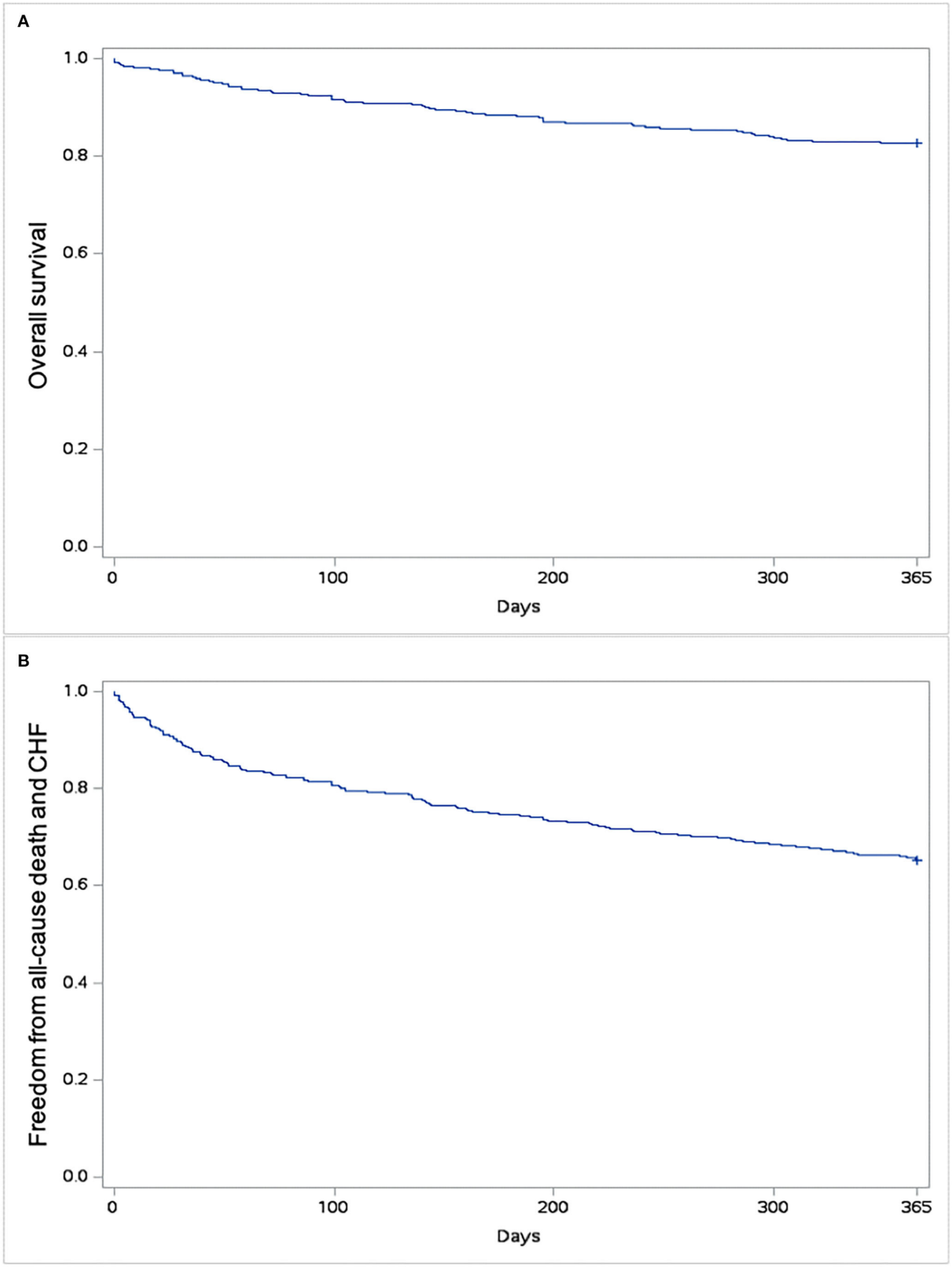

FIGURE 3
Kaplan–Meyer estimates of survival **(A)** and freedom from all-cause mortality and/or rehospitalization due to congestive heart failure (CHF) **(B)**.

(25) and 17% in the SURTAVI trial (26). This raises the question of the need to assess the potential futility in patients undergoing TAVR. Clinical futility means the lack of clinical benefit within the first year after treatment, and it has been variably defined

TABLE 3 Independent predictors of 1-year mortality in LFLG AS treated with new-generation THV.

Clinical variables	HR	P- value	CI 95%	
Age, years	1.00	0.873	0.97	1.04
Female sex	0.68	0.167	0.40	1.17
Porcelain aorta	1.84	0.161	0.78	4.34
Hostile chest	2.75	0.126	0.75	10.01
COPD	1.78	0.036	1.04	3.05
Previous PCI	0.53	0.052	0.28	1.01
Concomitant PCI	0.50	0.178	0.19	1.37
e-GFR	0.99	0.122	0.98	1.00
EuroSCORE II	1.02	0.021	1.00	1.04
Mean aortic transvalvular gradient	0.98	0.189	0.95	1.01

COPD, chronic obstructive pulmonary disease; e-GFR, estimated glomerular filtration rate; PCI, percutaneous coronary intervention; THV, transcatheter heart valve.

TABLE 4 Independent predictors of combined 1-year mortality and rehospitalization due to congestive heart failure in LFLG AS treated with new-generation THV.

Clinical variables	HR	*p*-value	CI 95%	
Age, years	1.00	0.763	0.98	1.03
Female sex	0.80	0.223	0.55	1.15
COPD	1.41	0.078	0.96	2.06
Neurological dysfunction	1.73	0.286	0.63	4.70
Previous aortic surgery	1.64	0.137	0.86	3.15
Diabetes	1.53	0.013	1.09	2.15
NYHA classes I and II	Ref			
NYHA class III	0.92	0.685	0.60	1.40
NYHA class IV	2.38	0.002	1.36	4.15

CHF, congestive heart failure; COPD, chronic obstructive pulmonary disease; NYHA, New York Heart Association.

TABLE 5 Early outcome of patients with LFLG AS treated with TAVR or SAVR.

Outcomes	SAVR, $n = 401$		TAVR, $n = 389$		*p*-value
	Missing		Missing		
30-Day death	0	18 (4.5)	0	13 (3.3)	0.407
Valve migration	0	0 (0.0)	2	7 (1.8)	0.007
Myocardial infarction	3	7 (1.8)	0	1 (0.3)	0.036
Major vascular complications	25	1 (0.3)	0	8 (2.1)	0.022
Permanent pacemaker	4	18 (4.5)	0	44 (11.3)	<0.001
Stroke	5	5 (1.3)	0	7 (1.8)	0.540
Cardiogenic shock	5	35 (8.8)	2	8 (2.1)	<0.001
Blood transfusion	25	210 (55.9)	2	41 (10.6)	<0.001
Transfused RBC units	0	2.0 ± 3.1	0	0.2 ± 0.8	<0.001
AKI	11	38 (9.7)	1	11 (2.8)	<0.001
PCI	3	1 (0.3)	0	0 (0.0)	0.323
Tamponade	4		0		0.319
Requiring surgery		6 (1.5)		2 (0.5)	
Requiring percutaneous treatment		1 (0.3)		2 (0.5)	
Infectious complications	11	24 (6.2)	0	15 (3.9)	0.148
PVL	37		0		<0.001
No/trivial		326 (89.6)		217 (55.8)	
Mild		32 (8.8)		144 (37.0)	
Moderate		4 (1.1)		25 (6.4)	
Severe		2 (0.6)		3 (0.8)	
AV pick gradient, mmHg	91	23.1 ± 10.3	22	14.6 ± 8.6	<0.001
AV mean gradient, mmHg	95	12.7 ± 6.8	7	7.8 ± 5.0	<0.001
Intensive care unit stay, days	7	4.0 ± 6.7	7	1.4 ± 2.3	<0.001

Continuous variables are reported as mean and standard deviation. Categorical variables are reported as counts and percentages (in parentheses).
AKI, acute kidney injury; AV, aortic valve; PCI, percutaneous coronary intervention; PVL, paravalvular leak; RBC, red blood cells; SAVR, surgical aortic valve replacement; TAVR, transcatheter aortic valve replacement.

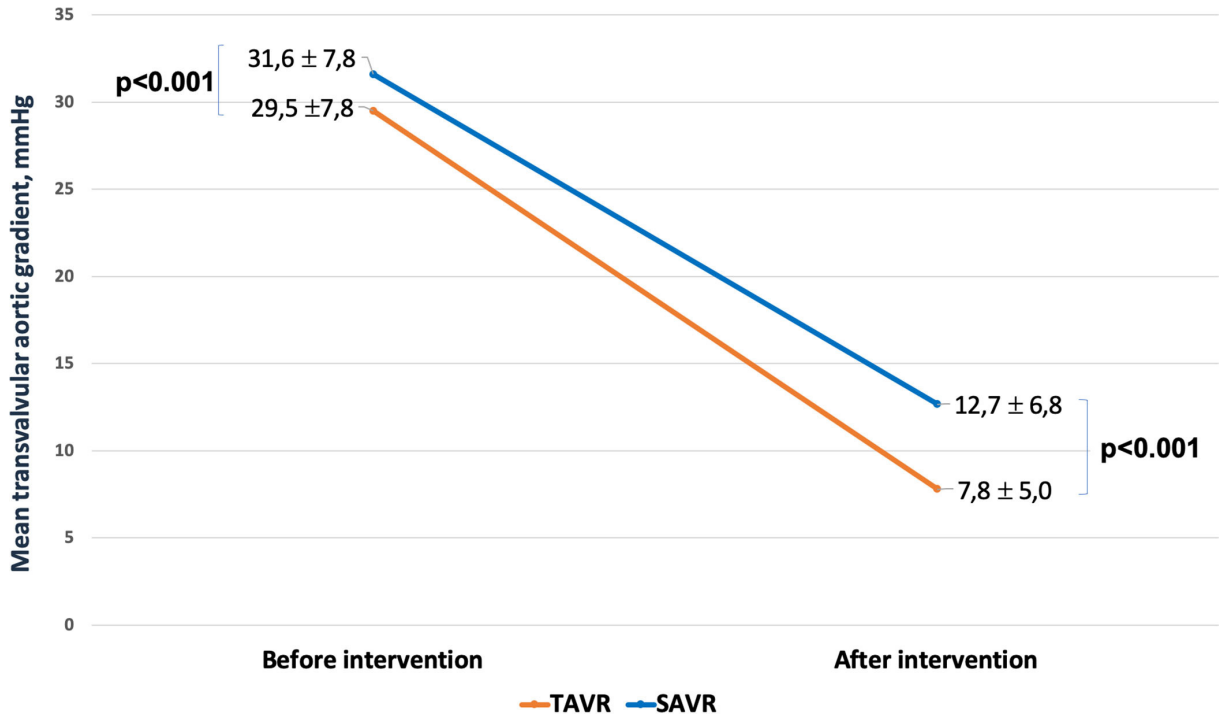

FIGURE 4
Change in mean transvalvular gradient after SAVR and TAVR.

as the composite of death, rehospitalization due to CHF, or lack in functional recovery and improvement in quality of life (27). We observed that COPD and EuroSCORE II were independent predictors of 1-year mortality after TAVR and that diabetes and NYHA class IV symptoms independently predicted 1-year death and/or rehospitalization due to CHF. Low baseline mean gradient, anemia, renal failure, and the presence of moderate or severe post-procedural PVL after TAVR have been identified as other predictors of poor outcome in these patients (16, 28–30). However, a validated risk assessment tool for potential futility of TAVR is still lacking and the identification of patients who may not fully benefit from TAVR remains a dilemma for the heart team during the decision-making process.

When compared with an historical series of LFLG AS patients who underwent SAVR, TAVR patients included in the OBSERVANT II study were older, at a higher surgical risk, more fragile, with more comorbidities, and at an advanced stage of disease. Notwithstanding, 30-day mortality and stroke were similar between the two cohorts. Looking at post-procedural mean transvalvular gradient, THVs performed better than surgical aortic valve prostheses. This superiority of THVs is well-known, in particular with the use of supra-annular devices (60.8% in our series) (31–33). This is a point in favor of TAVR when discussing the best therapeutic option in the case of LFLG AS, as the more complete is the relief of afterload mismatch, the higher is the probability of LV recovery (34, 35). On the contrary, THVs still suffer from a higher rate of PVL and conduction disorders needing PPM implantation. The impact of PVL and PPM on clinical outcome and LV recovery after TAVR is still a matter of debate, and the scientific evidence on this field are controversial. Previous reports suggested that mild PVL is commonly observed after TAVR and usually leads to a benign outcome (36). However, a meta-analysis of 45 studies including around 13,000 patients concluded that moderate or greater post-TAVR PVL was associated with a more than 2-fold increase in overall all-cause mortality (37). Moreover, conduction disorders and PPM leading to cardiac dyssynchrony can be badly tolerated by an already impaired LVEF, as suggested by Weber et al. (11).

Beyond these differences, at risk-adjusted analysis for other confounding factors, we found that 1-year clinical outcome was similar between TAVR and SAVR patients. The same finding was reported by a sub-analysis of the PARTNER trial, where, after a small early hazard associated with SAVR in the first 30 days, both TAVR and SAVR similarly improved outcome with respect to medical therapy alone (13). These results have been further confirmed by a recent meta-analysis, showing that aortic valve replacement was associated with a significant decrease in all-cause mortality regardless of surgical or transcatheter approach and in all subclasses of LG AS (38).

There are some study limitations that deserve to be acknowledged. First, this is a prospective registry without an external event adjudication committee and echocardiographic

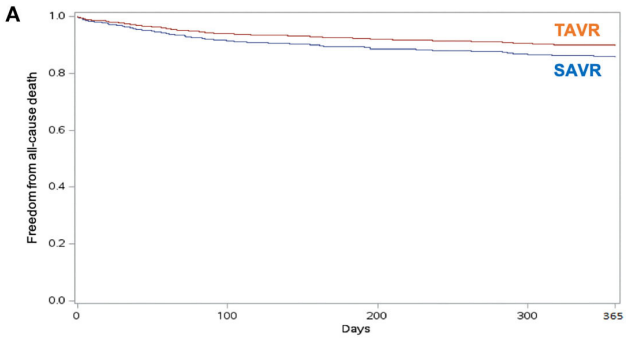

Parameters	HR	CI 95%		p value
TAVR	0,70	0,45	1,09	0,113
Age	1,04	1,01	1,07	0,005
Female sex	0,89	0,60	1,33	0,568
COPD	1,97	1,30	2,98	0,001
Previous aortic intervention	1,66	0,85	3,25	0,138
Angina	1,82	1,04	3,18	0,035
Previous cardiac surgery	1,76	1,11	2,78	0,016
Active cancer	3,69	1,82	7,47	0,000
Previous PCI	0,58	0,32	1,02	0,059
LVEF <30%	1,38	0,85	2,25	0,193
e-GFR	0,98	0,97	0,99	0,000

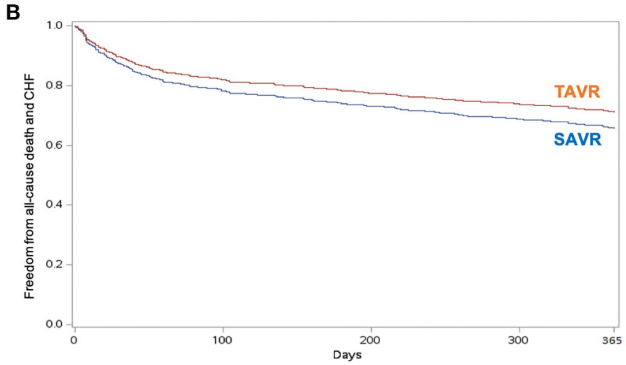

Parameters	HR	CI 95%		p value
TAVR	0,81	0,60	1,09	0,168
Age	1,01	0,99	1,03	0,356
Female sex	1,03	0,78	1,37	0,831
Dialisi	0,50	0,24	1,04	0,063
COPD	1,35	0,98	1,85	0,068
Home oxygen therapy	1,81	1,04	3,15	0,037
Previous aortic intervention	1,59	0,96	2,63	0,073
Liver disease	1,98	0,86	4,57	0,110
Diabetes	1,38	1,06	1,79	0,017
LVEF <30%	1,68	1,21	2,35	0,002
NYHA III	0,91	0,67	1,24	0,555
NYHA IV	1,42	0,92	2,19	0,109
eGFR	0,99	0,98	1,00	0,001
EuroScore II	1,01	1,00	1,02	0,179

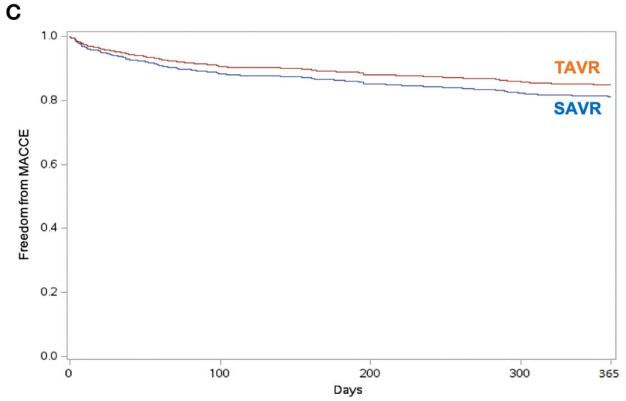

Parameters	HR	CI 95%		p value
TAVR	0,791	0,534	1,171	0,241
Age	1,032	1,007	1,058	0,012
Female sex	0,887	0,62	1,27	0,514
Dialisis	1,888	0,943	3,78	0,073
COPD	1,525	1,03	2,259	0,035
Home oxygen therapy	1,703	0,857	3,385	0,129
Previoius aortic intervention	1,631	0,886	3,003	0,116
Previous cardiac surgery	1,381	0,904	2,108	0,135
Diabetes	1,366	0,979	1,908	0,067
Active cancer	2,838	1,46	5,518	0,002
NYHA III	0,798	0,542	1,177	0,256
NYHA IV	1,243	0,745	2,074	0,404
eGFR	0,986	0,978	0,995	0,002

FIGURE 5
Adjusted proportional hazards estimates of outcomes after TAVR and SAVR. **(A)** Survival; **(B)** Survival freedom from the composite of mortality and hospital rehospitalization due to CHF; **(C)** Survival freedom from MACCE (all-cause mortality, stroke, myocardial infarction, and coronary revascularization). COPD, chronic obstructive pulmonary disease; e-GFR, estimated glomerular filtration rate; LVEF, left ventricular ejection fraction; NYHA, New York Heart Association; PCI, percutaneous coronary intervention; SAVR, surgical aortic valve replacement; TAVR, transcatheter aortic valve replacement.

data were site-reported without analysis in a centralized core laboratory. Second, no data were available on either Agatston calcium score or contractile reserve evaluated by low-dose dobutamine echocardiography. However, recent evidence suggest no impact of contractile reserve on outcome after TAVR (39). Third, frailty was estimated through a simple toolset (Geriatric Status Scale) including only basic daily life activities and cognitive impairment; however, other variables relative to nutritional status (BMI, albumin, hemoglobin) were collected separately. Data about futility are underreported with respect to VARC-3 definition (23), as we included only death and rehospitalization due to CHF, while data about quality of life at follow-up are lacking. Moreover, we do not know the reasons for death (cardiac or not cardiac) at follow-up. Additionally, TAVR and SAVR cohorts are from different time periods (2010–2012 for SAVR group and 2016–2018 for TAVR group), thus potentially reflecting different patient's selection and decision-making process by the local heart teams. However, as a matter of fact, no major changes in surgical techniques and technologies have been introduced during that time frame. Accordingly, we

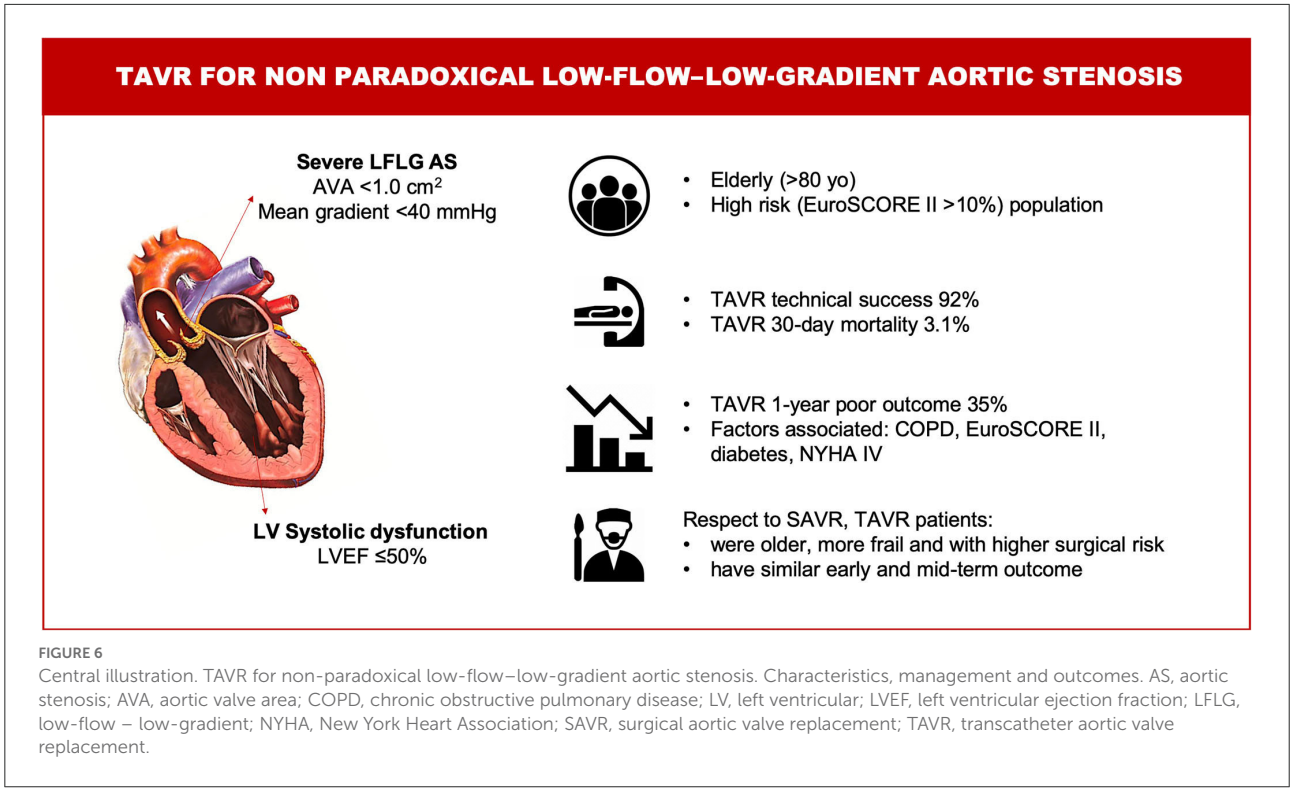

FIGURE 6
Central illustration. TAVR for non-paradoxical low-flow–low-gradient aortic stenosis. Characteristics, management and outcomes. AS, aortic stenosis; AVA, aortic valve area; COPD, chronic obstructive pulmonary disease; LV, left ventricular; LVEF, left ventricular ejection fraction; LFLG, low-flow – low-gradient; NYHA, New York Heart Association; SAVR, surgical aortic valve replacement; TAVR, transcatheter aortic valve replacement.

would not expect a significant variation in the results if a more contemporaneous surgical series had been available. Finally, both OBSERVANT I and OBSERVANT II are multicenter studies, and thus, the "center effect" should theoretically be considered. However, the small number of patients per center fulfilling inclusion criteria for this sub-analysis does not allow considering the variable "center" in the models, which would become highly unstable from the statistical point of view.

In conclusion, in patients with non-paradoxical LFLG AS, TAVR was as safe and effective as SAVR at early and mid-term intervals. TAVR was associated with a lower risk of severe early adverse events and therefore might be of benefit over SAVR in elderly with non-paradoxical LFLG AS. Attention should be paid to procedural planning to optimize hemodynamic acute result and reduce the risk of PVL and PPM. The risk of futility is impending, and predictors of poor outcome are still a matter of debate. Further studies are needed to address these issues and improve patients' selection.

Data availability statement

The raw data supporting the conclusions of this article will be made available by the authors, without undue reservation.

Ethics statement

The studies involving human participants were reviewed and approved by Segreteria del Comitato Etico per la Sperimentazione Clinica della Provincia di Padova, U.O.S.D. The patients/participants provided their written informed consent to participate in this study.

Author contributions

CF, GT, and FS contributed to conception and design of the study. SR organized the database. PD'E performed the statistical analysis. CF wrote the first draft of the manuscript. GB, FBi, MB, CT, FBe, MR, and GU wrote sections of the manuscript. All authors contributed to manuscript revision, read, and approved the submitted version.

Funding

The OBSERVANT study was supported by a grant (Fasc. 1M30) from the Italian Ministry of Health and Istituto Superiore di Sanità. The OBSERVANT II study was supported by the Italian Ministry of Health within the call Ricerca Finalizzata 2016 (code PE-2016-02364619).

Conflict of interest

The authors declare that the research was conducted in the absence of any commercial or financial relationships

that could be construed as a potential conflict of interest.

Publisher's note

All claims expressed in this article are solely those of the authors and do not necessarily represent those of their affiliated organizations, or those of the publisher, the editors and the reviewers. Any product that may be evaluated in this article, or claim that may be made by its manufacturer, is not guaranteed or endorsed by the publisher.

Supplementary material

The Supplementary Material for this article can be found online at: https://www.frontiersin.org/articles/10.3389/fcvm.2022.991729/full#supplementary-material

References

1. Vahanian A, Beyersdorf F, Praz F, Milojevic M, Baldus S, Bauersachs J, et al. 2021 ESC/EACTS Guidelines for the management of valvular heart disease. *Eur Heart J.* (2021) 43:561–632. doi: 10.1093/eurheartj/ehab395

2. Clavel M-A, Magne J, Pibarot P. Low-gradient aortic stenosis. *Eur Heart J.* (2016) 37:2645–57. doi: 10.1093/eurheartj/ehw096

3. Tarantini G, Buja P, Scognamiglio R, Razzolini R, Gerosa G, Isabella G, et al. Aortic valve replacement in severe aortic stenosis with left ventricular dysfunction: determinants of cardiac mortality and ventricular function recovery. *Eur J Cardiothorac Surg.* (2003) 24:879–85. doi: 10.1016/s1010-7940(03)00575-x

4. Connolly HM, Oh JK, Schaff HV, Roger VL, Osborn SL, Hodge DO, et al. Severe aortic stenosis with low transvalvular gradient and severe left ventricular dysfunction:result of aortic valve replacement in 52 patients. *Circulation.* (2000) 101:1940–6. doi: 10.1161/01.cir.101.16.1940

5. Pereira JJ, Lauer MS, Bashir M, Afridi I, Blackstone EH, Stewart WJ, et al. Survival after aortic valve replacement forsevere aortic stenosis with low transvalvular gradients and severe left ventricular dysfunction. *J Am Coll Cardiol.* (2002) 39:1356–63. doi: 10.1016/S0735-1097(02)01759-X

6. Vaquette B. Valve replacement in patients with critical aortic stenosis and depressed left ventricular function: predictors of operative risk, left ventricular function recovery, and long term outcome. *Heart.* (2005) 91:1324–9. doi: 10.1136/hrt.2004.044099

7. Levy F, Laurent M, Monin JL, Maillet JM, Pasquet A, Le Tourneau T, et al. Aortic valve replacement for low-flow/low-gradient aortic stenosis. *J Am Coll Cardiol.* (2008) 51:1466–72. doi: 10.1016/j.jacc.2007.10.067

8. Tribouilloy C, Lévy F, Rusinaru D, Guéret P, Petit-Eisenmann H, Baleynaud S, et al. Outcome after aortic valve replacement for low-flow/low-gradient aortic stenosis without contractile reserve on dobutamine stress echocardiography. *J Am Coll Cardiol.* (2009) 53:1865–73. doi: 10.1016/j.jacc.2009.02.026

9. Tarantini G, Covolo E, Razzolini R, Bilato C, Frigo AC, Napodano M, et al. Valve replacement for severe aortic stenosis with low transvalvular gradient and left ventricular ejection fraction exceeding 0.50. *Ann Thorac Surg.* (2011) 91:1808–15. doi: 10.1016/j.athoracsur.2011.02.057

10. Clavel MA, Webb JG, Rodés-Cabau J, Masson JB, Dumont E, De Larochellière R, et al. Comparison between transcatheter and surgical prosthetic valve implantation in patients with severe aortic stenosis and reduced left ventricular ejection fraction. *Circulation.* (2010) 122:1928–36. doi: 10.1161/CIRCULATIONAHA.109.929893

11. Weber M, Brüggemann E, Schueler R, Momcilovic D, Sinning J-M, Ghanem A, et al. Impact of left ventricular conduction defect with or without need for permanent right ventricular pacing on functional and clinical recovery after TAVR. *Clin Res Cardiol.* (2015) 104:964–74. doi: 10.1007/s00392-015-0865-9

12. Contorni F, Fineschi M, Iadanza A, Santoro A, Mandoli GE, Cameli M. How to deal with low-flow low-gradient aortic stenosis and reduced left ventricle ejection fraction: from literature review to tips for clinical practice. *Heart Fail Rev.* (2022) 27:697–709. doi: 10.1007/s10741-021-10090-0

13. Herrmann HC, Pibarot P, Hueter I, Gertz ZM, Stewart WJ, Kapadia S, et al. Predictors of mortality and outcomes of therapy in low-flow severe aortic stenosis: a Placement of Aortic Transcatheter Valves (PARTNER) trial analysis. *Circulation.* (2013) 127:2316–26. doi: 10.1161/CIRCULATIONAHA.112.001290

14. Lauten A, Figulla HR, Möllmann H, Holzhey D, Kötting J, Beckmann A, et al. TAVI for low-flow, low-gradient severe aortic stenosis with preserved or reduced ejection fraction: a subgroup analysis from the German Aortic Valve Registry (GARY). *EuroIntervention.* (2014) 10:850–9. doi: 10.4244/EIJV10I7A145

15. Elhmidi Y, Piazza N, Krane M, Deutsch M-A, Mazzitelli D, Lange R, et al. Clinical presentation and outcomes after transcatheter aortic valve implantation in patients with low flow/low gradient severe aortic stenosis. *Catheter Cardiovasc Interv.* (2014) 84:283–90. doi: 10.1002/ccd.25366

16. Ribeiro HB, Lerakis S, Gilard M, Cavalcante JL, Makkar R, Herrmann HC, et al. Transcatheter aortic valve replacement in patients with low-flow, low-gradient aortic stenosis: the TOPAS-TAVI registry. *J Am Coll Cardiol.* (2018) 71:1297–308. doi: 10.1016/j.jacc.2018.01.054

17. Barbanti M, Tamburino C, D'Errigo P, Biancari F, Ranucci M, Rosato S, et al. Five-year outcomes of transfemoral transcatheter aortic valve replacement or surgical aortic valve replacement in a real world population. *Circ Cardiovasc Interv.* (2019) 12:e007825. doi: 10.1161/CIRCINTERVENTIONS.119.007825

18. Seccareccia F, Tarantini G, Bedogni F, Berti S, Santoro G, Tamburino C, et al. [OBSERVANT II: OBservational Study of Effectiveness of transcatheter aortic valve implantation with new geneRation deVices for severe Aortic steNosis Treatment. Study protocol]. *G Ital Cardiol.* (2017) 18:14S—26. doi: 10.1714/2718.27731

19. Rosato S, Biancari F, D'Errigo P, Barbanti M, Tarantini G, Bedogni F, et al. One-year outcomes after surgical versus transcatheter aortic valve replacement with newer generation devices. *J Clin Med.* (2021) 10:3703. doi: 10.3390/jcm10163703

20. Costa G, D'Errigo P, Rosato S, Biancari F, Marcellusi A, Tarantini G, et al. One-year outcomes and trends over two eras of transcatheter aortic valve implantation in real-world practice. *J Clin Med.* (2022) 11:1164. doi: 10.3390/jcm11051164

21. Tamburino C, Barbanti M, D'Errigo P, Ranucci M, Onorati F, Covello RD, et al. 1-Year outcomes after transfemoral transcatheter or surgical aortic valve replacement: results from the Italian OBSERVANT study. *J Am Coll Cardiol.* (2015) 66:804–12. doi: 10.1016/j.jacc.2015.06.013

22. Rockwood K, Stadnyk K, MacKnight C, McDowell I, Hébert R, Hogan DB. A brief clinical instrument to classify frailty in elderly people. *Lancet.* (1999) 353:205–6. doi: 10.1016/S0140-6736(98)04402-X

23. VARC-3 WRITING COMMITTEE, Généreux P, Piazza N, Alu MC, Nazif T, Hahn RT, et al. Valve Academic Research Consortium 3: updated endpoint definitions for aortic valve clinical research. *Eur Heart J.* (2021) 42:1825–57. doi: 10.1093/eurheartj/ehaa799

24. Arnold SV, Reynolds MR, Lei Y, Magnuson EA, Kirtane AJ, Kodali SK, et al. Predictors of poor outcomes after transcatheter aortic valve replacement: results from the PARTNER (Placement of Aortic Transcatheter Valve) trial. *Circulation.* (2014) 129:2682–90. doi: 10.1161/CIRCULATIONAHA.113.007477

25. Leon MB, Smith CR, Mack MJ, Makkar RR, Svensson LG, Kodali SK, et al. Transcatheter or surgical aortic-valve replacement in intermediate-risk patients. *N Engl J Med.* (2016) 374:1609–20. doi: 10.1056/NEJMoa1514616

26. Reardon MJ, Van Mieghem NM, Popma JJ, Kleiman NS, Søndergaard L, Mumtaz M, et al. Surgical or transcatheter aortic-valve replacement in intermediate-risk patients. *N Engl J Med.* (2017) 376:1321–31. doi: 10.1056/NEJMoa1700456

27. Lindman BR, Alexander KP, O'Gara PT, Afilalo J. Futility, benefit, and transcatheter aortic valve replacement. *JACC Cardiovasc Interv.* (2014) 7:707–16. doi: 10.1016/j.jcin.2014.01.167

28. Zusman O, Kornowski R, Witberg G, Lador A, Orvin K, Levi A, et al. Transcatheter aortic valve implantation futility risk model development and validation among treated patients with aortic stenosis. *Am J Cardiol.* (2017) 120:2241–6. doi: 10.1016/j.amjcard.2017.09.007

29. Geisler D, Rudziński PN, Hasan W, Andreas M, Hasimbegovic E, Adlbrecht C, et al. Identifying patients without a survival benefit following transfemoral and transapical transcatheter aortic valve replacement. *J Clin Med.* (2021) 10:4911. doi: 10.3390/jcm10214911

30. Fraccaro C, Al-Lamee R, Tarantini G, Maisano F, Napodano M, Montorfano M, et al. Transcatheter aortic valve implantation in patients with severe left ventricular dysfunction: immediate and mid-term results, a multicenter study. *Circ Cardiovasc Interv.* (2012) 5:253–60. doi: 10.1161/CIRCINTERVENTIONS.111.964213

31. Regazzoli D, Chiarito M, Cannata F, Pagnesi M, Miura M, Ziviello F, et al. Transcatheter Self-expandable valve implantation for aortic stenosis in small aortic annuli: the TAVI-SMALL registry. *JACC Cardiovasc Interv.* (2020) 13:196–206. doi: 10.1016/j.jcin.2019.08.041

32. Hase H, Yoshijima N, Yanagisawa R, Tanaka M, Tsuruta H, Shimizu H, et al. Transcatheter aortic valve replacement with Evolut R versus Sapien 3 in Japanese patients with a small aortic annulus: the OCEAN-TAVI registry. *Catheter Cardiovasc Interv.* (2021) 97:E875–86. doi: 10.1002/ccd.29259

33. Bleiziffer S, Rudolph TK. Patient prosthesis mismatch after SAVR and TAVR. *Front Cardiovasc Med.* (2022) 9:761917. doi: 10.3389/fcvm.2022.761917

34. Ruel M, Al-Faleh H, Kulik A, Chan KL, Mesana TG, Burwash IG. Prosthesis-patient mismatch after aortic valve replacement predominantly affects patients with preexisting left ventricular dysfunction: effect on survival, freedom from heart failure, and left ventricular mass regression. *J Thorac Cardiovasc Surg.* (2006) 131:1036–44. doi: 10.1016/j.jtcvs.2005.10.028

35. Mohty D, Dumesnil JG, Echahidi N, Mathieu P, Dagenais F, Voisine P, et al. Impact of prosthesis-patient mismatch on long-term survival after aortic valve replacement: influence of age, obesity, and left ventricular dysfunction. *J Am Coll Cardiol.* (2009) 53:39–47. doi: 10.1016/j.jacc.2008.09.022

36. Colli A, Besola L, Salizzoni S, Gregori D, Tarantini G, Agrifoglio M, et al. Does pre-existing aortic regurgitation protect from death in patients who develop paravalvular leak after TAVI? *Int J Cardiol.* (2017) 233:52–60. doi: 10.1016/j.ijcard.2017.02.005

37. Athappan G, Patvardhan E, Tuzcu EM, Svensson LG, Lemos PA, Fraccaro C, et al. Incidence, predictors, and outcomes of aortic regurgitation after transcatheter aortic valve replacement: meta-analysis and systematic review of literature. *J Am Coll Cardiol.* (2013) 61:1585–95. doi: 10.1016/j.jacc.2013.01.047

38. Ueyama H, Kuno T, Harrington M, Takagi H, Krishnamoorthy P, Sharma SK, et al. Impact of surgical and transcatheter aortic valve replacement in low-gradient aortic stenosis: a meta-analysis. *JACC Cardiovasc Interv.* (2021) 14:1481–92. doi: 10.1016/j.jcin.2021.04.038

39. Buchanan KD, Rogers T, Steinvil A, Koifman E, Xu L, Torguson R, et al. Role of contractile reserve as a predictor of mortality in low-flow, low-gradient severe aortic stenosis following transcatheter aortic valve replacement. *Catheter Cardiovasc Interv.* (2019) 93:707–12. doi: 10.1002/ccd.27914

frontiers | Frontiers in Cardiovascular Medicine

TYPE Original Research
PUBLISHED 11 October 2022
DOI 10.3389/fcvm.2022.856028

OPEN ACCESS

EDITED BY
Elena Aikawa,
Brigham and Women's Hospital and Harvard Medical School, United States

REVIEWED BY
Hoda Hatoum,
Michigan Technological University, United States
Atsushi Sugiura,
University of Bonn, Germany
Qun-Shan Wang,
Shanghai Jiao Tong University, China

*CORRESPONDENCE
Katharina Hellhammer
k.hellhammer@contilia.de

SPECIALTY SECTION
This article was submitted to Heart Valve Disease, a section of the journal Frontiers in Cardiovascular Medicine

RECEIVED 16 January 2022
ACCEPTED 20 September 2022
PUBLISHED 11 October 2022

CITATION
Hellhammer K, Schueler R, Eißmann M, Schumacher B, Wolf A, Bruder O, Schmitz T and Lambers M (2022) Safety of transesophageal echocardiography during transcatheter edge-to-edge tricuspid valve repair: A single-center experience.
Front. Cardiovasc. Med. 9:856028.
doi: 10.3389/fcvm.2022.856028

Safety of transesophageal echocardiography during transcatheter edge-to-edge tricuspid valve repair: A single-center experience

Katharina Hellhammer[1]*, Robert Schueler[1], Mareike Eißmann[1], Brigitte Schumacher[2,3], Alexander Wolf[1], Oliver Bruder[1,4], Thomas Schmitz[1] and Moritz Lambers[1]

[1]Contilia Heart and Vascular Center, Department of Cardiology and Angiology, Elisabeth Hospital Essen, Essen, Germany, [2]Department of Internal Medicine and Gastroenterology, Elisabeth Hospital Essen, Essen, Germany, [3]Faculty of Medicine, University Duisburg-Essen, Essen, Germany, [4]Faculty of Medicine, Ruhr University Bochum, Bochum, Germany

Objectives: We aimed to determine transesophageal echocardiography (TEE) related complications during Transcatheter edge-to-edge tricuspid valve repair (TTVR).

Background: Transesophageal echocardiography is essential to guide structural heart disease (SHD) interventions. TTVR has become an evolving procedure for high-risk patients not suitable for surgery. Whether this complex procedure is associated with TEE related complications is not known so far.

Methods: We retrospectively analyzed 64 consecutive patients undergoing TTVR between 2019 and 2021 with the TriClip system (Abbott, Chicago, IL, USA) at our center. All procedures were performed under general anesthesia (GA). TEE related complications were classified as major and minor complications.

Results: Transesophageal echocardiography related complications were observed in two patients (3.1%) with one major complication (1.6%) and one minor complication (1.6%). In one patient perforation of the esophageal mucosa requiring red blood cell transfusion was observed, the other patient had hematemesis due to minor esophageal and gastric lesions without the need for blood transfusion. Both patients recovered during hospital stay with no persistent symptoms at discharge.

Conclusions: Transesophageal echocardiography related complications during TTVR are clinically relevant occurring in 3.1% of the patients. Further investigations are needed to identify potential risk factors and patients at high risk to develop a TEE related complication in the course of TTVR.

KEYWORDS

transcatheter tricuspid valve repair, interventional imaging, transesophageal echocardiography, safety, complications

Introduction

Transcatheter structural heart disease (SHD) interventions for left sided pathologies have become an inherent part in daily clinical practice. For tricuspid regurgitation (TR) treatment options have been limited so far. While tricuspid repair during left heart surgery is widely accepted in patients with severe primary or secondary TR (1), isolated repair of the tricuspid valve has shown to be unfavorable due to high surgical risk (2, 3). As TR is a highly prevalent disease, associated with high morbidity and mortality (4, 5), the clinical need for treatment options remains essential. Recently, transcatheter edge-to-edge tricuspid valve repair (TTVR) with the TriClip system (Abbott, Chicago, IL, USA) has emerged as a safe and (6) effective treatment option as current data suggests (7, 8). Transesophageal echocardiography (TEE) is indispensable to guide this complex intervention. Of note, deep transesophageal and transgastric views are necessary to evaluate clip position, grasping of the leaflets and leaflet insertion. Complications which have been described to be associated with periinterventional TEE are bleeding events of the upper gastro-intestinal tract, perforations of the esophagus or esophagogastric tears, dysphagia or lesions of the oropharynx (6, 9, 10). A complication rate ranging from 0.2 to 1.2% has been reported, considering these data were raised from patients undergoing cardiac surgery (6, 11). Recent data focusing on TEE related adverse events during transcatheter structural heart interventions reported a higher event rate of 5.3%−6.1% (10, 12). Patients undergoing TTVR were not included in these studies.

Whether the manipulation of the TEE probe during this complex procedure is associated with adverse events is not known so far. We therefore aimed to evaluate the incidence of TEE related complications in patients undergoing TTVR.

Methods

In a single-center study we analyzed 64 consecutive patients undergoing TTVR with the TriClip system between 04/2019 and 06/2021. All patients referred to this procedure were included in this study, no exclusion criteria were defined. All interventions were performed under general anesthesia (GA). Procedural steps have been described previously (7). In brief, the procedural steps are as follows: after obtaining a femoral vein access, the guide is positioned in the junction of the inferior vena cava and right atrium. Fluoroscopy and 2/3D transesophageal echocardiography is used to guide the procedurals steps. The TriClip delivery system is placed over the tricuspid valve and properly orientated perpendicular to the line of coaptation of the tricuspid valve leaflets. The clip is opened and advanced into the right ventricle. After optimal positioning, the clip is pulled back and the leaflets are grasped. Leaflet insertion, reduction of TR and orientation of the clip is evaluated. In case of insufficient reduction of TR or inadequate leaflet insertion, the clip can be re-opened to perform another grasping maneuvre.

Baseline patient characteristics, procedural data and in-hospital data were obtained. Laboratory results were taken 1 day prior to the intervention. Oral anticoagulation (NOAK) was paused 1 day prior to procedure. In case of oral anticoagulation with a vitamin k antagonist, an international normalized ration (INR) $\leq$2 was obtained before the patient was referred to the intervention. Procedure time was defined as time from start of the procedure till final closure of femoral access site. Time under TEE was defined as time starting from insertion of the probe till retraction of the probe at the end of the procedure. TEE was conducted using a GE Vivid^{TM} E95 with a 6VT-D probe (GE Healthcare Systems, USA) and was performed by a cardiologist with wide experience in transesophageal echocardiography and guidance of transcatheter structural heart interventions. Transcatheter tricuspid valve repair was performed by two experienced interventional cardiologists, performing structural heart interventions for several years. An activated clotting time >250 s was obtained throughout the intervention by administration of unfractionated heparin. Procedural success was defined as implantation of at least one TriClip device with TR reduction of at least one grade. Tricuspid regurgitation was assessed using standard 2D color Doppler methods and graded using a five-class grading scheme: mild, moderate, severe, massive and torrential (13).

TEE related complications were classified as minor and major complications. A major complication was considered to meet one of the following criteria: (1) upper gastro-intestinal bleeding requiring inotropes or blood transfusion, (2) mechanical lesions as perforations of esophagus or stomach requiring endoscopic or surgical intervention, and (3) persistent dysphagia requiring further diagnostic. Minor TEE related complications were considered as dysphagia or perioral hypesthesia persisting within 24 h after procedure, hematemesis without need for blood transfusion.

Statistical analysis was performed using SPSS Statistic (IBM, Inc.). Procedure time, Time under TEE and device time were expressed as median (min-max) ± standard deviation. All other continuous variables were expressed as means ± standard deviation. Categorial variables were specified in percentage and absolute numbers.

Abbreviations: cAVK, cerebrovascular artery disease; COPD, chronic obstructive pulmonary disease; GA, general anesthesia; INR, international normalized ratio; OSAS, obstructive sleep-apnoe syndrome; pAVK, peripheral artery vascular disease; PMVR, percutaneous mitral valve repair; SHD, structural heart disease; TEE, transesophageal echocardiography; TR, tricuspid regurgitation; TTVR, transcatheter edge-to-edge tricuspid valve repair.

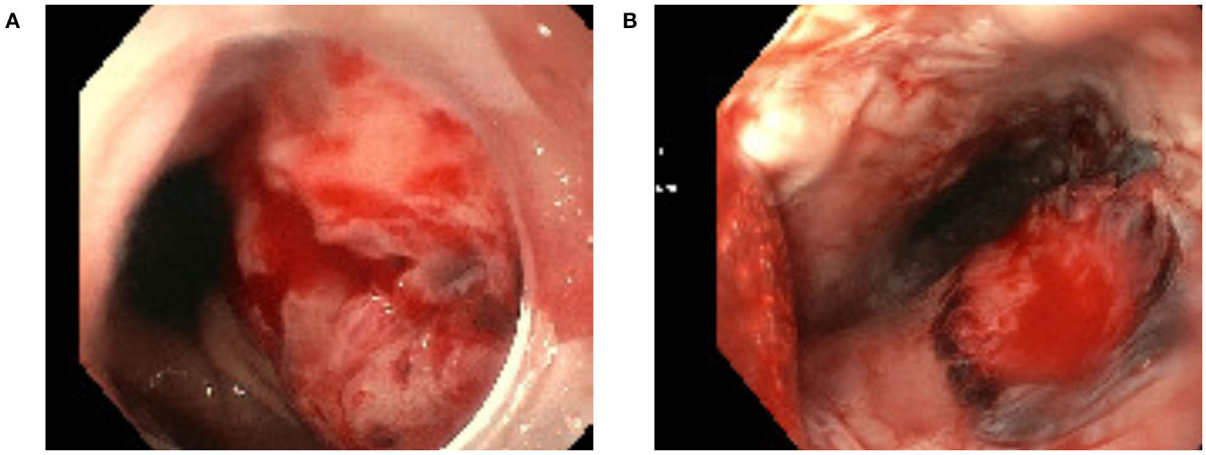

FIGURE 1
Esophageal mucosa perforation related to transesophageal echocardiography **(A)** and esophageal lesion related to transesophageal echocardiography **(B)**.

TABLE 1 TEE related complications.

	All patients ($n = 64$)
Overall complication rate, *n* (%)	2 (3.1)
Major complication, *n* (%)	1 (1.6)
Minor complication, *n* (%)	1 (1.6)

Results

We observed a TEE related complication in 2 (3.1%) patients. Of these, one presented with a major complication due to a perforation of esophageal mucosa leading to an upper-gastro-intestinal bleeding which required transfusion of two red blood cell concentrates (Figure 1A). In the second patient, hematemesis occurred caused by multiple esophageal and gastric lesions as seen by endoscopy (Figure 1B). Hematemesis stopped spontaneously and no other actions had to be taken in this patient.

Transesophageal echocardiography related complications are listed in Table 1.

Mean age of our cohort was 80 ± 6.4 years. Patients presented with multiple comorbidites of which atrial fibrillation was the most common in 89.1% ($n = 57$) of the patients. Mean logistic EuroSCORE was 19.3 ± 13.0. Baseline characteristics are shown in Table 2.

All patients underwent TTVR under GA. Median procedure time was 128 (46–220) min ± 36.7 with a successful procedure in 93.8% ($n = 60$) of the patients. In four patients the procedure was interrupted as the Clip could not be implanted due to insufficient grasping. No in-hospital deaths were observed. Procedural and in-hospital data is shown in Table 3.

We looked in detail at the two patients who presented with a TEE related complication (Tables 2, 3). Procedure time was prolonged with 170 (149–190) min ± 29.0. One patient was known to suffer from gastroesophageal reflux disease whereas in the second patient there was no history of previous gastroesophageal disease.

Discussion

To our best knowledge, this is the first study evaluating the incidence of TEE related complications during TTVR. We observed TEE related complications in 3.1% of the patients.

Transcatheter edge-to-edge repair has recently successfully applied in patients with severe TR and shown to be safe and effective (7, 8, 14, 15). For procedural success guidance of TEE during this complex intervention is essential. Mid esophageal and transgastric views of the tricuspid valve are very important views while performing this procedure. As the intervention can be challenging with a prolonged procedure time, prolonged manipulation with the TEE probe may cause mechanical or bleeding complications. Complication rate of TEE in diagnostic routine has been described with 0.2%−0.5% (16). During SHD interventions, recent data found a TEE related adverse event in 6.1% of patients undergoing either percutaneous mitral valve repair (PMVR), closure of left atrial appendage or closure of paravalvular leakage (10). A prolonged procedural time under TEE was identified as a predictor for a TEE related complication and was highest in patients undergoing PMVR. These patients had a 10-fold higher risk to develop a major TEE related complication. In our study, the overall incidence of a TEE

TABLE 2 Baseline characteristics.

	All patients ($n = 64$)	Patients with a TEE related complication ($n = 2$)
Age, years	80 ± 6.2	81 ± 2.8
Male, *n* (%)	26 (40.6)	1 (50.0)
Body mass index (kg/m^2)	24.9 ± 5.4	27.4 ± 6.6
Logistic EuroSCORE (%)	19.3 ± 13.0	15.2 ± 13.7
CHA_2DS_2-VASc Score	4.7 ± 1.2	4.5 ± 0.7
HAS-BLED Score	3.0 ± 0.9	2.5 ± 0.7
Coronary artery disease, *n* (%)	34 (53.1)	1 (50.0)
Previous heart surgery, *n* (%)	16 (25.0)	1 (50.0)
Atrial fibrillation, *n* (%)	57 (89.1)	2 (100)
pAVK, *n* (%)	5 (7.8)	0 (0.0)
cAVK, *n* (%)	7 (10.9)	0 (0.0)
OSAS, *n* (%)	3 (4.7)	0 (0.0)
COPD, *n* (%)	5 (7.8)	0 (0.0)
Diabetes mellitus, *n* (%)	13 (20.3)	0 (0.0)
Dialysis, *n* (%)	0 (0.0)	0 (0.0)
Anemia, *n* (%)	23 (35.9)	1 (50.0)
Immunotherapy, *n* (%)	1 (2.2)	0 (0.0)
Glomerular filtration rate (ml/min)	52 ± 19.2	63 ± 15.5
Hemoglobin (g/dl)	11.3 ± 1.7	10.8 ± 1.6
Thrombocytes, 10^3/µl	221 ± 77	218 ± 12.7
INR	1.3 ± 0.3	1.3 ± 0.1
Gastroesophageal pathologies, *n* (%)	7 (10.9)	1 (50.0)
- Gastroesophageal reflux disease, *n* (%)	3 (4.7)	1 (50.0)
- Chronic gastritis, *n* (%)	4 (6.3)	0 (0.0)
Dual antiplatelet therapy, *n* (%)	2 (3.1)	0 (0.0)
Oral anticoagulation, *n* (%)	55 (85.9)	2 (100)
Proton-pump inhibitor, *n* (%)	28 (43.8)	1 (50.0)

cAVK, cerebrovascular artery disease; COPD, chronic obstructive pulmonary disease; INR, international normalized ratio; OSAS, obstructive sleep-apnoe syndrome; pAVK, peripheral artery vascular disease; TEE, transesophageal echocardiography.

TABLE 3 Procedural data and in-hospital data.

	Patients without a TEE related complication ($n = 62$)	Patients with a TEE related complication ($n = 2$)
Procedure time (min)	120 (46–220) ± 35.3	170 (149–190) ± 29.0
Time under TEE (min)	76 (22–180) ± 35.7	125 (99–150) ± 36.1
Number of implanted Clips	1.6 ± 0.7	1.5 ± 0.7
TR reduction (grades)	2.1 ± 0.8	2.0 ± 1.4
Total length of stay (day)	7.5 (3–23) ± 4.4	15 (9–21) ± 8.5
Length of stay on ICU (day)	0 (0–2) ± 0.4	3.5 (2–5) ± 2.1
Procedural success, *n* (%)	57 (91.9)	2 (100)
In-hospital mortality, *n* (%)	0 (0.0)	0 (0.0)

ICU, intensive care unit; TEE, transesophageal echocardiography; TR, tricuspid regurgitation.

related complication was 3.1% with one major and one minor complication. We could not identify potential risk factors for the occurrence of a TEE related complication. The two patients presenting with a TEE related complication had a prolonged procedure time and therefore a longer time under TEE. Time under TEE may have an impact on adverse events as well in patients undergoing TTVR which has to be investigated in further studies. As transgastric views, where the probe is anteflexed toward the gastric fundus, are frequently used during this procedure, gastric lesions may occur more often, as observed in one of our patients.

Further considerations regarding the occurrence of TEE related complications may concern patient characteristics. Patients referred to TTVR are often a high-risk population presenting with multiple comorbidities (14) of which some may increase the risk of developing a TEE related complication. Besides, the procedure itself might as well be a risk factor for the occurrence of complications with its prolonged procedure time and therefore prolonged time under TEE. Previously reported complications after TTVR have been major bleedings, new onset of atrial fibrillation or single leaflet device attachment (14). These complications were not specific related to TEE. In our study, one of the two patients with a complication was suffering from gastroesophageal reflux disease. No routinely esophagogastroscopy was performed prior to intervention in our patients. This might be considered, at least in patients with known esophageal or gastric pathologies to decrease the risk for a TEE related complication. This complementary information might help to assess the periinterventional risk and identify patients who might need further treatment prior to intervention as for example high-dose PPI therapy.

Conclusions

In conclusion, a TEE related was observed in 3.1% of the patients undergoing TTVR. Further prospective studies are needed to identify potential risk factors associated to the occurrence of a TEE related complications to improve the safety of TEE during TTVR.

Limitations

The study has several limitations. First, it was a retrospective single-center study. Some events might not be recorded as they were self-limiting or felt not to be worth of mentioning in the medical data sheet. The number of complications might therefore be underestimated. As there was no systematic investigation of the upper gastrointestinal tract, subclinical lesions might as well be missed. Secondly,

operator specific occurrence of events cannot fully be excluded, though procedures were performed by a fixed team, highly experienced in structural heart disease interventions. Thirdly, due to the limited number of events, no potential risk factors associated with TEE related complications could identified. This aspect has to be investigated in further prospective studies. Fourthly, the sample size was rather small to detect potential complications. Further multicentre, prospective studies are needed to obtain data from a large patient cohort and detect potential complications.

Data availability statement

The raw data supporting the conclusions of this article will be made available by the authors, without undue reservation.

Ethics statement

Ethical approval was not provided for this study on human participants because in accordance with the Local Ethics Committee requirements an ethical approval was not needed due to retrospective data analysis. Written informed consent for participation was not required for this study in accordance with the national legislation and the institutional requirements.

Author contributions

KH and ML study concept, design, and supervision. KH, RS, ME, ML, BS, and AW acquisition and analysis or interpretation of data. KH writing and original draft preparation of the manuscript. TS, OB, and RS discussion and critical revision of the interpretation for important intellectual content. All authors reviewed the manuscript.

Conflict of interest

The authors declare that the research was conducted in the absence of any commercial or financial relationships that could be construed as a potential conflict of interest.

Publisher's note

References

1. Baumgartner H, Falk V, Bax JJ, Bonis M de, Hamm C, Holm PJ, et al. 2017 ESC/EACTS Guidelines for the management of valvular heart disease. *Eur Heart J.* (2017) 38:2739–91. doi: 10.1016/j.rec.2017.12.013

2. Zack CJ, Fender EA, Chandrashekar P, Reddy YNV, Bennett CE, Stulak JM, et al. National trends and outcomes in isolated tricuspid valve surgery. *J Am Coll Cardiol.* (2017) 70:2953–60. doi: 10.1016/j.jacc.2017.10.039

3. Alqahtani, F, Berzingi, CO, Aljohani, S, Hijazi, M, Al-Hallak, A, Alkhouli, M. Contemporary trends in the use and outcomes of surgical treatment of tricuspid regurgitation. *J Am Heart Assoc*. (2017) 6:e007597. doi: 10.1161/JAHA.117.007597

4. Nath J, Foster E, Heidenreich PA. Impact of tricuspid regurgitation on long-term survival. *J Am Coll Cardiol.* (2004) 43:405–9. doi: 10.1016/j.jacc.2003.09.036

5. Topilsky Y, Inojosa JM, Benfari G, Vaturi O, Maltais S, Michelena H, et al. Clinical presentation and outcome of tricuspid regurgitation in patients with systolic dysfunction. *Eur Heart J.* (2018) 39:3584–92. doi: 10.1093/eurheartj/ehy434

6. Lennon MJ, Gibbs NM, Weightman WM, Leber J, Ee HC, Yusoff IF. Transesophageal echocardiography-related gastrointestinal complications in cardiac surgical patients. *J Cardiothorac Vasc Anesth.* (2005) 19:141–5. doi: 10.1053/j.jvca.2005.01.020

7. Nickenig G, Weber M, Lurz P, von Bardeleben RS, Sitges M, Sorajja P, et al. Transcatheter edge-to-edge repair for reduction of tricuspid regurgitation: 6-month outcomes of the TRILUMINATE single-arm study. *Lancet.* (2019) 394:2002–11. doi: 10.1016/S0140-6736(19)32600-5

8. Orban M, Besler C, Braun D, Nabauer M, Zimmer M, Orban M, et al. Six-month outcome after transcatheter edge-to-edge repair of severe tricuspid regurgitation in patients with heart failure. *Eur J Heart Fail.* (2018) 20:1055–62. doi: 10.1002/ejhf.1147

9. Piercy M, McNicol L, Dinh DT, Story DA, Smith JA. Major complications related to the use of transesophageal echocardiography in cardiac surgery. *J Cardiothorac Vasc Anesth.* (2009) 23:62–5. doi: 10.1053/j.jvca.2008.09.014

10. Freitas-Ferraz AB, Rodés-Cabau J, Junquera Vega L, Beaudoin J, O'Connor K, Turgeon PY, et al. Transesophageal echocardiography complications associated with interventional cardiology procedures. *Am Heart J.* (2020) 221:19–28. doi: 10.1016/j.ahj.2019.11.018

11. Kallmeyer IJ, Collard CD, Fox JA, Body SC, Shernan SK. The safety of intraoperative transesophageal echocardiography: a case series of 7200 cardiac surgical patients. *Anesth Analg.* (2001) 92:1126–30. doi: 10.1097/00000539-200105000-00009

12. Afzal S, Zeus T, Hofsähs T, Kuballa M, Veulemans V, Piayda K, et al. Safety of transoesophageal echocardiography during structural heart disease interventions under procedural sedation: A single-centre study. *Eur Heart J Cardiovasc Imaging.* (2022). doi: 10.1093/ehjci/jeab280. [Epub ahead of print].

13. Hahn RT, Zamorano JL. The need for a new tricuspid regurgitation grading scheme. *Eur Heart J Cardiovasc Imaging.* (2017) 18:1342–3. doi: 10.1093/ehjci/jex139

14. Lurz, P. Stephan von Bardeleben, R, Weber, M, Sitges, M, Sorajja, P, Hausleiter, J, et al. Transcatheter edge-to-edge repair for treatment of tricuspid regurgitation. *J Am Coll Cardiol.* (2021) 77:229–39. doi: 10.1016/j.jacc.2020.11.038

15. Nickenig G, Kowalski M, Hausleiter J, Braun D, Schofer J, Yzeiraj E, et al. Transcatheter treatment of severe tricuspid regurgitation with the Edge-to-Edge MitraClip technique. *Circulation.* (2017) 135:1802–14. doi: 10.1161/CIRCULATIONAHA.116.024848

16. Hilberath, JN, Oakes, DA, Shernan, SK, Bulwer, BE, D'Ambra, MN, Eltzschig, HK. Safety of transesophageal echocardiography. *J Am Soc Echocardiogr*. (2010) 23:1115–27. quiz 1220–1. doi: 10.1016/j.echo.2010.08.013

frontiers | Frontiers in Cardiovascular Medicine

TYPE Original Research
PUBLISHED 31 October 2022
DOI 10.3389/fcvm.2022.942430

OPEN ACCESS

EDITED BY
Maria Nunes,
Federal University of Minas Gerais, Brazil

REVIEWED BY
Joshua D. Hutcheson,
Florida International University, United States
Robert Kiss,
McGill University, Canada

*CORRESPONDENCE
Payam Akhyari
Pakhyari@ukaachen.de

†PRESENT ADDRESS
Sebastian J. Bauer,
Payam Akhyari and Mareike Barth,
Department of Cardiac Surgery,
University Hospital
Rheinisch-Westfälische Technische Hochschule (RWTH), Aachen, Germany

SPECIALTY SECTION
This article was submitted to Heart Valve Disease, a section of the journal Frontiers in Cardiovascular Medicine

RECEIVED 12 May 2022
ACCEPTED 12 October 2022
PUBLISHED 31 October 2022

CITATION
Selig JI, Krug HV, Küppers C, Ouwens DM, Kraft FA, Adler E, Bauer SJ, Lichtenberg A, Akhyari P and Barth M (2022) Interactive contribution of hyperinsulinemia, hyperglycemia, and mammalian target of rapamycin signaling to valvular interstitial cell differentiation and matrix remodeling.
Front. Cardiovasc. Med. 9:942430.
doi: 10.3389/fcvm.2022.942430

Interactive contribution of hyperinsulinemia, hyperglycemia, and mammalian target of rapamycin signaling to valvular interstitial cell differentiation and matrix remodeling

Jessica I. Selig[1], H. Viviana Krug[1], Caroline Küppers[1], D. Margriet Ouwens[2,3,4], Felix A. Kraft[1], Elena Adler[1], Sebastian J. Bauer[1†], Artur Lichtenberg[1], Payam Akhyari[1*†] and Mareike Barth[1†]

[1]Department of Cardiac Surgery, Medical Faculty, University Hospital Düsseldorf, Heinrich Heine University Düsseldorf, Düsseldorf, Germany, [2]Institute of Clinical Biochemistry and Pathobiochemistry, German Diabetes Center (DDZ), Düsseldorf, Germany, [3]German Center for Diabetes Research (DZD), Munich, Germany, [4]Department of Endocrinology, Ghent University Hospital, Ghent, Belgium

Diabetes and its major key determinants insulin resistance and hyperglycemia are known risk factors for calcific aortic valve disease (CAVD). The processes leading to molecular and structural alterations of the aortic valve are yet not fully understood. In previous studies, we could show that valvular interstitial cells (VIC) display canonical elements of classical insulin signaling and develop insulin resistance upon hyperinsulinemia and hyperglycemia accompanied by impaired glucose metabolism. Analyses of cultured VIC and aortic valve tissue revealed extracellular matrix remodeling and degenerative processes. Since PI3K signaling through mammalian target of rapamycin (mTOR) is involved in fibrotic processes of the heart, we aim at further functional investigation of this particular Akt-downstream signaling pathway in the context of diabetes-induced CAVD. Primary cultures of VIC were treated with hyperinsulinemia and hyperglycemia. Phosphorylation of mTOR(Ser^{2448}) was determined by Western blot analysis after acute insulin stimulus. Inhibition of mTOR phosphorylation was performed by rapamycin. Phosphorylation of mTOR complex 1 (MTORC1) downstream substrates 4E-BP1(Thr$^{37/46}$) and P70S6K(Thr^{389}), and MTORC2 downstream substrate Akt(Ser^{473}) as well as the PDK1-dependent phosphorylation of Akt(Thr^{308}) was investigated. Markers for extracellular matrix remodeling, cell differentiation and degenerative changes were analyzed by Western blot analysis, semi-quantitative real-time PCR and colorimetric assays. Hyperinsulinemia and hyperglycemia lead to alterations of VIC activation, differentiation and matrix remodeling as

10.3389/fcvm.2022.942430

well as to an abrogation of mTOR phosphorylation. Inhibition of mTOR signaling by rapamycin leads to a general downregulation of matrix molecules, but to an upregulation of α-smooth muscle actin expression and alkaline phosphatase activity. Comparison of expression patterns upon diabetic conditions and rapamycin treatment reveal a possible regulation of particular matrix components and key degeneration markers by MTORC1 downstream signaling. The present findings broaden the understanding of mitogenic signaling pathways in VIC triggered by hyperinsulinemia and hyperglycemia, supporting the quest for developing strategies of prevention and tailored treatment of CAVD in diabetic patients.

KEYWORDS

valvular interstitial cells (VIC), calcific aortic valve disease (CAVD), rapamycin, insulin resistance, hyperinsulinemia, hyperglycemia, mammalian target of rapamycin (mTOR), MTORC1/2

Introduction

Early disturbances in insulin sensitivity and hyperglycemia (HG) (1, 2) are risk factors for the development of diabetes (3), which is a global burden with increasing prevalence (4, 5). Diabetes in turn is associated with an elevated risk for cardiovascular diseases, including calcific aortic valve disease (CAVD) (6–9). Here, studies report that aortic valve leaflets of diabetics are more prone to inflammation (10), oxidative stress (11) and remodeling (12), and show an enhanced micro-calcification together with an up-regulation of pro-osteogenic markers (13).

In previous work, we could show that valvular interstitial cells (VIC) are sensitive to short-term treatment by diabetic conditions such as hyperinsulinemia (HI) and HG (14). Here, it could be shown that VIC express the insulin receptor, insulin-like growth factor 1 receptor and glucose transporter 1. Beside impaired glucose metabolism, VIC develop an insulin resistance upon HI and HG with disturbed Akt/GSK-3α/β signaling, whilst HG alone was sufficient to induce insulin resistance. Consecutively, alterations in VIC differentiation and early signs of remodeling could be observed (14). Further analysis of aortic valve tissue in a three-dimensional approach revealed that these processes are further modulated by their biomechanical environment and that particular mitogenic signaling pathways such as downstream PI3K signaling are involved (15). Nevertheless, it remains incompletely understood whether HI, HG or the combination of both trigger molecular alterations of VIC and whether downstream PI3K signaling or alternative insulin-sensitive pathways are responsible for these processes.

PI3K signaling through mammalian target of rapamycin (mTOR) is known to be involved in fibrotic processes of several organs and tissues including the myocardium (16). Here, especially the treatment of myocardial dysfunction with mTOR inhibitors like rapamycin has gained attention, particularly in diabetes-related pathologies [reviewed in (17)]. Downstream mTOR signaling is regulated through two mTOR containing complexes: mTOR complex 1 (MTORC1) and MTORC2, both of which have diverse downstream effects and mechanisms in the heart (18). MTORC1 consists amongst others of the adaptor proteins RAPTOR (regulatory-associated protein of mTOR) and DEPTOR (DEP domain containing mTOR-interacting protein). MTORC1 downstream signaling leads to phosphorylation of P70S6K (ribosomal protein S6 kinase 1) and 4E-BP1 (eukaryotic translation initiation factor 4E (eIF4E)-binding protein 1). MTORC2 comprises RICTOR (rapamycin-insensitive companion of mTOR) instead of RAPTOR and activates Akt signaling (17). MTORC1 and MTORC2 signaling have been investigated in the context of myocardial dysfunction and type 2 diabetes (17, 18), whereas knowledge about their role in CAVD and diabetes is still scarce. Understanding of signaling pathways involved in pathological diabetes-induced processes of aortic valve disease, however, is crucial for the development of future preventive or therapeutic strategies. Thus, the present work aims at the investigation of mTOR and mTOR downstream signaling and its role in CAVD.

Materials and methods

Primary ovine valvular interstitial cells and treatments

Primary ovine VIC were isolated from aortic valves of fresh ovine hearts (n = 7) derived from a local abattoir as described before (14). Aortic valve leaflets were dissected and minced into small pieces. Tissue pieces were incubated in either

normoglycemic (NG; 1 g/L glucose) or HG (4.5 g/L glucose) medium in gelatin-covered flasks until VIC grew out. After three to four passages VIC were seeded in gelatin-covered 6-well plates and treated with NG or HG medium with or without 100 nM insulin (Sigma-Aldrich, St. Louis, MO, USA; cat. no. I5523) for 5 days with medium changes every second day [for details please refer to (14)]. Inhibition of mTOR phosphorylation was performed by chronic treatment with 10 nM rapamycin (cat. no. 9904, Cell Signaling, Dallas, TX, USA) using dimethyl sulfoxide (DMSO; Sigma-Aldrich; cat. no. D8418) as vehicle.

For the acute insulin stimulus, supernatant of the cells of all treatment groups was aspirated and the cells were washed twice with PBS. After a starvation period of 4 h in medium without FCS and insulin, VIC were treated with insulin (group: with acute insulin stimulus) or not (group: without acute insulin stimulus). To evaluate the optimal insulin concentration cells were initially treated either with 10 nM or with 100 nM insulin for 10 min. In the further process, 10 nM insulin was used for the acute stimulus. Afterward, cells were washed twice with cold PBS and were lysed for SDS-PAGE and Western blot as described before (14).

SDS-PAGE and Western blot analysis

Lysates were conducted to SDS-PAGE and separated proteins were blotted on nitrocellulose. Protein signals were detected using the following primary antibodies purchased from Cell Signaling: mTOR (cat. no. 2983); phospho-mTOR(Ser^{2448}) (cat. no. 2971); 5′-adenosine monophosphate (AMP)-activated protein kinase (AMPKα; cat. no. 2603); phospho-AMPKα(Thr^{172}) (cat. no. 2535); ribosomal protein S6 kinase beta-1 (P70S6K; cat. no. 2708); phospho-P70S6K(Thr^{389}) (cat. no. 9234); 4E-BP1 (cat. no. 9452); phospho-4E-BP1(Thr$^{37/46}$) (cat. no. 9459); Akt (cat. no. 4691), phospho-Akt(Ser^{473}) (cat. no. 4060), and phospho-Akt(Thr^{308}) (cat. no. 13038). Detection of housekeeping protein GAPDH (cat. no. 2118) or β-actin (cat. no. 4967) on the according membranes was used for normalization of protein signals. Signals of primary antibodies were detected by using the following secondary antibodies: Goat IgG anti-rabbit IgG (H + L)-HRP (cat. no. 111-035-003, Jackson ImmunoResearch, Ely, UK) and goat IgG anti-mouse IgG & IgM (H + L)-HRP (cat. no. 115-035-044, Jackson ImmunoResearch). Molecular weight was determined by using a PageRuler Prestained Protein ladder (cat. no. 26616; Thermo Fisher Scientific, Waltham, MA, USA). Detection of protein signals was performed by using an Amersham Imager 600 (GE Healthcare, Chalfont St Giles, UK) and intensity of protein bands was analyzed by Image Quant TL software (GE Healthcare). Detection of 4E-BP1 and Akt as well as the corresponding phosphorylated antibodies was performed with IRDye 800 CW goat anti rabbit (cat. no. 926-32211, LI-COR biosciences, Lincoln, NE, USA) and IRDye 680 LT goat anti mouse (cat. no. 926-68020, LI-COR biosciences) as secondary antibodies using an Odyssey scanner (LI-COR biosciences).

Western blot images of **Supplementary Figure 1** and **Figures 3**, **4** were cropped since additional conditions have been tested for control experiments on these blots. Uncropped images of the appropriate blots are depicted in **Supplementary Figures 2–4**, respectively.

mRNA analysis by semi-quantitative real-time PCR

Isolation of total RNA, cDNA synthesis as well as semi-quantitative real-time PCR was performed as previously described (10). Primer sequences were as follows: collagen type 1 (*COL1A1*; forward 5′-AAGACATCCCACCAGTCACC-3′, reverse 5′-TAAGTTCGTCGCAGATCACG-3′), elastin (*ELN*; forward 5′- AGTTCCTGGAGGCGTCTTCT-3′, reverse 5′ CAC CTGGCTTAGCTGGTTTC-3′), biglycan (*BGN*; forward 5′-TCTGCTCCGCTACTCCAAGT-3′, reverse 5′-TTGTTGTCC AAGTGCAGCTC-3′), decorin (*DCN*; forward 5′ CCAAAGTG CGAAAGTCTGTG-3′, reverse 5′-TTCAATGCCTGAGCTCT TCA-3′), α-smooth muscle actin (*ACTA2*; forward 5′-GATA GAGCACGGCATCATCA-3′, reverse 5′-GAAGGGTTGGATG CTCTTCA-3′), osteopontin (*OPN*; forward 5′-GATGGCCG AGGTGATAGTGT-3′, reverse 5′-TCGTCTTCTTAGGTGCG TCA-3′), alkaline phosphatase (*ALP*; forward 5′-CAACACC AACGTGGCTAAGA-3′, reverse 5′-GTTGTGGTGGAGCTG ACCTT-3′), matrix metalloproteinase 2 (*MMP2*; forward 5′-TGACAAGGACGGCAAGTATG-3′, reverse 5′-GTAAGATGT GCCCTGGAAGC-3′), hyaluronic acid synthase 2 (*HAS2*; forward 5′-TCACCCAGTTGGTCTTGTCC-3′, reverse 5′-GG TCAAGCATGGTGTCTGAA-3′), and matrix metalloprotei nase 9 (*MMP9*; forward 5′-TAGCACGCACGACATCTTTC-3′, reverse 5′-GCCCACATAGTCCACCTGAT-3′). Relative mRNA expression analysis was performed by $2^{-\Delta\Delta Ct}$ method using CT means of the following reference genes: β-tubulin (forward 5′-CCTACAACTGGACCGCATCT-3′, reverse 5′-AAAGGACCTGAGCGAACAGA-3′), 60S ribosomal protein L13a (*RPL13a*; forward 5′-GATCCCACCACCCTATGACA-3′, reverse 5′-CTTCAGACGCACAACCTTGA-3′), and 60S ribosomal protein L29 (*RPL29*; forward 5′-CCAAGTCCAAG AACCACACC-3′, reverse 5′-TATCGTTGTGATCGGGGTTT-3′). In the following, gene names are written in italics.

Detection of alkaline phosphatase activity

Using the PierceTM PNPP Substrate Kit (cat. no. 37620, Thermo Fisher Scientific), the concentration of cell released

alkaline phosphatase (n = 3) was measured using supernatants of the media before inhibitor treatment and then every second day. The assay was performed according to the manufacturers' instructions using a microplate reader (Infinite M1000 Pro) by measuring the absorbance at 405 nm.

Detection of cytotoxicity

The CyQUANT^{TM} LDH cytotoxicity assay (cat. no. C20300, Thermo Fisher Scientific) was used to determine the amount of lactate dehydrogenase (LDH) released into the media of the cells. Therefore, supernatants were collected at the day of cell harvest and the colorimetric assay was performed according to the manufacturer's instructions using a microplate reader (Infinite M1000 Pro). Data was normalized to total protein content.

Statistical analysis

Statistical analysis was performed using GraphPad Prism version 7 (GraphPad Software, San Diego, CA, USA). Data is presented as mean ± SEM. Statistical analysis of data originating from Western blot analysis was performed using two-way ANOVA with Sidak's multiple comparison test. Statistical analysis of data originating from semi-quantitative real-time PCR, ALP and LDH analysis was performed using Kruskal–Wallis test with Dunn's *post hoc* test. For comparison of two groups, Mann–Whitney U test or Wilcoxon signed rank test was applied. p-Values < 0.05 were considered as statistically significant.

Results

Hyperglycemia and hyperinsulinemia abrogate PI3K signaling in valvular interstitial cells

To elucidate the impact of diabetic conditions on PI3K signaling, Western blot analysis of mTOR signaling was performed in VIC (**Figure 1**). Acute insulin stimulation led to a significant increase in mTOR(Ser^{2448}) phosphorylation (p = 0.012) under NG, an effect which was abrogated by treatment with HI or HG as well as by the combination of both treatments. Upon acute insulin stimulus, HI inhibited phosphorylation of mTOR(Ser^{2448}) under NG treatment by 43% (p = 0.003) as well as under HG treatment by 48% (p = 0.009) (**Figures 1A,B**). Compared to NG conditions, the combination of HG and HI led to a significant decrease of mTOR(Ser^{2448}) phosphorylation upon acute insulin stimulus by 57% ($p < 0.0001$). HG treatment alone did not lead to a significant decrease of mTOR(Ser^{2448}) phosphorylation upon acute insulin stimulus compared to the appropriate NG condition. Basal phosphorylation (**Figures 1A,B**) as well as protein abundance of total mTOR (**Figure 1B'**) was not affected by diabetic conditions. In contrast to mTOR, AMPK signaling was not impaired by diabetic conditions (**Figure 2**).

Impact of diabetic conditions and mammalian target of rapamycin inhibition on mammalian target of rapamycin complex 1 and mammalian target of rapamycin complex 2 signaling

For rapamycin treatment, the optimal rapamycin concentration was evaluated, revealing that 10 nM rapamycin efficiently decreased basal phosphorylation of mTOR(Ser^{2448}) (**Supplementary Figure 1**) whilst cell morphology was not affected (not shown). In order to evaluate mTOR signaling, downstream targets of MTORC1 and MTORC2 were investigated.

Mammalian target of rapamycin complex 1 signaling upon diabetic conditions and rapamycin treatment

Hyperinsulinemia under NG conditions led to a significantly higher 4E-BP1(Thr$^{37/46}$) phosphorylation both under basal conditions (p = 0.0006) and upon acute insulin stimulus (p = 0.0006). Acute insulin stimulus led to a significant increase of 4E-BP1(Thr$^{37/46}$) under NG (p = 0.007) as well as under HG (p = 0.038) conditions compared to the corresponding basal conditions, whereas HI treatment abrogated this effect. Rapamycin treatment led to attenuated inducible 4E-BP1(Thr$^{37/46}$) phosphorylation by acute insulin (**Figures 3A,B**). Generally, upon acute insulin stimulus, rapamycin treatment led to a lower phosphorylation levels of 4E-BP1(Thr$^{37/46}$) both under NG (p = 0.038) and NG + HI (p = 0.073) conditions as well as under HG (p = 0.018) and HG + HI (p = 0.014) conditions compared to the corresponding untreated group (**Figures 3A,B**). Basal phosphorylation as well as total 4E-BP1 abundance was not altered (**Figure 3B'**). Phosphorylation of P70S6K(Thr^{389}) was not altered by rapamycin treatment (**Figures 3C,D**). Total P70S6K was not altered (**Figure 3D'**).

Mammalian target of rapamycin complex 2 signaling upon diabetic conditions and rapamycin treatment

Compared to the corresponding basal group, acute insulin stimulus led to a significantly increased phosphorylation of Akt(Ser^{473}) under NG (p = 0.002) and HG (p = 0.002)

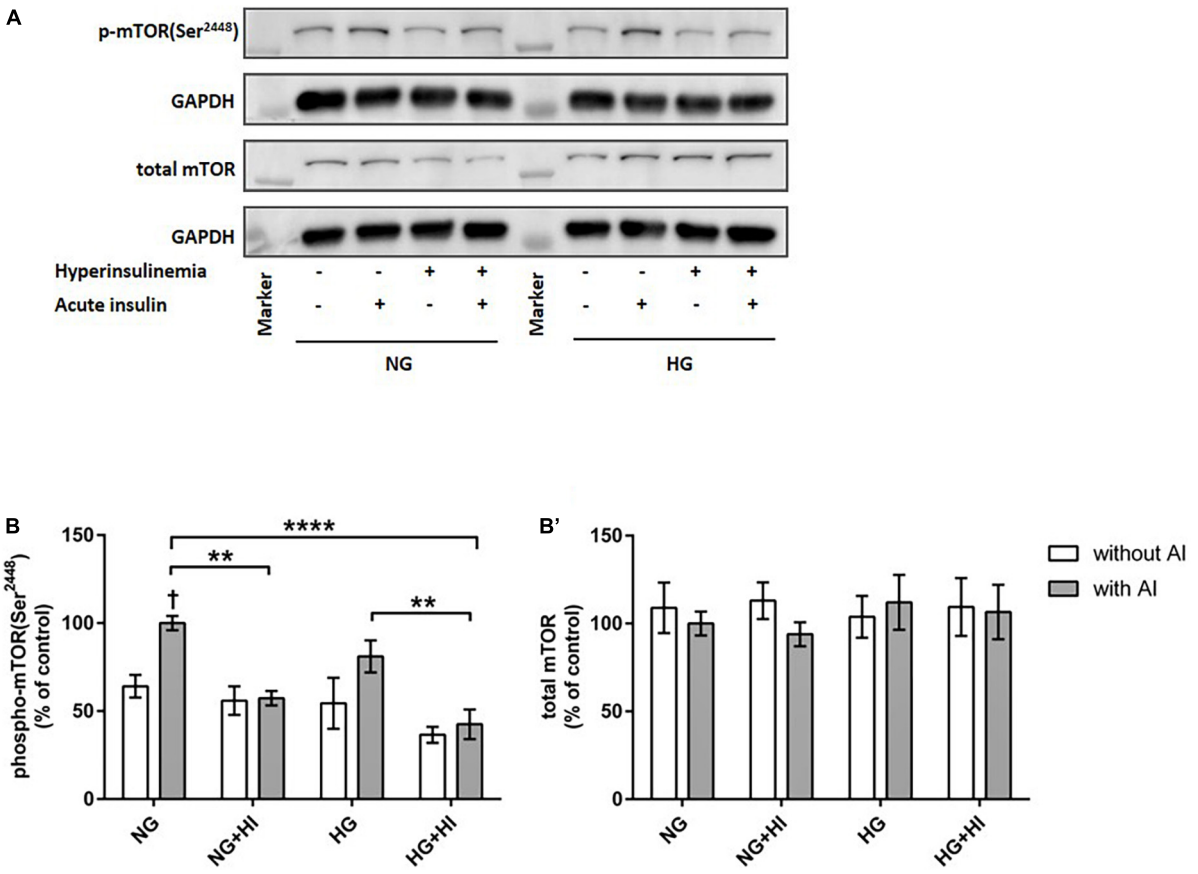

FIGURE 1
Diabetic conditions abrogate mTOR phosphorylation. Phosphorylation of mTOR(Ser^{2448}) upon hyperinsulinemia under normoglycemia and hyperglycemia was measured in cultured ovine VIC (n = 7). Representative Western blot images show phosphorylated and total mTOR expression **(A)**. Quantification of protein signals showed that hyperinsulinemia led to significantly decreased phosphorylation levels of mTOR(Ser^{2448}) as well as to an abrogation of inducible phosphorylation upon acute insulin stimulus **(B)**. Total amount of mTOR was not altered **(B')**. Data was normalized to GAPDH and expressed relative to normoglycemic conditions with acute insulin stimulus. NG, normoglycemia; HI, hyperinsulinemia; HG, hyperglycemia; AI, acute insulin stimulus. **p-Values < 0.01 and ****p-values < 0.0001 between indicated groups; $^{\dagger}p$-values < 0.05 compared to basal condition without acute insulin stimulus. Lanes of protein ladder represent 35 and 250 kDa, respectively.

treatment (Figures 4A,B). HI treatment abrogated inducible phosphorylation of Akt(Ser^{473}) and led to a significantly reduced Akt(Ser^{473}) phosphorylation under NG + HI (p = 0.0022) as well as under HG + HI treatment (p = 0.0026) upon acute insulin stimulus compared to NG and HG alone. A similar effect was observed upon rapamycin treatment; here, phosphorylation was increased under NG (p = 0.004) and HG (p = 0.002) treatment upon acute insulin stimulus compared to basal conditions and was abrogated by HI treatment. Generally, treatment with rapamycin led to a significantly increased phosphorylation level of Akt(Ser^{473}) upon acute insulin stimulus under NG (p = 0.002), NG + HI (p = 0.004), HG (p = 0.002) and HG + HI (p = 0.002) conditions (Figures 4A,B) compared to the according untreated group.

Detection of Akt(Thr^{308}) phosphorylation proved to be difficult due to generally low expression levels and unspecific binding (Figure 4B'). Acute insulin stimulus led to an increased phosphorylation under HG conditions in the untreated group (p = 0.011), whereas phosphorylation was not inducible under NG (p = 0.620), NG + HI (p = 0.805) and HG + HI (p = 0.710) conditions. Under rapamycin treatment, acute insulin stimulus led to an increased Akt(Thr^{308}) phosphorylation compared to the according basal condition under NG (p = 0.018) as well as under HG (p = 0.007) conditions. HI treatment abrogated this effect (Figure 4B'). Similar to phosphorylation of Akt(Ser^{473}), rapamycin treatment led to generally higher expression levels of phosphorylated Akt(Thr^{308}) upon acute insulin stimulus compared to the according untreated groups (NG: p = 0.0006; NG + HI: p = 0.005; HG: p = 0.018; HG + HI: p = 0.0006). Total Akt abundance was not influenced by acute insulin stimulus compared to basal conditions. However, rapamycin led to generally higher Akt expression levels compared to the untreated groups (Figure 4C).

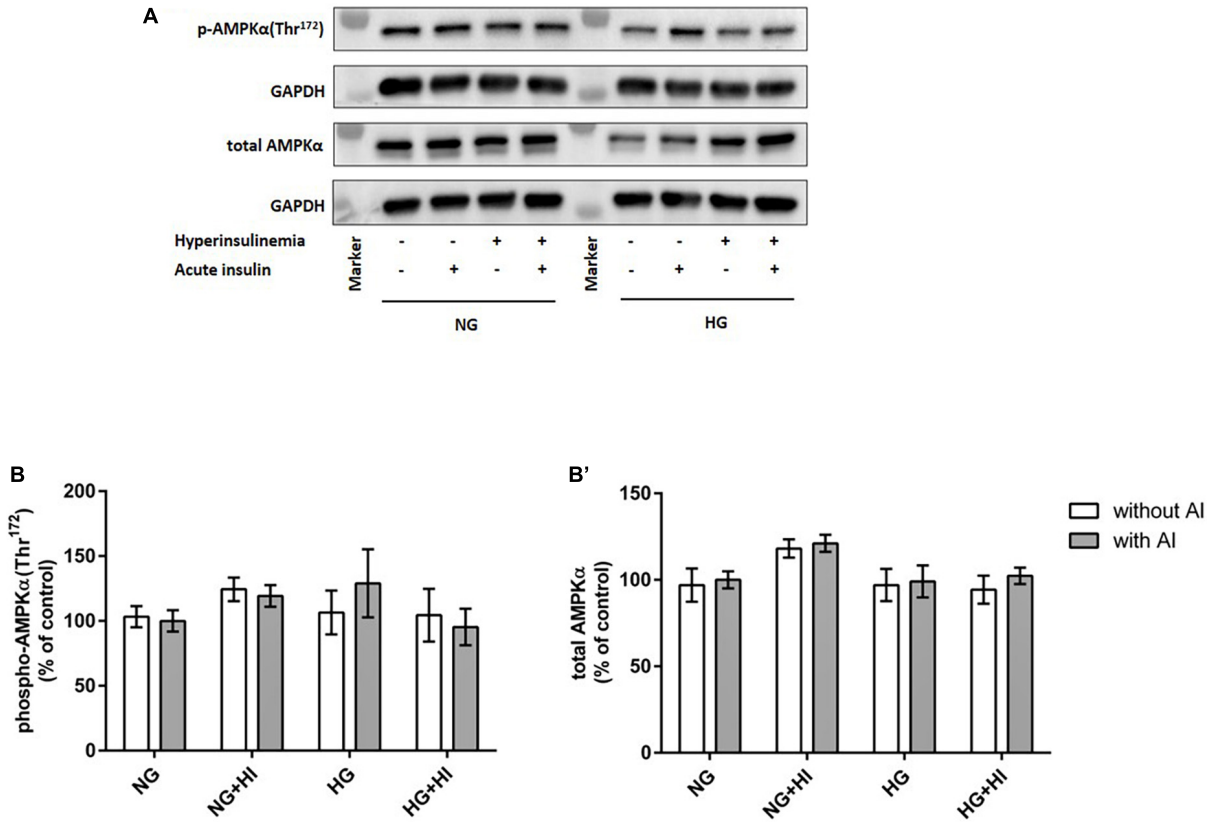

FIGURE 2
AMPK phosphorylation is not impaired by diabetic conditions. Phosphorylation of AMPK(Thr^{172}) upon hyperinsulinemia under normoglycemia and hyperglycemia was measured in cultured ovine VIC (n = 7). Representative Western blot images show phosphorylated and total AMPKα expression **(A)**. Quantification of protein signals showed that neither acute insulin stimulus nor hyperinsulinemia or hyperglycemia led to alterations in AMPK(Thr^{172}) phosphorylation **(B)**. Total amount of AMPK was not altered by the treatments **(B')**. Data was normalized to GAPDH and expressed relative to normoglycemic conditions with acute insulin stimulus. NG, normoglycemia; HI, hyperinsulinemia; HG, hyperglycemia; AI, acute insulin stimulus. Lanes of protein ladder represent 35 and 70 kDa, respectively.

Valvular interstitial cells differentiation and matrix remodeling under diabetic conditions and mammalian target of rapamycin inhibition

Next, we analyzed the impact of diabetic conditions as well as the impact of rapamycin as an inhibitor of mTOR signaling on VIC differentiation and matrix remodeling. For rapamycin treatment, the optimal rapamycin concentration was evaluated, revealing that 10 nM rapamycin efficiently decreased basal phosphorylation of mTOR(Ser^{2448}) (**Supplementary Figure 1**) whilst cell morphology was not affected (not shown).

Valvular interstitial cells activation and viability

Upon stress or tissue damage, VIC change their quiescent fibroblastoidal phenotype toward an activated myofibroblastoidal phenotype with higher contractility, which is indicated by an increased expression of ACTA2 (19–21). The term "VIC activation" used in this work thus refers to this phenomenon, and does not necessarily involve concomitant enhanced matrix remodeling as commonly described for pathological changes in CAVD (recently reviewed in (22).

Hyperinsulinemia treatment led to a significant downregulation of *ACTA2* gene expression in VIC under NG (p = 0.016) as well as under HG conditions (p = 0.047) compared to NG control conditions. HG treatment alone had no effect (p = 0.469). Inhibition of mTOR signaling by rapamycin treatment led to a significant upregulation of *ACTA2* gene expression under NG (p = 0.016) as well as under HG conditions (p = 0.031) compared to NG control conditions. HI treatment seemed to mitigate these effects. Comparison between rapamycin and HI treatment revealed opposed effects with highly significant difference (p = 0.0005; **Figure 5A**). LDH activity as a marker for cytotoxicity was not significantly altered by diabetic conditions, nor by rapamycin treatment under NG conditions. Rapamycin treatment in combination with HG treatment, however, led to a significantly higher LDH activity

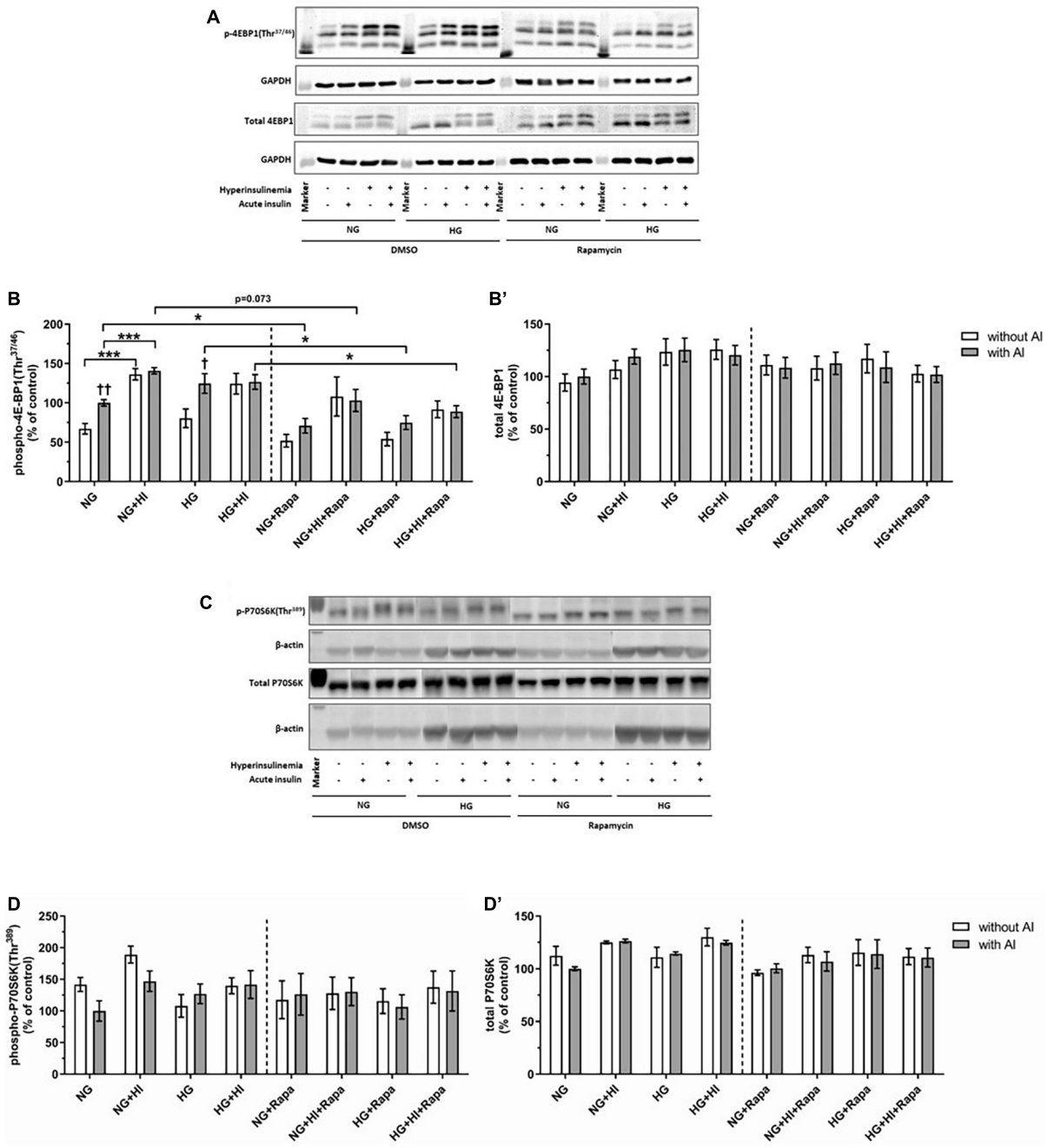

FIGURE 3
Mammalian target of rapamycin complex 1 signaling upon diabetic conditions and rapamycin treatment. Phosphorylation of 4E-BP1(Thr$^{37/46}$) and P70S6K(Thr^{389}) upon hyperinsulinemia under normoglycemia and hyperglycemia was measured in cultured ovine VIC (n = 6 for 4E-BP1 and n = 4 for P70S6K). Representative Western blot images show phosphorylated and total 4E-BP1 **(A)** and P70S6K expression **(C)**. Quantification of 4E-BP1 protein signals showed that rapamycin treatment led to generally lower phosphorylation levels of 4E-BP1(Thr$^{37/46}$) upon acute insulin stimulus. In absence of rapamycin, acute insulin stimulus led to significantly higher phosphorylation levels of 4E-BP1(Thr$^{37/46}$) whilst hyperinsulinemia abolished the effect of inducible phosphorylation **(B)**. Total amount of 4E-BP1 was not altered **(B')**. Quantification of P70S6K protein signals showed that neither acute insulin stimulus nor hyperinsulinemia or hyperglycemia led to alterations in P70S6K(Thr^{389}) phosphorylation **(D)**. Total amount of P70S6K was not altered by the treatments **(D')**. Data was normalized to GAPDH or β-actin, and expressed relative to normoglycemic conditions with acute insulin stimulus. NG, normoglycemia; HI, hyperinsulinemia; HG, hyperglycemia; AI, acute insulin stimulus; Rapa, rapamycin. *p-Values < 0.05 and ***p-values < 0.001 between indicated groups; $^{\dagger}p$-values < 0.05 and $^{\dagger\dagger}p$-values < 0.01 compared to basal condition without acute insulin stimulus. Lanes of protein ladder represent 15 kDa (4E-BP blots) and 35 kDa (GAPDH blots) as well as 70 kDa (P70S6K blots) and 35 kDa (β-actin blots), respectively.

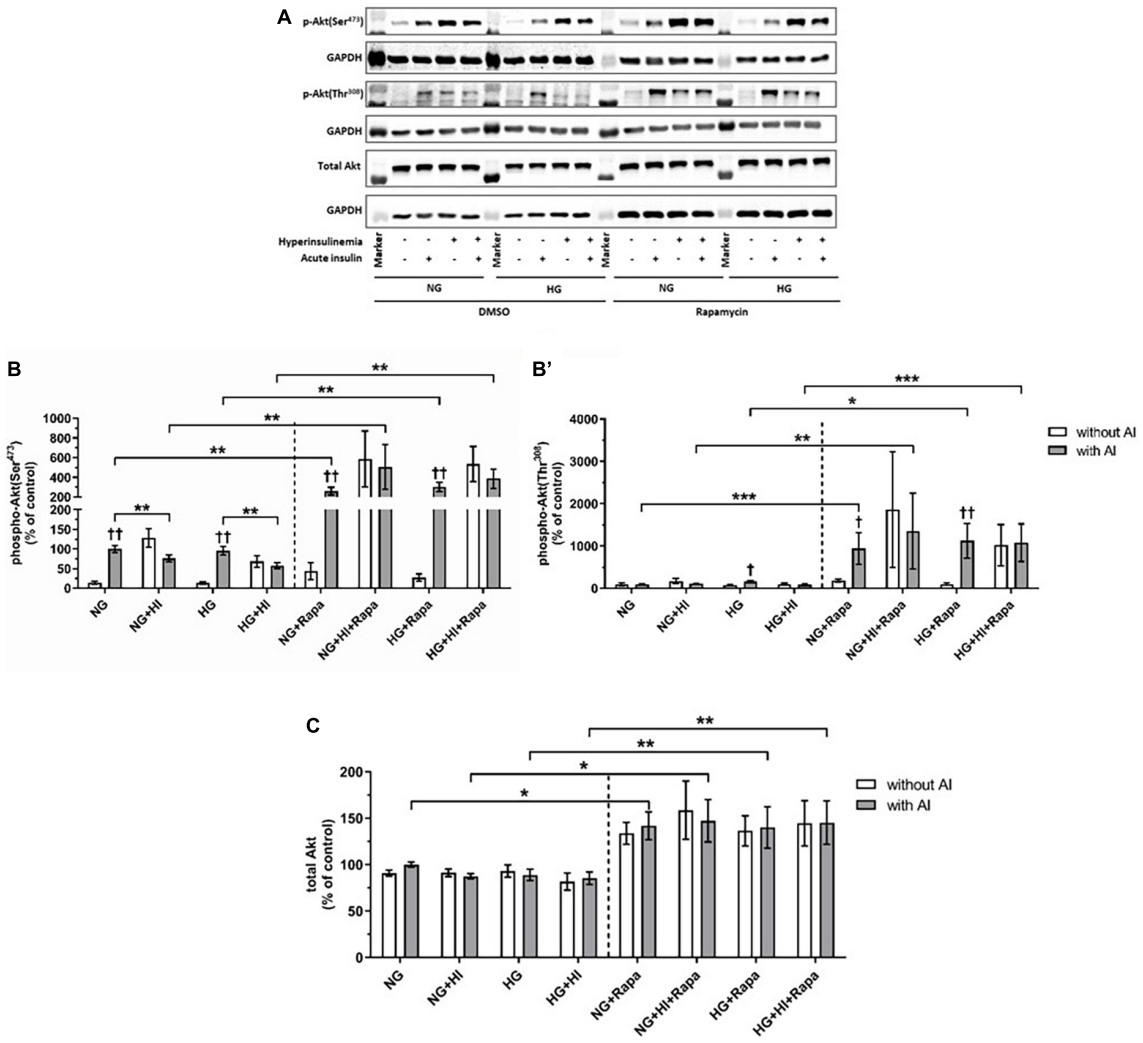

FIGURE 4
Mammalian target of rapamycin complex 2 signaling upon diabetic conditions and rapamycin treatment. Phosphorylation of Akt(Ser^{473}) and Akt(Thr^{308}) upon hyperinsulinemia under normoglycemia and hyperglycemia was measured in cultured ovine VIC (n = 6). Representative Western blot images show phosphorylated and total Akt expression **(A)**. Quantification of Akt protein signals showed that rapamycin treatment led to a generally higher Akt(Ser^{473}) **(B)** and Akt(Thr^{308}) **(B')** phosphorylation upon acute insulin stimulus. Acute insulin stimulus led to significantly higher phosphorylation levels of Akt(Ser^{473}) whilst hyperinsulinemia abolished the effect of inducible phosphorylation under control conditions as well as upon rapamycin treatment **(B)**. Akt(Thr^{308}) phosphorylation was significantly upregulated by acute insulin stimulus under HG conditions **(B')**. Upon rapamycin treatment, hyperinsulinemia abolished inducible phosphorylation Akt(Thr^{308}) by acute insulin stimulus **(B')**. Total amount of Akt showed a generally higher expression level upon rapamycin treatment, whereas neither acute insulin stimulus nor hyperinsulinemia or hyperglycemia led to alterations of Akt expression **(C)**. Data was normalized to GAPDH and expressed relative to normoglycemic conditions with acute insulin stimulus. NG, normoglycemia; HI, hyperinsulinemia; HG, hyperglycemia; AI, acute insulin stimulus; Rapa, rapamycin. *p-Values < 0.05, **p-values < 0.01, and ***p-values < 0.001 between indicated groups; $^{\dagger}p$-values < 0.05 and $^{\dagger\dagger}p$-values < 0.01 compared to basal condition without acute insulin stimulus. Lanes of protein ladder represent 70 and 55 kDa (Akt blots) and 35 kDa (GAPDH blots), respectively.

both without HI (p = 0.047) and with HI (p = 0.047) when compared to NG conditions (Figure 5B).

Structural extracellular matrix molecules and matrix metalloproteinases

COL1A1 gene expression was not significantly altered by diabetic conditions. Rapamycin treatment in contrast, led to significantly decreased *COL1A1* gene expression compared to NG control conditions independent of diabetic conditions (p = 0.016; Figure 6A). Comparison between rapamycin and HI treatment revealed significantly lower *COL1A1* gene expression under rapamycin treatment (p = 0.033). Gene expression of *ELN* was significantly downregulated by HG + HI treatment with similar effect upon rapamycin treatment alone (p = 0.016) as well as in combination with HI (p = 0.031) when compared to NG control conditions (Figure 6B). Combined treatment

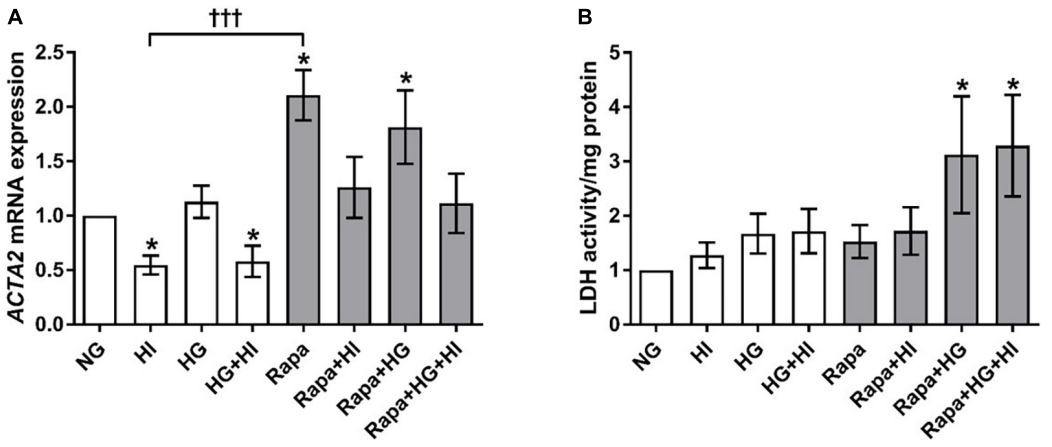

FIGURE 5
Valvular interstitial cells activation and viability under diabetic conditions and mTOR inhibition. Impact of diabetic conditions and mTOR inhibition on gene expression of *ACTA2* **(A)** and on LDH activity **(B)** was analyzed. HI led to a decrease of *ACTA2* gene expression, whereas rapamycin led to a remarkable and statistically highly significant opposite effect. *ACTA2*, α-smooth muscle actin; LDH, lactate dehydrogenase; HI, hyperinsulinemia; HG, hyperglycemia; Rapa, rapamycin. *p-Values < 0.05 of direct comparison to normoglycemic control; †††p-value < 0.001 of intergroup comparisons.

of rapamycin with HG or HG + HI conditions led to a slight trend toward lower *ELN* gene expression in comparison to NG control conditions ($p = 0.078$). *MMP2* gene expression was significantly upregulated under HI conditions ($p = 0.016$) and by a slight trend under HG + HI conditions ($p = 0.078$; Figure 6C). Comparison between HI and rapamycin treatment revealed a visible difference, however not statistically different ($p = 0.323$), whereas comparison between HI and HI + rapamycin showed a significant opposed effect ($p = 0.018$). *MMP9* gene expression levels were not detectable (not shown).

Glycosylated matrix molecules

Analysis of glycosylated matrix molecules revealed a significant upregulation of *BGN* gene expression upon HI treatment ($p = 0.031$) as well as upon HG + HI treatment ($p = 0.016$; Figure 7A). Rapamycin treatment led to a numerically small effect but significantly lower *BGN* gene expression when compared to NG control conditions ($p = 0.031$). Comparison between HI and rapamycin treatment showed significantly different gene expression of *BGN* ($p = 0.010$). Interestingly, when the subset of rapamycin-containing treatments is considered, rapamycin entirely abolished the effects of diabetic conditions on the expression of *BGN* as observed within the subset of conditions without rapamycin. *DCN* gene expression was in general upregulated by diabetic conditions when compared to NG control conditions ($p = 0.016$; Figure 7B). Rapamycin treatment in combination with HI or HG conditions led to numerically small but significantly lower *DCN* gene expression when compared to NG control conditions ($p = 0.016$). Comparison between HI and rapamycin treatment showed significantly different gene expression of *DCN* ($p = 0.008$). Similar to the observations on *BGN* gene expression, rapamycin led to a general abrogation of the elevating effect of diabetic conditions on *DCN* gene expression. *HAS2* gene expression was significantly upregulated by diabetic conditions either by HI ($p = 0.003$), HG ($p = 0.019$) or combined treatment with HI + HG ($p = 0.037$; Figure 7C). Rapamycin treatment in contrast, did not alter *HAS2* gene expression, whereas additional stimulation with HI led to significantly higher *HAS2* gene expression when compared to NG control conditions ($p = 0.016$). Comparison between HI and rapamycin treatment showed significantly different *HAS2* gene expression levels ($p = 0.0004$), with an overall inhibition of the stimulatory impact of diabetic conditions on *HAS2* gene expression.

Valvular interstitial cells chondro-osteogenic differentiation

OPN gene expression was significantly upregulated by HG treatment ($p = 0.023$). Rapamycin treatment did not alter *OPN* gene expression. However, *OPN* gene expression levels upon HI or HI + HG treatment were comparable to those under rapamycin treatment (Figure 8A). HI and HG + HI treatment led to significantly decreased ALP activity when compared to NG control conditions ($p = 0.031$; Figure 8B). Rapamycin treatment, however, led to a generally higher ALP activity when compared to NG control conditions ($p = 0.031$) except for the combination with HG + HI which led to a trend toward higher ALP activity ($p = 0.063$). Comparison between HI and rapamycin treatment revealed significantly opposed effects on ALP activity ($p = 0.027$). Collectively, rapamycin abrogated the inducing effect of HG on *OPN* gene expression and had a strong enhancing effect on ALP activity that contrasts the effects observed under HI.

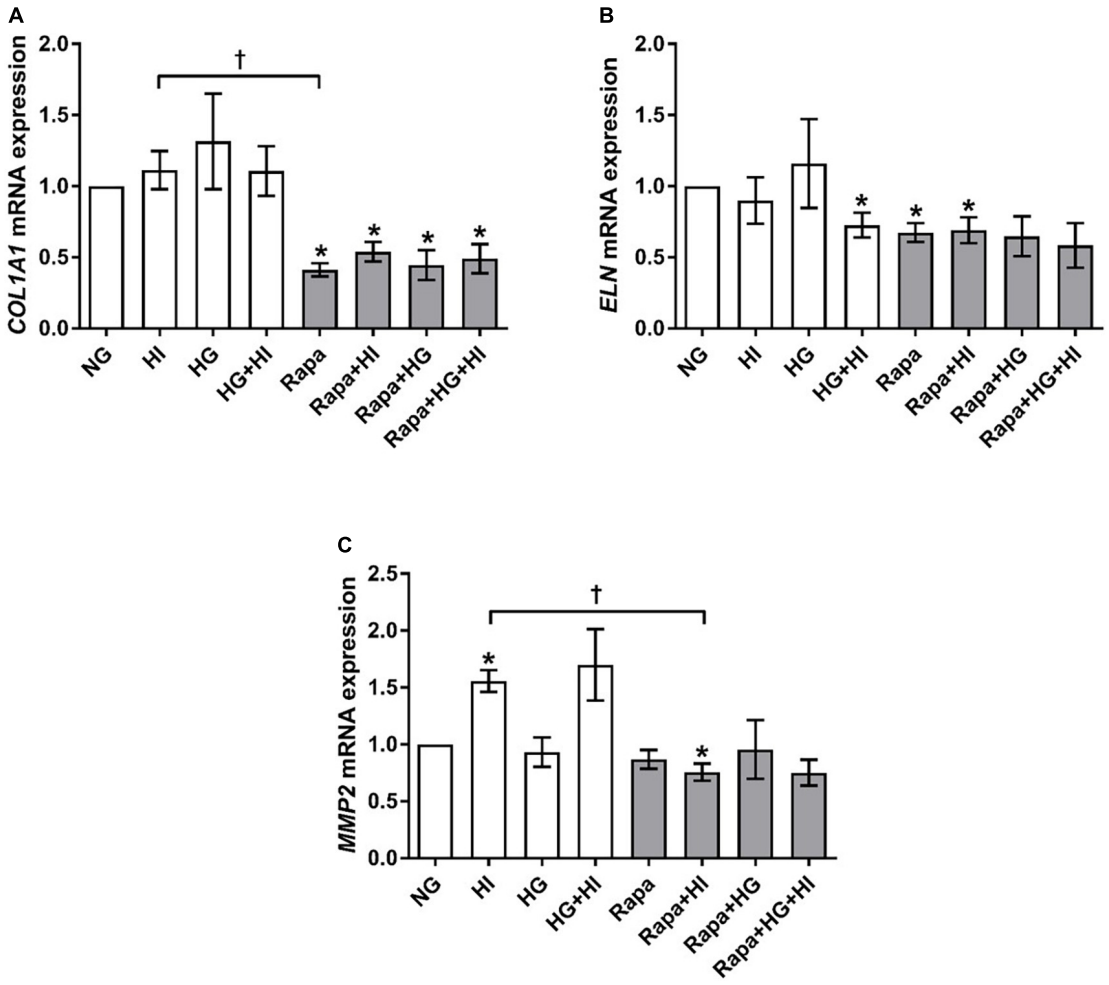

FIGURE 6
Expression of structural extracellular matrix molecules and matrix metalloproteinase under diabetic conditions and mTOR inhibition. Impact of diabetic conditions and mTOR inhibition on gene expression of *COL1A1* **(A)**, *ELN* **(B)**, and *MMP2* **(C)** was analyzed. Diabetic conditions had no significant impact on *COL1A1* gene expression, whereas rapamycin treatment led to a reduction of *COL1A1* gene expression **(A)**. *ELN* gene expression was reduced by HG + HI as well as by rapamycin treatment compared to NG conditions **(B)**. *MMP2* gene expression was induced by HI. Rapamycin + HI led to decreased *MMP2* gene expression. *COL1A1*, collagen type 1; *MMP2*, matrix metalloproteinase 2; *ELN*, elastin; HI, hyperinsulinemia; HG, hyperglycemia; Rapa, rapamycin. **p*-Values < 0.05 of direct comparison to normoglycemic control; $^{\dagger}p$-values < 0.05 of intergroup comparisons.

Discussion

The present work shows that chronic insulin treatment leads to decreased mTOR signaling by abrogating mTOR phosphorylation in VIC. Chronic insulin exposure as well as HG conditions in turn lead to VIC activation, chondro-osteogenic differentiation, and matrix remodeling. Inhibition of mTOR signaling by rapamycin altered the impact of diabetic conditions with respect to various components of the extracellular matrix as well as of markers of activation and chondro-osteogenic differentiation. Remarkably, the effect of mTOR inhibition in front of effects observed for diabetic conditions was not uniform: Rapamycin treatment resulted in a modulation of VIC regulation, partly resembling an amplification of HI or HG induced effects whilst also reflecting a marked inhibitory impact on other factors. These results suggest that mTOR is involved in intracellular transmission of diabetic stimulus on VIC but is not the only signaling pathway by which diabetic conditions regulate aortic valve morphology.

Mammalian target of rapamycin complex 1 and mammalian target of rapamycin complex 2 signaling under diabetic conditions

Hyperinsulinemia led to a decreased susceptibility of 4E-BP1(Thr$^{37/46}$) for phosphorylation upon acute insulin stimulus.

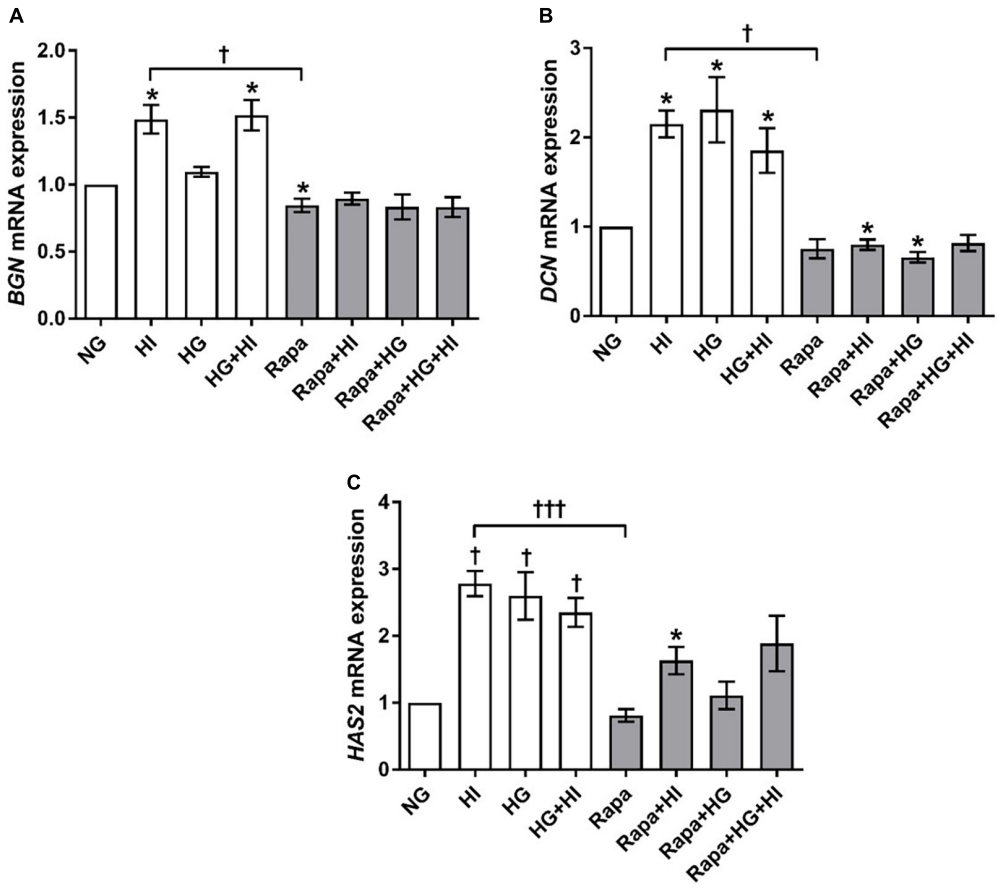

FIGURE 7
Expression of glycosylated matrix molecules under diabetic conditions and mTOR inhibition. Impact of diabetic conditions and mTOR inhibition on *BGN* **(A)**, *DCN* **(B)**, and *HAS2* **(C)** gene expression was analyzed. *BGN* gene expression is upregulated by HI but downregulated by rapamycin treatment **(A)**. *DCN* gene expression was upregulated by diabetic conditions, whereas rapamycin treatment did not alter *DCN* gene expression **(B)**. *HAS2* gene expression was upregulated by diabetic condition. Rapamycin treatment alone did not alter *HAS2* gene expression, whereas combination with HI led to increased expression levels **(C)**. *BGN*, biglycan; *DCN*, decorin; *HAS2*, hyaluronic acid synthase 2; HI, hyperinsulinemia; HG, hyperglycemia; Rapa, rapamycin. **p*-Values < 0.05 of direct comparison to normoglycemic control; $^{\dagger}p$-values < 0.05 of intergroup comparisons in relation to NG treatment; $^{\dagger\dagger\dagger}p$-values < 0.001 of intergroup comparisons.

This might be indicative for an impaired MTORC1 downstream signaling in VIC upon chronic diabetic conditions, as it has been described before for HUVECS and smooth muscle cells *in vitro*. Here, impaired phosphorylation of 4E-BP1 has been observed even after 5 min of HI (23). However, skeletal muscle of diabetics did not show alterations in 4E-BP1 phosphorylation (24). In contrast to reports on renal epithelial cells showing increased 4E-BP1 phosphorylation under HG treatment (25), this was not the case for VIC under HG treatment. Response to diabetic conditions thus seems to differ between different cell types and tissues and the presented results suggest that VIC share an alternating subset of features with several other cell types. Similar to 4E-BP1(Thr$^{37/46}$), a decrease of P70S6K(Thr^{389}) phosphorylation has been described *in vitro* in HUVECS and smooth muscle cells after a short-time incubation with HI (23). Reports focused on cancer cells showed an increase in phosphorylation levels of P70S6K after 15 min of HI followed by an adaptation to long-term exposure to HI (26). In the present work, phosphorylation levels of P70S6K(Thr^{389}) did not show significant changes under diabetic conditions in VIC which might be related to specific differences in short-term vs. long-term HI treatments. Time course experiments as well as examination of valvular tissue of diabetics might therefore lead to a better understanding of diabetes-induced P70S6K(Thr^{389}) phosphorylation in VIC. However, it has been shown that P70S6K acts *via* different phosphorylation sites by MTORC1 activation alone or in combination with other kinases (27, 28). Thus, future experiments might also aim at the investigation of alternative phosphorylation sites of P70S6K besides (Thr^{389}).

As we have shown before, in the present work HI led to impaired Akt(Ser^{473}) signaling under NG as well as under HG conditions (14). Under the applied conditions, Akt(Thr^{308}) phosphorylation is not as sensitive to HI as Akt(Ser^{473}) phosphorylation. Moreover, Akt(Thr^{308}) phosphorylation

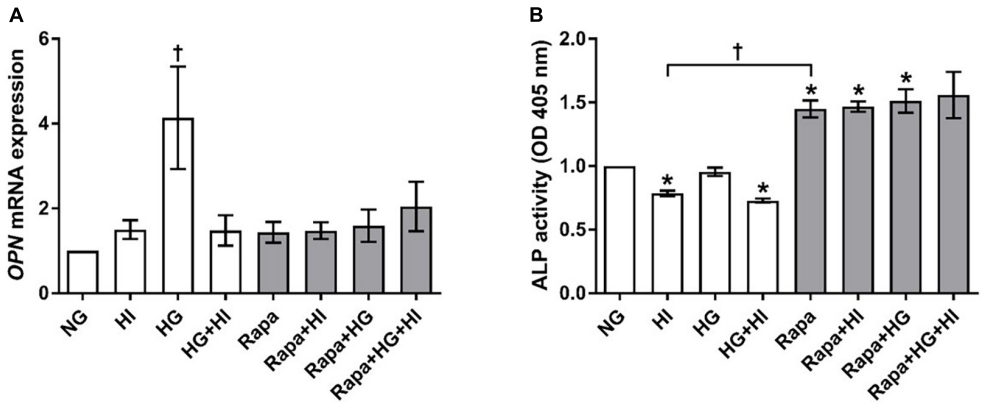

FIGURE 8
Expression of degeneration markers under diabetic conditions and mTOR inhibition. Impact of diabetic conditions and mTOR inhibition on *OPN* gene expression **(A)** and ALP activity **(B)** was analyzed. HG treatment led to a significant upregulation of *OPN* gene expression, whereas HI as well as rapamycin treatment kept *OPN* gene expression low **(A)**. ALP activity was reduced by HI treatment, whereas rapamycin treatment led to increased ALP activity. *OPN*, osteopontin; ALP, alkaline phosphatase; HI, hyperinsulinemia; HG, hyperglycemia; Rapa, rapamycin.
*p-Values < 0.05 of direct comparison to normoglycemic control; †p-values < 0.05 of intergroup comparisons as indicated or in relation to NG treatment.

seems to be mainly impaired by HG conditions. Susceptibility of both Akt(Ser^{473}) and Akt(Thr^{308}) phosphorylation to impaired signaling upon HI is more pronounced under rapamycin treatment. Here, Akt(Thr^{308}) phosphorylation shows a similar pattern as Akt(Ser^{473}) phosphorylation. This effect here seen in VIC might probably be due to MTORC1 inhibition by rapamycin and a resulting inhibition of the negative feedback loop, which then enhances activation of Akt(Ser^{473}) signaling (29) thereby triggering subsequent Akt(Thr^{308}) signaling. However, enhanced susceptibility of Akt(Thr^{308}) phosphorylation by prior Akt(Ser^{473}) activation has been shown already by Sarbassov et al. (30).

Mammalian target of rapamycin complex 1 and mammalian target of rapamycin complex 2 signaling under mammalian target of rapamycin inhibition

Rapamycin was initially considered as a potent inhibitor of translation and thus, e.g., inhibiting tumor growth through inhibition of MTORC1 complex and downstream inhibition of 4E-BP1 and P70S6K signaling (31). However, inhibition of 4E-BP1 phosphorylation of, e.g., 4E-BP1(Thr$^{37/46}$) by rapamycin seems to be unstable in long-term treatment (48 h +) and is particularly described to be cell type dependent (32). However, the effect of rapamycin on MTORC1 downstream signaling and especially on 4E-BP1 and P70S6K phosphorylation has scarcely been described for VIC (33). Our data show that rapamycin is able to decrease 4E-BP1(Thr$^{37/46}$) phosphorylation in VIC upon acute insulin stimulus even after 5 days of treatment. In addition, rapamycin also reduces the susceptibility of 4E-BP1 to inducible phosphorylation by acute insulin stimulus.

Moreover, phosphorylation of P70S6K(Thr^{389}) was not influenced by rapamycin treatment in VIC. This might be due to the relatively low rapamycin concentration chosen for our experiments (10 nM), whereas others also reported cell line dependent responsiveness with this concentration (34). Murine VIC treated with 100 nM rapamycin showed a decrease in P70S6K phosphorylation (35), which might be indicative for the need of higher concentrations of rapamycin. Apart from the mentioned report based upon a 1-h treatment with rapamycin (35), to our knowledge, long-term effects on P70S6K have not yet been reported for VIC. However, adverse effects of rapamycin or time-dependent suspension of mTOR pathway inhibition has been reported before for other cells (32). Effects of *in vivo* long-term rapamycin treatment on MTORC1 downstream targets P70S6K and 4E-BP1 have been described recently for vascular tissue showing a reduction of these both MTORC1 targets (36). Interestingly, inhibition of the phosphorylation of these two MTORC1 downstream targets by rapamycin is described to be temporarily different. In the reported model, inhibition of P70S6K phosphorylation alleviates over time, whereas inhibition of 4E-BP1 phosphorylation aggravates after day 7 after administration (36). Evaluation of a time- and/or dose-dependent rapamycin action or the impact or more specific mTOR inhibitors like torin on the responsiveness of VIC therefore might be necessary to investigate the role of 4E-BP1 and P70S6K in this setting in detail.

Previous reports have suggested that short-term rapamycin treatment inhibits MTORC1 whereas long-term treatment inhibits also MTORC2 and impairs subsequent Akt signaling

(37). The definition of "long-term" treatment though is ambiguous since clinical application certainly is not comparable to *in vitro* experimental treatments. However, impact of rapamycin treatment on MTORC2 has been described to be cell type dependent (37) and dependent on the time of rapamycin treatment or administration, respectively. Reports on administration of rapamycin *in vivo* up to 21 days describe unchanged MTORC2 downstream activation in vascular tissue (36) whereas *in vitro* treatment of fibroblasts with rapamycin for 4 days abolished Akt signaling (38).

Based on this, it is not clear whether MTORC2 is impaired by 5 days treatment with rapamycin in our approach, since we do not see impaired Akt signaling but rather increased Akt phosphorylation of both Akt(Ser^{473}) und Akt(Thr^{308}). Since Akt(Thr^{308}) is not mTOR dependent, we did not expect a decrease here, but would have excepted an impaired Akt(Ser^{473}) phosphorylation. Increase in Akt signaling in VIC might therefore be due to a not yet sufficient inhibition of MTORC2 together with the inhibition of the negative feedback loop of MTORC1 leading to enhanced activation of Akt signaling (29, 39). As Sarbassov et al. have reported earlier, also PI3K/PDK1 regulated Akt(Thr^{308}) phosphorylation depends on Akt(Ser^{473}) phosphorylation (30) and can be influenced by rapamycin treatment, which has been also shown recently in CRISPR/Cas9-based knockout of RICTOR (40). Nevertheless, our data on Akt signaling cannot dissect whether a possible inactivation of MTORC2 took place and if so, to which extend this would influence Akt(Ser^{473}) phosphorylation when compared to the enhanced activation due to a loss of MTORC1 negative feedback. In conclusion, interplay of MTORC1/MTORC2 in the balance of Akt phosphorylation is delicate and cell type specific, even more so with respect to the question of the impact of long-term usage of rapamycin.

Impact of diabetic conditions on valvular interstitial cells differentiation and valvular matrix

Diabetes is associated with a higher risk to develop aortic stenosis (7, 9) however, knowledge about the impact of HI and HG on aortic valve molecular composition is still limited. Aortic valves of diabetics are more prone to chondro-osteogenic differentiation and matrix remodeling than the valves of non-diabetics (11- 13). Animal studies analyzing the pathophysiology of the aortic valve in presence of diabetes further support the findings of clinical observations (41, 42). The present work shows that HI and HG as hallmarks of diabetes significantly alter the aortic valve on a cellular level, i.e., VIC differentiation and matrix remodeling. Similar to previous investigations, HI suppresses activation of VIC (14), whereas HG alone did not alter *ACTA2* expression, which was also observed by others (43). Diabetic conditions generally increased matrix remodeling, indicated by elevated expression of *MMP2* and proteoglycans, mainly but not exclusively due to HI treatment. HG treatment alone altered *DCN* and *HAS2* gene expression but was not sufficient to alter other matrix molecules as has been reported for VIC in three-dimensional *in vitro* approaches (43). Here, biomechanical stimuli seem to enhance some effects on matrix remodeling, an observation which we could corroborate in previous studies involving aortic valve tissue culture in different biomechanical environments (15).

It is surprising that ALP activity in VIC is rather downregulated by HI, since aortic valve tissue of human diabetics (13) as well as aortic valve tissue in a murine diabetes-induced atherosclerosis model (42) showed increased levels of ALP. Discrepancies in these findings may be due to the isolated investigation of VIC with selected stimuli, i.e., HG and HI, *versus* the complex pathophysiology involving dyslipidemia and inflammation, both of which have been described to take place in diabetes. Taken together, HI and HG treatment lead to molecular alterations of VIC, which can be also found in preclinical models of diabetes-induced aortic valve degeneration.

Impact of rapamycin on valvular interstitial cells differentiation and valvular matrix

Mammalian target of rapamycin signaling mediates fibrotic remodeling of several tissues including the myocardium (16). Inhibition of mTOR by rapamycin or so-called "rapalogs" is used to prevent heart failure and cardiac remodeling [reviewed in (18, 44)]. Such pharmacological intervention has also been suggested as a promising approach to prevent myocardial dysfunction in diabetes (45, 46). Nevertheless, reports on the role of mTOR in degenerative changes in cardiac valves, and specifically in VIC are scarce (47). In the present work, rapamycin treatment of VIC evokes a general downregulation of gene expression of several matrix components like *COL1A1*, *ELN* as well as of *BGN* and *DCN*. However, effects of mTOR inhibitors vary amongst cell types of different origin and with diverse actions of rapalogs of different generations or depending on the applied techniques (e.g., RNA interference vs. Rapalink-1), providing heterogeneous or even contrary findings, e.g., for proteoglycans (48, 49) or matrix metalloproteinases (50, 51). In the present work, rapamycin treatment led to an increased gene expression of *ACTA2*. Interestingly, especially the effect on alpha smooth muscle actin (α-SMA) activation seems to be cell type dependent as well as susceptible to different mTOR inhibitors. For example, an increase in α-SMA expression was reported for vascular smooth muscle cells (52) and mesangial cells upon sirolimus treatment (53). In

contrast, an inhibitory effect of rapamycin on α-SMA expression could be shown in endothelial-like cells (38) and fibroblasts (39). Long-term treatment with rapamycin led to a reduced α-SMA expression together with impaired MTORC2 downstream signaling *via* Akt in fibroblasts (38). A lack of decreased *ACTA2* expression in our approach thus might imply that our 5 days rapamycin treatment has yet not been enough to provoke inhibition of MTORC2 signaling with subsequent inhibition of myofibroblastoidal differentiation of VIC. However, these effects seem to be highly dependent on the starving status of the cells, since opposite effects have been described for unstarved cells (38).

Osteogenic markers such as osteopontin or alkaline phosphatase in contrast, seem to be in general rather downregulated by rapamycin as it has been shown for VIC (48) as well as for vascular smooth muscle cells (52). Discrepancies between our findings of unchanged *OPN* gene expression and an increased ALP activity and reports on downregulation of these markers might therefore be due to different treatment durations, an issue that is also discussed in the clinical application of mTOR inhibitors (54). Taken together, in our setting, rapamycin treatment leads to an activation of VIC together with an upregulation of ALP activity. Thus, the role of ALP may be subjected to further translational studies and might be a promising candidate for clinical investigation.

Potential involvement of mammalian target of rapamycin signaling in valvular interstitial cells differentiation and matrix remodeling under diabetic conditions

Our analyses show that chronic insulin treatment leads to an abrogation of mTOR phosphorylation in VIC even after short-time cultivation. In contrast to findings on upstream Akt signaling (14), HG conditions alone are not sufficient to impair mTOR signaling. Here, the reduction of mTOR phosphorylation was highest under combined HG conditions and chronic insulin exposure. Furthermore, AMPK is characterized as an upstream mTOR inhibitor, sensing glucose changes and inhibiting mTOR in episodes of glucose starvation (55, 56). In the present work, AMPK phosphorylation was not altered by varying glucose concentrations, which might be indicative for a mainly aerobic metabolism of VIC (57). Moreover, previous studies have shown that VIC mainly express the insulin-independent glucose transporter 1 but not glucose transporter 4 (14), which would be regulated by AMPK in case of metabolic imbalance (58).

In front of the background that diabetic conditions deplete mTOR signaling, the question arises which mitogenic effect induced by diabetic conditions can be ascribed to a regulation by mTOR signaling. Here, effects of rapamycin treatment should lead to similar expression patterns if not even further pronounced patterns as compared to the treatment with diabetic conditions. This effect was present for the gene expression of *ELN*, a structural matrix component, which was significantly downregulated both by treatment with HI + HG as well as by rapamycin treatment. The same holds true for *OPN* expression as a marker for chondro-osteogenic differentiation of VIC, which is upregulated by HG treatment, whereas HI treatment impedes this effect. Here, rapamycin treatment led to similar expression patterns. This is indicative for diabetes induced matrix remodeling and differentiation being mediated by mTOR signaling at this point. Most of the other investigated targets in the present work did not show comparable patterns of reaction. Concerning certain effects, even contrary reactions between diabetic conditions and rapamycin treatment were observed, e.g., in case of *ACTA2*, *MMP2*, and *BGN* gene expression as well as in case of ALP activity. In the case of latter subjects, the alterations induced by diabetic conditions do not seem to be mediated by mTOR signaling but rather by alternative pathways such as sonic hedgehog signaling, which has been described as relevant for osteoblastic differentiation under HG (59).

Concerning the question whether these observations can be attributed to mTOR downstream signaling *via* MTORC1 or MTORC2, similar effects in VIC provoked by diabetic conditions and rapamycin treatment might be seen in MTORC1 downstream 4E-BP1 signaling, where HI impairs susceptibility of VIC to induced phosphorylation, which can be also shown for rapamycin. Nevertheless, future investigations are needed to dissect the detailed involvement of MTORC1 downstream signaling in the course of VIC differentiation, remodeling and degeneration under diabetic conditions and mTOR inhibition.

Conclusion

Diabetic conditions lead to molecular alterations of VIC as well as to impaired mTOR signaling with different susceptibility to HG and HI. Inhibition of mTOR signaling by rapamycin treatment results in decreased matrix expression but also in an activation of VIC together with an upregulation of ALP activity. Particular matrix components and chondro-osteogenic markers reveal an mTOR-mediated reaction of VIC to diabetic conditions with potential involvement of MTORC1 downstream signaling *via* impaired 4E-BP1 phosphorylation. However, these data underscore the need for further investigations using MTORC1-specific inhibitors. Moreover, these findings foster the hypothesis of diabetes-induced initiation and progression of CAVD and further suggest that the involved molecular events may be only partly mediated by mTOR signaling. Further investigations therefore might aim at tailored treatment with mTOR inhibitors considering patients at increased risk for the development of CAVD, i.e., diabetics.

Limitations of the study

Hyperinsulinemia and HG are hallmarks of diabetic complications. However, isolated application of these two factors does not reflect the pathophysiology of diabetes with its complex aspects of inflammation, disturbed protein metabolism and dyslipidemia. Thus, the findings of the present work focus on the isolated effects of insulin and glucose on mTOR signaling, which should be further validated in translational studies, i.e., animal models of diabetes.

The use of *in vitro* [two-dimensional (2D)] cell culture bears several limitations, e.g., the influence of the interaction with other cell types of the tissue of origin, the lack of cell–matrix interactions or, especially in the case of the aortic valve, the lack of shear stress-induced mechanisms. Thus, findings of *in vitro* experiments have to be regarded with great attention concerning their comparability with whole tissue examinations and need to be confirmed by three-dimensional analysis and in translational approaches. Nevertheless, *in vitro* culture environments offer advantages for basic studies of isolated parameters if used in a reproducible and stable model.

The use of a non-human (i.e., ovine) VIC cell source is also afflicted with limitations, since these cells will differ from the corresponding human source in relation to mechanics, physiology, and immunology. Although ovine VIC have advanced to a reliable model for functional studies on CAVD, direct comparability to human-derived VIC is restricted and validation in human-derived cell lines therefore is inevitable. Our approach using ovine VIC is mainly owed to the lack of human healthy donor valves and a heterogeneous population of patients concerning age, medication and co-morbidities. Ovine VIC therefore represent a "healthy" phenotype that is hardly achievable with human specimen and allows analysis without patient-related side effects.

Although rapamycin is a clinically proven agent for the treatment of heart failure and post-infarction cardiac remodeling, it might lead to conflicting or confounding results *in vitro*, since it is inferior in completely blocking MTORC1 together with MTORC2 in comparison to, e.g., torin (60, 61). Thus, findings concerning rapamycin-induced effects on MTORC1 have to be interpreted carefully.

In the present investigations, DMSO was used as a solvent for rapamycin. DMSO is known to have unwarranted effects on cell proliferation and differentiation, which we sought to minimize by using concentrations of 0.1% DMSO.

Data availability statement

The original contributions presented in this study are included in the article/**Supplementary material**, further inquiries can be directed to the corresponding author.

Author contributions

MB and JS: conceptualization, formal analysis, and project administration. MB, JS, DO, and PA: methodology. JS, MB, and PA: validation. HK, CK, FK, and EA: investigation. AL: resources. HK and MB: data curation and visualization. MB and PA: writing—original draft preparation. MB, JS, AL, DO, SB, and PA: writing—review and editing. JS, MB, AL, and PA: supervision. JS: data curation and visualization. All authors contributed to the article and approved the submitted version.

Funding

This research was funded by German Research Foundation (DFG) to MB (grant number: 421961956).

Acknowledgments

We thank K. Bartkowski and K. Freidel for their competent assistance with Western blots. Moreover, we also thank the S. Bunnenberg Foundation for the generous support of the Cardiovascular Research Facilities at the Heinrich Heine University Düsseldorf.

Conflict of interest

The authors declare that the research was conducted in the absence of any commercial or financial relationships that could be construed as a potential conflict of interest.

Publisher's note

Supplementary material

The Supplementary Material for this article can be found online at: https://www.frontiersin.org/articles/10.3389/fcvm.2022.942430/full#supplementary-material

References

1. Beulens J, Rutters F, Ryden L, Schnell O, Mellbin L, Hart HE, et al. Risk and management of pre-diabetes. *Eur J Prev Cardiol.* (2019) 26:47–54.

2. Vas PRJ, Alberti KG, Edmonds ME. Prediabetes: moving away from a glucocentric definition. *Lancet Diabetes Endocrinol.* (2017) 5:848–9. doi: 10.1016/S2213-8587(17)30234-6

3. Perreault L, Faerch K. Approaching pre-diabetes. *J Diabetes Complic.* (2014) 28:226–33.

4. Makaroff LE. The need for international consensus on prediabetes. *Lancet Diabetes Endocrinol.* (2017) 5:5–7.

5. Guariguata L, Whiting DR, Hambleton I, Beagley J, Linnenkamp U, Shaw JE. Global estimates of diabetes prevalence for 2013 and projections for 2035. *Diabetes Res Clin Pract.* (2014) 103:137–49. doi: 10.1016/j.diabres.2013.11.002

6. Yan AT, Koh M, Chan KK, Guo H, Alter DA, Austin PC, et al. Association between cardiovascular risk factors and aortic stenosis: the CANHEART aortic stenosis study. *J Am Coll Cardiol.* (2017) 69:1523–32. doi: 10.1016/j.jacc.2017.01.025

7. Larsson SC, Wallin A, Hakansson N, Stackelberg O, Back M, Wolk A. Type 1 and type 2 diabetes mellitus and incidence of seven cardiovascular diseases. *Int J Cardiol.* (2018) 262:66–70.

8. Ljungberg J, Johansson B, Engstrom KG, Albertsson E, Holmer P, Norberg M, et al. Traditional cardiovascular risk factors and their relation to future surgery for valvular heart disease or ascending aortic disease: a case-referent study. *J Am Heart Assoc.* (2017) 6:5.

9. Cai X, Zhang Y, Li M, Wu JH, Mai L, Li J, et al. Association between prediabetes and risk of all cause mortality and cardiovascular disease: updated meta-analysis. *BMJ.* (2020) 370:m2297.

10. Natorska J, Wypasek E, Grudzien G, Sobczyk D, Marek G, Filip G, et al. Does diabetes accelerate the progression of aortic stenosis through enhanced inflammatory response within aortic valves? *Inflammation.* (2012) 35:834–40. doi: 10.1007/s10753-011-9384-7

11. Kopytek M, Ząbczyk M, Mazur P, Undas A, Natorska J. Accumulation of advanced glycation end products (AGEs) is associated with the severity of aortic stenosis in patients with concomitant type 2 diabetes. *Cardiovasc Diabetol.* (2020) 19:92. doi: 10.1186/s12933-020-01068-7

12. Barth M, Selig JI, Klose S, Schomakers A, Kiene LS, Raschke S, et al. Degenerative aortic valve disease and diabetes: implications for a link between proteoglycans and diabetic disorders in the aortic valve. *Diab Vasc Dis Res.* (2019) 16:254–69. doi: 10.1177/1479164118817922

13. Mosch J, Gleissner CA, Body S, Aikawa E. Histopathological assessment of calcification and inflammation of calcific aortic valves from patients with and without diabetes mellitus. *Histol Histopathol.* (2017) 32:293–306. doi: 10.14670/HH-11-797

14. Selig JI, Ouwens DM, Raschke S, Thoresen GH, Fischer JW, Lichtenberg A, et al. Impact of hyperinsulinemia and hyperglycemia on valvular interstitial cells - a link between aortic heart valve degeneration and type 2 diabetes. *Biochim Biophys Acta Mol Basis Dis.* (2019) 1865:2526–37. doi: 10.1016/j.bbadis.2019.05.019

15. Selig JI, Boulgaropoulos J, Niazy N, Ouwens DM, Preuss K, Horn P, et al. Crosstalk of diabetic conditions with static versus dynamic flow environment-impact on aortic valve remodeling. *Int J Mol Sci.* (2021) 22:13. doi: 10.3390/ijms22136976

16. Jimenez-Uribe AP, Gomez-Sierra T, Aparicio-Trejo OE, Orozco-Ibarra M, Pedraza-Chaverri J. Backstage players of fibrosis: NOX4, mTOR, HDAC, and S1P; companions of TGF-beta. *Cell Signal.* (2021) 87:110123. doi: 10.1016/j.cellsig.2021.110123

17. Suhara T, Baba Y, Shimada BK, Higa JK, Matsui T. The mTOR signaling pathway in myocardial dysfunction in type 2 diabetes mellitus. *Curr Diab Rep.* (2017) 17:38.

18. Sciarretta S, Forte M, Frati G, Sadoshima J. The complex network of mTOR signalling in the heart. *Cardiovasc Res.* (2022) 118:424–39.

19. Stephens EH, Han J, Trawick EA, Di Martino ES, Akkiraju H, Brown LM, et al. Left-ventricular assist device impact on aortic valve mechanics, proteomics and ultrastructure. *Ann Thorac Surg.* (2018) 105:572–80. doi: 10.1016/j.athoracsur.2017.08.030

20. Barth M, Mrozek L, Niazy N, Selig JI, Boeken U, Sugimura Y, et al. Degenerative changes of the aortic valve during left ventricular assist device support. *ESC Heart Failure.* (2022) 9:270–82.

21. Ma H, Killaars AR, DelRio FW, Yang C, Anseth KS. Myofibroblastic activation of valvular interstitial cells is modulated by spatial variations in matrix elasticity and its organization. *Biomaterials.* (2017) 131:131–44. doi: 10.1016/j.biomaterials.2017.03.040

22. Dayawansa NH, Baratchi S, Peter K. Uncoupling the vicious cycle of mechanical stress and inflammation in calcific aortic valve disease. *Front Cardiovas Med.* (2022) 9:783543. doi: 10.3389/fcvm.2022.783543

23. Terruzzi I, Pellegatta F, Luzi L. Differential p70S6k and 4E-BP1 regulation by insulin and amino acids in vascular endothelial and smooth muscle cells. *Acta Diabetol.* (2005) 42:139–46. doi: 10.1007/s00592-005-0193-z

24. Møller AB, Kampmann U, Hedegaard J, Thorsen K, Nordentoft I, Vendelbo MH, et al. Altered gene expression and repressed markers of autophagy in skeletal muscle of insulin resistant patients with type 2 diabetes. *Sci Rep.* (2017) 7:43775. doi: 10.1038/srep43775

25. Lu Q, Chen YB, Yang H, Wang WW, Li CC, Wang L, et al. Inactivation of TSC1 promotes epithelial-mesenchymal transition of renal tubular epithelial cells in mouse diabetic nephropathy. *Acta Pharmacol Sin.* (2019) 40:1555–67.

26. Baricevic I, Roberts DL, Renehan AG. Chronic insulin exposure does not cause insulin resistance but is associated with chemo-resistance in colon cancer cells. *Hormone Metab Res Hormon Und Stoffwechselforschung Hormones Metab.* (2014) 46:85–93.

27. Arif A, Jia J, Willard B, Li X, Fox PL. Multisite phosphorylation of S6K1 directs a kinase phospho-code that determines substrate selection. *Mol Cell.* (2019) 73:446–57e6. doi: 10.1016/j.molcel.2018.11.017

28. Bahrami BF, Ataie-Kachoie P, Pourgholami MH, Morris DL. p70 Ribosomal protein S6 kinase (Rps6kb1): an update. *J Clin Pathol.* (2014) 67:1019–25. doi: 10.1136/jclinpath-2014-202560

29. O'Reilly KE, Rojo F, She QB, Solit D, Mills GB, Smith D, et al. mTOR inhibition induces upstream receptor tyrosine kinase signaling and activates Akt. *Cancer Res.* (2006) 66:1500–8.

30. Sarbassov DD, Guertin DA, Ali SM, Sabatini DM. Phosphorylation and regulation of Akt/PKB by the rictor-mTOR complex. *Science.* (2005) 307:1098–101.

31. Fingar DC, Blenis J. Target of rapamycin (TOR): an integrator of nutrient and growth factor signals and coordinator of cell growth and cell cycle progression. *Oncogene.* (2004) 23:3151–71.

32. Choo AY, Yoon SO, Kim SG, Roux PP, Blenis J. Rapamycin differentially inhibits S6Ks and 4E-BP1 to mediate cell-type-specific repression of mRNA translation. *Proc Natl Acad Sci USA.* (2008) 105:17414–9. doi: 10.1073/pnas.0809136105

33. Tan Y, Wang JY, Yi RL, Qiu J. [Effect of rapamycin on proliferation of rat heart valve interstitial cells *in vitro*]. *Nan Fang Yi Ke Da Xue Xue Bao J Southern Med Univ.* (2016) 36:572–6.

34. Bernard S, Poon AC, Tam PM, Mutsaers AJ. Investigation of the effects of mTOR inhibitors rapamycin and everolimus in combination with carboplatin on canine malignant melanoma cells. *BMC Veterinary Res.* (2021) 17:382. doi: 10.1186/s12917-021-03089-0

35. Ghatak S, Misra S, Moreno-Rodrigue RA, Hascall VC, Leone GW, Markwald RR. Periostin/β1integrin interaction regulates p21-activated kinases in valvular interstitial cell survival and in actin cytoskeleton reorganization. *Biochimica Biophys Acta General Subjects.* (2019) 1863:813–29. doi: 10.1016/j.bbagen.2018.12.015

36. Guo X, Fereydooni A, Isaji T, Gorecka J, Liu S, Hu H, et al. Inhibition of the Akt1-mTORC1 axis alters venous remodeling to improve arteriovenous fistula patency. *Sci Rep.* (2019) 9:11046.

37. Sarbassov DD, Ali SM, Sengupta S, Sheen JH, Hsu PP, Bagley AF, et al. Prolonged rapamycin treatment inhibits mTORC2 assembly and Akt/PKB. *Mol Cell.* (2006) 22:159–68. doi: 10.1016/j.molcel.2006.03.029

38. Bernard M, Dieudé M, Yang B, Hamelin K, Underwood K, Hébert MJ. Autophagy fosters myofibroblast differentiation through MTORC2 activation and downstream upregulation of CTGF. *Autophagy.* (2014) 10:2193–207. doi: 10.4161/15548627.2014.981786

39. Wan X, Harkavy B, Shen N, Grohar P, Helman LJ. Rapamycin induces feedback activation of Akt signaling through an IGF-1R-dependent mechanism. *Oncogene.* (2007) 26:1932–40. doi: 10.1038/sj.onc.1209990

40. Ruicci KM, Plantinga P, Pinto N, Khan MI, Stecho W, Dhaliwal SS, et al. Disruption of the RICTOR/mTORC2 complex enhances the response of head and neck squamous cell carcinoma cells to PI3K inhibition. *Mol Oncol.* (2019) 13:2160–77.

41. Le Quang K, Bouchareb R, Lachance D, Laplante MA, El Husseini D, Boulanger MC, et al. Early development of calcific aortic valve disease and left ventricular hypertrophy in a mouse model of combined dyslipidemia and type 2

diabetes mellitus. *Arterioscler Thromb Vasc Biol.* (2014) 34:2283–91. doi: 10.1161/ATVBAHA.114.304205

42. Tucureanu MM, Filippi A, Alexandru N, Ana Constantinescu C, Ciortan L, Macarie R, et al. Diabetes-induced early molecular and functional changes in aortic heart valves in a murine model of atherosclerosis. *Diab Vasc Dis Res.* (2019) 16:562–76. doi: 10.1177/1479164119874469

43. Ciortan L, Macarie RD, Cecoltan S, Vadana M, Tucureanu MM, Mihaila AC, et al. Chronic high glucose concentration induces inflammatory and remodeling changes in valvular endothelial cells and valvular interstitial cells in a gelatin methacrylate 3D model of the human aortic valve. *Polymers.* (2020) 12:12. doi: 10.3390/polym12122786

44. Sciarretta S, Forte M, Frati G, Sadoshima J. New insights into the role of mTOR signaling in the cardiovascular system. *Circ Res.* (2018) 122:489–505.

45. Samidurai A, Ockaili R, Cain C, Roh SK, Filippone SM, Kraskauskas D, et al. Differential regulation of mTOR complexes with miR-302a attenuates myocardial reperfusion injury in diabetes. *iScience.* (2020) 23:101863. doi: 10.1016/j.isci.2020.101863

46. Das A, Durrant D, Koka S, Salloum FN, Xi L, Kukreja RC. Mammalian target of rapamycin (mTOR) inhibition with rapamycin improves cardiac function in type 2 diabetic mice: potential role of attenuated oxidative stress and altered contractile protein expression. *J Biol Chem.* (2014) 289:4145–60. doi: 10.1074/jbc.M113.521062

47. Deng XS, Meng X, Song R, Fullerton D, Jaggers J. Rapamycin decreases the osteogenic response in aortic valve interstitial cells through the stat3 pathway. *Ann Thorac Surg.* (2016) 102:1229–38. doi: 10.1016/j.athoracsur.2016.03.033

48. Nie D, Zhou Y, Wang W, Zhang J, Wang JH. Mechanical overloading induced-activation of mtor signaling in tendon stem/progenitor cells contributes to tendinopathy development. *Front Cell Dev Biol.* (2021) 9:687856. doi: 10.3389/fcell.2021.687856

49. Mavrogonatou E, Papadopoulou A, Fotopoulou A, Tsimelis S, Bassiony H, Yiacoumettis AM, et al. Down-regulation of the proteoglycan decorin fills in the tumor-promoting phenotype of ionizing radiation-induced senescent human breast stromal fibroblasts. *Cancers.* (2021) 13:8. doi: 10.3390/cancers13081987

50. Chi OZ, Liu X, Cofano S, Patel N, Jacinto E, Weiss HR. Rapalink-1 increased infarct size in early cerebral ischemia-reperfusion with increased blood-brain barrier disruption. *Front Physiol.* (2021) 12:706528. doi: 10.3389/fphys.2021.706528

51. Wang X, Li L, Li M, Dang X, Wan L, Wang N, et al. Knockdown of mTOR by lentivirusmediated RNA interference suppresses atherosclerosis and stabilizes plaques *via* a decrease of macrophages by autophagy in apolipoprotein Edeficient mice. *Int J Mol Med.* (2013) 32:1215–21. doi: 10.3892/ijmm.2013.1494

52. Xu Z, Liu X, Wang Z, Tao J, Han Z, Gu M, et al. Effect of sirolimus on arteriosclerosis induced by advanced glycation end products *via* inhibition of the ILK/mTOR pathway in kidney transplantation recipients. *Eur J Pharmacol.* (2017) 813:1–9. doi: 10.1016/j.ejphar.2017.06.038

53. Esposito C, Valentino R, Villa L, Serpieri N, Mangione F, Grosjean F, et al. Effects of sirolimus on human mesangial cells. *Trans Proc.* (2010) 42:1344–6.

54. Bellumkonda L, Patel J. Recent advances in the role of mammalian target of rapamycin inhibitors on cardiac allograft vasculopathy. *Clin Trans.* (2020) 34:e13769.

55. Inoki K, Zhu T, Guan KL. TSC2 mediates cellular energy response to control cell growth and survival. *Cell.* (2003) 115:577–90.

56. Gwinn DM, Shackelford DB, Egan DF, Mihaylova MM, Mery A, Vasquez DS, et al. AMPK phosphorylation of raptor mediates a metabolic checkpoint. *Mol Cell.* (2008) 30:214–26.

57. Bertrand L, Auquier J, Renguet E, Ange M, Cumps J, Horman S, et al. Glucose transporters in cardiovascular system in health and disease. *Pflugers Arch.* (2020) 472:1385–99.

58. Yang J, Holman GD. Insulin and contraction stimulate exocytosis, but increased AMP-activated protein kinase activity resulting from oxidative metabolism stress slows endocytosis of GLUT4 in cardiomyocytes. *J Biol Chem.* (2005) 280:4070–8. doi: 10.1074/jbc.M410213200

59. Jiang ZL, Jin H, Liu ZS, Liu MY, Cao XF, Jiang YY, et al. Lentiviralmediated Shh reverses the adverse effects of high glucose on osteoblast function and promotes bone formation *via* sonic hedgehog signaling. *Mol Med Rep.* (2019) 20:3265–75. doi: 10.3892/mmr.2019.10540

60. Thoreen CC, Kang SA, Chang JW, Liu Q, Zhang J, Gao Y, et al. An ATP-competitive mammalian target of rapamycin inhibitor reveals rapamycin-resistant functions of mTORC1. *J Biol Chem.* (2009) 284:8023–32.

61. Benjamin D, Colombi M, Moroni C, Hall MN. Rapamycin passes the torch: a new generation of mTOR inhibitors. *Nat Rev Drug Dis.* (2011) 10:868–80. doi: 10.1038/nrd3531

frontiers | Frontiers in Cardiovascular Medicine

TYPE Original Research
PUBLISHED 09 January 2023
DOI 10.3389/fcvm.2022.1032755

OPEN ACCESS

EDITED BY
Marie Billaud,
Department of Surgery, Brigham and Women's Hospital and Harvard Medical School, United States

REVIEWED BY
Marie-José Goumans,
Leiden University Medical Center (LUMC), Netherlands
Alexander Fletcher,
University of Glasgow, United Kingdom

*CORRESPONDENCE
Nimrat Grewal
✉ n.grewal@lumc.nl

SPECIALTY SECTION
This article was submitted to Heart Valve Disease, a section of the journal Frontiers in Cardiovascular Medicine

RECEIVED 31 August 2022
ACCEPTED 20 December 2022
PUBLISHED 09 January 2023

CITATION
Grewal N, Dolmaci O, Jansen E, Klautz R, Driessen A, Lindeman J and Poelmann RE (2023) Are acute type A aortic dissections atherosclerotic? *Front. Cardiovasc. Med.* 9:1032755. doi: 10.3389/fcvm.2022.1032755

Are acute type A aortic dissections atherosclerotic?

Nimrat Grewal[1,2,3]*, Onur Dolmaci[1,2], Evert Jansen[1], Robert Klautz[1,2], Antoine Driessen[1], Jan Lindeman[4] and Robert E. Poelmann[5,6]

[1]Department of Cardiothoracic Surgery, Amsterdam University Medical Center, Amsterdam, Netherlands, [2]Department of Cardiothoracic Surgery, Leiden University Medical Center, Leiden, Netherlands, [3]Department of Anatomy and Embryology, Leiden University Medical Center, Leiden, Netherlands, [4]Department of Vascular Surgery, Leiden University Medical Center, Leiden, Netherlands, [5]Institute of Biology, Animal Sciences and Health, Leiden University, Leiden, Netherlands, [6]Department of Cardiology, Leiden University Medical Center, Leiden, Netherlands

Background: Type A aortic dissections (TAAD) are devastating aortic complications. Patients with Marfan syndrome, a bicuspid aortic valve or a thoracic aortic aneurysm have an increased risk to develop a TAAD. These predisposing conditions are characterized by a histologically thin intimal layer and hardly any atherosclerosis. Little is known about the susceptibility for atherosclerosis in patients with a type A aortic dissection.

Objective: We aim to systematically describe atherosclerotic lesions in TAAD patients.

Materials and methods: A total of 51 patients with a TAAD (mean age 62.5 ± 10.8 years, 49% females) and 17 control patients (mean age 63 ± 5.5 years, 53% females) were included in this study. Cardiovascular risk factors were assessed clinically. All sections were stained with Movat pentachrome and hematoxylin eosin. Plaque morphology was classified according to the modified AHA classification scheme proposed by Virmani et al.

Results: In the TAAD group thirty-seven percent were overweight (BMI > 25). Diabetes and peripheral arterial disease were not present in any of the patients. Fifty-nine percent of the patients had a history of hypertension. The intima in TAAD patients was significantly thinner as compared to the control group (mean thickness 143 ± 126.5 μm versus 193 ± 132 μm, $p < 0.023$). Seven TAAD patients had a normal intima without any form of adaptive or pathological thickening. Twenty-three TAAD patients demonstrated adaptive intimal thickening. Fourteen had an intimal xanthoma, also known as fatty streaks. A minority of 7 TAAD patients had progressive atherosclerotic lesions, 4 of which demonstrated pathological intimal thickening, 3 patients showed early fibroatheroma, late fibroatheroma and thin cap fibroatheroma. In the control group the majority of the patients exhibited progressive atherosclerotic lesions: three pathologic intimal thickening, two early fibroatheroma, six late fibroatheroma, one healed rupture and two fibrotic calcified plaque.

10.3389/fcvm.2022.1032755

Discussion: This study shows that TAAD patients hardly exhibit any form of progressive atherosclerosis. The majority of TAAD patients showcase non-progressive intimal lesions, whereas the control group mostly demonstrated progressive intimal atherosclerotic lesions. Findings are independent of age, sex, or the presence of (a history of) hypertension.

KEYWORDS

type A aortic dissection, cardiovascular risk, atherosclerosis, embryology, intima

1. Introduction

A type A aortic dissection is a life-threatening condition caused by a tear in the intimal layer, which allows blood to surge through the middle layer of the wall, causing the vascular layers to separate (dissect) from one another. Epidemiologically, patients with hypertension, connective tissue disorders or a bicuspid aortic valve (BAV) are at highest risk to develop a thoracic aortic aneurysm or aortic dissection (TAAD) (1, 2). Traditionally, cardiovascular risk factors such as aging, dyslipidaemia, smoking, chronic kidney disease, and diabetes were related to the occurrence of TAADs. Thoracic aortic aneurysms and dissections can, however, develop in the absence of cardiovascular risk factors and affect young individuals as a result of genetic disorders (3, 4). The mechanisms initiating and stimulating the progression of an aortic dissection are still poorly understood. More recently attention has been drawn toward the intrinsic pathology of the aortic vessel wall. Bicuspid aortic valve and Marfan syndrome (MFS) are both associated with an extremely high risk to develop a thoracic aortic dissection (5, 6). During the last decade, a number of studies dealing with the embryonic development of aortopathy in BAV and MFS have significantly improved our knowledge on the etiology (7, 8). In both conditions an altered neural crest cell and second heart field contribution, separately or in combination, can account for a maturation defect of the vascular smooth muscle cells resulting in a structurally different aortic root and ascending aortic wall (8, 9). Besides undifferentiated vascular smooth muscle cells in the medial layer, significant differences in the intimal layer have also been noted in BAV and MFS. The intima has been found significantly thinner in the BAV and MFS patient groups as compared to individuals with a tricuspid aortic valve (TAV). Vascular smooth muscle cells and smooth muscle cell-derived cells are a major source of plaque cells and extracellular matrix at all stages of atherosclerosis (10). Clinically, both BAV and MFS are characterized by significantly less atherosclerosis. Findings which are in line with earlier studies highlighting that thoracic aortic aneurysms are associated with decreased systemic atherosclerosis (11). We postulate that the combination of a thin intimal layer and a defect in vascular smooth muscle cell differentiation might act protective for the development of atherosclerosis in the vessel wall. Less is, however, known about the role of atherosclerosis in patients with a type A aortic dissection. Recently we concluded that patients with a type A aortic dissection also demonstrate a significantly thinner intimal layer, even in the absence of a genetic syndrome or a bicuspid aortic valve (12). Considering the overlap in pathogenetic mechanisms between BAV, MFS, and type A aortic dissections it is particularly interesting to study the presence of atherosclerosis in aortic dissections.

Earlier studies have suggested that patients with a type A aortic dissection are less prone for atherosclerosis, however, this has been concluded on basis of imaging studies (11, 13). The novelty of this paper is that we study atherosclerosis on tissue level and can detect early stages of atherosclerosis which would be missed by only studying the images of transesophageal echocardiography or computed tomography images (11, 14). The aim of this study is to systematically classify atherosclerotic lesions in the type A aortic dissection population according to the adapted AHA classification as proposed by Virmani et al. (15).

2. Materials and methods

2.1. Patients and tissue samples

Fifty-one ascending aortic wall samples were obtained from the aortotomy site as residual aortic wall material during an ascending aortic replacement in patients with an acute type A aortic dissection at the Leiden University Medical Center, Leiden, Netherlands. Patients with a proven genetic disorder (e.g., Marfan disease) or a bicuspid aortic valve were excluded. Seventeen control aortas were obtained during post-mortem autopsies.

Sample collection was uniform in all patients: ascending aortic wall specimen were obtained from the aortotomy site. The aortotomy site is classically in the middle of the ascending aorta, just beneath the pericardial fold. Circular tissue was obtained and embedded in paraffin. The complete circular ascending aortic wall was sectioned to avoid sampling of the aortic tissue.

Sample collection and handling was carried out according to the official guidelines of the Medical Ethical Committee of Leiden University Medical Center and the code of conduct of the Dutch Federation of Biomedical Scientific Societies.[1] Autopsy has been performed according to the guidelines of the pathology department. Tissue collection was performed according to the regulations and protocols for secondary tissue use of the department of pathology at the Leiden University Medical Center. Written informed consent was obtained.

After excision, specimens were fixed in 4% formalin (24 h), decalcified in a formic acid-formate buffer (120 h), and embedded in paraffin. Transverse sections (4 μm) were mounted on precoated Starfrost slides (Klinipath BV, Duiven, Netherlands).

2.2. Histological classification of the lesions

The sectioning and staining protocols have been described previously (16). Hematoxylin-eosin (HE) and Movat pentachrome staining was performed for the histological evaluation of all samples of each circular aortic specimen. Sections were studied with a Leica BM5000 microscope equipped with plan achromatic objectives (Leica Microsystems, Wetzlar, Germany). Each section was individually classified according to the modified classification of the AHA as proposed by Virmani et al. (15), by two independent observers with no knowledge of the characteristics of the aortic patch (**Table 1**). Across the circular ascending aortic wall tissue the plaque with the most advanced grade of atherosclerosis according to Virmani et al. (15) called the "dominant plaque" was analyzed for this study.

Given a role of inflammation in atherosclerosis we also studied the presence of inflammatory infiltrates in the intimal layer of type A aortic dissection and control patients. As inflammatory cells are acute phase proteins, an abundance of these cells is encountered in the dissected medial layer. To study inflammatory cells associated with intimal atherosclerosis, we studied the influx of inflammatory cells in the intimal layer using the HE and MOVAT pentachrome stained sections, indexed from zero (no inflammatory cells), 1 (a few cells), 2 (groups of cells) to 3 (large clusters of cells).

2.3. Statistical analysis

All numerical data are presented as the mean ± standard deviation. Statistical differences were evaluated with the Mann–Whitney U test for comparison between the groups. One, two and three way ANCOVA, binary logistic regression and linear regression analysis were performed to correct for age, sex and hypertension. Significance was assumed when $p < 0.05$ with SPSS 26.0 (SPSS Inc., Chicago, IL, USA) was used for the statistical analyses.

3. Results

3.1. Patient population

A total of 51 patients with a type A aortic dissection were included in the study. The mean age of the study population was 62.5 ± 10.8 years. Females and males were evenly distributed in the study group (49% females). All patients had a tricuspid aortic

1 www.FMWV.nl

TABLE 1 Atherosclerotic lesions in type A aortic dissection patients.

Morphological description	Associated AHA classification	*N*	Mean age	Female (%)
Normal aorta	–	7	63.3 ± 9.3	42.9%
Non-progressive intimal lesions				
Adaptive intimal thickening	I	24	62.1 ± 10	61%
Intimal xanthoma	II	13	62.6 ±	14%
Progressive atherosclerotic lesions				
Pathological intimal thickening	III	4	64.2 ± 7	100%
Early fibroatheroma	IV	1	51	100%
Late fibroatheroma	IV/V_a	1	65	100%
Thin-cap fibroatheroma	–	1	66	0%
Plaque rupture	VI	0	–	–
Healing rupture	VI	0	–	–
Fibrotic calcified plaque	$V_{b,c}$, VII	0	–	–

valve and no underlying aortic genetic disease was identified after genetic screening by the institutional geneticist.

The mean body-mass index of all patients was 26.01 kg/m^2; 19 patients (37%) were considered overweight (BMI > 25). Smoking status was not known for most patients. Diabetes and peripheral arterial disease were not present in any of the patients. Chronic obstructive pulmonary disease was seen in one patient. Fifty-nine percent of the patients had a history of hypertension (antihypertensive medication or systolic blood pressure > 140 mmHg and diastolic > 90 mmHg in the period).

The control group of 17 patients were obtained post-mortem. The mean age of the control patients was 63 ± 5.5 years. Females and males were evenly distributed in the controls (53% females). All control patients had a non-cardiac cause of death, had a tricuspid aortic valve and no underlying genetic disease was known. Data on cardiovascular risk factors could not be retrieved for all control patients.

3.2. Morphometric measurements

The intima is defined as the area between the inner surface of the aortic wall, lined by the endothelial cells and the first elastic lamellae of the media (**Figure 1**). The mean intimal thickness in all type A dissection patients was 143 ± 126.5 μm. No significant difference in intimal thickness was observed when corrected for age and sex or in the presence of (a history of) hypertension (Age vs intimal thickness p = 0.406; sex vs intimal thickness: OR 1.00 (95% CI 1.00–1.01), p = 0.669; Hypertension vs intimal thickness OR 1.00 (95% CI 1.00–1.00), p = 0.860). In control patients the mean intimal thickness was 193 ± 132 μm, which is significantly thicker as compared to the type A aortic dissection patients (p < 0.023).

3.3. Non-progressive intimal lesions in type A aortic dissection patients

Atherosclerotic lesions in the intima were scored according to the modified classification of the AHA as proposed by Virmani et al. (15), **Table 1**. Seven patients had a normal intima without any form of adaptive or pathological thickening (**Figure 2A**). The intimal layer had a mean thickness of 81 ± 62.7 μm in these patients. Mean age in this group was 63.3 ± 9.3 years and 43% was female.

Twenty-three type A aortic dissection patients demonstrated adaptive intimal thickening (**Figure 2B**). In these patients the intimal thickening consisted mainly of smooth muscle cells with an increase in proteoglycan-rich matrix. Mean intimal thickness in this group was 103.4 ± 56 μm, and mean age was 62.1 ± 10 years. Sixty-one percent of the patients with adaptive intimal thickening were female.

As soon as macrophage-derived foam cells become evident in the intima the lesions are referred to as intimal xanthoma, also known as fatty streaks (**Figure 2C**). These lesions were seen in 14 patients, with a mean age of 62.6 ± 14.9 years and 14% was female. Mean thickness of the intima was 151.6 ± 94.4 μm.

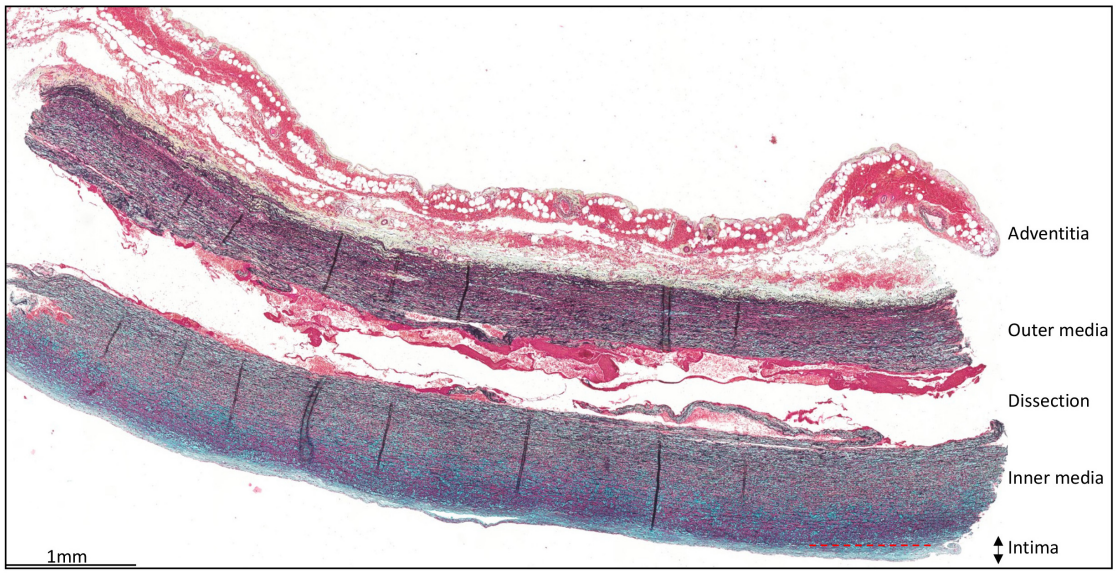

FIGURE 1
Transverse histologic section (4 μm) of a type A aortic dissection aortic specimen. The vessel wall layers are indicated: adventitia, media, and intima. The intimal layer is defined as the area between the endothelial cells lining the luminal surface and the lamina elastica interna. Scale bar shown in figure.

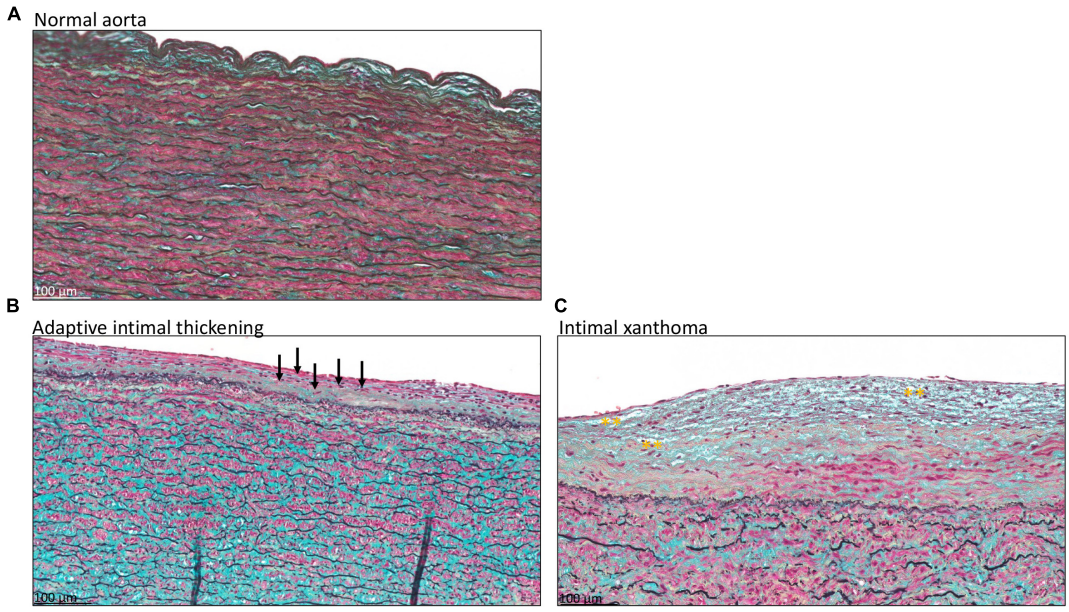

FIGURE 2
Transverse histologic section of type A aortic dissection aortic specimen (4 µm), stained with MOVAT pentachrome. **(A)** Shows a normal intimal layer, without any signs of adaptive or pathological thinning. In panel **(B)** an adaptive thickened intima is seen with mainly vascular smooth muscle cells in the proteoglycan-rich matrix, a few of which are depicted with black arrows. **(C)** Intimal xanthoma is seen in a patient with macrophage derived foam cells in the matrix, highlighted with yellow asterisks. Scale bar shown in the figures.

3.4. Progressive atherosclerotic lesions in type A aortic dissection patients

A total of seven patients had progressive atherosclerotic lesions (Figure 3 and Table 1). The mean age of these patients was 62.7 ± 7.2 years and 86% was female. Four out of these seven patients demonstrated pathological intimal thickening with a mean intimal thickness of 244.0 ± 156.2 µm (Figure 3A). Mean age of the four patients was 64.2 ± 7 years, all of which were female. The remaining three patients showed early fibroatheroma (Figure 3B), late fibroatheroma (Figure 3C) and thin cap fibroatheroma (Figure 3D).

The severity of the atherosclerotic lesions was independent of age, sex, and the cardiovascular risk factor hypertension (age vs atherosclerosis classification $p = 0.976$; sex vs atherosclerosis classification: OR 0.99 (95% CI 0.63–1.56), $p = 0.960$; hypertension vs atherosclerosis classification: OR 1.14 (95% CI 0.72–1.78); $p = 0.587$).

3.5. Atherosclerotic lesions in control patients and intimal inflammation

Non-progressive atherosclerotic lesions (intimal xanthoma) were seen in only three patients (Table 2). Patients from the control group predominantly exhibited progressive atherosclerotic lesions. Three patients showed pathological intimal thickening (Figure 4A), two had early fibroatheroma (Figure 4B), six demonstrated late fibroatheroma (Figure 4C), one had a healed rupture (Figure 4D), and two had a fibrotic calcified plaque (Figure 4E and Table 2). Sex was randomly distributed across the non- and progressive atherosclerotic lesions.

As inflammatory cells are associated with the development of atherosclerosis, we studied the infiltration of inflammatory cells in the intimal layer. The qualitative amount of inflammatory cells was significantly higher in the control group as compared to the type A aortic dissection patients ($p < 0.0001$) (Figures 4F, G).

4. Discussion

In this study we analyzed atherosclerotic lesions in type A aortic dissection patients. We found a very low incidence of progressive atherosclerotic lesions in the study population. Major cardiovascular risk factors for atherosclerosis (i.e., age, sex, hypertension, and diabetes mellitus) were not associated with atherosclerosis. The control group on the other hand demonstrated predominantly progressive atherosclerotic lesions. The intimal layer further showed significantly more influx of inflammatory cells in the control patients as compared to the intimal layer in type A aortic dissections, this finding is in line with earlier suggestions that inflammation may

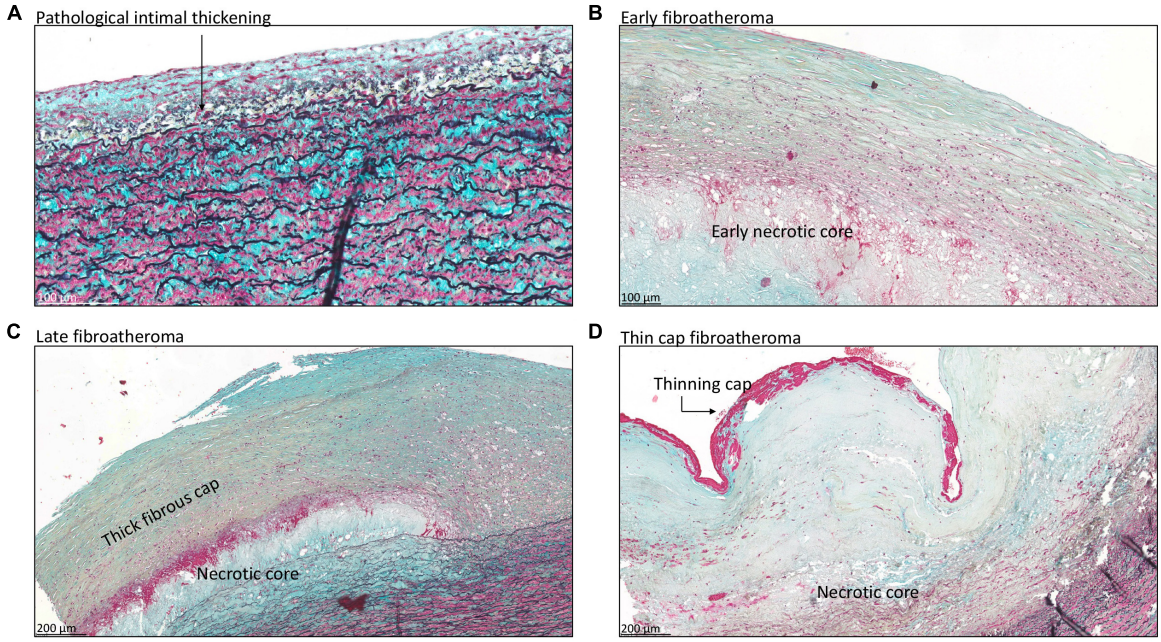

FIGURE 3
Transverse histologic section (4 µm) of type A aortic dissection aortic specimen, stained with MOVAT pentachrome. **(A)** Shows pathological intimal thickening, characterized by the presence of lipid pools deep within the intima near the intimal medial border with overlying vascular smooth muscle cells (black arrow). Fibroatheroma is seen in panels **(B–D)**, with an early necrotic core in panel **(B)**, thick fibrous cap in panel **(C)**, and thinning of the fibrous cap in panel **(D)**. Scale bar shown in the figures.

TABLE 2 Atherosclerotic lesions in control patients.

		Type A dissections group	Control group
Morphological description	Associated AHA classification	*N*	*N*
Normal aorta	–	7 (14%)	0
Non-progressive intimal lesions			
Adaptive intimal thickening	I	24 (47%)	0
Intimal xanthoma	II	13 (25%)	3 (18%)
Progressive atherosclerotic lesions			
Pathological intimal thickening	III	4 (8%)	3 (18%)
Early fibroatheroma	IV	1 (2%)	2 (12%)
Late fibroatheroma	IV/V_a	1 (2%)	6 (35%)
Thin-cap fibroatheroma	–	1 (2%)	0
Plaque rupture	VI	0	0
Healing rupture	VI	0	1 (6%)
Fibrotic calcified plaque	$V_{b,c}$, VII	0	2 (12%)

contribute to the development of atherosclerosis. The presence of inflammatory cells in the intimal layer of the ascending aorta is an interesting finding and further studies should be performed to characterize the type of inflammatory cells present. Findings of this study are consistent with previous observations that conditions predisposing for the development of a type A aortic dissection, being patients with Marfan syndrome, a bicuspid aortic valve and a thoracic aortic aneurysm, also associate with a lower prevalence of atherosclerosis (11, 17).

A type A aortic dissection is a life-threatening aortic complication. Although several risk factors have been described predisposing individuals for this lethal condition, the exact pathogenesis has not yet been identified (18). Roughly, the development of an aortic dissection requires three main

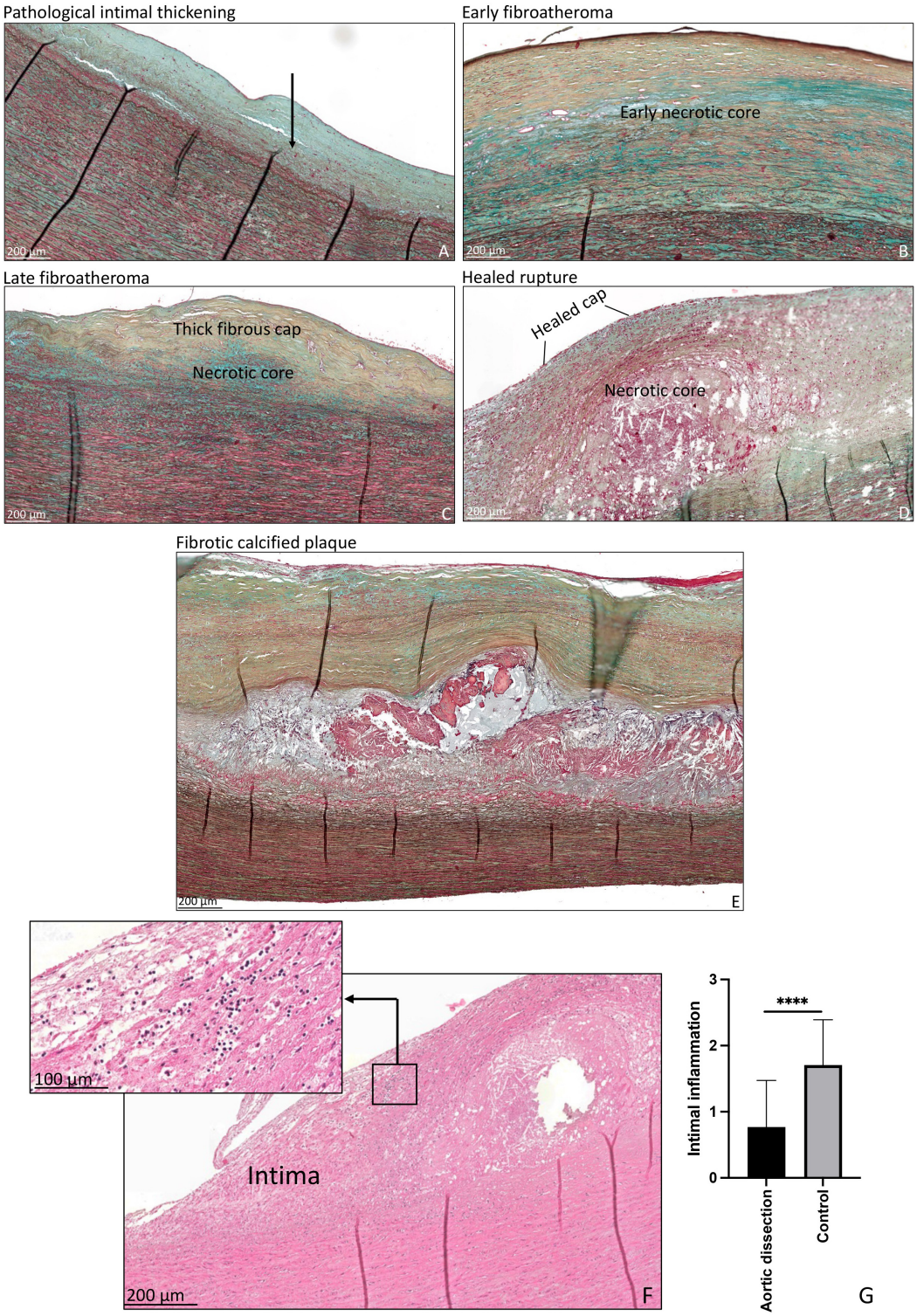

FIGURE 4
Transverse histologic section (4 µm) of control aortic specimen, stained with MOVAT pentachrome **(A–E)** and hematoxylin eosin **(F)** staining. **(A)** Shows pathological intimal thickening, lipid pools are seen deep within the intima near the intimal medial border with overlying vascular smooth muscle cells (black arrow). **(B)** Shows early fibroatheroma, with an early necrotic core. **(C)** Shows late fibroatheroma with a thick fibrous cap overlying the necrotic core. Healed rupture is seen in panel **(D)** and a fibrotic calcified plaque in panel **(E)**. Intimal inflammation is seen in panel **(F)**, the insert demonstrates a detail of the inflammatory cells. The qualitative amount of inflammatory cells was significantly higher in the control group as compared to the type A aortic dissection patients ($p < 0.0001$) **(G)**. ****$p < 0.0001$. Scale bar shown in the figures.

pathological conditions, being mechanical wall stress, a susceptible intimal layer and medial degeneration (12, 19). Our previous study had shown that medial pathology in type A aortic dissections is comparable with thoracic aneurysms in patients with a tricuspid aortic valve with smooth muscle cell nuclei loss, mucoid extracellular matrix accumulation and elastic fiber fragmentation and loss (12). The intimal layer was, however, significantly thinner as compared to the tricuspid thoracic aortopathy patients, resembling the intima in patients with Marfan syndrome and a bicuspid aortic valve (20, 21). As aortic dissections commence with a tear in the intimal layer, it is particularly interesting to understand whether the pathology present is comparable to degenerative or genetic thoracic aortopathy.

Age is an important factor in the atherosclerotic process and is related with a significant change in the physiological and pathological properties of the vessel wall (22, 23). Studies focusing on the natural history of atherosclerosis have shown that advanced atherosclerotic disease is common in people over 45. In this study we excluded patients with a genetic syndrome and/or a bicuspid aortic valve, and all patients analyzed were aged and presented with so-called degenerative thoracic aortopathy. In the study population age did not differ significantly between the sub-groups of non-and progressive intimal lesions as suggested by Virmani et al. (15). Moreover, 86% of the patients had no signs of progressive intimal atherosclerosis, with the majority demonstrating a normal aorta or adaptive intimal thickening even at an advanced age. This is contrast to the control group of comparable age and gender distribution, which predominantly exhibited progressive atherosclerotic lesions. A comparative study performed by Heng et al. used heart transplant recipients as control aortic tissue and found no atherosclerosis in this group (24). These patients were, however, almost 5–6 years younger than the patients studied in our paper. This could explain the difference in our findings. Future studies should pay additional attention to the cardiovascular risk factors in the control group. Our data further suggests that in the type A dissection population progressive aortic atherosclerosis occurs more often in women than in men, an observation that concurs with clinical observations showing that peripheral artery disease develops earlier and at a relatively high rate in women (25, 26). In the control group a female predominance was not observed in the progressive aortic atherosclerotic lesions.

Earlier studies have suggested that patients with a thoracic aortic aneurysm or aortic dissection demonstrate less atherosclerotic lesions (11, 13, 17, 27). These studies used imaging modalities such as TEE or CT scanning to score atherosclerotic lesions across the aorta (28). In this paper we studied the histological classification of atherosclerosis on aortic tissue level to be able to also detect early stages of atherosclerosis which would be missed by only studying the images of transesophageal echocardiography or computed tomography images (11, 14). As more than 90% of the type A aortic dissections commence within the first few centimeters of the ascending aortic wall, and the aortic root and arch are not always involved, we uniformly studied the ascending aorta in all patients. In our earlier studies we have paid particular attention to the role of shear stress on the histopathology of the aortic wall in patients with a bicuspid and tricuspid aortic valve, with and without dilatation and found no difference in the amount of atherosclerosis (29). With magnetic resonance imaging the area with maximum shear stress in the ascending aortic wall was compared to the opposite site (non-jet side). Differences were appreciated in the intimal thickness, but without features of atherosclerosis (29).

We recognize that atherosclerosis is a pathological entity, even though our study has dealt with many limitations by performing histopathological analysis and avoiding sampling errors, the lesions represent a very short segment of ascending aorta, and areas of atheroma may be missed. Staining for smooth muscle cells and immune cell markers should be considered in future studies to confirm our findings. Our study is further limited by the low number of control patients versus the dissected specimen. Even though genetic screening is performed in the patients to exclude an aortic genetic disease, unknown genetic mutations associated with sporadic type A dissections can be missed.

Our findings emphasize that a type A aortic dissection occurs in the absence of clinical cardiovascular risk factors as diabetes, dyslipidaemia and peripheral arterial and despite aging most patients have minimal atherosclerotic lesions. We postulate that a thin intimal layer could increase susceptibility for a future aortic dissection, but at the same time acts protective for systemic atherosclerosis.

Data availability statement

The raw data supporting the conclusions of this article will be made available by the authors, without undue reservation.

Ethics statement

The studies involving human participants were reviewed and approved by the Medical Ethical Committee of Leiden University Medical Center. The patients/participants provided their written informed consent to participate in this study.

Author contributions

NG conceived and designed the experiments, performed the experiments, analyzed and interpreted the data, contributed reagents and materials, and wrote the manuscript. OD, EJ, and

AD wrote the manuscript. RK conceived and designed the experiments, contributed reagents and materials, and wrote the manuscript. JL contributed reagents and materials and wrote the manuscript. RP conceived and designed the experiments, analyzed and interpreted the data, contributed reagents and materials, and wrote the manuscript. All authors contributed to the article and approved the submitted version.

Conflict of interest

The authors declare that the research was conducted in the absence of any commercial or financial relationships that could be construed as a potential conflict of interest.

The reviewer M-JG declared a shared affiliation with the authors NG, OD, JL, and RP to the handling editor at the time of review.

Publisher's note

All claims expressed in this article are solely those of the authors and do not necessarily represent those of their affiliated organizations, or those of the publisher, the editors and the reviewers. Any product that may be evaluated in this article, or claim that may be made by its manufacturer, is not guaranteed or endorsed by the publisher.

References

1. Harris C, Croce B, Cao C. Type A aortic dissection. *Ann Cardiothorac Surg.* (2016) 5:256. doi: 10.21037/acs.2016.05.04

2. Benedetto U, Sinha S, Dimagli A, Cooper G, Mariscalco G, Uppal R, et al. Decade-long trends in surgery for acute type a aortic dissection in England: a retrospective cohort study. *Lancet Reg Health Eur.* (2021) 7:100131. doi: 10.1016/j.lanepe.2021.100131

3. Bossone E, Masiello P, Panza A, Alfano A, Tedesco L, Priante O, et al. Acute aortic dissection in the young: clinical series. *Minerva Chir.* (2007) 62:305–7.

4. Vapnik JS, Kim JB, Isselbacher EM, Ghoshhajra BB, Cheng Y, Sundt TM III, et al. Characteristics and outcomes of ascending versus descending thoracic aortic aneurysms. *Am J Card.* (2016) 117:1683–90. doi: 10.1016/j.amjcard.2016.02.048

5. Michelena HI, Khanna AD, Mahoney D, Margaryan E, Topilsky Y, Suri RM, et al. Incidence of aortic complications in patients with bicuspid aortic valves. *JAMA.* (2011) 306:1104–12. doi: 10.1001/jama.2011.1286

6. Roman MJ, Devereux RB. Aortic dissection risk in Marfan syndrome. *J Am Coll Cardiol.* (2020) 75:854–6. doi: 10.1016/j.jacc.2019.12.042

7. Grewal N, Groot AC, Lindeman JH, Klautz A, Driessen A, Klautz RJM, et al. Normal and abnormal development of the aortic valve and ascending aortic wall: a comprehensive overview of the embryology and pathology of the bicuspid aortic valve. *Ann Cardiothorac Surg.* (2022) 11:380–8. doi: 10.21037/acs-2021-bav-14

8. Granata A, Serrano F, Bernard WG, McNamara M, Low L, Sastry P, et al. An iPSC-derived vascular model of Marfan syndrome identifies key mediators of smooth muscle cell death. *Nat Genet.* (2017) 49:97–109. doi: 10.1038/ng.3723

9. Harmon AW, Nakano A. Nkx2-5 lineage tracing visualizes the distribution of second heart field-derived aortic smooth muscle. *Genesis.* (2000) 2013:862–9.

10. Basatemur GL, Jørgensen HF, Clarke MCH, Bennett MR, Mallat Z. Vascular smooth muscle cells in atherosclerosis. *Nat Rev Cardiol.* (2019) 16:727–44.

11. Achneck H, Modi B, Shaw C, Rizzo J, Albornoz G, Fusco D, et al. Ascending thoracic aneurysms are associated with decreased systemic atherosclerosis. *Chest.* (2005) 128:1580–6. doi: 10.1378/chest.128.3.1580

12. Grewal N, Velders BJJ, Gittenberger-de Groot AC, Poelmann R, Klautz RJM, Van Brakel TJ, et al. A systematic histopathologic evaluation of type-A aortic dissections implies a uniform multiple-hit causation. *J Cardiovasc Dev Dis.* (2021) 8:12. doi: 10.3390/jcdd8020012

13. Agmon Y, Khandheria BK, Meissner I, Schwartz GL, Sicks JD, Fought AJ, et al. Is aortic dilatation an atherosclerosis-related process? clinical, laboratory, and transesophageal echocardiographic correlates of thoracic aortic dimensions in the population with implications for thoracic aortic aneurysm formation. *J Am Coll Cardiol.* (2003) 42:1076–83.

14. Weissler-Snir A, Greenberg G, Shapira Y, Weisenberg D, Monakier D, Nevzorov R, et al. Transoesophageal echocardiography of aortic atherosclerosis: the additive value of three-dimensional over two-dimensional imaging. *Eur Heart J Cardiovasc Imaging.* (2014) 16:389–94. doi: 10.1093/ehjci/jeu195

15. Virmani R, Kolodgie FD, Burke AP, Farb A, Schwartz SM. Lessons from sudden coronary death: a comprehensive morphological classification scheme for atherosclerotic lesions. *Arterioscler Thromb Vasc Biol.* (2000) 20:1262–75.

16. Grewal N, Gittenberger-de Groot AC, Thusen JV, Wisse LJ, Bartelings MM, DeRuiter MC, et al. The development of the ascending aortic wall in tricuspid and bicuspid aortic valve: a process from maturation to degeneration. *J Clin Med.* (2020) 9:908. doi: 10.3390/jcm9040908

17. Dolmaci OBLJ, Lindeman JHN, Driessen AHG, Klautz RJM, van Brakel TJ, Hans-Marc J. The extent of coronary artery disease in patients with stenotic bicuspid versus tricuspid aortic valves. *J Am Heart Assoc.* (2021) 10:e020080.

18. Howard DP, Banerjee A, Fairhead JF, Perkins J, Silver LE, Rothwell PM. Population-based study of incidence and outcome of acute aortic dissection and premorbid risk factor control: 10-year results from the Oxford vascular study. *Circulation.* (2013) 127:2031–7. doi: 10.1161/CIRCULATIONAHA.112.000483

19. Akutsu K. Etiology of aortic dissection. *Gen Thorac Cardiovasc Surg.* (2019) 67:271–6. doi: 10.1007/s11748-019-01066-x

20. Grewal N, Goumans MJ, deRuiter M, Klautz RJ, Poelmann R, Mulder B, et al. Aortopathy in bicuspid aortic valve and Marfan syndrome is characterized by a lack of activation potential of the epicardium in the ascending aorta. *Int J Pathol Clin Res.* (2017) 3:51. doi: 10.23937/2469-5807/1510051

21. Grewal N, Gittenberger-de Groot AC. Pathogenesis of aortic wall complications in Marfan syndrome. *Cardiovasc Pathol.* (2018) 33:62–9.

22. van Dijk RA, Virmani R, von der Thusen JH, Schaapherder AF, Lindeman JH. The natural history of aortic atherosclerosis: a systematic histopathological evaluation of the peri-renal region. *Atherosclerosis.* (2010) 210:100–6. doi: 10.1016/j.atherosclerosis.2009.11.016

23. O'Rourke MF. Arterial aging: pathophysiological principles. *Vasc Med.* (2007) 12:329–41. doi: 10.1177/1358863X07083392

24. Heng E, Stone JR, Kim JB, Lee H, MacGillivray TE, Sundt TM. Comparative histology of aortic dilatation associated with bileaflet versus trileaflet aortic valves. *Ann Thorac Surg.* (2015) 100:2095–101. doi: 10.1016/j.athoracsur.2015.05.105

25. Leng GC, Papacosta O, Whincup P, Wannamethee G, Walker M, Ebrahim S, et al. Femoral atherosclerosis in an older British population: prevalence and risk factors. *Atherosclerosis.* (2000) 152:167–74. doi: 10.1016/S0021-9150(99)00447-5

26. Diehm C, Schuster A, Allenberg JR, Darius H, Haberl R, Lange S, et al. High prevalence of peripheral arterial disease and co-morbidity in 6880 primary care patients: cross-sectional study. *Atherosclerosis.* (2004) 172:95–105. doi: 10.1016/S0021-9150(03)00204-1

27. Dolmaci OB, Driessen AHG, Klautz RJM, Poelmann R, Lindeman JHN, Grewal N. Comparative evaluation of coronary disease burden: bicuspid valve disease is not atheroprotective. *Open Heart.* (2021) 8:e001772. doi: 10.1136/openhrt-2021-001772

28. Khoury Z, Gottlieb S, Stern S, Keren A. Frequency and distribution of atherosclerotic plaques in the thoracic aorta as determined by transesophageal echocardiography in patients with coronary artery disease. *Am J Card.* (1997) 79:23–7. doi: 10.1016/S0002-9149(96)00670-4

29. Grewal N, Girdauskas E, deRuiter M, Goumans MJ, Lindeman JH, Disha K, et al. The effects of hemodynamics on the inner layers of the aortic wall in patients with a bicuspid aortic valve. *Int Mol Med.* (2017) 4:5. doi: 10.15761/IMM.1000308

Frontiers in
Cardiovascular Medicine

Innovations and improvements in cardiovascular treatment and practice

Focuses on research that challenges the status quo of cardiovascular care, or facilitates the translation of advances into new therapies and diagnostic tools.

Discover the latest Research Topics

See more →

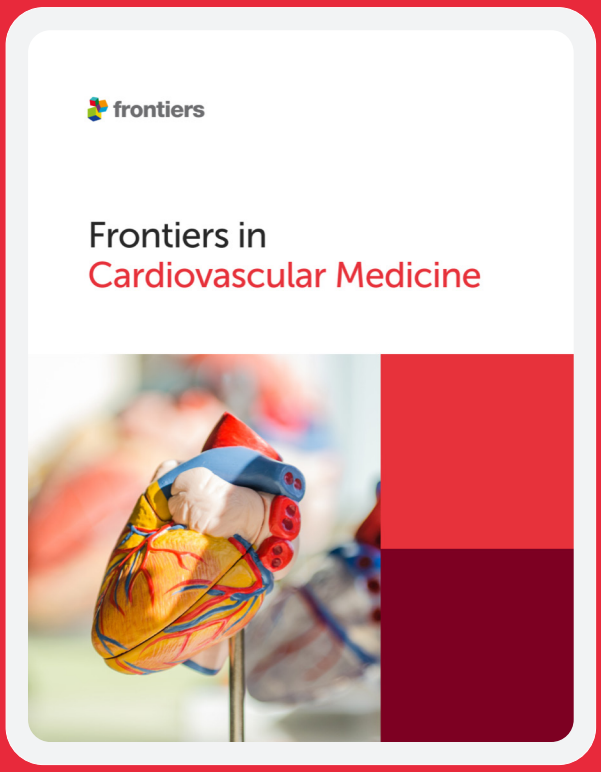

Frontiers

Avenue du Tribunal-Fédéral 34
1005 Lausanne, Switzerland
frontiersin.org

Contact us

+41 (0)21 510 17 00
frontiersin.org/about/contact